On the Structure and Distribution

of

Quasi-Stellar Radio-Sources

by

G. M. Rowan-Robinson

Presented as a thesis for the degree of

Doctor of Philosophy in the University of London

June, 1969

Preface.

The work contained in this thesis is essentially original, and has not been submitted for any previous degree. Much of Chapter I has been published in papers I and II attached to this thesis.

I am grateful to the Science Research Council for a Research Studentship which made this work possible. The computing was performed at the Computer Centre at the University of Sussex and at Queen Mary College, to the staff to whom thanks are due for much assistance in the writing of programs.

Finally, I am deeply indebted to my supervisor, Professor W H. McCrea, F.R S., for his continued interest and guidance throughout the course of this work.

Summary.

Assuming the redshifts of quasars are cosmological, their distribution in space is investigated by means of new test, the luminosity-volume test (Chapter I), which is shown to be far more powerful than the magnitude-redshift test. In most relativistic cosmological models, strong evolutionary factors must be influencing the distribution of quasars in space, and possible explanations are discussed qualitatively and quantitatively. The similar behaviour of the stronger radio-galaxies strengthens the link between the two classes of source.

Less direct information about more remote parts of space is obtained by the interpretation of the radio source-counts (Chapter III) and the integrated radio and X-ray background intensities (Chapter IV). Assumptions have to be made about the physical properties of sources, particularly the magnetic field, and a number of different models for the structure of radio-sources are discussed in Chapter II. Evidence is presented against the idea that the radio-emitting components are ejected from the parent galaxies at relativistic speeds. Models are considered in which relativistic electrons are generated continuously in the radiating components.

A number of the tacit assumptions underlying previous interpretations of radio source-counts are examined in detail. Longair's often quoted result that the radio source-counts indicate a real dimination in the density of sources at earlier epochs is shown to be false. Significant dependence on cosmological model is found, particularly at lower flux-levels, and comparatively empty universes are preferred. Density evolution is consistent with the source-counts only if there is a luminosity-dependent truncation, which could be caused by the black-body radiation if the luminosity of sources is a function of the magnetic field.

The observed X-ray background is hard to explain in terms of interaction of the black-body radiation with relativistic-electrons in radio-sources, unless sources have exceptionally low magnetic fields.

CONTENTS

Chapter II: Structure of radio-galaxies and quasars

Chapter III: Interpretation of radio source-counts

CHAPTER ONE

Summary.

The properties of the relativistic cosmologies are summarized in section 2, and consideration of a flow diagram of the two cosmological parameters emphasizes the special significance of the de Sitter, Milne and Einstein-de Sitter models. The influence of the "volume effect" on the magnitude redshift test is evaluated in section 3, and in section 4 a new test, the luminosity-volume test, is described. It is found that some kind of secular evolution must influence the distribution in space of both the quasars (sections 5 and 12) and the stronger radio-galaxies (section 14). Possible evolutionary effects are discussed in section 6, and the parameters required with simple mathematical forms of evolution estimated in section 10 and 14. If it is assumed that the coordinate number-density, or the typical luminosity, of sources have a negative exponential dependence on the scale-factor, similar parameters are obtained for both quasars and radio-galaxies. This is a significant result if there is some link between the two classes of object. At early epochs the number-density of sources would be about 10^4 times greater than that at the present epoch, or the typical luminosities of sources would be about 100 times greater than at the present epoch. The characteristic epochs beyond which the distribution of sources would look fairly uniform correspond to redshifts of about 10 and 5 respectively.

The non-uniform distribution of the radio-galaxies shows that the strict steady-state cosmology is not saveable by ad hoc hypotheses about the redshifts of quasars. The "local" theory for quasars is discussed in Appendix 5, and while earlier arguments do not seem strong enough to rule out such a theory, it can be shown that if the redshifts of quasars are essentially independent of distance, their distribution in space is still inconsistent with the steady-state cosmology.

I. Introduction.

Throughout most of this work I assume that the redshifts of quasars are cosmological (1). Although severe difficulties exist for this view (2, 4 - 6), the other possible explanations that have been presented in detail to date (8,9) pose more difficulties than they solve (10 - 12).

Pessimism has been expressed whether, even if quasars are at cosmological distances, they are of much value to cosmology (13, 14). The two classical tests, the magnitude-redshift test and the number-counts of sources, are only effective in distinguishing between cosmological models in situations where the dispersion in luminosity is small. While this is the case for the optical luminosities of galaxies, it is certainly not true for the radio-luminosities of radio-galaxies, or for either the optical or radio luminosities of quasars (if the redshifts of quasars are cosmological). This pessimism is unjustified, since the additional factor of completeness down to a limiting flux-level enables a far more powerful test, the "luminosity-volume" test, to be applied. This test combines the essential features of both the redshift-magnitude and number-count tests and uses more information than either. A simple extension enables evolutionary hypotheses to be tested.

Radio number-counts of all sources provide clear evidence that evolutionary factors are affecting at least a sub-population of the

sources (15 - 18). Two kinds of evolution have been considered in some detail in earlier interpretations of the radio number-counts (18 - 20):

(a) Density evolution: the fraction of material in the form of active sources is a function of epoch.

(b) Radio luminosity-evolution: the typical luminosity of sources is a function of epoch, while the fraction of material in the form of active sources and the form of the dispersion of luminosities are independent of epoch.

Longair (18) has shown that to obtain consistency with number-counts to low flux-levels and the extragalactic contribution to the integrated background radio emission all classes of source cannot be supposed to evolve. If the evolution is then due to an indistinguishable sub-population of the sources, the distinction between hypotheses (a) and (b) disappears (18). However if the evolution takes place in a recognizable sub-population (e.g. the quasars) then we are dealing with distinct hypotheses and can hope to test between them. Earlier suggestions that the magnitude-redshift diagram for quasars supported luminosity rather than density evolution (22, 23) were shown to be incorrect(24). The present results are still stronger: luminosity evolution of the form considered in references 18 - 20 , 22, 23 is inconsistent with a wide range of cosmological

model, whereas consistency with all models can be obtained using density evolution.

However, it is important to consider whether results obtained using a particular mathematically simple form of evolution may not depend rather strong on that mathematical form. The truncation of the evolving population beyond a redshift of about 4(18) may fall in this category. In this work I suggest other forms of evolution which do not require such a truncation.

The cosmological models tested are the familiar relativistic models, including the possibility of a non-zero cosmological constant, the steady-state cosmology and a class of Brans-Dicke models.

2. The models

(i) summary of properties:

The properties of the relativistic cosmological models are discussed in many standard references (e.g. 25, 26, 27), but for completeness we summarize here the relations we need.

The observed flux in the frequency range ν_0 to $\nu_0 + d\nu_0$, from a source emitting $F(\nu_e)\,d\nu_e$ in the corresponding range of emitted frequency ν_e to $\nu_e + d\nu_e$, is given by

$$f(\nu_0)\,d\nu_0 = \frac{F(\nu_e)\,d\nu_e\,(1 + k r_0^2/4)^2}{R_0^2 r_0^2 Z^2} \qquad (1)$$

where $\dfrac{\nu_e}{\nu_0} = 1 + z = Z$

and $$\int_{t_e}^{t_0} \frac{dt}{R} = \int_0^{r_0} \frac{dr}{1 + k r^2/4} \qquad (2)$$

Writing $\mathcal{F} = \log_{10} F(\nu_0)$, $\mathcal{f} = \log_{10} f(\nu_0)$ equation (1)

becomes $\mathcal{F} = \mathcal{f} + \log_{10} \dfrac{R_0^2 r_0^2 Z^2}{(1 + k r_0^2/4)^2} - 0.4K$ (3)

where the K-correction takes account of the selectivity of the atmosphere and the apparatus, and of the shift of the spectrum across the observed frequency band. The forms we have used for optical and radio K-corrections are presented in appendix I.

From Einstein's equations for uniform, pressure-free universes, the scale-factor $R(t)$ satisfies the equations

$$\ddot{R} = -4\pi G \rho R/3 + \Lambda R/3 \qquad (4)$$

$$(\dot{R})^2 = 8\pi G \rho R^2 / 3 + \Lambda R^2/3 - kc^2 \qquad (5)$$

where Λ is the cosmological constant and the density, ρ, satisfies the equation $\rho R^3 = \rho_0 R_0^3$, subscripts zero referring to the present epoch. Then if we write $H = \dot{R}/R$, $q = -\ddot{R} R/\dot{R}^2$ (6)

and $\sigma = 4\pi G \rho / 3H^2$, (7)

equations (4) and (5) become

$$\Lambda/3 = (\sigma - q) H^2 = (\sigma_0 - q_0) H_0^2 \qquad (8)$$

and

$$k c^2 = (3\sigma - q - 1) H^2 R^2 = (3\sigma_0 - q_0 - 1) H_0^2 R_0^2 \qquad (9)$$

(ii) Flow diagram for the models:

Having solved equations (4) and (5) for $R(t)$, and writing $Z = R_0/R$, we can use equations (5), (8) and (9) to obtain

$$H^2(t) = H_0^2 \{ \sigma_0 - q_0 + (1 + q_0 - 3\sigma_0) Z^2 + 2\sigma_0 Z^3 \} = H_0^2 . Y(z)$$

$$\sigma(t) = \sigma_0 Z^3 / Y(z)$$

$$q(t) = \{ \sigma_0 (Z^3 - 1) + q_0 \} / Y(z) .$$

Thus if H_0, σ_0, q_0 are known at the present epoch, then H, σ, q are known for all epochs, past and future. The behaviour of the models can be illustrated by a flow diagram (Fig. 1a). This diagram, and an illuminating discussion of the $\sigma - q$ representation, can be found in Refsdal and Stabell (28). For our purposes the interesting feature to note is that there are just 3 fixed points in this diagram: the Einstein de Sitter model ($\sigma = q = 1/2$),

the de Sitter model ($\Omega = 0$, $q = -1$), and the Milne model ($\Omega = q = 0$). These represent asymptotic states of the universe: the Einstein de Sitter model is the initial state of all non-empty models except those to the left of the curve A , while the Milne and de Sitter models are the final states of monotonic expanding models (all those to the left of the curve B) with $\Lambda = 0$ and $\Lambda \neq 0$, respectively. Oscillating models are those to the right of the curve B. A and B correspond to those models which approach the Einstein static universe as $t \longrightarrow \pm \infty$ respectively (i.e. A is the Eddington-Lemaître model).

The loci to the left of the curve A correspond to those models which "bounce" under the action of cosmological repulsion. As Solheim (29) has remarked, most of these models are ruled out if the redshifts of quasars are cosmological, since they give upper limits to Z which are inconsistent with values already obtained for quasars. In fact for these models to be correct we must be indistinguishibly close to the de Sitter model at the present epoch. Their philosophical attraction is that they are the only non-empty models which do not possess a singularity.

From the point of view of the testing of models, the most interesting situations arise if (Ω_0 , q_0) are <u>not</u> near any of the 3 fixed points. For then we know the future of the universe and its past history (at least back to the epoch where the pressure becomes

significant). But if (σ_0, q_0) are near to one of the fixed points in the $\sigma - q$ plane, we cannot tell whether the universe has always had these values of σ and q, or whether it is in an asymptotic state.

The smoothed-out density of the material actually observed to date $(7 \times 10^{-31}$ gm cm$^{-3})$, (30), and the present value of the Hubble constant $(H_0^{-1} = 1.2 \times 10^{10}$ years), suggest that our present position in the $\sigma - q$ plane may be rather close to the $\sigma = 0$ axis. Difficulties in reconciling the ages of the oldest stars with the age of the universe may force us to the left of the point M and perhaps rather near to the point S. But considerations of this kind are subject to enormous uncertainty. The disadvantage of the $\sigma - q$ representation is that phases where the universe is static lie at infinity. Accordingly, we transform Fig. 1a by

$$s = \frac{\sigma}{\frac{1}{2} + \sigma} \quad , \qquad t = \frac{q}{\frac{1}{2} + |q|} \qquad \text{(Fig. 1b)}$$

so that all models satisfy $0 \leq s \leq 1$, $-1 \leq t \leq 1$, and the points ES, M, S in Fig. 1 become $(\frac{1}{2}, \frac{1}{2})$, $(0,0)$, $(0, -\frac{2}{3})$. $\Lambda = 0$ corresponds to $s = t$ and $k = 0$ to

$4st - 5s - t + 2 = 0 , \quad t \geq 0$

$6st + 5s - 3t - 2 = 0 , \quad t \leq 0.$

The Einstein static model (E) has $s = 1 , \ t = 0 ,$ and the static phases in the two types of oscillating model are labelled E+ (or models to the left of A in Fig. 1a $R = 0 , \ \ddot{R} > 0$) and E - (for models to the right of B in Fig. 1a ; $R = 0 , \ \ddot{R} < 0$) and have $s = 1 , \ t = \pm 1$ respectively. The Lemaître models are those whose flow lines lie close to the boundary $s = 1$.
The instability of the Einstein model is illustrated by the fact that if a slight perturbation causes $\ddot{R}$ to become non-zero, t changes discontinuously from 0 to ± 1.

The flow illustrated in this diagram is somewhat anomalous: an infinite time is required to reach the sink S. E- , E+ are points of reflection except for the two Eddington-Lemaître loci, which take an infinite time to arrive at, and depart from, these points, respectively.

3. Influence of volume effect on magnitude-redshift test

(i) magnitude-redshift test

The results of attempts to distinguish between these models using the magnitude-redshift test for the brightest galaxies in clusters have been

reviewed and extended by Solheim (29), who has computed exact theoretical relations instead of the power-series expansions used in earlier work (31 , 32). His best values for the cosmological parameters are

$$q_0 = -0.06 \quad , \quad \tau_0 = 4.53 \quad ,$$

though these values are appreciably modified if the galaxies are assumed to change their luminosity with epoch (29,33).

The acceptable models appear as a region of the $\tau_0 - q_0$ plane (the "model" diagram). He also applies this procedure to optical data for fifteen quasars. However, it is necessary to take account of the severe selection effect imposed by the limiting radio magnitude for these objects (9 flux-units if we confine our attention to identifications from the 3C catalogue (37, 38)), and also of the "volume effect" discussed below. In the present work we have rather more data available (37 redshifts), we take account of these selection effects, and we also perform the test in a different and more powerful way.

A number of other authors have discussed the observational data for quasars with respect to particular cosmological models. McCrea (34)

plotted the absolute optical magnitudes of quasars against redshift for 3 models : the Milne model ($\sigma_0 = q_0 = 0$), the de Sitter model ($\sigma_0 = 0$, $q_0 = -1$; the steady-state model gives the same diagram), and a particular model used by Schmidt for which $\sigma_0 = q_0 = 1$.

McCrea pointed out that the luminosity, $F_1(z)$ say, of the most luminous source out to redshift z should be an increasing function of z, simply as a probability effect. The Schmidt model then seemed to be rendered improbable by the fact that the nearest quasars, 3C 273, would be intrinsically the most luminous, in this model. The rate of increase of $F_1(z)$ appeared improbably steep in the steady-state model, on the other hand.

(ii) The volume effect.

Some quantitative estimate of the importance of the effect may be made as follows. We assume that the proper number-density of quasars at any epoch, $\nu(t)$, is proportional to the smoothed-out cosmological density, $\rho(t)$, and that the luminosity-function (18) for quasars is independent of epoch. That is, at epoch t let the number of sources per unit proper volume having $\log_{10}F$ in the range

$\mathcal{F}$ to $\mathcal{F} + d\mathcal{F}$ be $\nu(t) . \varphi(\mathcal{F})\, d\mathcal{F}$

where

$$\int_{-\infty}^{+\infty} \varphi(\mathcal{F})\, d\mathcal{F} = 1.$$

Define the coordinate number-density,

$$\eta(t) = \zeta(t) . \frac{R^3(t)}{R_0^3} \qquad (10)$$

thus if $\zeta(t) \propto \nu(t)$, then $\eta(t) = \text{const.} = \eta(t_0) = \eta_0$, say.

The element of proper volume is

$$\frac{R^3(t)\, r^2\, dr\, \sin\theta\, d\theta\, d\varphi}{(1 + k r^2/4)^3}$$

so the total number of sources in the range of luminosity $\mathcal{F}$ to $\mathcal{F} + d\mathcal{F}$ out to redshift z is

$$N(\mathcal{F}, z)\, d\mathcal{F} = \eta_0 R_0^3 . \nu(z) . \varphi(\mathcal{F})\, d\mathcal{F}$$

where

$$\gamma(z) = \int_0^{r_0(z)} \frac{4\pi r^2 \, dr}{(1 + k r^2/4)^3} \qquad (11)$$

Then the expected luminosity, $F_N(z)$, of the Nth most luminous source out to redshift z will be roughly the solution of the equation

$$\eta_0 R_0^3 . \gamma(z) . y . \int_{\mathcal{F}_N(z)}^{\infty} \varphi(\mathcal{F}) \, d\mathcal{F} = N ,$$

where $\mathcal{F}_N(z) = \log_{10} F_N(z)$, and y is the fraction of the sky covered by the sources.

Let

$$\Phi(x) = \int_{-\infty}^{x} \varphi(\mathcal{F}) \, d\mathcal{F}$$

Then

$$\mathcal{F}_N(z) = \Phi^{-1} \left\{ 1 - \frac{N}{\eta_0 R_0^3 . \gamma(z) . y} \right\} \qquad (12)$$

where

$$\Phi^{-1} \{ \Phi(x) \} = x \qquad (13)$$

For example if (a)

$$\varphi(\mathcal{F}) = \frac{1}{\sqrt{2\pi a^2}} \cdot \exp \{ -(\mathcal{F} - \mathcal{F}_0)^2 / 2a^2 \}$$

Then

$$\mathcal{F}_N(z) = \mathcal{F}_0 + a \cdot \mathrm{erf}^{-1} \{ 1 - \frac{N}{\pi_0 R_0^3 \cdot \nu(z) \cdot y} \} \qquad (14)$$

and if (b)

$$\varphi(\mathcal{F}) = b \cdot \log_e 10 \cdot 10^{-b(\mathcal{F} - \mathcal{F}_1)} \quad \text{for} \quad \mathcal{F} \geq \mathcal{F}_1$$

$$= 0 \quad \text{for} \quad \mathcal{F} < \mathcal{F}_1$$

then

$$\Phi(\mathcal{F}) = 1 - 10^{-b(\mathcal{F} - \mathcal{F}_1)},$$

and

$$\mathcal{F}_N(z) = \mathcal{F}_1 + \frac{1}{b} \cdot \log_{10} \left\{ \frac{R_0^3 \cdot y \cdot \eta_0 \cdot \gamma(z)}{N} \right\} \qquad (15)$$

$$= \text{const.} + \frac{1}{b} \log_{10} \gamma(z)$$

Some idea of the importance of the volume effect for the optical redshift-magnitude diagram for quasars may be gained from Fig. 2a which shows $F_1(z)$ for two simple luminosity functions of type (a) and (b), in the de Sitter model. The parameters chosen are $a = 0.8$, $b = 1.5$, $4\pi \eta_0 . y = 10^{-3}$ per $\left(\frac{c}{H_0} \right)^3$.

We are not claiming that the optical luminosity function for quasars is actually of either of these forms, but merely demonstrating how severe the effect of a large dispersion in luminosity can be. Clearly a large part of the divergence of the data from the normal de Sitter m-z curve could be due to this effect, so that analysis of the kind performed by Solheim (29) is unlikely to give accurate results for quasars. However, if from counts and from identifications we can obtain information about η_0 and the form of $\varphi(\mathcal{F})$, then it is in principle possible to test cosmological models by comparing equation (12) with observed locus of the Nth most luminous source out to redshift z, for different values of

N. Fig. 2b shows $\mathcal{F}_N$ against $\log_{10} \gamma$ for the steady-state model, with $N = 2, 4, 8$, where $\mathcal{F}$ denotes the luminosity at 178 MHz. Under hypothesis (b) above, the 3 loci would be parallel straight lines, equally spaced. The best set of this form satisfies

$$\mathcal{F}_N = -21.91 + 1.70 \log_{10} \gamma - 0.87 \log_{10} N .$$

Comparing this with equation (15), the inequality of the coefficients of $\log \gamma$ and $- \log N$ shows that the quasars cannot be uniformly distributed in space in the steady-state model. Either the number-density of sources changes with epoch such that

$$N(z) \propto \gamma(z)^{1.70/0.87} \simeq \gamma^2(z) , \quad \text{where} \quad N(z) = \int_{\infty}^{-\infty} N(\mathcal{F};z)\, d\mathcal{F},$$

or the typical luminosity of a source change with epoch, such that

$$P \propto \gamma^{1.70 - 0.87} \propto \gamma^{0.83} .$$

However, hypothesis (b) is not too good a fit of the data, and in general it is very unsatisfactory to have a test which depends on knowing the form of the luminosity function. Also the selection effect imposed by the fact that quasars are identified at optical frequencies

(optically weak emitters will only be seen at small redshifts) is not allowed for. The test we shall describe in section 4 takes full account of the volume effect, but does not require knowledge of η_0 or $\phi(\mathcal{F})$.

McVittie and Stabell (35) have also considered plots of the optical luminosity of quasars against redshift in several models and argue that although evolution would be necessary in models with $q_0 = \sigma_0 = 0$ and $q_0 = \sigma_0 = 1$, this is not the case for the model $q_0 = 1$, $\sigma_0 = 3$, for example. In section 5 we show that <u>none</u> of the relativistic models are consistent with the present data for quasars, without some kind of evolutionary factors.

McVittie and Stabell (35), and Kafka (14) have allowed for the volume effect in a rather different manner from that described above. Confining their attention to a fixed range of optical luminosity they compare the number of sources out to redshift z with $\phi(z)$. This is equivalent to the "luminosity-volume" test we describe in the next section, but is limited in two ways. Firstly it does not take account of the serious selection effect imposed by the 3C limiting flux-level.* And secondly it uses the available information in such an inefficient way that, as Kafka admits, no conclusions of real statistical significance can be drawn with the present data.

Rees and Sciama (36) showed that in different ranges of radio luminosity in the steady-state model there was an excess of quasars at large redshift. The inconsistency is even more striking when correction is made for the effect of optical selection, and when the optical luminosities are also considered.

---

* In more recent work Kafka (54) now takes account of the effect but still does not combine the information in an efficient enough way to obtain significant results.

4. Luminosity-volume test

The central suggestion of this chapter is that for quasars the magnitude-redshift test be replaced by the "luminosity-volume" test. Suppose that (i) the number of quasars per unit proper volume, $\zeta(t)$, is proportional to the smoothed-out cosmical density at that epoch; (ii) the distribution of luminosities of quasars (i.e. the form of $\varphi(\mathcal{F})$) is the same at all epochs.

Then the total number of sources out to the epoch corresponding to redshift z is

$$N(z) = \int_{-\infty}^{+\infty} N(\mathcal{F}, z)\, d\mathcal{F} = \eta_0 R_0^3 . \gamma(z) \qquad (16)$$

$\gamma(z)$ is the comoving coordinate volume of the sphere bounded by sources whose light is redshifted by z.

Then in any particular model that we wish to test we consider the distribution of luminosity $\mathcal{F}$ (see equation 3) with respect to volume γ: that is, we transform the magnitude-redshift diagram to a luminosity-volume diagram. If assumptions (i) and (ii) hold, we should expect to find, in any given range of luminosity, equal numbers of sources in any two equal volumes of comoving coordinate space. However, as a result of the limitations of our telescopes, not all quasars

are visible. Confining our attention to 3C quasars, only those brighter than the limiting flux-level are visible. An optical identification can then only be made if the quasar is brighter than the limiting optical magnitude. Moreover, the degree of completeness of the identifications may be different in different ranges of magnitude, an effect which could be reinforced by non-random selection of objects for redshift measurements. However, although such effects may well be present, it is not necessary that the set of quasars with known redshift at our disposal be complete, but only that it be representative down to the limiting flux-levels. Throughout this work we assume that the set of 37 quasars listed in Table I is representative down to the 3C limiting flux-level of 9 flux-units, and down to the 18th visual magnitude.

Penston and Rowan-Robinson (3) have suggested that the 3C quasars with visual magnitudes fainter than 18 are not distributed isotropically on the sky. Preferring to suppose that this is some effect of observational selection that the universe is inhomogeneous on the large scale (39), we shall make a correction for this effect at a later stage. For the moment we treat our set of quasars as it it were representative down to the 19th magnitude, which, since there are only two quasars with $V > 19$ in our set, we shall regard as the limiting magnitude for quasars.

Fig. 3 shows optical and radio luminosity-volume diagrams for a particular cosmological model (the Einstein de Sitter model). The cutoffs imposed by the limiting flux-levels are calculated by eliminating z between

$$\hat{\mathcal{F}} = \hat{f} + \log_{10} \frac{R_0^2 r_0^2 (1+z)^2}{(1 + k r^2/4)^2} - 0.4\, K(z) \qquad (17)$$

and $\hat{\mathcal{V}} = \mathcal{V}(z)$ (18)

where $\hat{f}$ is the limiting flux level and K the appropriate K-correction (see Appendix I : the radio cutoff is shown for sources with spectral index $\alpha = 0.8$).

Clearly, a source with luminosity $\mathcal{F}$ and redshift z will only be observable if $\mathcal{V}(z) \leq \hat{\mathcal{V}}(\mathcal{F})$. A difficulty here is that in the radio case, $\hat{\mathcal{V}}(\mathcal{F})$ is different for sources with different spectral indices. This has been taken into account but the error introduced by taking the radio cutoff to be that appropriate to sources with the mean spectral index (about 0.8) is not very great.

The vertical lines to the right of the two diagrams correspond to a redshift of 2.2 , beyond which no quasar has yet been observed. Thus in the radio diagram the line $A_1A_2A_3$ bounds the observable region of the luminosity-volume plane. If we define the line $B_1B_2B_3$ by the relations

$$\Upsilon = \Upsilon(2.2)/2 \qquad \text{for} \qquad \mathcal{F} \geq \hat{\mathcal{F}}(2.2)$$

and

$$\Upsilon = \hat{\Upsilon}(\mathcal{F})/2 \qquad \text{for} \qquad \mathcal{F} < \hat{\mathcal{F}}(2.2) ,$$

then $B_1B_2B_3$ divides $A_1A_2A_3$ into two regions in which, under assumptions (i) and (ii), we should expect to find equal numbers of sources.

Before we compare the numbers of quasars actually found in such equivalent regions, we have to allow for the fact that the set of quasars in $A_1A_2A_3$ is affected by optical selection. Sources which are intrinsically faint optically can only be found at small redshifts on account of the optical cutoff. Similarly the optical diagram is affected by radio selection, since sources intrinsically faint radio-wise can only be found at small redshifts on account of the radio cutoff.

For a set of sources free from optical selection out to redshift z_1 we should confine our attention to sources with

$$\mathcal{F}_{opt} \geq \hat{\mathcal{F}}_{opt}(z_1). \tag{19}$$

However, if we choose $z < z_1$ such that $\Upsilon(z) \geq \frac{1}{2}\,\Upsilon(z_1)$, then by relaxing condition (19) to

$$\mathcal{F}_{opt} \geq \hat{\mathcal{F}}_{opt}(z),$$

sources will be missed only from the further half of the observable region of space. Since it transpires that there are significantly more quasars in this further half for all the relativistic cosmologies, our conclusions (that the numbers in the two equivalent volumes of observable space are unequal) are merely reinforced. In Fig. 3b we show $\mathcal{F}_{opt} = \hat{\mathcal{F}}_{opt}(1.4)$, for example (the broken line). Optical selection operates against sources falling in the shaded region in Fig. 3b, since they would have $V > 19$. It seems unlikely that many sources are "missing" anyway.

Similarly, for a set of quasars free from radio selection out to z_2 we should confine our attention to sources with $\mathcal{F}_{rad} \geq \hat{\mathcal{F}}_{rad}(z_2)$. In view of the probable incompleteness of the identifications for $18 < V \leq 19$, we shall apply the optical luminosity-volume test to sources with $V \leq 18$ only.*

---

* It may seem logically unsatisfactory to take the optical limiting magnitude as 19 when correcting the radio-data for optical selection, and as 18 when performing the optical luminosity-volume test. However, in the latter case it is necessary only that we choose some magnitude brighter than or equal to the actual limiting magnitude, so our procedure is certainly consistent if the data is representative in the range $18 < V \leq 19$ (though wasteful of information). On the other hand if our set of quasars is incomplete in the range $18 < V \leq 19$, then the effect is much severer for the optical luminosity-volume test than for the correction of the radio-data for optical selection, since many of the "missing" sources would be excluded anyway from the radio test by the condition $\mathcal{F}_{opt} \geq \mathcal{F}_{opt}(1.4)$.

Since only 2 out of our 37 sources have $V \leq 18$ and $z > 1.15$, presumably due to radio selection, we take $z_2 = 1.15$. The line $C_1C_2C_3$ now bounds the region of interest in Fig. 3b. A set of quasars mainly free from radio selection out to redshift 1.15 can be obtained by demanding $\mathcal{F}_{rad} \geq \hat{\mathcal{F}}_{rad}(0.8)$: a few sources in the shaded region of Fig. 3a would be missed, and these would fall entirely in the further of the 2 equivalent regions. The point of this procedure is that we more than double the fraction of the available data brought into play.

Finally, the line $D_1D_2D_3$ in Fig. 3b is defined by

$$\gamma = \hat{\gamma}(\mathcal{F})/2 \quad \text{for} \quad \mathcal{F} < \hat{\mathcal{F}}_{opt}(1.15)$$

and

$$\gamma = \gamma(1.15)/2 \quad \text{for} \quad \mathcal{F} \geq \hat{\mathcal{F}}_{opt}(1.15)$$

Then if n_A, n_B, n_C, n_D are the numbers of quasars found the regions A,B of Fig. 3a and C,D of Fig. 3b, respectively, we expect $n_A = n_B$, $n_C = n_D$, if hypotheses (i) and (ii) are satisfied. To test whether the numbers obtained are consistent with these expectations,

we compare the quantity:

$$\frac{(n_A - n_B)^2}{(n_A + n_B)} + \frac{(n_C - n_D)^2}{(n_C + n_D)}$$

with the χ^2 variable with 2 degrees of freedom. A probability can then be assigned, from this combined radio and optical luminosity-volume test, to the chosen cosmological model under assumptions (i) and (ii).

5. Relativistic cosmological models without evolutionary effects.

The procedure described above has been applied, with the aid of a computer, to a grid of cosmological models in the range: $-1 \leq q_0 \leq 3$, $0 \leq z_0 \leq 3$, which includes most of the region of interest in the $z_0 - q_0$ plane.

Recently Lemaître's models have been readvocated (40, 88, 89): these lie to the right of but close to curve A in Fig. 1, and have the possibility of an antipole. Whereas $\hat{F}(z)$ is monotonic increasing for most models, in certain models it can reach a maximum and then start to decrease, eventually tending to zero at the

antipole.

We may write equation (2) as

$$\frac{r_0}{1 + \frac{1}{4} r_0^2} = \sin \chi$$

in the case $k = +1$, where $\chi = \int_{t_e}^{t_0} \frac{cdt}{R}$,

so the antipole is the point where $\chi = \pi$.

The application of the luminosity-volume test to the Lemaître models has been discussed in Paper III attached to this thesis. Although these models have dramatically different properties to those specified by the inequalities given above, it may well be that the latter include all the serious possibilities. In particular we note Sandage's (86) recent reiteration of Humason, Mayall and Sandage's (31) conclusion that the evidence from the brightest galaxies in clusters favours a positive value of q_0. Against this must be set the fact that the cluster data is very unrepresentative with respect to volume of space. This is illustrated by Fig. 3c, which shows the distribution of optical luminosity against volume of space for the data of Humason Mayall and Sondage, in the de Sitter model ($\Omega_0 = 0$, $q_0 = -1$).

In asserting that this model is inconsistent with the data, great weight is being attached to the 3 remotest clusters.

Actually we have tested models with $\sigma_0 > 3$ and $q_0 > 3$, but these give no new results and anyway imply unreasonable values for the average density of the universe ($\rho_0 > 6 \times 10^{-29}$ gm cm^{-3}) and the total age of the universe ($t_0 < 7.5 \times 10^9$ years), respectively. The formulae used are summarized in Appendix 2. No model gives a probability above a few percent, so we may conclude with some confidence that none of these models are consistent with the present data for quasars. In fact outside a narrow strip $-1 \leq q_0 \leq -0.5$, $0 \leq \sigma_0 \leq 0.1$, no model give a probability greater than 0.1 per cent. Here we are at odds with McVittie and Stabell (35), who consider that the model with $q_0 = 0$, $\sigma_0 = 3$ is acceptable. Our procedure assigns a probability of less than 0.01 percent to this model. Evolutionary factors must be affecting the distribution of quasars if <u>any</u> of the relativistic models are to apply.

Similarly if the optical luminosity-volume alone is applied (suitably corrected for the effects of radio-selection) no consistant model can be found. Although the probabilities are rather higher from this weaker test, all the models are ruled out at the 90 percent level of

significance. The least inconsistent models are those near to the de Sitter model ($\sigma_0 = 0$, $q_0 = -1$). These results should be compared with those of Solheim from applying the magnitude-redshift test to the cluster data of Baum (32) and Humason, Mayall and Sandage (31). His outermost contour includes an area of the $\sigma_0 - q_0$ plane very much larger than the whole of that which we have considered, yet corresponds to a probability of nearly 40 per cent. Such a comparison demonstrates the great power of the luminosity-volume test, given a set of objects like the quasars to which it can be applied.

It is tempting at this point to conclude that the evolutionary factors required to give consistency with these cosmological models cannot be such as to affect the radio-emission only: this was stated in Paper I. However, if the radio-luminosity of sources was greater in the past, then the procedure described in the previous section does not correctly eliminate the effect of radio selection from the optical luminosity-volume test. In fact, by introducing a sufficiently strong evolutionary effect of this kind, the apparent non-uniformity in the distribution of optical luminosities can be made to disappear in most cosmological models. This is discussed in Appendix 3, where an alternative and independently derived form of the luminosity-volume test

due to Schmidt (90) is also discussed.

The best way to rule out the possibility of radio luminosity evolution only, is to examine the distribution in space of a set of quasars identified entirely at optical frequencies. Braccesi's report (87) of a source-count slope of -1.8 for quasars at infrared frequencies suggests that if the number-density of quasars at any epoch is proportional to the smoothed out cosmological density at that epoch, then the typical optical luminosity must also have been greater in the past, for the relativistic models to apply. Presumably the optical and radio emissions would then have to arise from a common mechanism. The evidence for a relationship between optical and radio luminosity is discussed in section 7.

An alternative, and perhaps simpler, explanation is that the fraction of material in the form of quasars is a decreasing function of the cosmical time. In either case; since optical counts by Sandage (41) down to 18.5 magnitudes ofthe Haro-Luyten catalogues of blue objects give a slope rather less steep than -1.0 ($d \log N / d\, m_{pg} = 0.38$), we may deduce that these quasars do not make a dominant contribution to those catalogues at 18.5 m. But a substantial contribution is, of course, not ruled out by this argument. Or putting the argument another way, if the quasars do make a dominant contribution to the Haro-Luyten

catalogues at faint magnitudes, then we have to rule out either the cosmological interpretation of the redshifts of quasars, or the relativistic cosmologies.

Before attempting to set some limits on the evolutionary parameters required to obtain consistency with relativistic models, we discuss some of the physical factors which might give rise to evolutionary effects. Some unrealistic assumptions made for reasons of mathematical simplicity may well vitiate some of the conclusions of earlier investigations.

6. Possible evolutionary factors affecting the distribution of quasars

Since only a small fraction of the available material at any epoch appears to be in the form of active quasars, it is quite uncertain that this fraction should be the same at different epochs. However, we may distinguish two situations of particular interest:-

(a) Quasars are violent outbursts in pre-existing agglomerations of matter. Such a view links them with the strong radio-galaxies, which they resemble in total radio power, in radio spectra, and in certain cases, in radio structure (e.g. 3C47). It is then reasonable to suppose that the fraction of matter in the form of active quasars at any (recent) epoch is independent of epoch. But this is certainly not necessary, for evolution

in number-density $r(t)$ may arise if the probability that an object has an outburst between epoch t and $t + dt$, $p(t)\,dt$, is a function of epoch, or if the typical lifetime of a source is a function of epoch.

Luminosity evolution may also occur, that is, the typical luminosity of a source may be a function of epoch.

The objects undergoing the outbursts must then have some knowledge of the cosmical epoch. Either they were all born simultaneously and are aware of their age (through some internal evolution), or the outbursts (and/or the associated radiation) are the results of interaction with uncondensed material whose properties change with epoch. Theories of the latter kind might be suitable for radio-galaxies, if it transpire that they too must evolve, since their radio-emission is often centered far from the optical galaxy. But they do not seem very likely for the very compact quasars, particularly as it is probable that the typical optical luminosity is required to be greater in the past if there is no evolution in number-density.

We shall investigate two simple mathematical forms of luminosity evolution:

a) $\bar{F}(t) \propto R(t)^{-Q_L}$, which we can write $\bar{F}(z) \propto (1 + z)^{Q_L}$

b) $\bar{F}(t) \propto \exp(-\text{const}\, R(t))$, which we can write

$$\bar{F}(z) \propto \exp\left\{ (1 + z_L) \cdot \left(1 - \frac{1}{1+z}\right) \right\}$$

For the cosmological models considered by Davidson and Davies (20, 21) in which $R(t)$ has a power law dependence on the cosmical time t, our form of evolution (a) is equivalent to that considered by Davidson and Davies namely a power law dependence of luminosity on cosmical time. Of the relativistic cosmological models, only the Einstein de Sitter model, with $R(t) \propto t^{2/3}$, is of the form considered by Davidson and Davies, so that only their results for this model can be compared with this work.

The disadvantage of evolutions of the form (a) is that they must be truncated at some finite value of z, z^* say, in order that a finite background radiation be obtained. Davidson and Davies (20) choose for z^* the point at which $\frac{d}{dz}\left\{ \hat{\mathcal{F}}(z) - Q_L \cdot \log_{10}(1+z) \right\} = 0$, which seems a completely arbitrary assumption and may strongly influence his conclusions. Longair (18) takes z^* as a parameter to be fitted to the observations, and requires a value for z^* of about 3 to obtain consistency with the source-counts and the integrated background in the Einstein de Sitter model.

But unless there are strong physical grounds for considering evolutions of the form (a), it seems rather premature to conclude that there is a real dearth of sources beyond $z = 3 - 4$ (18). An example of a form of evolution that does not require such a truncation is provided by from (b), where the typical luminosity at any epoch declines exponentially with epoch. We investigate this form in order to demonstrate that definitive conclusions can not be obtained by confining attention to from (a) only, rather than for any special merit in an exponential evolution. The actual form of evolution cannot really be determined until the structure of the sources has been settled. But as in illustration of the way different models for the emission might give rise to different evolutionary parameters, we note that:

$Q_L = 3$ corresponds to $\bar{F}(t) \propto \ldots(t)$, which could arise if the emission were the result of the interaction of high-velocity shocks or ejected material with intergalactic material:

$Q_L = 3.5$ corresponds to $\bar{F}(t) \propto H(t)^{(1+y)/2}$, $H(t) \propto R(t)^{-2}$, $y = 2.5$, which could arise if the emission were the synchroton radiation of electrons with a power-law energy spectrum of index 2.5, in a universal magnetic field: as the universe expands the magnetic pressure is supposed to expand adiabatically ($H^2 R^4 = \text{constant}$).

(b) Quasars correspond to the formation of galaxies

If galaxies burn up some 20 percent of their Hydrogen during the final stages of their formation, perhaps inside massive objects, then objects emitting energy at about the rate found in quasars would be expected (43). If this stage is short compared with cosmological time-scales, then the number-density of quasars would be proportional to the rate of galaxy formation. In this case it would be extremely unreasonable to suppose that the number-density of quasars is independent of epoch. For comparison, the rate of star-formation is often taken to have a power-law dependence on the gas density. Or perhaps an exponential dependence would be more appropriate. We have tested both of the forms:

c) $r_i(t) \propto (1 + z)^{Q_D}$

d) $r_i(t) \propto \exp\{(1 + z_D).(1 - 1/(1 + z))\}$ where Q_D, z_D are parameters.

Evolution (c) has to be truncated at some z^*, but not form (d).

7. Modified luminosity-volume test.

In order to test cosmological models when evolutionary effects of the kind discussed in the preceding section are present,

we modify the luminosity-volume diagrams in a simple way, described in (24). We consider the distribution of "corrected" luminosity, $\mathcal{F}'$, with respect to "weighted" volume, $\mathcal{V}'$. Assuming that the increase of luminosity with redshift is the same for all classes of quasars, we divide out this increase and compare the distribution of the luminosities as they would be at the present epoch in different ranges of volume, weighted by the postulated increase in number-density with redshift. Thus for the four types of evolution suggested in the previous section:

(a) $$\mathcal{F}' = \mathcal{F} - Q_L . \log_{10} (1 + z)$$

(b) $$\mathcal{F}' = \mathcal{F} - (1 + z_L).(1 - \frac{1}{1 + z}) . \log_{10} e$$

(c) $$\mathcal{V}' = \int_0^{r_0} \frac{4\pi r^2 . (1 + z)^{Q_L} . dr}{(1 + k r^2/4)^3}$$

(d) $$\mathcal{V}' = \int_0^{r_0} \frac{4\pi r^2 . \exp(1 + z_D) . (1 - \frac{1}{1 + z}) . dr}{(1 + k r^2/4)^3}$$

Now it is an assumption underlying our analysis that the radio and optical luminosities are independent. Since we are requiring radio

and optical luminosities to be influenced by the same evolutionary factors in cases (a) and (b), we need to consider whether there is a detailed correlation between radio and optical luminosities. Such a correlation might appear if the optical and radio emissions were produced by the same mechanism, and would invalidate results obtained by the modified luminosity-volume test. In Fig. 5 we have plotted the optical against radio luminosity for quasars with $z \leq 0.6$. Quasars with large redshift can only be observed if they are intrinsically powerful both optically and radio-wise: thus a spurious correlation between optical and radio luminosity is introduced if all quasars are plotted in this diagram. Moreover for quasars with large redshifts the effects of cosmological model and evolutionary hypothesis are very large. Fig. 5 shows luminosities as calculated in the Milne model, but the results are not very different for other models.

Fig. 5 shows clearly that there is no detailed correlation between optical and radio luminosities, so that the procedure described in section 4 will be valid.

8. An upper limit to the rate of luminosity evolution

Before we proceed to test evolutions of the form (a) - (d), it is

advisable to consider whether arbitrarily large values of the parameters Q_L and z_L are acceptable. The effect of correcting the luminosities of all the sources is to reduce the value of $\hat{f}(z)$ for any given value of z, by an amount which increases with z. In fact there is a value of z for which $\hat{f}(z)$ reaches a maximum, decreasing for larger values of z. The consequences of this redshift falling within the range of redshift covered by our set of quasars can be seen from Figs. 6a, b, which show the optical and radio luminosity-volume diagrams for the Einstein de Sitter model, corrected for luminosity evolution of form (a) with $Q_L = 3.07$. In this case $\hat{f}(z)$ has a maximum at redshift 2.2, and if this form of evolution is correct then we should expect large numbers of quasars with redshifts greater than 2.2 and fluxes above the 30 limiting flux-level. Now although a sharp decline in the optical continuum emission beyond Lyman α (44) could explain the absence of such objects amongst those 3C sources identified with blue quasi-stellar objects, they should be visible as red stellar objects. Fig. 6b shows the effect of such a sharp cutoff (arbitrarily taken as $F(\nu) \propto \nu^{-5}$) on the distribution of visual luminosities. Clearly very many objects should be found in 3C with redshifts between 2.2 and 3.5 (note that the scale has

been compressed beyond $\nu = 0.25$). Beyond $z = 3.5$, the radio-sources would correspond to empty fields down to 19 magnitudes. Now although there are one or two tentative identifications of 3C sources with red stellar objects (45), and about 30 sources associated with empty fields (46), many of the latter are likely to be distant radio-galaxies. Thus the identifications of 3C do not permit large numbers of quasars beyond redshift 2.2, and evolutions so extreme as to produce the situation illustrated in Fig. 6 can be ruled out. We are loath to introduce some ad hoc cutoff in the distrubtion of quasars beyond $z = 2.2$ until the less extreme models, where the radio cutoff provides a fairly natural explanation of the absence of 3C quasars beyond $z = 2.2$, have been eliminated.

Thus in any model we restrict our attention to values of Q_L for which the maximum in $\hat{f}(z)$ occurs at $z > 2.2$. This limitation is indicated by a dash-dotted line in Figs. 4, 7 - 10.

Models which require Q_L less than but close to this limiting value are clearly unsatisfactory, by the same argument. For this reason the models in the top right-hand corners of Figs. 4a and b are probably ruled out, even though they give consistency with the modified luminosity-volume test.

Finally, we may remark that it is a peculiarity of all models

with luminosity evolution that the corrected luminosity of 3C 273 the quasar with the smallest redshift in our set, is the largest of all: this peculiarity also applies to some cosmological models even without luminosity evolution (34).

9. Correction for the incompleteness of the data for $V > 18$

We cannot hope to obtain accurate values for the evolutionary parameters if the selection effect postulated by Penston and Rowan-Robinson (3) is present. Without some such effect we have to admit that the quasars with large redshift are distributed anisotropically, so that analysis of the present kind is invalid. Since the quasars with $V > 18$ cover about half as much of the sky as those with $V \leq 18$, the simplest correction is to include each of the sources with $V > 18$ twice. Such a correction influences the radio luminosity-volume test only: the general effect is to increase the values of the evolutionary parameters slightly, though the results are not changed much qualitatively.*

---

* See Appendix 3 for results using more recent data.

10. Evolutionary parameters in the relativistic models.

Some of our results are summarized in Figs. 4, 7 - 10. The models we have tested are as follows:

i) a grid of models in the range: $-1 \leq q_0 \leq 3$, $0 \leq \ldots_0 \leq 3$; luminosity evolution (a) with $Q_L = 2.5$, 3 (Figs. 4a and b)

ii) models with $\ldots = 0$, $k = 0$, and $\ldots_0 = 0$ respectively: luminosity evolution (a) for a range of Q_L (Figs. 7a, b, and c).

iii) models with $\ldots = 0$ and $\ldots_0 = 0$; luminosity evolution (b) , and density evolutions (c) and (d) for ranges of the respective parameters z_L , Q_D , z_D (Fig. 8a , b ; 9a and b).

iv) de Sitter, Milne and Einstein de Sitter models: combined evolutions of type (a) and (c) (Figs. 10a,b, and c).

In each figure we show interpolated contours of 10 and 20 percent probabilities that the present available data is consistent with the given model. Models giving probabilities below 10 percent can probably be ruled out, even when the limitations of the present work are borne in mind. We regard models giving probabilities higher than 20 per cent as acceptable, though many of these will

almost certainly be ruled out when more complete data down to a lower flux-level is available. We discuss each of the four evolutionary hypotheses described in section 6, in turn:

(a) power-law luminosity evolution, which has been favoured by a number of authors, is the most vulnerable of the four hypotheses to this kind of analysis. There are few models in which this kind of evolution gives consistency with the data. Fig. 7a shows that of the models with zero cosmological constant, the only satisfactory models are those with q_0 close to zero. The best values for q_0 are in the range 0.005 to 0.03, corresponding to a smoothed out density at the present epoch of 10^{-31} to 6.10^{-31} gm per cc. The close agreement with values obtained from counting up the actual galaxies observed (30) should be regarded as coincidental until there are some strong grounds for believing that evolution of this kind is affecting the distribution of luminosities of quasars.

When a non-zero cosmological constant is included, the most satisfactory models are those with q_0 close to zero (Figs. 4a and b); 7b). Of the completely empty models by far the most satisfactory is the de Sitter model, and those with $q_0 > 1$ are ruled out. Thus exactly those models which might have been expected from consideration

of the actual density of material observed to date, and from the problem of the long ages of the oldest stars, are preferred on this evolutionary hypothesis.

(b) Exponential luminosity evolution gives consistency with the data at the 10 percent level for all the cosmological models tested to date (Figs. 8a and b). In view of the advantage of this form of evolution already discussed, namely that no arbitrary truncation of the distribution is required, this result provides considerable incentive for further investigation of evolutions of this type. At the 20 percent level models with $\Lambda = 0$, $q_0 > 1$, are ruled out, but all the empty models are acceptable. For interest we show the 30 percent contours also in Figs. 8a and b: these look very like the 20 percent contours in Figs. 7a and b, suggesting that when more data is available, similiar conclusions will be reached as for case (a). The best values for the parameter z_L are in the range 5 to 6: the significance of z_L is that between the epochs corresponding to $z = \infty$ and $z = z_L$ the typical luminosity of quasars has been reduced by a factor $1/e$. At the present epoch the typical luminosity is between 10^{-3} and $10^{-2.5}$ of the value at epoch $t = 0$.

(c) This analysis is extremely insensitive to power-law density evolution, in the sense that for all models quite a wide range of the parameter Q_D is consistent with the data (Figs. 9a and b). Thus the earlier conclusion of the present author (24), that density evolution was at least as consistent with the data as luminosity evolution, can now be strengthened to the statement:

density evolution gives much better consistency with the data than luminosity evolution.

We may note that of the models with zero cosmological constant, the empty models require the least severe evolution: and that of the empty models (including those with non-zero cosmological constant) the de Sitter requires by far the least severe evolution.

(d) Similarly insensitive results are obtained for exponential density evolution, with the best values of z_D being in the range 7 - 13. Here the significance of the parameters z_D is that between the epochs corresponding to $z = \infty$ and $z = z_D$ the fraction of material in the form of active quasars has decreased by a factor $1/e$. At the present epoch that fraction is only between 10^{-3} and 10^{-5} of the value at $t = 0$. If we consider quasars to be the birth-pangs

of galaxies, then we may conclude that most of the galaxies had formed by the epoch corresponding to redshift 10 ± 3.

The comparison of the Milne, de Sitter and Einstein de Sitter models is very interesting (Figs. 10a, b and c). Density evolution alone is consistent with the data for all three models, as also are intermediate cases with combined luminosity and density evolution. Luminosity evolution alone is consistent with the de Sitter model for $2 \leq Q_L \leq 3.5$. For the Milne model a rather small range about $Q_L = 2.5$ is consistent : with more data a more detailed analysis may enable this possibility to be completely ruled out. With the Einstein de Sitter model only values of Q_L which give rise to the difficulty discussed in section 8 are consistent.

11 Comparison with earlier work

(i) Longair (18) has interpreted the Cambridge radio source-counts in terms of power-law luminosity and density evolutions of the most luminous sources, in the Einstein de Sitter model. The best parameters he obtained ($Q_L = 3.3$, $Q_D = 5.7$) agree well with those obtained in this analysis of the available data for quasars. However, as

we have remarked in the previous section, luminosity evolution with Q_L of order 3 or more in the Einstein de Sitter model would require the existence of a large number of sources in 3C to be identified with quasi-stellar objects with redshifts greater than 2.2. This difficulty could only be overcome by supposing that there is a real truncation of the quasars at redshift 2.2 : this value is significantly lower than the value required by Longair in his analysis ($z^* = 3$). This difficulty is less severe in the Milne and de Sitter models.

(ii) Davidson and Davies (21) have argued that the hypothesis of galactic collisions can be ruled out (without additional luminosity evolution) on the grounds of the source-counts, for models with $R(t) \propto t^{-n}$. While we do not necessarily wish to advocate this hypothesis, we note that this case, which corresponds to power-law density evolution with $Q_D = 3$, is not ruled out for the quasars in the de Sitter model. Of course the de Sitter model is not of the form considered by Davidson and Davies, but this demonstrates that the range of models considered by them does not necessarily include the full range of properties shown by the relativistic models.

(iii) Although the density-evolution hypothesis does not allow us to specify the cosmological model, we may compare the results obtained for the luminosity-evolution hypothesis (a) with those obtained using the brightest galaxies in clusters (29, 31 - 33). If the cosmological constant is set equal to zero, and allowance is made for the evolution of the stars in galaxies, both analyses agree in demanding a value for q_0 close to zero. When models with non-zero cosmological constant are considered our analysis gives the de Sitter as the most favourable model. For consistency of this model with the cluster data rather steeper optical luminosity-evolution would be required than has been considered to date (33).

12. Other cosmological models.

(i) The Steady-State model

Mathematically, the Steady-State model is equivalent to the de Sitter model with negative power-law density-evolution, with $Q_D = 3$. The combined optical and radio luminosity-volume tests give a probability of only 0.01 percent for this model.

(ii) Brans-Dicke models with $k = 0$.

Brans and Dicke (47) have given the solution of the cosmological equations obtained from their scalar-tensor theory of gravitation

for the case $k = 0$: the models are given by $R(t) \propto t^{(2+2\omega)/(4+3\omega)}$ where ω is a constant of the theory which can range from zero to infinity. As $\omega \rightarrow \infty$ these models tend to the Einstein de Sitter model. We have tested these models for a range of ω : for $\omega \geq 4$ they give results identical to the Einstein de Sitter model (see Fig. 11, $Q_L - \omega$). The value of ω inferred by Dicke from his interpretation of his measurements of the solar oblateness is about 6 (48). Thus there is little prospect of distinguishing between the rival theories of gravitation on the basis of cosmological tests.

13. Conclusions for quasars.

If the redshifts of quasars are cosmological our tentative conclusions are that:

(i) no relativistic model is consistent with the data for quasars without some evolutionary factor that affects both radio and optical distributions.

ii) the luminosity-evolution hypothesis is far more vulnerable to the luminosity-volume test than density-evolution.

(iii) luminosity-evolution with a power-law dependence on the scale-factor requires $q_0 < 0.035$ if $\Lambda = 0$, with the best value being $0.005 \leq q_0 \leq 0.03$, or $10^{-31} \leq \rho_0 \leq 6.10^{-31}$,

in very good agreement with Oort's value (30) for the average smoothed-out density of matter in galaxies. If models with non-zero cosmological constant are also considered, the best models are those near to the de Sitter model in the $\sigma_0 - q_0$ plane, which give very long ages to the universe.

(iv) luminosity-evolution with an exponential dependence on the scale-factor gives better consistency with the data than power-law evolution, but the best models are the same as those given in (iii).

(v) density-evolution gives consistency with all models, though the least severe evolution is required in the de Sitter model. With exponential evolution the epoch at which the number density of quasars is $1/e$ times that at $t = 0$ is given by $z = 10 \pm 3$.

Some of these conclusions may be modified when all quasars in 3C have their redshifts measured, but it seems exceedingly unlikely that (i) and (ii) can be altered. These alone are sufficient to demonstrate the great power of the luminosity-volume test. While some of the features of this test have occurred independently to a number of authors (14, 35, 36), the two factors that enable significant conclusions to be reached are allowance for selection effects imposed by the limiting flux-levels and the combination of the available information into a single probability.

14. Application to radio-galaxies

The optical luminosities of radio-galaxies show small dispersion (41), so the effect of the limiting visual magnitude of 20 is simply to confine our identifications to redshifts smaller than 0.4 - 0.5. Moreover we can obtain from the observed visual magnitude of a galaxy a rough estimate of its redshift, in those cases where the redshift has not yet been determined. At present redshifts are available in the literature (55 - 59) for 59 of the 147 galaxies identified with radio-sources in the Revised 3C catalogue (38) corresponding to 80 percent of those identified to date with $V \leq 15$ magnitude, but only 20 percent of those identified with $15 < V \leq 20$. Fig. 12 shows the distribution of redshift of these galaxies against visual magnitude, as estimated by Wyndham (60) : six galaxies with redshifts less than 0.01 (3C 71, 231, 270, 272, 1,274, 386) are omitted. In what follows we shall confine our attention to "strong" radio galaxies, i.e. those with luminosity greater than 10^{23} w/ster/(c/s), so that of these 6 nearby radio galaxies, only 3C 274 will concern us.

Sources of the same luminosity and spectral shape would satisfy a relation of the form

$$V = A + 5.\log_{10} z + K(z) + 5.\log_{10} \{ D(z)/z \} \qquad (20)$$

where z is the redshift

$K(z)$ is the "K-correction" (31),

and $D(z)$ is the "luminosity distance" (26).

For small z equation (20) can be approximated by

$$V = A + 5 \log_{10} z + B z \qquad (21)$$

where A and B are constants.

Loci of this form with $A = 20.5$, $B = 4, 5, 6$, are shown in Fig. 12: that with $B = 5$ is the best line of form (21) through the data.

The scatter of the points in Fig. 12 is primarily due to the approximate nature of the magnitude estimates, which are probably not more accurate than $\pm$ 1m. Other factors are the dispersion in intrinsic

luminosity of the galaxies, the effect of galactic obscuration, and differences in spectral shape for different types of galaxy. Corrections could be applied for the latter two effects, but the approximate nature of the data hardly makes this worthwhile at the present. We shall see that errors of up to a magnitude do not alter our basic conclusions.

Naturally we shall not attempt to determine cosmological parameters from equation (21), since there is the possibility of systematic error in the magnitude estimates, quite apart from the random errors mentioned above. In what follows we assume only that equation (21), with $A = 20.5$ and $B = 5$, is valid to within a magnitude for the uncorrected visual magnitudes of radio-galaxies. For the 88 galaxies identified with 3CR radio-sources for which no redshifts are available, we estimate the redshift from equation (21) with $A = 20.5$, $B = 5$. For a total of 142 strong radio-galaxies we then investigate the distrubution of intrinsic radio luminosity against volume, in various cosmological models: we wish to test whether, in any given range of radio luminosity, equal numbers of sources are found in equivalent volumes of space. The total volume of space in which sources of a given luminosity are visible is limited by (i) the limiting radio flux-level of the 3CR catalogue, (ii) for sources of sufficiently high radio luminosity, a more severe limitation arises from the limiting

optical magnitude of about 20 magnitudes, which we assume to be equivalent to the restriction $z \leq 0.4$. For each range of radio-luminosity considered, the observable volume of space is divided into two. The numbers found are tabulated in Table 2. The columns labelled (a) refer to the nearer half of the observable volume, and (b) the farther.

Because the properties of the relativistic cosmological models do not differ much out to the redshifts at which these galaxies are found, it is unlikely that the results will depend very sensitively on the cosmological parameters; (the situation is quite different for the quasars, which are visible out to much larger redshifts). The models we have investigated in detail are the Einstein de Sitter ($\sigma_0 = q_0 = 1/2$), Milne ($\sigma_0 = q_0 = 0$) and de Sitter ($\sigma_0 = 0$, $q_0 = -1$) models. These are the fixed points in the $\sigma - q$ plane (54), and correspond to asymptotic states of homogeneous, isotropic, pressure-free universes. (In paper III the Lemaître models ($q_0 < -1$) have been investigated in the same way. Fig. 7 of paper III shows the radio luminosity-volume diagram for a particular Lemaître model). For comparison, the results obtained for the steady-state model are given in column 4. From the last row of Table 2 we see that for all these four

models the total number of strong radio-galaxies found in the farther region (b) is significantly larger than in region (a). The distributions do not differ greatly from model to model.

The incompatibility of the steady-state model (in which evolutionary effects are not permitted) with the radio-galaxy data is perhaps more serious evidence against that model than the distribution of the quasars (39), since doubts have frequently been raised as to the cosmological nature of the large redshifts of quasars. Conversely, a major impetus of these doubts, the prospect of attributing the steep radio-source counts entirely to the quasars (18, 46, 61) would be removed if the present results are confirmed by more accurate data.

To test whether the results could be significantly affected by the uncertainties in the estimated magnitudes, the optical magnitudes of the 88 galaxies for which we have estimated the redshift using equation (2) have been decreased by one magnitude (increasing the magnitudes merely reinforces the inequality between the totals for regions (a) and (b)). The corresponding numbers of sources found in regions (a) and (b) are shown in Table 3 for all luminosities greater than 10^{23}. Since from Table 2 we see that the inequality between the totals in regions (a) and (b) is caused primarily by sources with luminosity greater than $10^{25.4}$, the totals are also shown for this restricted range of luminosity.

The numbers of sources found in regions (a) and (b) are still significantly different, even if the optical magnitudes of all the galaxies are in error by a magnitude in the same direction, particularly for the higher range of luminosity. A more likely situation is that errors of up to 1 magnitude exist, but in either direction, so that the totals found in Table 1 are probably not greatly in error. Rows 5 - 6 of Table 3 show the effect of changing the value of B in equation (2), which again does not alter the basic conclusion. Finally, since it may be argued that in view of the paucity of redshifts for galaxies with $19 \leq V \leq 20$, it is inadmissable to use an extrapolation of the form (2) in this range, row 6 shows the results obtained when attention is confined to galaxies with $V \leq 19$ ($z \leq 0.3$). Incompleteness of the identifications in the fainter ranges of optical magnitude would merely reinforce our conclusions: against this must be offset the greater possibility of incorrect identifications.

These preliminary results provide the strongest impetus for the completion of redshift measurements of radio-galaxies in the 3C catalogue. The evidence seems very strong that for consistency with the usual cosmological models, some evolutionary factor must affect the distribution of the strong radio-galaxies. The effect is clearest for

galaxies with radio-luminosity greater than about $10^{25.4}$, but since such a small volume of space is visible for the lower ranges of luminosity, no clear effect would be expected for these anyway. Of the models proposed by Longair (18) in his attempt to explain the Cambridge radio-source counts, his model (d), density evolution of all sources with radio-luminosity greater than $10^{26.8}$, is definitely unsuitable. But his model (b), luminosity evolution of all sources with luminosity greater than $10^{25.4}$, is entirely in agreement with the present work (though Longair preferred to interpret this evolution as due to the quasars only). But it seems unproved that the evolution does not operate down to luminosities a factor of, say, 10 lower than this. A different way of seeing the existence of this evolutionary effect is to perform radio source-counts on the 3CR radio-galaxies, after those which are intrinsically weak radiowise have been removed. Table 4 lists all 3CR radio galaxies with $\mathcal{F} < 24.9$ in the E, M and S models, and also in the Eddington-Lemaître model with $Z_m = 2.95$ (see Paper II for definition of Z_m). Owing to the differences between the models, the number of such objects depends slightly on model (35 in E and M, 32 in S, 31 in EL). However all such objects have $V \leq 15.5$ and the class of such identifications with 3CR sources

is certainly complete. Moreover practically all have had their redshifts measured (32 out of 35 objects in Table 4), so there is very little uncertainty about the composition of this set of weak radio emitters.

Source-counts, at 178 Mc/s, are shown in Fig. 13 for all 3CR radio-galaxies and for strong radio-galaxies only. The slope of the former locus is -1.6 ± 0.1, in agreement with Veron's (46) value of -1.55. The strong radio-galaxies ($P \geq 10^{24.9}$) on the other hand, give a slope of -1.8 ± 0.1, significantly steeper than the Euclidean value of -1.5. Further discussion on this point will be given in Chapter III.

Clearly the completion of redshift measurements for 3CR radio-galaxies is a program of great importance, to test more reliably the existence of the effect claimed here.

As in section 7, the evolutionary hypothesis of the form discussed in section 6 can be tested by means of the modified luminosity-volume test.

The values of the parameters Q_L, z_L, Q_D, z_D required to give consistency of the radio-galaxy data with various cosmological models are given in columns i - iv in Table 5, together with the corresponding values for the quasars, taken from

section 10). There is remarkably close agreement of the parameters required for the exponential evolutions of both quasars and radio-galaxies (cols. ii and iv). In view of the arbitrariness of the particular forms of evolution we have considered, this agreement cannot be taken as evidence of a link between radio-galaxies and quasars. But if such a link is accepted (see for example, Ref. 62) then these forms of evolution seem very promising. Their consistency with radio-source counts to low flux-levels, and with the integrated radio background, will be discussed in Chapter III.

Although our discussion has been confined to 3 particular relativistic models, similar results are found for all models in the range

$$0 \leq z_0 \leq 3, \quad -1 \leq q_0 \leq 3.$$

It seems that for radio-galaxies the evolutionary factor far outweighs any differences between the cosmological models. The explanation of this evolution must await more detailed knowledge of the structure of radio-galaxies: whether, for example, they correspond to early or late stages in the life of a galaxy, and whether interaction with an intergalactic gas or magnetic field is an essential feature of their activity.

CHAPTER TWO

Summary.

Before proceeding to interpret the radio source-counts and integrated radio and X-ray backgrounds in Chapter III and IV, it is necessary to consider the physical parameters of radio-sources, especially the magnetic field.

In section 1 the different types of object identified with extragalactic radio-sources are summarized, and in section 2 the empirical relationship between the physical parameters in these sources is investigated. The component separation in double sources appears to be an increasing function of radio-luminosity, which suggests that luminosity increases with age if all sources are part of a single evolutionary sequence. The effect of the assumptions underlying the equipartition argument is examined in section 2.3. If the equipartition argument applies in radio-galaxies, either the components travel out from the parent galaxy with relativistic velocities, or the relativistic electrons are generated continuously in the components.

A model of double radio-galaxies proposed by Ryle and Longair, invoking relativistically moving components, is examined in some detail in section 3, and two other possible models are discussed in sections 4 and 5. Consideration of the several quadruple radio-sources known seems to rule out the possibility of relativistically moving

components (section 3.2), particularly when the Ryle-Longair model is made self-consistent (section 3.3).

Two possible ways of replenishing the energy in the radiating components are from the kinetic energy of the components, by interaction with a postulated surrounding medium (section 4), and from the energy of a shock generated in the parent galaxy (section 5). While a heuristic explanation of the double nature of most strong radio-sources can be given for this latter model, some difficulties are outlined in sections 5.1 and 5.2.

If the magnetic field in the radiating components is sufficiently high, the black-body radiation (if it is cosmological in origin) will only influence the distribution of sources with large redshifts (section 6).

1. Types of extragalactic radio source.

A major difficulty in the interpretation of radio source-counts to low flux-levels in different cosmological models is that there are several different types of extragalactic source. The main classes found at 178 MHz, down to the 3C level (9 f.u.), are (56)

(a) emission from "normal" spiral galaxies like our own and M.31, or irregulars like M82, often from extended sources centred on the optical galaxy.

(b) emission from "radio-galaxies", in a large fraction of cases from 2 emitting regions at appreciable displacements on either side of the optical galaxy. The optical galaxies associated with these strong radio-emitters are usually classed as ellipticals or N-galaxies.

(c) quasi-stellar radio sources, many of which have similar radio-properties to class (b), but some of which have very small radio-diameters and show strong radio-variations.

The distinction between these 3 classes is by no means sharp. Radio-wise there is a smooth transition between classes (b) and (c), and the same is true optically for quasars and N-galaxies (some of which show emission-line spectra, optical variations, and evidence for a non-thermal contribution to the optical continuum (63)).

The transition between classes (a) and (b) occurs at a radio-luminosity of about 10^{24} w m^{-2} $ster^{-1}$ Hz^{-1} , but it is not clear whether this is due to the crossover at this luminosity of the luminosity functions for two distinct classes of object, or to a critical value of some physical parameter on which the radio luminosity depends. The difference in optical type between classes (a) and (b) may be a consequence of the radio-event.

Evidence has been presented that quasars and radio-galaxies behave differently at higher frequencies ($> 10^3$ MHz) , (64) , quasars tending to show much more violent and short-lived emission at these frequencies than radio-galaxies. Although the major energy output of some quasars may well be in the millimetre wavelength region, the interpretation of counts at lower frequencies (178 or 408 MHz) are not thereby invalidated. Anomalous behaviour at higher frequencies will only influence the lower frequency counts if a significant proportion of sources at any flux-level have redshifts sufficients to shift the higher frequency emission down to the lower frequencies, i.e. if $z > 10$. It will be shown that the proportion of sources with such large redshift is likely to be negligible down to 10^{-2} flux-units (10^{-26} w m^{-2} Hz^{-1}) at 178 MHz.

The question of the dependence of counts on spectral shape and a frequency will be considered in detail in Chapter III.

2. Physical parameters in radio-galaxies and quasars.

All three classes of source are believed to emit by the synchrotron mechanism (65), for which, if the magnetic field in the emitting region has simple structure, and for the optically thin case,

$$P(\nu) = A(\alpha) . K . H^{1+\alpha} . \nu^{-\alpha} \qquad (1)$$

where the electron energy spectrum is taken to be

$$N(y)\,dy = K . y^{-1-2\alpha} . dy \qquad (2)$$

and y = electron energy / $m_e c^2$.

α is assumed to be a constant for each source (a reasonable approximation for most sources in the frequency range 38 - 1400 MHz (50).

There are 3 relevant parameters: H, α, K, the latter being related to the total number of relativistic electrons in the radiating region. Of these 3 fundamental parameters, only α can be measured directly.

Given knowledge of the radio structure, and certain simplifying assumptions, estimates can be made of K and H.

2.1. Relation between spectral index and radio luminosity.

The data for 142 radio galaxies and 42 quasars are summarized in Fig. 14, $\mathcal{F}_{178}$ for the Einstein de Sitter model against α (see Table 6). For the radio-galaxies there is some evidence for a relation between spectral index and luminosity, the stronger sources having steeper radio spectra. The spectrum of radio emission due to a single generation of electrons losing their energy by the synchrotron mechanism would tend to steepen with age (50), so either the stronger emitters are the older sources, or else sources of different luminosity cannot be thought of as part of a simple evolutionary sequence due to a single generation of electrons (both of these conclusions may be correct).

The mean line in Fig. 14 about which the radio-galaxies are distributed has equation

$$\bar{\alpha} = 0.85 + 0.075 \left(\mathcal{F} - 25{:}4 \right) \qquad (3)$$

The quasars do not conform to this relation, tending to have significantly smaller values of α than the radio-galaxies of similar luminosity.

In this respect they ressemble the weaker radio-galaxies, and this has been used as an argument in favour of the "local" theory for quasars (9). However, the quasars and weaker radio-galaxies could be phenomena of similar age , but of vastly different power (see section 2.2).

There is a selection effect which would contribute (slightly) to the dearth of low luminosity sources with large α. Sources with the same luminosity and redshift z would be observed to have flux-densities $(1+z)^{-\alpha}$, so in observations down to a particular flux-level, sources with larger α would be discriminated against. However, sources with $\mathcal{F} < 24.5$ have $z < 0.1$, so $\mathcal{F} < 0.04.\ \alpha$ and this selection effect is very slight. The effect of relation (3) and of the dispersion in α, on the interpretation of source-counts, will be considered in Chapter III.

2.2 Structure of radio-galaxies.

Of 82 more extended 3C sources for which detailed radio-maps have been published (66), the only unambiguous singles are:

3C 68.2 , 231 , 264, 272.1, 280.1, 323.

(All are identified with galaxies except 3C 280.1 , a quasar).

Of these the only object definitely belonging to class (b) is 3C 323 for which $\log_{10} P = 25.8$. The remaining objects in class (b)

are either doubles, or candidates for doubles observed almost end-on.

Ryle and Longair (62) have offered the ingenious suggestion that in quasars in which only one component is observed, a second component may exist, but with its flux severely reduced by a relativistic Doppler effect. Their model will be examined in section 3. For the moment we confine attention to the known extended identified doubles (quasars or radio-galaxies).

For these we have 2 main pieces of information: the projected linear separation of the components, d, and the size of the individual components, D. Figs. 15 a, b, and c show $\mathcal{F}$ - log d, $\mathcal{F}$ - log D, and log D - log d (the diameter along the radio axis of the brightest component is given in each case: 2 values of D are shown for 3C 402, which has 2 components of similar brightness, but very different size). In each figure different symbols are used to indicate sources with different values of log d/D (Fig. 15a), log d (Fig. 15b), and $\mathcal{F}$ (Fig. 15c). The limitation imposed by the finite resolving power of the telescope is indicated by loci of sources with the 3C limiting flux-level and apparent angular dimensions of 20" (Fig. 15a) and 10" (Fig. 15b).

However, from the analysis of Allen et al (67) it would appear that the percentage of 3C sources which will lie far to the left

of these lines is rather small. Out of 133 3C sources investigated by them, for over 80 percent the smallest dimension associated with a major component was $\geq 6''$, and for only 4 sources was this smallest dimension $< 1''$ (although the percentage of sources with some structure smaller than 1" is appreciably higher, particularly amongst the quasars).

From Figs. 15a, b and c we may infer that

(i) the maximum separation (and in view of the remark above, probably the mean separation also) in double radio-galaxies and quasars is an increasing function of luminosity.

(ii) the ratio of separation to component diameter is an increasing function of luminosity.

(iii) there is no particular correlation of component dimension with luminosity.

(Obviously these three remarks are not independent of each other).

If these sources are part of an evolutionary sequence, then apart from the strong compact sources 3C 123, 147, 245, 249 and 405, the inference would be that the weaker sources are younger than the stronger sources, i.e., the luminosity increases with age. However, component separation may be a measure of velocity of ejection rather than age, and in this case the radio-luminosity needs to increase with velocity.

2.3. Equipartition argument.

From equation (22), the value of the product KH^{1+a} is known. For emitting regions of known diameter, absence of a low frequency cut-off due to synchrotron self-absorption down to a given frequency sets an upper limit on H, which is however rather a weak condition for most sources.

The condition is (68)

$$B\theta^{-4} = 10^{-36.77}\ \nu_s^5 / S^2$$

where B is in gauss

θ is in seconds of arc

ν_s is the self-absorption frequency in H_z

and S is f.u.

so $\theta = 10$, $\nu_s < 10^7$, $S = 10$ give $B < 1.7$ gauss.

For a few sources with very small radio diameters (or unresolved) the condition is more interesting (68) and for 3C 287 seems to imply that the energy in magnetic field is less than the energy in particles, although this conclusion can be evaded by assuming that the emission at different frequencies comes from different components.

For the remaining sources some relation between K and H must be assumed, and it is of interest to calculate H_{eq}, the field that

gives equipartition of energy between relativistic particles and magnetic field, since this value gives the minimum total energy in the source.

The value of H_{eq} depends on two assumptions:

(i) the range of electron energies (y_1, y_2) for which equation (23) is valid

(ii) the ratio of the total energy in relativistic particles to the energy in electrons, f.

Now the energy in relativistic electrons,

$$E_{el} = \int_{y_1}^{y_2} N(y) \, . \, y \, m_e c^2 \, . dy$$

$$= K \, . \, m_e c^2 \left[\frac{y_1^{-(2\alpha - 1)} - y_2^{-(2\alpha - 1)}}{2\alpha - 1} \right] , \quad \alpha \neq \tfrac{1}{2}$$

$$= K \, . \, m_e c^2 \log (y_2 / y_1) , \quad \alpha = \tfrac{1}{2} .$$

The total energy is paticles is then $E_{part} = f E_{el}$,

the magnetic energy $E_{mag} = \frac{H^2 V}{4\pi}$ where V is the volume of the emitting region pervaded by field H and so the total energy $E_{tot} = E_{part} + E_{mag}$.

For a given source P, a, V are treated as constant, (y_1, y_2) as known function of H, and K to be determined as a function of H s.t. E_{tot} is a minimum.

Suppose $y_i = g_i H^x$, $i = 1,2,.$

Then $$E_{tot} = f\, m_e c^2 \quad \frac{[g_1^{-(2a-1)} - g_2^{-(2a-1)}]}{(2a-1)\, A\,(a)} \; PH^{-1-a-x(2a-1)} + \frac{H^2 V}{4\pi}$$

so $$\frac{dE_{tot}}{dH} = 0 \text{ if } H^{3+a+x(2a-1)} = \frac{2\pi P f\, m_e c^2 [g_1^{-(2a-1)} - g_2^{-(2a-2)}]\{1+a+x(2a-1)\}}{(2a-1)\; A\;(a)\;.\;V}$$

and

$$(E_{tot})_{min} = \left[1 + \frac{2}{1+a+x(2a-1)}\right] \frac{V}{4\pi}$$

$$\left\{ \frac{2\pi\, Pf\, m_e c^2 \,[g_1^{-(2a-1)} - g_2^{-(2a-1)}]\,\{1+a+x(2a-1)\}}{(2a-1)\; A\;(a)\;.V} \right\}^{\lambda}$$

where $\lambda = \dfrac{2}{3+a+x(2a-1)}$

E.g. (a) $y_i = \text{const}, \quad x = 0$

$$g_i = y_i = 10^{-3.3}\, \nu_i^{1/2}\, H^{-1/2}$$

$$(E_{tot})_{min} = h_a(\alpha) \cdot P^{\frac{2}{3+\alpha}} V^{1-\frac{2}{3+\alpha}}$$

(b) $\nu_i = \text{const}, \quad x = -\frac{1}{2}$

$$g_i = 10^{-3.3}\, \nu_i^{1/2}$$

$$(E_{tot})_{min} = h_b(\alpha)\, P^{4/7}\, V^{3/7}$$

(c) $y_i \propto H^{1/2}$ [RL]

$$g_i = \frac{y_i}{H^{1/2}} = \frac{10^{-3.3}\, \nu_i^{1/2}}{H}$$

$$(E_{tot})_{min} = h_c(\alpha)\, P^{\frac{4}{5+2\alpha}} V^{1-\frac{4}{5+2\alpha}}$$

The variation of h and $(E_{tot})_{min}$ with a is shown for a number of values of the parameters

x , f , g_1 , g_2 , P , V in Fig. 16.a.

The dependence on the parameters x, g_1, g_2, is at least as strong as the dependence on a, so it is important that these parameters should correspond to the source model being considered.

The values of P_{1400} , V and of $(E_{tot})_{min}$, H_{eq} for case (b) with $\nu_1 = 10\ MH_z$, $\nu_2 = 10^4\ MH_z$, $f = 100$, have been given by MacDonald et al (66) for each component of 52 identified, resolved, radio-sources, assuming the simplest possible geometry for the emitting regions. The relationship between P and V is of particular importance if it is believed that radio-galaxies form a simple evolutionary sequence. For example, according to the picture of Ryle and Longair (62) the more extended radio-galaxies (and quasars) belong to an evolutionary sequence in which the luminosity decreases as the volume of the emitting region (a blob of relativistic plasma) expands adiabatically. Fig. 16b, a plot of P_{1400} against V, does not support this view. While the selection effect discussed above in connection with Figs. 15a and b explains the cutoff to the left of the distribution (i.e. at smaller values of V), the maximum emitting

volume corresponding to each radio-luminosity is an increasing function of luminosity. The dispersion about Ryle and Langair's evolutionary sequence is more evident than the sequence.*

---

* If the emitting regions have relativistic velocities v with respect to the parent galaxy (and corresponding expansion velocities), then the luminosity will be modified by a factor $Z^{3+\alpha}$, and the volume by $\sim Z^3$, where $Z = (1 + v/c \cos \theta) / \sqrt{1 - v^2/c^2}$, and θ is the angle between the direction of motion as the time of sight. Thus, the apparent relation $P \propto V$ will be modified only slightly.

The corresponding distributions of H_{eq} and $(E_{tot})_{min}$ against P_{1400} are shown in Figs. 16c and d. The majority of the resolved components have $10^{-4.6} < H_{eq} < 10^{-4}$, with mean of order $10^{-4.3}$. When the unresolved components are taken into consideration, a higher value of the mean equipartition field will be obtained, but probably not much higher (according to the data of Allen et al (67)).

The actual magnetic field in the emitting regions may, of course, bear no relation to H_{eq}. But it is of some interest that the life-time of electrons radiating at 10^9 H_z in a field, $H = 10^{-4}$ gauss,

$$\tau_s = 10^{12.2}\, \nu^{-1/2} H^{-3/2} = 10^{13.7} \text{ secs} = 10^{6.2} \text{ years},$$

while the maximum separation observed in doubles is also of this order. Thus either (i) more than one generation of electrons is involved (ii) $v \sim c$ (iii) $H < H_{eq}$.

3. Models for double radio-sources with relativistic motions.

If the relativistic electrons required to produce the synchrotron emission at radio frequencies are created in a single initial event within the parent galaxy, and if the magnetic field pervading these blobs of relativistic plasma is of order the equipartition value, H_{eq}, then we saw in the last section that the velocities with which the blobs move away from the parent galaxy must be of order the velocity of light. Apart from the difficulty of understanding the initial event which not only accelerates the electrons, but also fires them out in the form of compact blobs, an unsatisfactory feature of this type of model is that the main energy losses while the blob of plasma is expanding are the adiabatic losses.

In this section some considerations presented by Ryle and Longair (62) with respect to models involving relativistic motions are examined in greater detail.

3.1. Ratio of fluxes from 2 sources moving in opposite directions with v close to c.

Suppose two similar radiating lumps A and B are ejected with velocity v from O at t = 0 in O's frame, and observed

from E subsequently at a time corresponding to t_0 in 0's frame, and t_a, t_r in A and B's frames. Then

$$t_a (1 - v/c \cos\varphi) = t_0 = t_r(1 + v/c \cos\varphi) \qquad (4)$$

where φ is the angle between the direction of motion and the line of sight. The light from the receding and approaching components is redshifted by

$$Z_r = 1 + z_r = \frac{1 + v/c \cos\varphi}{\sqrt{1 - v^2/c^2}} \quad \text{and}$$

$$Z_a = 1 + z_a = \frac{1 - v/c \cos\varphi}{\sqrt{1 - v^2/c^2}} ,$$

and the fluxes are dimmed, due to the motion, by

$Z_r^{3+\alpha}$ and $Z_a^{3+\alpha}$, where it is assumed that both sources have spectral index α. Thus the ratio of the fluxes

$$\frac{S_a}{S_r} = \frac{P_a}{P_r} \left(\frac{Z_r}{Z_a} \right)^{3+\alpha} = \frac{P(t_a)}{P(t_r)} \left(\frac{1 + v/c \cos\varphi}{1 - v/c \cos\varphi} \right)^{3+\alpha}$$

where $P(t)$ is the luminosity of a blob at time t. Thus

$$\frac{S_a}{S_r} = \frac{P(t_a)}{P(t_r)} \left(\frac{t_a}{t_r} \right)^{3+\alpha}, \quad \text{by (4)} \qquad (5)$$

If the velocity v is close to c, then the factor $\left(\frac{1 + v/c \cos \Phi}{1 - v/c \cos \Phi} \right)^{3+\alpha}$ will be very large. However, in the majority of double radio-sources the fluxes are not very unequal. Out of 60 doubles, 53 (88 per cent) have flux ratios smaller than 2.5 : 1, and 31 (52 percent) " " " " " 1.4 : 1.

From equation (5) we must conclude that $P(t)$ is a sharply declining function of t, such that

$$P(t) \sim t^{-3-\alpha} \qquad (6)$$

This was pointed out by Scheuer (69), and in Ryle and Longair's Fig. 2 (62), log P - log t, is the explanation of the lines of slope $\sim$ -4 which join the 2 components of each double. It is these lines which make the "mean" locus, in which $P \propto t^{-3}$ for the extended sources, plausible. As we have seen from Fig. 15a, there is no support for an evolution of this type when data from different doubles are compared.

3.2 Quadruple sources.

Out of 82 sources studies by MacDonald et al (66) 5(3C , 33.1 , 61.1 , 184.1 , 234, 452) consist of 4 sources along an axis, and 4 out of these 5 have an optical object (a galaxy) situated fairly centrally on the axis. It is reasonable to suppose that we are observing products of two separate events of the type discussed in section 3.1 , and we shall denote the parameters for the 2 events by

$$t_0^i \ , \ v_i \ , \ t_{a,r}^i \ , \ Z_{a,r}^i \ , \ S_{a,r}^i , i = 1,2,$$

(the inner, more recent event corresponding to $i = 1$).

Now if we consider the two sources moving in the same direction for example the approaching components:

$$\frac{S_a^1}{S_a^2} = \frac{P(t_a^1)}{P(t_a^2)} \left\{ \frac{Z_a^2}{Z_a^1} \right\}^{3+\alpha}$$

$$= \frac{P\{ t_0^1 / (1 - v_{1/c} \cos \varphi) \}}{P\{ t_0^2 / (1 - v_{2/c} \cos \varphi) \}} \left\{ \frac{(1 - v_{2/c} \cos \varphi) / \sqrt{1 - v_2^2 / c^2}}{(1 - v_{1/c} \cos \varphi) / \sqrt{1 - v_1^2 / c^2}} \right\}^{3+\alpha}$$

$$= \frac{P(t_0^1)}{P(t_0^2)} \left\{ \frac{\sqrt{1 - v_1^2/c^2}}{\sqrt{1 - v_2^2/c^2}} \right\}^{3+\alpha} \quad \text{if} \quad P \propto t^{-3-\alpha}$$

$$= \left\{ \left(\frac{t_0^2}{t_0^1} \right) \sqrt{\frac{1 - v_1^2/c^2}{1 - v_2^2/c^2}} \right\}^{3+\alpha} = \frac{S_r^1}{S_r^2} \quad , \text{ similarly.} \qquad (7)$$

For example if $v_1 = v_2$ and $t_0^2 = 2 t_0^1$, $S_a^1 \sim 14\, S_a^2$

and if $t_0^2 = 3 t_0^1$ (probably necessary for 3C 452), $S_a^1 \sim 70\, S_a^2$.

But out of 10 pairs, in no case does the ratio of the flux of the inner member to the outer exceed 1.5 (in the 3 most extreme cases the ratio is 0.18 , 0.26 and 0.46). Thus we need $v_1 \neq v_2$ and in fact v must decrease with time such that

$$\sqrt{1 - v^2/c^2} \quad \propto \quad t \qquad (8)$$

So far we have assumed that there is no deceleration of the blobs and that the initial velocities are the same in both directions. Under these

assumptions equation (8) refers to the initial velocity.

Now it is under these assumptions that Ryle and Longair's estimates of the velocities in different doubles are valid (we shall discuss the method in the next section). The table shows their suggested mean relation for v as a function of t

Log t =	5	5.5	6	6.5
v/c	.9	.8	.45	.1
$1 - v^2/c^2$	.19	.36	.80	.99
$\log (1 - v^2/c^2)$	-.72	-.44	-.1	-.004
$\frac{\log (1 - v^2/c^2)}{\log t}$		.56	.68	-.2
$\frac{1}{2}$ (log t - 6.4)	-.7	-.45	-.2	

Comparison of rows 3 and 5 show that their data is fairly well represented by

$$\sqrt{1 - v^2/c^2} = (t/10^{6.4})^{1/4}, \quad t \text{ in years.}$$

This is not nearly as steep a decline of v with t as required by relation (8), and the inner components would be expected to be much brighter than the outer.

But anyway the only natural deduction from the fact that v decreases with the time t that has elapsed since the ejection, is that the blobs are being decelerated, and in that case the above analysis must be modified.

3.3 Velocity of individual components decreases with time

If $v = v(t)$, the distance travelled in time t

$$s(t) = \int_0^t v(x)\,dx = t.\bar{v}(t), \quad \text{where } \bar{v}(t) = \frac{1}{t}\int_0^t v(x)\,dx$$

and so equation (25) must be replaced by

$$t_a\left(1 - \frac{\bar{v}(t_a)}{c}\cos\varphi\right) = t_0 = t_r\left(1 + \frac{\bar{v}(t_r)}{c}\cos\varphi\right) \qquad (9)$$

Ryle and Longair estimate $v\cos\varphi$ from equation (4) using the fact that

if the velocities of approaching and receding components are the same and independent of t, then the ratio of apparent angular displacements of the blobs from the parent galaxy

$$\frac{\theta_a}{\theta_r} = \frac{t_r}{t_a} .$$

However this relation now has to be replaced by

$$\frac{\theta_a}{\theta_r} = \frac{t_r \cdot \bar{v}(t_r)}{t_a \cdot \bar{v}(t_a)} \qquad (10)$$

If $\bar{v}(t)$ does not change too rapidly with t (which is rather likely, as we shall show below) then the method of Ryle and Longair gives a good estimate of $\bar{v}(t_0) \cos\varphi$. In fact

$$\frac{\bar{v}(t_0) \cdot \cos\varphi}{c} \simeq \frac{\theta_a - \theta_r}{\theta_a + \theta_r} \qquad (11)$$

If $d_c = \frac{r(z_G).R_0}{1+\frac{1}{4}k.r^2(z_G)} \cdot \frac{1}{1+z_G}$, where z_G is the cosmological redshift of the parent galaxy, then

$$\frac{d_c(\theta_a + \theta_r)}{\bar{v}(t_0).\sin\varphi} \simeq \frac{t_0}{1-\left(\frac{\bar{v}(t_0).\cos\varphi}{c}\right)^2} \qquad (12)$$

Thus if there is a relation between $\bar{v}(t_0)$ and t_0, a corresponding relation should appear in the

$d_c(\theta_a + \theta_r) - \left(\frac{\theta_a - \theta_r}{\theta_a + \theta_r}\right)$ plane, blurred somewhat by the effect of orientation.

These quantities have been calculated from the data of MacDonald et al (66), and plotted in Fig. 17, for 38 sources in which the optical object identified with the double radio source lies near the radio axis (see Table 6). These include the 15 objects used by Ryle and Longair, although two of the identifications used by them are not confirmed by MacDonald et al (3C 332, due to a change of the estimated position of the source, and 3C 356 (a), which Schmidt has shown

to be a star (91)). A number of the sources have several associated candidates for parenthood, and these are all shown in Fig. 17. With the new data, it is very difficult to see any correlation between the 2 quantities plotted. The majority of the points are uniformly distributed with $0 < d_{\mathcal{L}}(\theta_a + \theta_r) < 500$ kpc and

$$0 < \frac{\theta_a - \theta_r}{\theta_a + \theta_r} < 0.25.$$

The few, more extreme, values of $\frac{\theta_a - \theta_r}{\theta_a + \theta_r}$ have average values of $d_{\mathcal{L}}(\theta_a + \theta_r)$, although it is true that the most extreme value, 0.84 for 3C 340, corresponds to one of the smaller linear separations. However, the most natural interpretation of Fig. 17 is that the blobs are ejected with unequal and not necessarily relativistic, velocities, and that in objects like 3C 340 only one component is the result of an ejection, the other being centred on the parent galaxy (cf M 87 and 3C 273). Nevertheless it is of interest to carry the argument a step further for the relativistic case.

First we calculate $\bar{v}(t)$ for a number of simple forms of $v(t)$.

(i) constant deceleration:

$v = v_0 - ft$, f constant ,

$= 0$ when $t = v_o/f$.

$\bar{v}(t) = v_0 - \frac{1}{2} ft = v_0/2$ when $v = 0$.

Thus while v decreases from v_0 to zero, $\bar{v}$ changes only from v_0 to $v_0/2$.

More generally, if $v = v_0 - ft^n$

$$\bar{v} = v_0 - \frac{f}{n+1} t^n$$

$$\longrightarrow \frac{n}{n+1} v_0 \text{ as } v \longrightarrow 0 .$$

ii) $\sqrt{1 - v^2/c^2} = (t/t_{max})^n$.

$$\bar{v}(t) = \frac{c}{t} \int_0^t \sqrt{1 - (t/t_{max})^{2n}} \, dt$$

$$n = 1 : \frac{\bar{v}(t)}{c} = \frac{t_{max}}{2t} \left\{ \sin^{-1}\left(t/t_{max}\right) + \frac{t}{t_{max}} \sqrt{1 - t^2/t^2_{max}} \right\}$$

$$\longrightarrow \pi/4 \quad \text{as} \quad t \longrightarrow t_{max}.$$

$$n = \frac{1}{2} : \frac{\bar{v}(t)}{c} = \frac{2t_{max}}{3t} \left\{ 1 - \left(1 - t/t_{max}\right)^{3/2} \right\} \longrightarrow \frac{2}{3} \quad \text{as} \quad t \longrightarrow t_{max}$$

$$n = \frac{1}{4} : \frac{\bar{v}(t)}{c} = \frac{4t_{max}}{t} \left[\frac{2}{15} - \frac{1}{3} \left\{ 1 - \sqrt{\frac{t_{max}}{t}} \right\}^{3/2} + \frac{1}{5} \left\{ 1 - \sqrt{\frac{t_{max}}{t}} \right\}^{5} \right.$$

$$\longrightarrow \frac{8}{15} \quad \text{as} \quad t \longrightarrow t_{max}.$$

Now $\bar{v}/c > \lambda$ all $t \Rightarrow \frac{t_a}{t_r} > \frac{1 + \lambda \cos \varphi}{1 - \lambda \cos \varphi}$

and

$$\frac{t_a}{t_r} > \left(\frac{1 + \lambda \cos \varphi}{1 - \lambda \cos \varphi} \right) \lambda \sim 6.5 \text{ if } \varphi = 0, \quad \lambda = \pi/4$$

1.8	$\pi/3$	$\pi/4$
1.3	$\pi/3$	2/3
0.9	$\pi/3$	8/15

Thus if $n = 1$, over half the points in Fig. 17 should have

$$\frac{\theta_a - \theta_r}{\theta_a + \theta_r} > 0.29$$

which is certainly false.

If $n = \frac{1}{2}$, over half should have $\frac{\theta_a - \theta_r}{\theta_a + \theta_r} > 0.13$

which is just about satisfied.

Since for $n \geq \frac{1}{4}$, $1 \geq \bar{v}(t) / c > \frac{1}{2}$ all t, the assumption made above that $\bar{v}(t)$ does not change too rapidly is valid, and so

$\frac{\theta_a - \theta_r}{\theta_a + \theta_r}$ is a good estimate of $\frac{\bar{v}(t_0) \cdot \cos \varphi}{c}$.

However $v(t)$ can now be very much less than $\bar{v}(t)$ and expression (5) becomes

$$\frac{S_a}{S_r} = \frac{P(t_a)}{P(t_r)} \left\{ \frac{1 + (v_r/c) \cos \varphi}{1 - (v_a/c) \cos \varphi} \cdot \frac{\sqrt{1 - v_a^2/c^2}}{\sqrt{1 - v_r^2/c^2}} \right\}^{3+\alpha}$$

$$= \frac{P(t_a)}{P(t_r)} \left(\frac{t_a}{t_r} \right)^{(3+\alpha)n} \left\{ \frac{1 + \cos\varphi \sqrt{1 - (t_r/t_{max})^{2n}}}{1 - \cos\varphi \sqrt{1 - (t_a/t_{max})^{2n}}} \right\}^{3+\alpha}$$

It is not now possible to obtain roughly equal fluxes for all orientations by a simple $P - t$ relation.

Now if $t_r, t_a \ll t_{max}$, and so $\bar{v}(t_a) \simeq \bar{v}(t_r) \simeq c$,

then $$\frac{S_a}{S_r} = \frac{P(t_0/(1 - \cos\varphi))}{P(t_0/(1 + \cos\varphi))} \cdot \left(\frac{1 + \cos\varphi}{1 - \cos\varphi} \right)^{(3+\alpha)(1+n)},$$

~ 1 if $P \propto t^{-x}$, where $x = (3 + \alpha)(1 + n)$.

But if now $t_r \ll t_a \simeq t_{max}$, so $\bar{v}(t_r) \simeq c$, $\bar{v}(t_a) \simeq \lambda c$, then

$$\frac{S_a}{S_r} = \left(\frac{1 + \cos\varphi}{1 - \lambda\cos\varphi} \right)^{-x+(3+\alpha)n} (1 + \cos\varphi)^{3+\alpha} = (1 - \lambda\cos\varphi)^{3+\alpha}$$

$$< \frac{1}{6} \text{ if } n = 1, \varphi > \pi/3.$$

Turning to the case of quadruple sources:

$$\frac{S_1}{S_2} = \left(\frac{t_0^1}{t_0^2}\right)^x \cdot \left\{ \frac{1 \pm \frac{\bar{v}_1}{c} \cos \varphi}{1 \pm \frac{\bar{v}_2}{c} \cos \varphi} \right\}^x$$

$$\cdot \left\{ \frac{(1 \pm v_2/c \cdot \cos \varphi) / \sqrt{1 - v_2^2/c^2}}{(1 \pm v_1/c \cdot \cos \varphi) / \sqrt{1 - v_1^2/c^2}} \right\}^{3+\alpha}$$

where + refers to the two receding sources,

and - refers to the two approaching sources,

$$= \left(\frac{t_1}{t_2}\right)^{3+\alpha} \left\{ \frac{1 \pm \cos \varphi \sqrt{1 - (t_2/t_{max})^{2n}}}{1 \pm \cos \varphi \sqrt{1 - (t_1/t_{max})^{2n}}} \right\}^{3+\alpha}$$

if $\sqrt{1 - v^2/c^2} = (t/t_{max})^n$ and $x = (3+\alpha)(1+n)$.

$t_1 \ll t_2 \ll t_{max}$: $\frac{S_1}{S_2} \simeq \left(\frac{t_1}{t_2}\right)^{3+\alpha} \ll 1$, all φ

$t_1 \ll t_2 \quad t_{max}$: $\frac{S_1}{S_2} \simeq \left(\frac{t_1}{t_2}\right)^{3+\alpha} \cdot \frac{1}{(1 \pm \cos \varphi)^{3+\alpha}}$

$\ll 1$ for receding components

~ 1 for approaching components if $\varphi = \pi/3$, $t_2 = 2t$.

Finally to convert Ryle and Longair's $\bar{v} - t$ relation directly into a $v - t$ relation we note that

$$v = \frac{d}{dt}(\bar{v}\, t) = \bar{v}\left(1 + \frac{d \log \bar{v}}{d \log t}\right).$$

The best value of n is found to be about 0.25 : certainly $n = 1$ does not fit the data.

To conclude, the tendency of both components in double radio-sources (and of all four in quadruples) to have similar fluxes makes it unlikely that the motions of the radio components are relativistic. If the relativistic electron belong to a single generation, the magnetic field must be considerably less than the equipartition value. The different separations of the two components must be due to different velocities, decelerations, or times of ejection.

4. The interaction of the moving components with the surrounding medium.

In any model in which the radio components are where they are because matter has travelled there, the interaction of this moving matter with the surroundings has to be considered. The maximum temperature of the intergalactic or intercluster medium is 10^6 ^oK (70) and the corresponding speed of sound 100 km/sec, so we are almost certainly dealing with supersonic motions and shock drag resistance. This is given essentially by the momentum destroyed per sec. in the tunnel swept out by the moving object, and in the relativistic case is

$$\frac{\pi \rho R^2 v^2}{1 - v^2/c^2} \quad , \text{ in the frame of the object.}$$

(One factor $\frac{1}{\sqrt{1 - v^2/c^2}}$ for the increase in apparent mass of the material hitting the object, and one factor for the time dilation), where ρ is the density of the ambient material in the rest frame, and R is the radius of the object assumed spherical. The drag on the object will be measured to have the same value in the rest-frame (by the law of transformation of force), so the equation of motion is

$$\frac{d}{dt}\left(\frac{Mv}{\sqrt{1 - v^2/c^2}}\right) = \frac{-\pi . R^2 v^2}{1 - v^2/c^2} \quad ,$$

where M is the proper mass of the object,

and if we write $w = v / \sqrt{1 - v^2/c^2}$

$$\frac{1}{w^2} \frac{dw}{dt} = - \frac{\pi}{M} R^2(t) \qquad (13)$$

Here we are now assuming that R is a function of time. Equation (34) now has the same form as for the non-relativistic case, with $v/\sqrt{1 - v^2/c^2}$ in place of v, and can be integrated:

$$\frac{1}{w} - \frac{1}{w_0} = \frac{\pi}{M} \int_0^t R^2(t)\, dt$$

where $w = w_0$ when $t = t_0$.

(i) $R = R_0$, constant:

$$w = \frac{w_0}{1 + a t} \quad , \quad \text{where} \quad a = \frac{\pi R_0^2 w_0}{M}$$

so $w = w_0/2$ after time $1/a$.

Now $v = w\sqrt{1 - v^2/c^2}$, so $v = \dfrac{w}{\sqrt{1 + w^2/c^2}} = \dfrac{w_0}{\sqrt{(1+at)^2 + w_0^2/c^2}}$.

Thus the distance travelled in time t,

$$S(t) = \int_0^t v\,dt = \frac{w_0}{a}\left[\sinh^{-1}\left\{\frac{(1+at)c}{w_0}\right\} - \sinh^{-1}\frac{c}{w_0}\right]$$

$$\sim \frac{w_0}{a}\log_e\frac{2a\,ct}{w_0} \quad \text{for large } t$$

$$= \frac{M}{\pi\rho R_0^2}\log_e\left(\frac{2\pi\rho R_0^2\,ct}{M}\right)$$

The velocity becomes small after a time which is a few multiples of $1/a$, and the distance travelled is of order $M/\pi\rho R_0^2$, independent of w_0.

Thus $R_0 \sim 10^{23}$ cm, $s > 10^{24}$ cm $\Rightarrow M > 10^7\odot$ if $\rho \geq 10^{-30}$ gm/cc.

(ii) $\dot{R} = U$, constant

$$R = Ut \ , \quad w = \frac{w_0}{1 + \pi \cdot t^3 w_0 U^2 / 3M}$$

characteristic time is now $\left\{ \frac{3M}{\pi \cdot w_0 U^2} \right\}^{1/3}$

and the distance travelled is $\left\{ \frac{3M w_0^2}{\pi \cdot U^2} \right\}^{1/3}$,

which is independent of w_0 if $U \alpha w_0$.

The energy that is consumed in this interaction, per sec,

$$\dot{E} = \frac{\pi \cdot v R^2}{\sqrt{1 - v^2/c^2}} \left\{ \frac{c^2}{\sqrt{1 - v^2/c^2}} - c^2 \right\} = \pi \cdot w R^2 c^2 \left\{ \sqrt{1 + w^2/c^2} - 1 \right\}$$

and if $v \sim w \sim 10^9$ cm/sec, $R \sim 10^{23}$ cm , then $\dot{E} \sim 10^{73} \cdot \rho$ ergs/sec.

$\sim 10^{44}$ ergs/sec if $\rho = 10^{-29}$ gm/cc

Finally, if the different luminosities correspond to different velocities of ejection, and the sources are snuffed out after a fixed time,

the fact that the maximum separation in doubles increases with luminosity could be explained.

5. A non-relativistic shock model.

We saw (Fig. 16c) that the dispersion in the equipartition field is much smaller than the dispersion in radio luminosities. This is a consequence of the fact that most sources satisfy a relation $P \propto V$ approximately, and this is not likely to be seriously altered when data is available on sources at present unresolved. If the equipartition argument is correct, and if the sources form an evolutionary sequence, we have to find a model in which the magnetic field remains constant while the emitting region increases its volume by several orders of magnitude.

One possibility is that the magnetic field provides the pressure support behind a shock travelling through a medium of uniform density.

The magnetic field would be of order $H_0 \sim \sqrt{8\pi \rho_0}\, v_0$, where the shock moves with velocity v_0 through a medium of density ρ_0.

The magnetic field energy is then proportional to the emitting volume (or region behind the shock),

and is formed at the expense of the energy in the shock. Some fraction of this energy may then be converted into relativistic particles (a fixed fraction, to give $P \propto V$). In this picture the cloud of relativistic particles is not created in some unspecified way in the initial explosion, but manufactured in situ out of magnetic energy. The explosion that gives rise to the shock is presumed to take place at the centre of a galaxy.

The compact radio-sources, including quasars, N-galaxies, and Seyferts like NGC 1275, would correspond to the phase where the shock travels through denser galactic material. If we use Colgate's relation (71) for the motion of a shock through the surface layers of a supernova, $v \propto \rho^{-1/4}$ then $H_0 \propto \rho^{1/4}$. Since $P \propto H^{3+\alpha}$ there would be a considerable decrease in brightness of the source as the shock passed out into the intergalactic medium. A possible history is illustrated in the sketch.

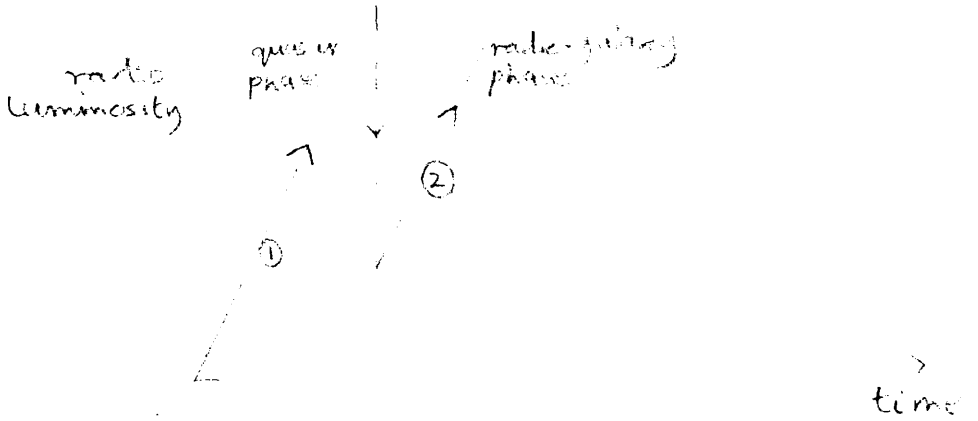

This model is similar to that of Ryle and Langair, excpet that during phase 2 the luminosity increases with time rather than decreases. Since the motions are non-relativistic the time scales for the whole radio galaxy phase will be much longer than the 10^6 years of Ryle and Longair's model.

If the galaxy (or its nucleus) is disc-shaped a natural explanation of the double nature of the sources can be found. A spherical blast wave would be refracted into a dumbell shape on passing out of the disc into the lower density surrounding medium, in which the shock velocity is appreciably higher.

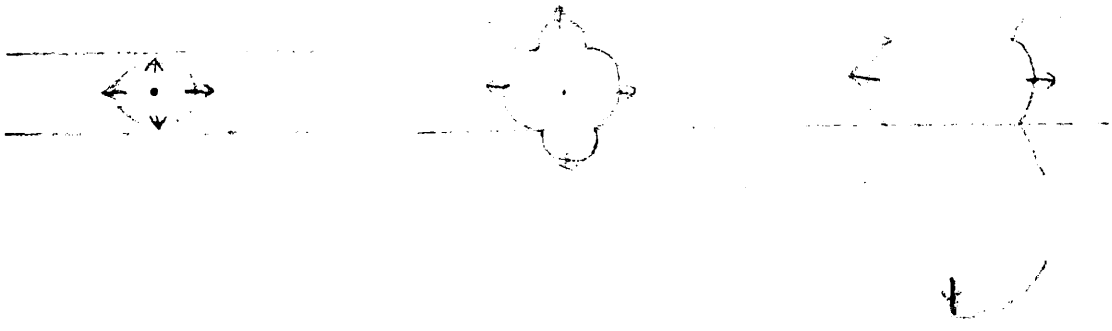

The origin of the shock wave may lie either in multiple supernovae outbursts (72), in the catastrophic evolution of a dense stellar system (73), or perhaps in the explosion of a supermassive object (74).

In section 2.3 the mean equipartition magnetic field was found to be about $10^{-4.3}$ gauss, in double radio-galaxies, and if the ratio of

magnetic to particle energy is f, this figure must be multiplied by

$f^{1/3 + a + x(2a-1)}$.

Thus $v_0 \sim 10^{-5} \rho_0^{-\gamma_2} f^{1/(3 + a + x(2a - 1))}$

Neither H_0 nor v_0 depend very strongly on f. The values of v_0 corresponding to various typical densities are:

$v_0 \sim 10^{10}$ cm/sec if $\rho_0 \sim 10^{-30}$, approximate average density of matter in galaxies

$\sim 2 \times 10^{9}$ ... 2×10^{-29}, the density of matter required to "close" the universe (if $\Lambda = 0$).

$\sim 10^{9}$ ... 10^{-28}, the average density of a cluster if the virial theorem is satisfied.

$\sim 3 \times 10^{7}$ ... 10^{-25}, the average density in the disc of the galaxy.

At the most luminous phase, the total energy in magnetic field and particles is of order 10^{60} ergs, so the energy in the shock must exceed this. One simple consequence of the passage of so strong a shock through a galaxy might be to sweep all the gas out of the galaxy and this might explain why ellipticals, with which strong radio-sources are usually associated, are deficient in gas with respect to spirals (75).

In fact, the total energy in the shock will be related to the maximum dimensions r of the source roughly by

$E \sim \frac{2\rho_0 r^3 v_0^2}{3}$, assuming a cone of 1 steradian is accelerated to velocity v_0

$\sim \frac{H_0^2 r^3}{12\pi} \sim 10^{-8.6+72-1.6}$ if $H_0 \sim 10^{-4.3}$, $r \sim 10^6$ l t years

$\sim 10^{62}$ ergs,

the rest mass energy of about 10^8 solar masses and the hydrogen-burning energy of about 10^{10} solar masses.

So far only heuristic considerations have been presented, but very little progress can be made quantitatively. First we shall note that in a plane transverse-field shock it is not possible both to

amplify the magnetic field greatly across the shock and convert most of the shock energy into magnetic field energy. Secondly, by analogy with the Taylor blast-wave solution, we shall note that it is unlikely that the magnetic field behind the shock will remain constant as the shock expands.

5.1. Plane shock, transverse field.

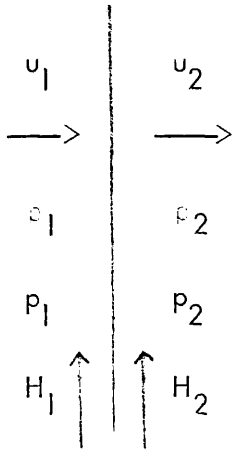

Consider a plane shock travelling at velocity u_1 perpendicular to the plane of the shock. In the frame of the shock let upstream and downstream variables have suffices 1 and 2, and suppose the magnetic field is tranvsverse to the motion.

Then the mass-conservation condition, and continuity of the

electric field, give

$$\frac{u_1}{u_2} = \frac{\rho_2}{\rho_1} = \frac{H_2}{H_1} = \eta .$$

The momentum condition is $\left[p + \rho u^2 + \frac{H^2}{8\pi} \right]_1^2 = 0$

or $$\frac{1}{\gamma} \left[\eta S_2^2 - S_1^2 \right] = u_1^2 \left(1 - \frac{1}{\eta} \right) - \frac{1}{2} a_1^2 \left(\eta^2 - 1 \right) \qquad (14)$$

where $a^2 = H^2/4\pi\rho$ and $S^2 = \gamma p/\rho$,

and the energy condition is $\left[\rho u \left\{ \frac{\gamma p}{(\gamma-1)\rho} + \frac{1}{2} u^2 \right\} + \frac{uH^2}{4\pi} \right]_1^2 = 0$

or $$\frac{1}{\gamma-1} \left[S_2^2 - S_1^2 \right] = \frac{1}{2} u_1^2 \left(1 - \frac{1}{\eta^2} \right) - a_1^2 \left(\eta - 1 \right) \qquad (15)$$

Eliminating S_2^2 between equations (14) and (15) :

$$\xi = \frac{H_2^2}{4\pi \rho_1 u_1^2} = \frac{\eta^2 a_1^2}{u_1^2} = \frac{\{y+1-\eta(y-1)\}\eta}{y+2\eta-\eta y+2S_1^2/a_1^2} .$$

The maximum value of η is $\frac{y+1}{y-1}$, and to get $\eta \gg 1$ and

$\xi = O(1)$, we need $y-1 \ll 1$, and then

$$\frac{4\pi p_2}{H_2^2} \sim \frac{\eta(y-1)}{2\{2-\eta(y-1)\}} .$$

Elliminating S_1^2 between equations (14) and (15)

$$u_2^2 = s_2^2 \left[1 - \frac{(y+1)\eta - 1}{(y+1)\eta - y + 1} \right] + a_2^2 \left[1 - \frac{(y-1)(y\eta+\eta-y+2)}{\eta\{(y+1)\eta-(y-1)\}} \right]$$

$< S_2^2 + a_2^2$ if $\eta > 1$, so the shock is stable. Now $\eta \gg 1$, $y \sim 1$ imply $\eta u_2^2 \sim S_2^2 + a_2^2$; the momentum and energy conditions become

$$\rho_1 u_1^2 \sim p_2 + \frac{1}{8\pi} H_2^2 , \quad \text{or} \quad u_1^2 \sim \left(\frac{S_2^2}{\gamma} + \frac{a_2^2}{2} \right) \eta$$

$$\text{and} \quad \frac{1}{2} u_1^2 \sim \frac{S_2^2}{\gamma-1} + \eta a_1^2 , \quad \text{or} \quad u_1^2 \sim \left(\frac{S_2^2}{\gamma-1} + a_2^2 \right) 2 .$$

Thus if the pressure support behind a strong shock is mainly magnetic ($a_2 \gg S_2$), we need most of the energy to be dissipated thermally. The magnetic field behaves like a gas with $\gamma = 2$: relativistic particles, on the other hand, for which $p = \frac{1}{3} \epsilon$, behave as if $\gamma = 1.5$.

5.2 3-dimensional shocks.

The only exact solutions known are due to Taylor (76), for spherically symmetric motions in which physical variables depend on only one spatial variable. The introduction of a magnetic field axis rules out the possible application of such simple solutions. However one amenable problem is that of a cylindrical shock moving radically outwards, the magnetic field being everywhere parallel to the axis of the cylinder.

In cylindrical polars (r , θ, z),

$\underline{u} = (u(r,t), 0,0), \quad \underline{H} = (0,0, H(r,t))$.

The continuity equation is

$$\dot{\rho} + \frac{1}{r^2} \frac{\partial}{\partial r} (\rho u r^2) = 0 \tag{16}$$

the equation of motion is

$$\rho \left\{ \dot{u} + u \frac{\partial u}{\partial r} \right\} + \frac{\partial p}{\partial r} + \frac{1}{4\pi} H \frac{\partial H}{\partial r} = 0 \tag{17}$$

and the equation for the field is

$$\dot{H} + \frac{1}{r} \frac{\partial}{\partial r} (H u r) = 0 \tag{18}$$

Equation (17) is the Taylor equation, with $(p + H^2/8\pi)$ in place of p. Thus if the shock front has equation $r = R(t)$, we can expect that behind the shock:

$$p + \frac{H^2}{8\pi} \propto \rho_0 \dot{R}^2(t)$$

$$R(t) \propto t^{2/5}$$

where ρ_0 is the undisturbed density,

for the blast-wave case in which the total energy carried by the wave is constant. Thus H will not be constant behind the shock, and this is likely to extend to the general 3-D case. Moreover if a blast wave in which the magnetic field plays an important role in the pressure support, the shock will travel faster perpendicular to the direction of the field, than parallel to it. This could even cause the very strong asymmetry observed in double radio-sources.

A second important factor, beside the possible existence of an aligned magnetic field, is that there may be strong density gradients in the vicinity of the initial explosion. For example if there is a plane of symmetry with the density decreasing with distance from the plane, the velocity of the shock will be greatest where the density is least, and there may be a mushrooming effect (as in an H-bomb explosion).

In what follows no particular weight will be attached to the model outlined above. But the evidence for a relativistically moving coherent blob of relativistic particles and magnetic field is not strong, and other possibilities should be considered. One of the main advantages

in supposing that the energy required in the radiating components is transported from the parent galaxy or quasar in the form of kinetic or shock energy, is that the relativistic electrons are not required to survive inverse Compton interaction with the optical photons from the parent object. This is a serious problem (77) and can be avoided only by supposing relativistic motions are present (78). Evidence against such motions has been presented in section 3.

6. The lifetime of sources.

The lifetime of sources clearly depends very much on which model is the correct one. But since all models invoke synchrotron radiation, the synchrotron life of the radiating electrons is a quantity of some interest. For electrons of energy y in a magnetic field H, this life is $\tau_s = 10^{7.6} / y H^2$ (65). If these electrons encounter radiation with energy-density U_{rad} they will also lose energy by inverse Compton radiation, so the life becomes

$$\tau = 10^{7.6} / y (H^2 + 4\pi U_{rad}).$$

Thus if U_{rad} is due to cosmical black-body radiation of temperature

2.7° K at the present epoch, the life of the radiating electrons will begin to be drastically reduced at epochs such that

$10^{-5.65}\ (1+z)^{2} \geq H$ (see chapter IV).

In models where the radiating life of the electrons determines the life of the source, there will be a corresponding reduction in the number density of sources.

CHAPTER THREE

Summary.

In section 1 the source models and types of evolution discussed in the previous chapters are summarized. The case to be investigated in greatest detail here is where all sources of a particular class have the same magnetic field, and either this field is strong enough so that the black-body radiation does not interact significantly with the relativistic electrons until epochs such that the redshift is ten or more, or the black-body radiation is not cosmological in origin. The simplest types of evolution are the exponential evolutions proposed in 1.6, characterized by one parameter only.

Three independent methods of description of the dependence of number-density on luminosity and epoch, and their appropriateness for different types of evolution, are outlined in section 2, since some confusion on this point is apparent in the literature.

Section 3 presents some theoretical considerations on number-counts of a set of sources with the same luminosity and spectral shape. It has often been tacitly assumed, on the basis of an examination of the first order term in a power series expansion, than the number-count slope for a set of uniformly distributed sources with the same luminosity and spectra is less than the Euclidean value of 1.5 for all cosmological models of interest. In section 3.1 this is proved for models

with $k \leq 0$: for $k > 0$, the statement is not true in general, and seems hard to prove even for the case $\Lambda = 0$, where numerical calculations indicate it to be true. In section 3.2 the number-count slope as the flux-level tends to zero is found to be non-zero only if $c_0 = 0$. In section 3.3 and 3.4 the log N - log S relation is evaluated for sources with exponential luminosity and density evolution in the Einstein de Sitter, Milne and de Sitter models: luminosity evolution is better able to account for the sharp change in the observed source-count slope at faint flux-levels. The effect of luminosity and density evolution on the first order term in the power series expansion of the source-count slope is evaluated in section 3.5, and a rough interpretation given of the counts of strong radio-galaxies described in 1.14 (see also Appendix 4).

Section 4 is essentially a rediscussion of Gower's "convolution of radio source-counts" (17). The counts are interpreted in terms of both density and luminosity evolution, and density evolution of all sources is found to be improbable. An interesting qualitative result is that the peak contribution to source-counts down to any flux-level is likely to come from sources with a luminosity that decreases with decreasing flux-density. The main contribution at faint flux-levels could come from a class of sources making an insignificant contribution at

higher flux-levels.

In section 5 the effect on counts of the dispersion in spectral indices is investigated, and is found to be not very great. To sufficient accuracy the sources may be treated as if they all had the mean spectral index. The dependence of the luminosity function on frequency introduced by this dispersion in spectral shape, is shown to be not too great in section 6, and section 7 deals with a related problem, the dependence of the source-counts on frequency. If the dispersion in spectral indices at high flux-levels is represented by a Gaussian, and is independent of flux-density, it is found that the shape of the source-counts should be independent of frequency over a wide range of frequency. The observed counts at 2770 MHz can be understood if, in one source in 500 at 178 MHz, the flux increases with frequency, rather than decreases as is usually the case. Such a population is known (a subset of the quasars), so there is in this sense no discrepancy between the counts at 178 and 2770 MHz.

In sections 8 - 11 the observed source-counts are interpreted in terms of exponential luminosity evolution of the stronger radio-galaxies (no evolution being assumed for other classes of source) in three asymptotic cosmological models. Significant differences are found between the three models, both in the goodness of fit, particularly at

low flux-levels where the models predict different asymptotic source-count slopes, and in the value of the critical luminosity above which the evolution is supposed to operate. The latter is the only parameter in the problem: the rate of evolution is essentially determined by the analysis of Chapter I , as also is the luminosity function (section 8). Thus the excellence of fit in the Milne model seems to be a significant result. Certainly if attention is confined to cosmological models with $\Omega = 0$, the counts are more easily understood in a low-density universe. Longair's claim that the source-counts provide evidence of a truncation in the density of sources beyond a redshift of 3 or 4 can be firmly repudiated. The effect of such a truncation is investigated. A truncation beyond a redshift of 10 would have a negligible effect: one at a redshift of 5 would blur the distinction between the cosmological models, as also does the statistical uncertainty in the observed luminosity function (section 11), and the effect of electron scattering (section 12).

In section 13 the effect of the dependence of spectral index on luminosity is found to be slight: a dependence of spectral index on epoch would have a similar effect to a modification of the rate of evolution.

Finally, in section 14 it is found to be impossible to account for the observed counts with exponential density evolution,

even with an arbitrary truncation, provided this truncation is independent of radio luminosity. However, as discussed in section 2, density evolution with a luminosity-dependant truncation will look very like luminosity evolution, and this possibility will be examined in Chapter IV.

1. Source models and types of evolution

Unless the magnetic field in quasars and radio-galaxies has an energy-density much greater than the black-body radiation at all epochs from which there is a significant contribution to the radio source-counts, then we have to take account of the dependence of the radio luminosity on magnetic field. In general this dependence will not be simple, but two cases are of particular interest:

(i) The magnetic field is the same for all sources (in a particular class), so that by equation (1) of section II.2 , $P \propto K$.

(ii) The particle energy, K , is the same in all sources, so that $P \propto H^{1+\alpha}$.

If there is no prospect of distinguishing between these two cases, there is no point in considering more complicated cases where both K and H depend on the phase of the source.

A source observed to have a particular luminosity at the present epoch would then have had different luminosities at earlier epochs if K and H vary with epoch. This could happen because galaxies or clusters of galaxies had different properties at earlier epochs, or as the result of interaction with intercluster material whose properties (density, magnetic field) change with epoch.

However this latter explanation will hardly serve for evolution in sources of class (a), the quasars and compact radio-galaxies, since the radio-emission comes from a region too small to know about intergalactic (or intercluster) conditions. Thus if interaction with a universal gas is the only cause of evolution in sources on a cosmological scale, we have to consider cosmological models in which quasars are uniformly distributed, i.e. certain Lemaître models. In paper III it was shown that a range of models can be found requiring no evolution in the quasars: but only the most extreme models ($q_0 < -2$) do not require evolution for the radio-galaxies.

In models with zero cosmical constant, on the other hand, evolution is required for both quasars and radiogalaxies. Interaction with a universal gas would then cause steeper evolution in radiogalaxies than quasars. This appears to be the case if power law evolutions are considered, though similar evolutionary rates are found in both classes of source if exponential evolutions are considered (see I.14).

The probability that sources of a particular luminosity class will exist may be a function of epoch, if there is evolution in the properties of the parent objects, or if the parent objects are still being formed over the epochs considered (so that the number density of parents varies with epoch). The number-density of sources will also

vary with epoch if the lifetime of sources does. For example, if the radiating life of the relativistic electrons is the controlling factor, the number density of sources will decrease with epoch due to inverse Compton losses, and strongly so once $10^{-5.65}(1+z)^2 > H$ (see chapter IV).

2. The dependence of the luminosity function on epoch

There are 3 completely general ways of describing the dependence of the coordinate number-density, η, on luminosity, $\mathcal{F}$, and redshift, z:

(i) slices of constant z, $\eta_z(\mathcal{F})$, i.e. the "luminosity function" at different epochs. This is useful if we have "density" evolution, with $\eta_z(\mathcal{F}) = j(z).\phi(\mathcal{F})$, i.e. the same relative distribution of luminosities is found at different epochs, but the density varies with epoch.

(ii) lines of constant number-density, $\eta(\mathcal{F}, z) =$ constant. This is useful in the case of "luminosity" evolution, where

$$\eta(\mathcal{F}, z) = \eta_0(\mathcal{F} - k(z)),$$

so these lines of constant η are parallel in the $\mathcal{F}$ - z plane. This is the case where the probability of occurrence, and the age, of sources of a particular type are independent of epoch, but the luminosity varies with epoch.

(iii) slices of constant luminosity, $\eta_{\mathcal{F}}(z)$, or "luminosity dependent density evolution". This is useful if we have density evolution truncated at a redshift dependent on luminosity, $z^*(\mathcal{F})$, for example where the luminosity of sources is dependent on magnetic field.

While these 3 methods of description are completely equivalent, the particular forms of evolution described above as "luminosity" and "density" evolution are not (though in Chapter I we saw that it is as yet difficult to rule out either type of evolution for any class of source). Note that if there exists a minimum luminosity for a class of source with "luminosity" evolution, then from viewpoint (iii) there is a luminosity-dependent truncation in the density of sources. But this is not the natural viewpoint for this type of evolution.

If the luminosity function has a power-law dependence on luminosity at the present epoch, say

$$\log_{10} \eta(\mathcal{F},0) = b - a\mathcal{F}, \quad \mathcal{F}_1 \leq \mathcal{F} \leq \mathcal{F}_2, \quad a > 0,$$

then in density evolution:

$$\log_{10} \eta(\mathcal{F}, z) = b + \log_{10} j(z) - a\mathcal{F}, \quad \mathcal{F}_1 \leq \mathcal{F} \leq \mathcal{F}_2$$

while in luminosity evolution:

$$\log_{10} \eta(\mathcal{F}, z) = b - a(\mathcal{F} - k(z)), \quad \mathcal{F}_1 + k(z) \leq \mathcal{F} \leq \mathcal{F}_2 + k(z).$$

So if $\log_{10} j(z) = a.k(z)$ both types of evolution give the same number-density for $\mathcal{F}_1 + k(z) \leq \mathcal{F} \leq \mathcal{F}_2$

(assuming $\log_{10} j(z)$ and $k(z)$ are both positive if $z > 0$).

However they are not <u>equivalent</u>, because they give different densities in the ranges $\mathcal{F}_1 \leq \mathcal{F} \leq \mathcal{F}_1 + k(z)$ and

$\mathcal{F}_2 \leq \mathcal{F} \leq \mathcal{F}_2 + k(z)$.

We now consider the effects on source-counts of cosmological model, evolutionary hypothesis, and dispersions in luminosity and spectral shape.

3. Number-counts for sources with the same luminosity and spectra

3.1. The condition that the number-count slope be less than 1.5

Let $N_\nu(f)$ be the number of sources brighter than S at frequency ν, per steradian, where $f = \log_{10} S$, and define

$$x_\nu(f) = - \frac{d \log_{10} N_\nu(f)}{d f}$$, the number-count slope.

Then if the sources have power law spectra, with spectral index α, and monochromatic luminosity P_ν (w/Hz/ster), by 1. (11)

$$N_\nu(f) = \eta_0 R_0^3 \mathcal{V}(z)$$

where

$$\mathcal{F}_\nu = \log_{10} P_\nu = f + 2 \log_{10} D(z) + (\alpha - 1) \log_{10} (1 + z) \qquad (1)$$

$D(z) = R_0 \, v \, (1 + z)$, the luminosity distance,

$$v = \frac{r}{1 + \frac{1}{4} k r^2}$$

$$\mathcal{Y}(z) = \int_0^{r(z)} \frac{r^2\,dr}{(1+\frac{1}{4}kr^2)^3} \quad .$$

For $k = -1$, $v = \sinh \chi$, $\mathcal{Y} = \frac{1}{2}\{ v\sqrt{1+v^2} - \log_e (v + \sqrt{1+v^2}) \}$

0, $v = \chi$, $\mathcal{Y} = v^3/3$ (2)

$+1$, $v = \sin \chi$, $\mathcal{Y} = \frac{1}{2}\{ \chi - \sin \chi \cos \chi \}$

where

$$\chi = \frac{c}{R_0 H_0} \int_1^{1+z} \frac{dx}{\sqrt{2q_0 x^3 + (1+q_0-3q_0)x^2 + q_0 - q_0}}$$

and

$$\frac{R_0 H_0}{c} = |3q_0 - q_0 - 1|^{-1/2}, \quad k \neq 0 \qquad (3)$$

$$= 1, \quad k = 0$$

From (1) and (3),

$$f = \text{const.} - 2\log_{10} v + \log_{10} |3\chi_0 - q_0 - 1| - (1+\alpha)\log_{10}(1+z) \qquad (4)$$

so that if $\mathcal{J} \leq v^3/3$ and $\frac{dv}{dz} \geq 0$ all z (and if $\alpha \geq -1$),

it is clear that $x_v(f) \leq 1.5$ all f. Obviously this condition is satisfied for $k = 0$, by (2).

If $k = -1$, $\frac{d\mathcal{J}}{dv} = \frac{v^2}{\sqrt{1+v^2}} < \frac{d}{dv}(v^3/3)$, all $v \neq 0$

and when $v = 0$, $\mathcal{J} = 0$, so $\mathcal{J} < v^3/3$ all $v > 0$.

Also $\frac{dv}{dz} = \cosh \chi \cdot \frac{d\chi}{dz} \geq 0$ all z,

so $x \leq 1.5$ for all models with $k \leq 0$.

But if $k = +1$, $(4n-1)\pi/2 < \chi < (4n+1)\pi/2$, n an integer,

$$\frac{d\mathcal{J}}{dv} = \frac{v^2}{\sqrt{1-v^2}} > \frac{d}{dv}(v^3/3), \quad v \neq 0.$$

In fact $|\mathcal{J}| > \frac{|v|^3}{3}$ all v.

Moreover $\frac{dv}{dz} = \cos\chi \cdot \frac{d\chi}{dz}$

< 0 when $(4n + 1)\,\pi/2 < \chi < (4n + 3)\,\pi/2$.

In fact $x_\nu(f) \longrightarrow \infty$ when $\frac{2}{v}\frac{dv}{dz} + \frac{1+a}{1+z} = 0$,

or $\tan\chi = \frac{-2(1+z)}{1+a} \cdot \frac{d\chi}{dz}$,

and there will certainly exist such a solution if

$\chi_{z \longrightarrow \infty} > \pi$.

Models of this type, in which the antipole is observable, are discussed in paper III. We note here that even if $\chi(\infty) < \pi$, x could be greater than 1.5.

If the cosmological constant is zero, $k = +1$ corresponds to $q_0 > \frac{1}{2}$, and (99)

$$v(z) = \sqrt{2q_0 - 1}\left\{\frac{q_0 z + (q_0 - 1)(\sqrt{1 + 2q_0 z} - 1)}{q_0^2 (1+z)}\right\},$$

so

$v(\infty) = 1$ if $q_0 = 1$ i.e., $\chi(\infty) = \pi/2$

and

$v(\infty) \longrightarrow 0$ as $q_0 \longrightarrow \infty$, i.e., $\chi(\infty) \longrightarrow \pi$.

Even though v is given explicitly, it does not seem possible to prove the result that seems evident from numerical computations, that $x \leq 1.5$ for all f in all models with $\Lambda = 0$, and that for given f, or given $N_\nu(f)$, $x_\nu(f)$ decreases as q_0 increases.

3.2 Asymptotic slope in general model

This will be important when interpreting the observed source-counts to low flux-level. We consider first models with $k = +1$: then

$$x = \pm \frac{v^3}{\mathcal{S}\sqrt{1 - v^2}\,[2 + \frac{1+\alpha}{1+z}\, v\, \frac{dz}{dv}]}$$

$+$ if $(4n - 1)\,\pi/2 < \chi < (4n + 1)\,\pi/2$

$-$ if $(4n + 1)\,\pi/2 < \chi < (4n + 3)\,\pi/2$

and

$$\frac{1+z}{v}\frac{dv}{dz} = (1+z)\cot\chi\sqrt{\frac{3\sigma_0 - 1 - q_0}{2\sigma_0(1+z)^3 + (1+q_0-3\sigma_0)(1+z)^2 + \sigma_0 - q_0}}$$

$\therefore$

$\longrightarrow 0$ as $z \longrightarrow \infty$ if $\sigma_0 \neq 0$ and $\chi(\infty) \neq n\pi$

so $x \longrightarrow 0$ if $\sigma_0 \neq 0$ and $\chi(\infty) \neq n\pi$.

$\sigma_0 \neq 0$, $\chi(\infty) = n\pi$:

$$\text{for } z \gg 1, \quad x \sim \frac{\pm v^3(-1)^n}{n\pi/2\,[2 + (1+a)\sqrt{2\sigma_0(1+z)}\,v(-1)^n]}$$

$\longrightarrow 0$ as $z \longrightarrow \infty$.

$$k = 0, \quad x = \frac{3}{2 + (1+a)\frac{v}{Z}\frac{dZ}{dv}} = \frac{3}{2 + (1+a)\frac{v}{Z}\sqrt{2\sigma_0 Z^3 + 1 - 2\sigma_0}}$$

$\longrightarrow 0$ as $Z \longrightarrow \infty$ if $\sigma_0 \neq 0$.

$$k = -1, \quad x = \frac{v^3}{\mathfrak{I}\sqrt{1+v^2}\,[2 + (1+a)\frac{v}{Z}\frac{dZ}{dv}]}$$

and

$$\frac{Z}{v}\frac{dv}{dZ} = Z \cdot \coth \chi \cdot \sqrt{\frac{1 + q_0 - 3\Omega_0}{2\Omega_0 Z^3 + (1 + q_0 - 3\Omega_0)Z^2 + \Omega_0 - q_0}}$$

$\longrightarrow > 0$ as $Z \longrightarrow \infty$ if $\Omega_0 \neq 0$,

so $x \longrightarrow 0$ as $Z \longrightarrow \infty$.

$\Omega_0 = 0$: $q_0 > -1$: $\frac{Z}{v}\frac{dv}{dZ} \sim \coth \chi \longrightarrow 1$ as $Z \longrightarrow \infty$

$$\mathcal{V} \sim \frac{v^2}{z} \quad \text{so} \quad x \longrightarrow \frac{2}{2 + (1 + \alpha)} = \frac{2}{3 + \alpha} \quad \text{as} \quad Z \longrightarrow \infty$$

$q_0 = -1$: $\frac{Z}{v}\frac{dv}{dZ} \longrightarrow 1$ as $Z \longrightarrow \infty$, $\mathcal{V} = v^3/3$

so $x \longrightarrow \frac{3}{3 + \alpha}$.

Thus, leaving aside models on or to the left of the Eddington-Lemaître locus in the $\Omega_0 - q_0$ plane (for which models there exists a finite maximum redshift) the asymptotic number-count slope is zero unless $\Omega_0 = 0$. It is also zero for the steady-state model, since $\mathcal{V} \sim \log_e Z$ for large Z, and $v = Z - 1$, so

$$x \sim \frac{1/\log_e Z}{3 + \alpha} \longrightarrow 0.$$

3.3 Counts with exponential luminosity evolution

$$\mathcal{F}(z) = \mathcal{F}(0) + Z_L \cdot \log_{10} e \cdot (1 - 1/Z)$$

$$k = 0: \qquad x = \frac{\frac{3}{r}\frac{dr}{dZ}}{\frac{2}{r}\frac{dr}{dZ} + \frac{1+\alpha}{Z} - \frac{Z_L}{Z^2}}$$

e.g.

$$\text{ES}: \quad r = 2\left[1 - Z^{-1/2}\right], \quad x = \frac{3}{2 + 4\left[Z^{1/2} - 1\right] - \frac{2Z_L\,(Z^{1/2} - 1)}{Z}}$$

$$\text{S}: r = Z - 1, \quad x = \frac{3}{2 + \frac{2(Z-1)}{Z} - \frac{Z_L\,(Z-1)}{Z^2}}$$

$$k = +1: \qquad x = \frac{v^3}{\gamma\sqrt{1 - v^2}\left[2 + (1+\alpha)\frac{v}{Z}\frac{dZ}{dv} - \frac{Z_L}{Z^2}\frac{v}{Z}\frac{dZ}{dv}\right]}$$

$$k = -1: \quad x = \frac{v^3}{\mathcal{J} \sqrt{1+v^2}\,[\,2 + (1 + a - \frac{Z_L}{Z^2})\ \frac{v}{Z}\ \frac{dZ}{dv}\,]}$$

e.g. in the Milne model:

$$v = \frac{Z^2 - 1}{2Z}, \qquad \frac{dv}{dZ} = \frac{Z^2 + 1}{2Z^2}, \qquad \sqrt{1+v^2} = \frac{Z^2 + 1}{2Z}$$

$$\mathcal{J} = \{\ \frac{Z^4 - 1}{8Z^2} - \frac{\log_e Z}{2}\ \}$$

$$x = \frac{(Z^2 - 1)^3}{4Z^2 (Z^2 + 1)\ \{\ Z^2/8 - 1/8Z^2 - \log_e Z/2\ \}\ [\,2 + (1+a - \frac{Z_L}{Z^2})\ \frac{Z^2 - 1}{Z^2 + 1}\,]}$$

3.4 Counts with exponential density evolution

$$k = 0: \quad \mathcal{J}'(z) = \int_1^Z r^2 \cdot e^{Z_D(1 - 1/Z)} \cdot dr$$

e.g. in the Einstein de Sitter model:

$$\mathcal{J}'(z) = 4 \int_1^Z (1 - Z^{-1/2})^2 \, e^{Z_D(1-1/Z)} \, Z^{-3/2} \, dZ$$

Let $x = Z_D/Z$, then $\mathcal{J}'(z) = 4 . e^{Z_D} . Z_D \int_{Z_D/Z}^{Z_D} \{ \frac{1}{Z_D^{3/2} x^{1/2}} -$

$$- \frac{2}{Z_D^2} + \frac{x^{1/2}}{Z_D^{5/2}} \} e^{-x} \, dx$$

$$= 4e^{Z_D} [(\frac{1}{Z_D^{1/2}} + \frac{1}{2Z_D^{3/2}}) 2 \int_{\sqrt{Z_D/Z}}^{\sqrt{Z_D}} e^{-t^2} \, dt$$

$$+ \frac{1}{Z_D^{3/2}} \{ \sqrt{\frac{Z_D}{Z}} \, e^{-Z_D/Z} - \sqrt{Z_D} \, e^{-Z_D} \}$$

$$+ \frac{2}{Z_D} \{ - e^{-Z_D/Z} + e^{-Z_D} \}]$$

$$= 8e^{Z_D} (\frac{1}{Z_D^{1/2}} + \frac{1}{2Z_D^{3/2}}) \int_{\sqrt{Z_D/Z}}^{\sqrt{Z_D}} e^{-t^2} \, dt$$

$$\frac{4}{Z_D} (\frac{1}{Z^{1/2}} - 2) \, e^{Z_D(1 - \frac{1}{Z})} + 4/Z_D .$$

in the de Sitter model:

$$\mathcal{J}'(z) = \int_1^Z (Z-1)^2 \, e^{Z_D(1-1/Z)} \, dZ$$

$$= e^{Z_D(1-1/Z)} \left[Z^3/3 - Z^2(Z_D/6+1) + Z(Z_D^2/6 + Z_D + 1)\right] - Z_D^2/6 - 5Z_D/6 - \frac{1}{3}$$

$$- Z_D \, e^{Z_D} (Z_D^2/6 + Z_D + 1) \left[\gamma(1,Z_D) - \gamma(1, Z_D/Z) \right]$$

where $\gamma(a,x) = \int_0^x e^{-y} y^{a-1} \, dy$ is the incomplete γ function.

$$k = -1: \quad \mathcal{J}'(z) = \int_1^Z e^{Z_D(1-1/Z)} \, \frac{r^2 \, dr}{(1 - \frac{1}{4} r^2)^3}$$

e.g. in the Milne model:

$$r = \frac{2(Z-1)}{Z+1}, \quad \mathcal{J}'(z) = \int_1^Z e^{Z_D(1-1/Z)} \left\{ \frac{Z}{4} - \frac{1}{2Z} + \frac{1}{4Z^3} \right\} dZ$$

$$= \frac{e^{Z_D(1 - 1/Z)}}{8} \left\{ Z^2 - ZZ_D + \frac{2}{Z_D^3} + \frac{2}{Z_D Z} \right\} - \frac{1}{4Z_D^2} - \frac{1}{4Z_D} + \frac{Z_D}{8} - \frac{1}{8}$$

$$+ (Z_D/8 - 1/2\, Z_D) [\gamma(1, Z_D) - \gamma(1, Z_D/Z)].$$

Figs. 18a,b and c shows log N - log S curves for 3 cosmological models, the Einstein de Sitter (E), Milne (M) and de Sitter (S) models, (i) with no evolution (ii) with exponential luminosity evolution, $Z_L = 6$ (iii) with exponential density evolution $Z_D = 10$, these parameters being consistent with the analysis of Chapter I for quasars and radio-galaxies.

The curves are labelled with values of redshift, and it will be seen that while the curves with evolution have similar slopes in the range $z < 1$, they differ greatly at large redshift. The luminosity evolution curves show a fairly rapid decrease of slope at faint fluxes, and the differences between the 3 models are much more marked than for the curves without evolution. The density evolution curves show no particularly rapid decrease of slope, and differ among themselves less than the curves without evolution. Thus there is little prospect of

explaining the observed counts on the basis of exponential density evolution, and this is confirmed by more detailed analysis. With exponential luminosity evolution, on the other hand, there is not only the prospect of explaining the counts without any cutoff at some redshift Z^*, but also the prospect of distinguishing between cosmological models.

3.5 Counts for small redshift.

Using expansions of $\mathcal{V}(z)$ and $D(z)$ as power series in z (27), it is easy to see that when the effects of evolution are included (either power-law or exponential), to the first order in z:

$$\log_{10} N(f) = \text{const.} + 3 \log_{10} z + \frac{3}{2}\left(\frac{Q_D}{2} - q_0 - 1\right)z$$

$$-f = \text{const.} + 2 \log_{10} z + (\alpha - q_0 - Q_L)\, z ,$$

both independent of Ω_0,

where Q_D is the parameter for density evolution and Q_L is the parameter for luminosity evolution.

To this order in z,

$$x = \frac{3}{2}\left[1 + z\left\{\frac{Q_D + 2Q_L}{4} - \frac{1+\alpha}{2}\right\}\right] \qquad (5)$$

The interesting point is that this is independent of σ_0 and q_0 (the steady-state theory, on the other hand, corresponds to $Q_L = 0$, $Q_D = -3$).

Fig. 19 shows the exact dependence of x on z for four cosmological models: the Einstein-de Sitter, Milne, de Sitter and Eddington-Lemaitre ($Z_m = 2.95$) models, together with a histogram of the visual magnitudes of strong 3C radio-galaxies ($\mathcal{F} > -27$) and the corresponding redshifts as estimated by equation (14) of 1.14. The dependence of x on a cosmological model over the range of z of interest for these objects is slight and equation (5) is a reasonable estimate. The median z for these objects is 0.17: substituting this, and the value $x \sim 1.8$ obtained in 1.14, we find

$$Q_D + 2Q_L \sim 10 \qquad (6)$$

which agrees very well the parameters found directly, by means of the modified luminosity - volume test, in 1.14.

4. Sources have the same spectral index, but a dispersion in luminosity

(i) no evolution:

$$\eta(\mathcal{F}, Z) = \eta_0 \, \Phi(\mathcal{F}) \quad \text{where} \quad \int_{-\infty}^{\infty} \Phi(\mathcal{F}) \, d\mathcal{F} = 1 \qquad (7)$$

Let $n_f(\mathcal{F}) \, d\mathcal{F}$ be the number of sources brighter than f having $\log_{10} P$ between $\mathcal{F}$ and $\mathcal{F} + d\mathcal{F}$, so

$$N(f) = \int_{-\infty}^{\infty} n_f(\mathcal{F}) \, d\mathcal{F} \qquad (8)$$

then $$n_f(\mathcal{F}) = \Phi(\mathcal{F}) \cdot \eta_0 R_0^3 \cdot \mathcal{J}(z) \qquad (9)$$

where $\mathcal{J}(z)$ is defined by 1.3.(8)

and

$$\mathcal{F} = f + 2 \log_{10} D(z) + (\alpha - 1) \log_{10} (1 + z) \qquad (10)$$

Now if all sources had the same luminosity $\mathcal{F}_0$

$$N(f) = \eta_0 R_0^3 \, \mathcal{J}(z) = N_0(f) \quad , \text{ say} \qquad (11)$$

where $\mathcal{F} = \mathcal{F}_0$ in equation (10).

In the general case

$$N(f) = \int_{-\infty}^{\infty} \eta_f(\mathcal{F})\, d\mathcal{F} = \int_{-\infty}^{\infty} N_0(f + \mathcal{F}_0 - \mathcal{F})\, \varphi(\mathcal{F})\, d\mathcal{F} \qquad (12)$$

This is the "convolution relation" referred to by Gower (17) but not explicitly stated by him.

(ii) density evolution:

$\eta(\mathcal{F}, z) = \eta_0 \cdot j(z) \cdot \varphi(\mathcal{F})$, where $j(0) = 1$

Equation (9) now becomes

$$n_f(\mathcal{F}) = \varphi(\mathcal{F}) \cdot \eta_0 R_0^3 \cdot \mathcal{J}'(z) \qquad (13)$$

where $\mathcal{J}(z) = \int_0^z j(x) \cdot d\mathcal{J}(x)$,

and (11) and (12) become

$$N_0(f) = \eta_0 R_0^3 \cdot \mathcal{J}'(z) \qquad (14)$$

$$N(f) = \int_{-\infty}^{\infty} N_0 (f + \mathcal{F}_0 - \mathcal{F}) . \varphi(\mathcal{F}) \, d\mathcal{F} ,$$

as before.

(iii) <u>luminosity evolution:</u>

$$\eta (\mathcal{F}, z) = \eta_0 . \varphi \{ \mathcal{F} - k(z) \}$$

where $k(0) = 0$.

Then

$$N(f) = \int_{-\infty}^{\infty} d\mathcal{F} \{ \int_0^z \eta_0 R_0^3 . \varphi \{ \mathcal{F} - k(x) \} . d\mathcal{V}(x)$$

$$= \int_{-\infty}^{\infty} d\mathcal{F}' \{ \int_0^z \eta_0 R_0^3 . \varphi (\mathcal{F}') . d\mathcal{V}(x),$$

where $\mathcal{F}' = \mathcal{F} - k(x)$,

$$= \int_{-\infty}^{\infty} N_0 (f + \mathcal{F}'_0 - \mathcal{F}') \varphi (\mathcal{F}') \, d\mathcal{F}'$$

where

$$\mathcal{F}'_0 = f + 2 \log_{10} D(z) + (\alpha - 1) \log_{10} (1 + z) + k(z) \qquad (15)$$

Thus the convolution relation holds for both luminosity and density evolution, and in fact for any evolution of the form

$$\eta(\mathcal{F},z) = \eta(z) \cdot \varphi\{\mathcal{F} - k(z)\}.$$

Relations (9) and (13), which we can summarize

$$n_f(\mathcal{F}) = N_0(f + \mathcal{F}_0 - \mathcal{F}) \cdot \varphi(\mathcal{F}) \qquad (16)$$

only hold for density evolution. But even for luminosity evolution, this relation holds with $\mathcal{F}'$ for $\mathcal{F}$.

If we can work out the luminosities of all sources down to some given flux-level, then the L.H.S. of (16) is an observable quantity. If we postulate the form of $N_0(f)$, then we can deduce the form of $\varphi(\mathcal{F})$. This is presumably the procedure followed by Gower.

From (16), the distribution $n_f(\mathcal{F})$ can, for given f, have a maximum at $\mathcal{F} = \tilde{\mathcal{F}}(f)$ if

$$\frac{d}{d\mathcal{F}}\{\varphi(\tilde{\mathcal{F}})\} / \varphi(\tilde{\mathcal{F}}) = \frac{\frac{d}{df} N_0(f + \mathcal{F}_0 - \tilde{\mathcal{F}})}{N_0(f + \mathcal{F}_0 - \tilde{\mathcal{F}})} = -x_0(f + \mathcal{F}_0 - \tilde{\mathcal{F}}) \qquad (17)$$

where

$$x_0(f) = - \frac{d \log_{10} N_0(f)}{df}$$

E.g. (a) $\varphi(\mathcal{F}) \propto \exp(-a\mathcal{F})$, where a is a positive constant, then

$$x_0(f + \mathcal{F}_0 - \tilde{\mathcal{F}}(f)) = a$$

so

$$f - \tilde{\mathcal{F}}(f) = \text{constant} = x_0^{-1}(a) - \mathcal{F}_0.$$

The condition that the turning-point be a maximum is easily show to be

$$\frac{dx_0(f)}{df} > 0.$$

Thus, as f decreases, so also does $\tilde{\mathcal{F}}(f)$,

i.e. the peak contribution to source-counts down to any flux level comes from sources with a luminosity that decreases with decreasing flux-density.

E.g. (b) $\varphi(\mathcal{F}) \propto \exp\left\{ - \frac{(\mathcal{F} - \mathcal{F}_0)^2}{2\sigma^2} \right.$

then

$$x_0 (f + \mathcal{F}_0 - \tilde{\mathcal{F}}(f)) = \frac{\tilde{\mathcal{F}}(f) - \mathcal{F}_0}{2} \quad , \quad \text{from (17),}$$

so

$$\frac{d\tilde{\mathcal{F}}(f)}{df} = \frac{2 \frac{dx_0}{df} \Big|_{f + \mathcal{F}_0 - \tilde{\mathcal{F}}(f)}}{1 + 2 \frac{dx_0}{df} \Big|_{f + \mathcal{F}_0 - \tilde{\mathcal{F}}(f)}}$$

> 0 if $\frac{dx_0}{df} > 0$ everywhere.

As above, this turning-point can be shown to be a maximum (the condition is

$$\frac{d}{d\mathcal{F}} \left\{ \frac{1}{\Phi(\mathcal{F})} \frac{d\Phi}{d\mathcal{F}} \right\} \Big|_{\tilde{\mathcal{F}}} < \frac{dx_0}{df} \Big|_{f + \mathcal{F}_0 - \tilde{\mathcal{F}}}).$$

While the luminosity function probably does not have exactly the form of either example above, the general point remains, that the main contribution to source-counts down to low flux-densities may come from a class of source which makes a negligible contribution at higher flux-levels.

To illustrate the properties of the convolution relation we adopt a slightly different approach to Gower. Rather than calculate the luminosity function from (16) we postulate that it is of the form (b) above, and calculate the number-counts for a wide range of parameters.

Like Gower (17), we suppose $N_0(f)$ has the form:

$$\log_{10} N_0(f) = x_1 (f_{00} - f_1), \quad f \geq f_{00} - F$$

$$= x_1 F + x_2 (f_{00} - F - f), \quad f < f_{00} - F$$

so that

$$x_0(f) = x_1, \quad f > f_{00} - F$$

$$= x_2, \quad f < f_{00} - F, \quad \text{with} \quad x_2 < x_1.$$

Then if

$$\varphi(\mathcal{F}) = \frac{1}{\sqrt{2\pi \sigma^2}} \exp\left\{ - \frac{(\mathcal{F} - \mathcal{F}_0)^2}{2\sigma^2} \right\}$$

it can be shown that (12) gives

$$N(f) = 10^{x_1(f_{00} - f) + \frac{x_1^2 \sigma^2 \log_e 10}{2}} \left\{ \frac{f - f_{00} + F - x_1 \sigma^2 \log_e 10}{\sigma} \right\}$$

$$+ 10^{(x_1 - x_2)F + x_2(f_{00} - f) + \frac{x_2^2 \sigma^2 \log_e 10}{2}} \cdot \left[1 - \Phi\left\{\frac{f - f_{00} + F - x_2 \sigma^2 \log_e 10}{\sigma}\right\}\right]$$

where

$$\Phi(x) = \frac{1}{\sqrt{2\pi}} \int_{-\infty}^{x} e^{-t^2/2}\, dt.$$

Writing

$$f_0 = f_{00} + \frac{x_1 \sigma^2 . \log_e 10}{2}, \quad \epsilon = f_0 - f,$$

$$N(f_0 - \epsilon) = 10^{x_1 \epsilon} \cdot \Phi\left\{\frac{F - \epsilon - x_1 \sigma^2 \log_e 10}{\sigma}\right\}$$

$$+10^{(x_1 - x_2)(F - x_2 \sigma^2 . \log_e 10) + x_2 \epsilon} \left[1 - \Phi\left\{\frac{F - \epsilon + (\frac{x_1}{2} - x_2) \sigma^2 . \log_e 10}{\sigma}\right\}\right]$$

$$= A + B, \text{ say.}$$

Then $x(f_0 - \epsilon) = \dfrac{x_1 A + x_2 B}{x_1 + x_2}$, a weighted mean

of A and B.

Note that

$$n_f(\mathcal{F}) = \frac{1}{\sqrt{2\pi\sigma^2}} \exp\left\{ - \frac{(\mathcal{F} - \mathcal{F}_0 - \sigma^2 x_1 \log_e 10)^2}{2\sigma^2} \right\}$$

$$\cdot 10^{x_1(f_{00} - f) + \frac{x_1^2 \sigma^2 \log_e 10}{2}} , \quad \mathcal{F} < \mathcal{F}_1.$$

$$= \frac{1}{\sqrt{2\pi\sigma^2}} \exp\left\{ - \frac{(\mathcal{F} - \mathcal{F}_0 - \sigma^2 x_2 \log_e 10)^2}{2\sigma^2} \right\}$$

$$\cdot 10^{(x_1 - x_2)F + x_2(f_{00} - f) + \frac{x_2^2 \sigma^2 \log_e 10}{2}} , \quad \mathcal{F} > \mathcal{F}_1 ,$$

where $\mathcal{F}_1 = f + \mathcal{F}_0 - f_{00} + F$,

which are Gaussians with peaks at $\mathcal{F}_0 + \sigma^2 x_i \log_e 10$,

$i = 1, 2$ respectively.

Thus if $f \gg \sigma^2 x_1 . \log_e 10 + f_{00} - F$

or if $f \ll \sigma^2 x_2 . \log_e 10 + f_{00} - F$,

the luminosity distribution will have the appearance of a simple Gaussian distribution. On the other hand if $\mathcal{F}_1$ falls in or near the interval $(\mathcal{F}_0 + x_2 \sigma^2 . \log_e 10 , \mathcal{F}_0 + x_1 \sigma^2 . \log_e 10)$, an asymmetric distribution will be produced.

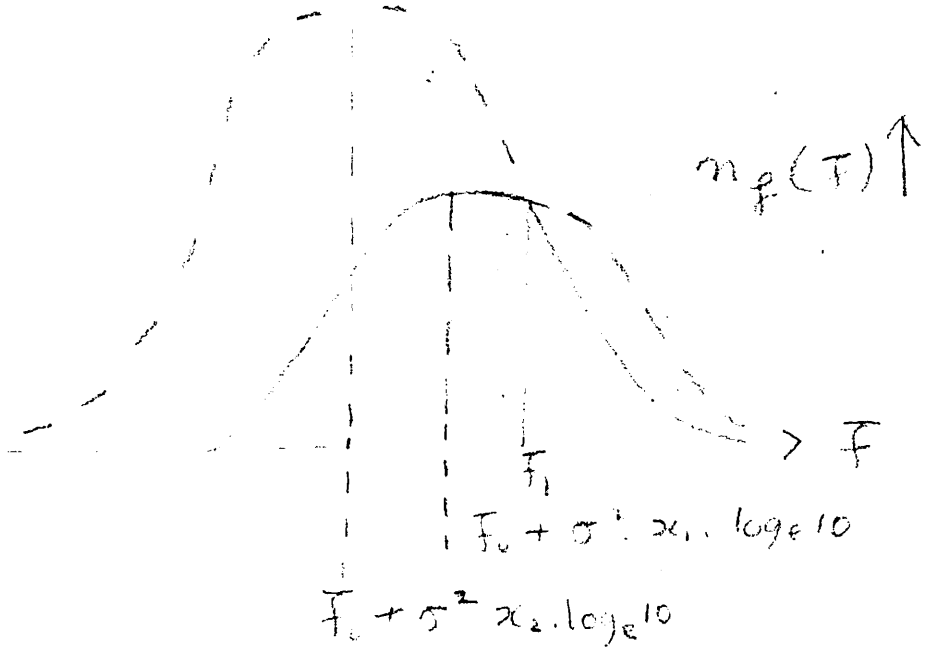

The luminosity distribution of Longair and Scott (100) is in fact quite well represented by a Gaussian, with $\sigma = 1 \pm .1$. But the situation illustrated in the figure cannot be ruled out because the high luminosity end of the distribution is very poorly determined, due to lack of complete redshift data for galaxies, and depends on cosmological model (and evolutionary hypothesis in the case of luminosity evolution).

Using a computer, the models which best fit the source-count data at 178 MHz have been selected from the grid of models

$\sigma = 0.9\ (0.05)\ 1.1$

$x_1 = 1.9\ (0.1)\ 2.1$

$x_2 = 0\ (0.2)\ 0.6.$

The counts were normalized so that $N(-24.1) = 1$, which determines f_0 in each case.

For almost all models a value of F could be found which gave reasonable consistency (to $\pm$ 0.06 in log N) with the data down to $f = -26.6$, the limit of the Ryle-Neville survey (101) and the range considered by Gower (17). The value of F ranged mainly between 3 and 4.

However, very few of these models gave a satisfactory fit to the data down to the 5C level. The best models are shown in Fig. 20, log N - f.

They have the parameters:

		x_1	x_2	F	$T_{178}(^oK)$	f_0
A	0.9	2.0	0.0	2.9	15.5	-24.08
B	0.9	2.0	0.6	2.8	22	-24.08
C	0.95	2.0	0.2	3.0	17.5	-24.07
D	1.0	2.1	0.0	3.0	19	-24.04
E	1.1	2.1	0.0	3.3	23	-24.02

Marginally the best fit is the model A. The corresponding integrated background temperature (related to $\int SdN$ - see III.9) is given in column 6, and is consistent with Bridle's (94) estimate of $30^o \pm 7^o$ for sources with spectral index 0.8 (slightly on the low side).

In the case of density evolution we can determine the redshift of the break in $\log N_0$, in any cosmological model, from

$$2\log_{10}D(z) + (\alpha - 1)\log_{10}(1+z) = \mathcal{F}_0 - f_{00} + F$$

$$= (\mathcal{F}_0 + \tfrac{1}{2}\sigma^2 x_1 . \log_e 10) - f_0 + F - \tfrac{1}{2}\sigma^2 x_1 . \log_e 10 . \qquad (18)$$

provided $\mathcal{F}_1(-25)$ is appreciably greater than $(\mathcal{F}_0 + \tfrac{1}{2}\sigma^2 x_1 . \log_e 10)$ we can identify the latter quantity with the peak luminosity at $\mathcal{F} \sim -26$ obtained by Longair and Scott (100), and then for model A:

$$2\log D(z) + (\alpha - 1)\log_{10}(1+z) \sim -26 + 24.08 + 2.9 - 1.87 = -0.89 \qquad (19)$$

so $z \sim 0.37$ if $q_0 = 1$

~ 0.29 if $q_0 = -1$.

A truncation in the number-density of sources at such small redshift seems quite inconsistent with the analysis of Chapter 1.

On the other hand if $N_0(f)$ is interpreted in terms of luminosity evolution, the truncation redshift would become very much larger, since the L.H.S. of (18) would then have the evolutionary factor subtracted from it.

However, with the above parameters (model A), $\mathcal{F}_1(-25) = -25.87$, only just above the peak at -26, so the observed distribution should look narrower than a Gaussian with $\sigma = 0.9$. This again makes density evolution unlikely.

Although this type of argument is of some interest, indicating that density evolution alone is unlikely to be satisfactory, its independence of cosmological model, and its assumption that all sources have the same evolutionary properties, render the method of little use in gaining insight into the meaning of the radio source-counts.

5. Sources have dispersion in spectral index and luminosity.

Let $\eta(\mathcal{F}, z)\, d\mathcal{F}$ be the number of sources having $\log_{10} P$ between $\mathcal{F}$ and $\mathcal{F} + d\mathcal{F}$ at epoch z, per unit comoving coordinate volume, and let $q(\alpha, \mathcal{F}, z)\, d\alpha$ be the fraction of sources of luminosity $\mathcal{F}$ having spectral index between α and $\alpha + d\alpha$, at epoch z, so $\int_{-\infty}^{\infty} q(\alpha, \mathcal{F}, z)\, d\alpha = 1$ all $\mathcal{F}$, z.

Define $\bar{\alpha}(\mathcal{F}, z) = \int_{-\infty}^{\infty} \alpha\, q(\alpha, \mathcal{F}, z)\, d\alpha$

$$\sigma_\alpha^2(\mathcal{F}, z) = \int_{-\infty}^{\infty} \{\alpha - \bar{\alpha}(\mathcal{F}, z)\}^2 q(\alpha, \mathcal{F}, z)\, d\alpha$$

and let $\mathcal{V}(z)$ be defined as in I.3.(11).

Then the number of sources per steradian brighter than

f ($= \log_{10} S$, where S is the flux density) is given by

$$N(f) = \int_{-\infty}^{\infty} da \int_{-\infty}^{\infty} d\mathcal{F} \int_{0}^{z} d(\quad) \, q(a,\mathcal{F},\quad) \cdot \left(\frac{R_0}{c_0}\right)^3 \cdot \frac{d\mathcal{V}(\quad)}{dz}$$

where $\mathcal{F} = f + 2\log_{10} D(z) + (a-1)\log_{10}(1+z)$, as in 3.1.(1).

We shall suppose $q(\mathcal{F},z) = q_0 \cdot a(z) \cdot \phi(\mathcal{F}')$

where $\mathcal{F}' = \mathcal{F} - \log_{10} b(z)$

$$\int_{-\infty}^{\infty} \phi(x)\, dx = 1$$

and $a(0) = b(0) = 1$.

Writing $q'(a, \mathcal{F}', \quad) \equiv q(a, \mathcal{F}, \quad)$

and $d\mathcal{V}'(\quad) \equiv a(\quad)\, d\mathcal{V}(\quad)$

then

$$N(f) = \eta_0 \left(\frac{R_0}{Ct_0} \right)^3 \int_{-\infty}^{\infty} \varphi(\mathcal{F}')\, d\mathcal{F}' \left[\int_{-\infty}^{\infty} da \int_0^z q'(a, \mathcal{F}', z) \cdot \frac{d\, \mathcal{D}'(z)}{dz}\, dz \right].$$

We shall see that if $q'(a, \mathcal{F}', z)$ is independent of $\mathcal{F}', z$, and $\sigma_a^2 \ll 1$, then the quantity in the square brackets is approximately $\mathcal{D}'\{z(\bar{a})\}$, where $z(\bar{a})$ is the solution of

$$\mathcal{F}' = \mathcal{F} - \log_{10} b(z) = f + 2 \log_{10} D(z) + (\bar{a} - 1) \log_{10} (1 + z). \quad (20)$$

We shall then consider the case $\bar{a} = \bar{a}(\mathcal{F}', z)$, and show that the effect on source counts of such a dependence of spectral index on luminosity and epoch is likely to be small.

Dropping primes, if $q(a, \mathcal{F}, z)$ is independent of $\mathcal{F}$ and z,

$$N(f) = \eta_0 \left(\frac{R_0 H_0}{c} \right)^3 \int_{-\infty}^{\infty} \varphi(\mathcal{F})\, d\mathcal{F} \int_{-\infty}^{\infty} q(a)\, \mathcal{D}\{z(a)\}\, da$$

and

$$\mathcal{Y}\{z(a)\} = \mathcal{Y}\{z(\bar{a})\} + (a-\bar{a})\left.\frac{d\mathcal{Y}}{da}\right|_{a=\bar{a}}$$

$$+ \frac{(a-\bar{a})^2}{2!}\left.\frac{d^2\mathcal{Y}}{da^2}\right|_{a=\bar{a}} + \cdots \qquad (21)$$

$$\therefore \int_{-\infty}^{\infty} q(a)\,\mathcal{Y}\{z(a)\}\,da = \sum_{0}^{\infty} J_n \left.\frac{d^n\mathcal{Y}}{da^n}\right|_{a=\bar{a}} \qquad (22)$$

where $J_n = \int_{-\infty}^{\infty} \frac{(a-\bar{a})^n}{n!}\,.q(a)\,da$

and $q(a)$ has to be such that the integrals J_n exist, for the expansion (21) to be valid. The first two non-zero terms of (22) are

$$\mathcal{Y}\{z(\bar{a})\} + \frac{\sigma_a^2}{2}\left.\frac{d^2\mathcal{Y}}{da^2}\right|_{a=\bar{a}}$$

and we shall evaluate the other terms under the assumption that

$$q(a) = \frac{1}{\sqrt{2\pi\sigma_a^2}} \exp\left\{\frac{-(a-\bar{a})^2}{2\sigma_a^2}\right\} \qquad (23)$$

which represents the observations well in the range 38 - 1400 MHz (50), with $\bar{\alpha} \sim 0.8$, $\sigma_\alpha \sim 0.15$.

Then

$$J_n = \frac{1}{\sigma_\alpha n! \sqrt{2\pi}} \int_{-\infty}^{\infty} (\alpha - \bar{\alpha})^n \exp\left\{ \frac{-(\alpha - \bar{\alpha})^2}{2\sigma_\alpha^2} \right\} d(\alpha - \bar{\alpha})$$

$$= \frac{1}{\sigma_\alpha n! \sqrt{2\pi}} \left\{ \left[-(\alpha - \bar{\alpha})^{n-1} \sigma_\alpha^2 \cdot \exp\left\{ \frac{-(\alpha - \bar{\alpha})^2}{2\sigma_\alpha^2} \right\} \right]_{-\infty}^{\infty} \right.$$

$$\left. + (n-1)\sigma_\alpha^2 \int_{-\infty}^{\infty} (\alpha - \bar{\alpha})^{n-2} \exp\left\{ \frac{-(\alpha - \bar{\alpha})^2}{2\sigma_\alpha^2} \right\} d\alpha \right\}$$

on integrating by parts,

$$= \frac{\sigma_\alpha^2}{n} J_{n-2} .$$

Now $J_1 = 0$ so $J_{2n+1} = 0$ all n

J_0 , so $J_{2n} = \alpha^{2n} / 2^n . n!$

So for the particular form of $q(\alpha)$ given by equation (23):

$$N(f) = \eta_0 \left(\frac{R_0 H_0}{C} \right)^3 \left\{ \mathcal{Y}(z(\bar{\alpha})) + \frac{\alpha^2}{2} \frac{d^2 \mathcal{Y}}{d\alpha^2} \Big|_{\alpha = \bar{\alpha}} \right.$$

$$\left. + \frac{\alpha^4}{2^2 . 2!} \frac{d^4 \mathcal{Y}}{d\alpha^4} \Big|_{\alpha = \bar{\alpha}} + \ldots \right\} .$$

Since $\alpha \sim 0.15$, the terms of order α^4 and higher are very small .

Now equation (20) gives

$$\alpha(z) = \frac{F - 2 \log_e v}{\log_e Z} - 1 \quad , \quad \text{where} \quad F = \frac{\mathcal{F} - f - 2 \log_{10} R_0}{\log_{10} e}$$

so

$$\frac{d\alpha}{dz} = \frac{- 2 v'/v - (\alpha + 1)/Z}{\log_e Z} = \frac{-1}{x \log_e Z} \frac{d \log_e \mathcal{Y}}{dZ} .$$

where

$$x = \frac{d \log_{10} N}{df} = \frac{- d \log_e \mathcal{Y}}{dZ} \Big/ - 2 v'/v - (\alpha + 1)/Z \quad .$$

Thus

$$\frac{d \mathcal{Y}}{d \alpha} = - x \, . \log_e \mathcal{Y} \, . \, \mathcal{Y}$$

and

$$\frac{d^2 \mathcal{Y}}{d \alpha^2} = \frac{1}{\alpha'} \frac{d}{dz} \left(\frac{d \mathcal{Y}}{d \alpha} \right)$$

$$= \frac{x \, . \log_e Z}{\frac{d \log_e \mathcal{Y}}{d z}} \left(\frac{dx}{dz} \, . \log_e \mathcal{Y} \, . \, \mathcal{Y} + \frac{x \, \mathcal{Y}}{Z} + x \, . \log_e Z \, . \, \frac{d \mathcal{Y}}{dz} \right)$$

$$= \frac{x x' (\mathcal{Y} \, . \log_e Z)^2}{\frac{d \mathcal{Y}}{dz}} + \frac{x^2 \mathcal{Y}^2}{\frac{d \mathcal{Y}}{dz}} \cdot \frac{\log_e Z}{Z} + \mathcal{Y} (x \log_e Z)^2$$

In the de Sitter model: $v = z$, $\mathcal{Y} = z^3/3$, $\mathcal{Y}' = z^2$,

$$x = \frac{3/z}{2/z + (1+\alpha)/(1+z)} = \frac{3(1+z)}{2 + z(3+\alpha)}$$

$$x' = \frac{-3(1+\alpha)}{\{2 + z(3+\alpha)\}^2}$$

so

$$\frac{d^2 y}{d\alpha^2} = \frac{-9(1+\alpha)(1+z)}{\{2+(3+\alpha)z\}^3} \cdot \frac{z^6 (\log_e Z)^2}{9z^2} + \frac{9(1+z)^2}{\{2+(3+\alpha)z\}^2} \cdot \frac{z^6 . \log_e Z}{9z^2(1+z)}$$

$$+ (\log_e Z)^2 \cdot \frac{z^3}{3}$$

$$= \frac{(1+z)z^3 \log_e Z}{\{2+z(3+\alpha)\}^2} \left\{ \frac{-(1+\alpha)z . \log_e Z}{2+z(3+\alpha)} + z + 3(1+z) . \log_e Z \right\}$$

$$\sim \frac{3z^3 \{\log_e (1+z)\}^2}{(3+\alpha)^2} \quad \text{for large } z.$$

Thus $N(f) \simeq n_0 \left(\frac{R_0 H_0}{c} \right)^3 . \mathcal{J}(z(\bar{a})) . \left\{ 1 + \frac{9 \cdot 2 \{ \log_e(1+z) \}^2}{2 (3 + \bar{a})^2} \right\}$

for faint f.

e.g. $Z = 100$, $\bar{a} = 0.8$, $\quad = 0.15 \longrightarrow \{ \} = 1.187$

so $\log_{10} N(f) - \log_{10} \mathcal{J}(z(\bar{a})) \sim 0.07$

(this corresponds to $f = \mathcal{F} - 7.6 = -33.6$ if $\mathcal{F} = -26$).

Fig. 21 shows $\log_{10} \left\{ 1 + \frac{2}{2} \frac{d^2 \mathcal{J}}{d a^2} \Big|_{a = \bar{a}} \right\} - f$

for ES,M,S models with exponential luminosity and density evolution ($Z_L = 6$, $Z_D = 10$) and $\mathcal{F} = -26$. Over the range of interest ($-24 > f > -28$) the effect of the dispersion in spectral indices is to increase the number of sources by less than 10 per cent in all cases and this is less than the effect of the uncertainty in $\bar{a}$.

In what follows we shall take $a = \bar{a}$.

6. Dependence of luminosity function on frequency.

Since only monochromatic source counts and luminosities are available, it is important to know whether it matters much at which

frequency we perform our analysis.

Let the number of sources at ν having $\log_{10} P_\nu$ between $\mathcal{F}_\nu$, $\mathcal{F}_\nu + d\mathcal{F}_\nu$, and spectral index (assumed constant for each source, i.e., independent of frequency) between α and $\alpha + d\alpha$ be

$$n_\nu(\mathcal{F})\, q_\nu(\alpha, \mathcal{F}_\nu)\, d\mathcal{F}_\nu\, d\alpha$$

where $\int_{-\infty}^{\infty} q_\nu(\alpha, \mathcal{F}_\nu)\, d\alpha = 1$ for all $\mathcal{F}_\nu$.

Since a source of luminosity $\mathcal{F}_\nu$ and spectral index α at frequency ν becomes one of luminosity $\mathcal{F}_\nu - \alpha \log_{10}(\nu_0/\nu)$ (and spectral index α) at frequency ν_0, the relation

$$n_\nu(\mathcal{F})\, q_\nu(\alpha, \mathcal{F}) = n_{\nu_0}(\mathcal{F} - \alpha \log_{10}(\nu_0/\nu))\, q_{\nu_0}(\alpha, \mathcal{F} - \alpha \log_{10}(\nu_0/\nu)) \tag{24}$$

holds identically.

Integrating with respect to a from $-\infty$ to $+\infty$:

$$\eta_\nu(\mathcal{F}) = \int_{-\infty}^{\infty} q_\nu(a, \mathcal{F} - a \log_{10} \nu_0/\nu)\, \eta_{\nu_0}(\mathcal{F} - a \log_{10} \nu_0/\nu)\, da \tag{25}$$

so

$$\frac{\partial \eta_\nu(\mathcal{F})}{\partial \log_{10} \nu} = \int_{-\infty}^{\infty} \frac{\partial}{\partial \mathcal{F}} \{ q_\nu(a, \mathcal{F} - a \log_{10} \nu_0/\nu)\, \eta_{\nu_0}(\mathcal{F} - a \log_{10} \nu_0/\nu) \}\, da$$

$$\longrightarrow \frac{\partial}{\partial \mathcal{F}} \{ \eta_\nu(\mathcal{F})\, \bar{a}_\nu(\mathcal{F}) \} \quad \text{as} \quad \nu_0 \longrightarrow \nu \tag{26}$$

where

$$\bar{a}_\nu(\mathcal{F}) = \int_{-\infty}^{\infty} q_\nu(a, \mathcal{F})\, a\, da$$

(provided q and η are sufficiently well-behaved functions).

Thus if $\bar{a}_\nu(\mathcal{F})$ is independent of $\mathcal{F}$ (for example if $q_\nu(a, \mathcal{F})$ is) then

$$\eta_\nu(\mathcal{F}) \text{ is a function of } \{ \mathcal{F} + \int \bar{a}_\nu\, d \log \nu \} \tag{27}$$

That is, the luminosity function at frequency ν is obtained from that at ν_2 simply by shifting the luminosity scale by

$$\int_{\nu_1}^{\nu_2} \bar{\alpha}_\nu \, d\log_{10} \nu .$$

But the relation (24) implies that not any $\eta_\nu(\mathcal{F})$ is permissible, since

$$\frac{\eta_\nu(\mathcal{F} - \alpha \log \nu/\nu_0)\, q_\nu(\alpha, \mathcal{F} - \alpha \log \nu/\nu_0)}{q_{\nu_0}(\alpha, \mathcal{F})}$$

must be independent of α

For example, suppose $\eta_{\nu_2}(\mathcal{F}) \propto \exp\left\{ - \frac{(\mathcal{F} - \bar{\mathcal{F}}_2)^2}{2\sigma_2^2} \right\}$

$$q_{\nu_2}(\alpha, \mathcal{F}) \propto \exp\left\{ - \frac{(\alpha - \bar{\alpha}_2)^2}{2\Sigma_2^2} \right\}$$

(independent of $\mathcal{F}$),

Then from (25)

$$\eta_{\nu_1}(\mathcal{F}) \propto \int_{-\infty}^{\infty} da \cdot \exp\left\{ - \frac{(\mathcal{F} - a \log \nu_2/\nu_1 - \bar{\mathcal{F}}_2)^2}{2\sigma_2^2} + \frac{(a - \bar{a}_2)^2}{2\Sigma_2^2} \right\}$$

$$= \int_{-\infty}^{\infty} \exp\{ - x(a) \} \, da \,, \quad \text{say.}$$

Let $f = \mathcal{F} - \bar{\mathcal{F}}_2$, $\quad = \log \nu_2/\nu_1$, and drop subscripts:

$$x(a) = \frac{f^2 - 2f a + a^2 \ldots}{2\ldots^2} + \frac{a^2 - 2a\bar{a} + \bar{a}^2}{2\Sigma^2}$$

$$= \frac{f^2}{2\ldots^2} - 2a\left\{ \frac{f}{2\ldots^2} + \frac{\bar{a}}{2\Sigma^2} \right\} + \frac{a^2}{2S^2}, \quad \text{where} \quad \frac{1}{S^2} = \frac{2}{\ldots^2} + \frac{1}{\Sigma^2}$$

i.e. $$S^2 = \frac{2\ldots^2 \Sigma^2}{\ldots^2 + \Sigma^2 \ldots^2}$$

$$= \frac{\{a - S^2[\frac{f}{2\ldots^2} + \frac{\bar{a}}{2\Sigma^2}]\}^2}{2S^2} + \frac{f^2}{2\ldots^2} - \frac{S^4(\frac{f}{2\ldots^2} + \frac{\bar{a}}{\Sigma^2})^2}{2S^2} + \text{const}$$

(28)

and so

$$\eta_{\nu_1}(\mathcal{F}) \;\alpha\; \exp\left\{ -\frac{f^2}{2}\left[\frac{1}{\sigma^2} - \frac{S^2\,\Sigma^2}{\sigma^4}\right] + f.\,\frac{S^2.\,\bar{\alpha}}{\sigma^2\,\Sigma^2}\right\}.$$

Now

$$\frac{1}{\sigma^2} - \frac{S^2\,\Sigma^2}{\sigma^4} = \frac{1}{\sigma^2 + \Sigma^2\,\Lambda^2} = \frac{S^2}{\sigma^2\,\Sigma^2}$$

so

$$\eta_{\nu_1}(\mathcal{F}) \;\alpha\; \exp\left\{ \frac{-(f - \bar{\alpha})^2}{2(\sigma^2 + \Sigma^2\,\Lambda^2)}\right\}$$

$$= \exp\left\{ \frac{-(\mathcal{F} - \bar{\mathcal{F}}_2 - \bar{\alpha}_2 \log \nu_2/\nu_1)^2}{2(\sigma_2^2 + \Sigma_2^2 \log_{10}^2 \nu_2/\nu_1}\right\} \qquad (29)$$

and this is of form (27) if and only if $\Sigma_2 = 0$.

In practice, for radio sources $\sigma \sim 1.0$, $\Sigma \sim .15$ at 178 MHz,

so

$$\left(\frac{\Sigma}{\sigma}\right)^2 \sim .02$$

andthe second term in the denominator of (29) is negligible for

$$| \log \nu / 178 | < 1 \cdot (\nu \text{ in MHz}).$$

Note also that

$$q_{\nu_1}(a, \mathcal{F}) \propto \exp\left\{ - x(a) + \frac{(f - \Delta \bar{a}_2)^2}{2(\sigma_2^2 + \Sigma_2^2 \Delta^2} \right\}$$

$$\propto \exp\left\{ \frac{-(a - \frac{\Delta f \Sigma_2^2 + \sigma^2 \bar{a}_2}{\sigma_2^2 + \Sigma_2^2 \Delta^2})^2}{2\sigma^2} \right\}, \quad \text{by (28)}$$

which is independent of $\mathcal{F}$ only if $\Sigma_2 = 0$.

Thus $q_\nu(a, \mathcal{F})$ independent of $\mathcal{F}$ at one frequency certainly does not imply $q_\nu(a, \mathcal{F})$ independent of $\mathcal{F}$ at any other frequency.

In fact if $q_\nu(a, \mathcal{F})$ is independent of $\mathcal{F}$ all ν then

$$\eta_{\nu_1}(\mathcal{F})\, q_{\nu_1}(a) = \eta_{\nu_2}(\mathcal{F} - a \log \nu_2 / \nu_1)\, q_{\nu_2}(a)$$

so

$$q_{\nu_1}(a) \cdot \frac{\partial \eta_{\nu_1}(\mathcal{F})}{\partial \mathcal{F}} = q_{\nu_2}(a) \frac{\partial \eta_{\nu_2}(\mathcal{F} - a \log \nu_2/\nu_1)}{\partial \mathcal{F}}$$

and

$$\frac{1}{\eta_{\nu_1}(\mathcal{F})} \cdot \frac{\partial \eta_{\nu_1}(\mathcal{F})}{\partial \mathcal{F}} \Big|_{\mathcal{F}} = \frac{1}{\eta_{\nu_2}(\mathcal{F})} \cdot \frac{\partial \eta_{\nu_2}(\mathcal{F})}{\partial \mathcal{F}} \Big|_{\mathcal{F}-a\log \nu_2/\nu}$$

Putting $a = 0$ implies $\frac{1}{\eta_\nu(\mathcal{F})} \cdot \frac{\partial \eta_\nu(\mathcal{F})}{\partial \mathcal{F}}$ is independent

of ν, and putting $\nu_1 = \nu_2$ on the L.H.S. implies that

$$\frac{1}{\eta_\nu(\mathcal{F})} \frac{\partial \eta_\nu(\mathcal{F})}{\partial \mathcal{F}}$$

is independent of $\mathcal{F}$. Thus

$$\log \eta_\nu(\mathcal{F}) = a\mathcal{F} + b(\nu)$$

where a is a constant, and for the total density of sources to be finite, this relation cannot hold for all $\mathcal{F}$ (from $-\infty$ to ∞).

However, although it is, strictly, incorrect to assume that the distribution of spectral indices is independent of luminosity, it will be found in section 11 of this chapter that the effect is not likely to be too serious. More serious might be a dependence of this distribution on epoch.

7. Number counts as a function of frequency.

There is an intimate relation between the spectral shape of a population of sources, and the dependence of source counts on frequency. We shall consider sources with spectra of the form $S(\nu) \propto \nu^{-\alpha}$, which is satisfied for the majority of radio sources over a wide range of frequencies (38 - 1400 MHz[50]).

Let $n_\nu(f)\,df$ be the number of sources between f and $f + df$ at frequency ν and let

$$N_\nu(f) = \int_f^\infty n_\nu(f)\,df$$

be the number of sources brighter than f. Let $p_\nu(\alpha,f)\,d\alpha$ be the fraction of sources of flux f at frequency ν having spectral indices between α and $\alpha + d\alpha$, so

$$\int_{-\infty}^{\infty} p_{\nu}(\alpha, f)\, d\alpha = 1 \quad \text{all } f, \nu .$$

Now a source with flux f and spectral index α at frequency ν_1 becomes a source of flux $f + \alpha \log \nu_1 / \nu_2$ (and the same spectral index) at frequency ν_2. Thus

$$\eta_{\nu_1}(f) \cdot p_{\nu_1}(\alpha, f) = \eta_{\nu_2}(f + \alpha \log \nu_1 / \nu_2) \cdot p_{\nu_2}(\alpha, f + \alpha \log \nu_1 / \nu_2) \tag{29}$$

Integrating both sides with respect to α

$$\eta_{\nu_1}(f) = \int_{-\infty}^{\infty} \eta_{\nu_2}(f + \alpha \log \nu_1 / \nu_2) \cdot p_{\nu_2}(\alpha, f + \alpha \log \nu_1 / \nu_2)\, d\alpha \tag{30}$$

Exactly as in the previous section we can prove that if $\bar{\alpha}_{\nu}(f)$ is independent of f, where

$$\bar{\alpha}_{\nu}(f) = \int_{-\infty}^{\infty} \alpha\, p_{\nu}(\alpha, f)\, d\alpha,$$

then the shape of the number-count curve is independent of ν.

Also that if $p_\nu(\alpha, f)$ is independent of f, then

$N_\nu(f) \propto S^{-x}$, where x is a constant, independent of frequency.

We shall now consider two simple forms for $N_{\nu_2}(f)$:

(i) $N_{\nu_2}(f) \propto S^{-x}$, i.e., $\log_{10} N_{\nu_2}(f) = \log_{10} N_2 + x(f_2 - f)$

then

$$n_{\nu_2}(f) = -\frac{\partial}{\partial f} N_{\nu_2}(f) = x \cdot N_{\nu_2}(f) \cdot \log_e 10$$

so

$$n_{\nu_1}(f) = x \cdot \log_e 10 \cdot N_2 \cdot S^{-x} \int_{-\infty}^{\infty} \left(\frac{\nu_2}{\nu_1}\right)^{\alpha x} \cdot p_{\nu_2}(\alpha, f + \alpha \log \nu_1/\nu_2) \cdot d\alpha .$$

This if $p_{\nu_2}(\alpha, f)$ is independent of f, the counts have the same shape at frequency ν_1. Also it follows from equation (29) that $p_{\nu_1}(\alpha_1, f)$ is also independent of f.

If the dispersion in spectral indices is dependent on f at ν_2, the count slope at ν_1 may be modified.

E g. if

$$p_{\nu_2}(\alpha, f) = \{ \alpha - \bar{\alpha}(f) \}, \quad \bar{\alpha}(f) = \bar{\alpha}_2 + k(f - f_2)$$

then

$$n_{\nu_1}(f) = x.\log_e 10 . N_2 . 10^{-x f + \bar{\alpha}(f) \log_{10} \nu_2 / \nu_1}$$

$$= x.\log_e 10 . N_2 . 10^{-(x - k\log_{10} \nu_2/\nu_1) f + \alpha_2 \log_{10} \nu_2/\nu_1 - k f_2}$$

so

$$x(\nu) = x + k . \log \nu / \nu_2 .$$

Nevertheless it is surprising that whatever the dispersion in spectral indices, provided only that it is independent of flux, the count slope is indepehdent of frequency.

However the observed number-count slope at 178 MHz is certainly not independent of flux-density so we now consider:

(ii) $\log_{10} N_{\nu_2}(f) = \log_{10} N_2 - \frac{(f - f_2)^2}{2\sigma^2}$, $f \geq f_2$. (31)

Then

$$n_{\nu_2}(f) = N_2 . \log_e 10 . \frac{(f - f_2)}{\sigma^2} . e^{\frac{-(f-f_2)^2 \log_e 10}{2\sigma^2}}$$

so

$$n_{\nu_1}(f) = \frac{N_2 . \log_e 10}{\sigma^2} \int_{-\infty}^{\infty} (f - f_2 + \alpha\ldots) \exp - \{ \frac{(f-f_2+\alpha\ldots)^2 \log_e 10}{2\sigma^2} \} p_{\nu_2}(\alpha, f-f_2+\alpha\ldots) d\alpha$$

where $\ldots = \log \nu_1 / \nu_2$

$$= \frac{N_2 \log_e 10 . \exp - \{ \frac{(f-f_2)^2 \log_e 10}{2\sigma^2} \}}{\sigma^2} \times \int_{-\infty}^{\infty} (f-f_2+\alpha\ldots) . \exp \{ \frac{2(f-f_2)\alpha\ldots + \alpha^2 \ldots^2) \log_e 10}{2\sigma^2} \}$$

$$\times p_{\nu_2}(\alpha , f - f_2 + \alpha\ldots) \, d\alpha .$$

$$g(f) = \frac{\bar{\alpha}^2}{2\Sigma^2} - \frac{\tilde{\alpha}(f)^2}{2S^2}$$

$$= \frac{\sigma^2 \bar{\alpha} \Delta \log_e 10 \{ \bar{\alpha} \Delta + 2(f-f_2) \} - \Sigma^2 (f-f_2)^2 \Delta^2 (\log_e 10)^2}{2\sigma^2 (\sigma^2 + \Sigma^2 \Delta^2 \log_e 10)}$$

Now

$$\int_{-\infty}^{\infty} \frac{\alpha . \exp \{ \frac{-(\alpha-\tilde{\alpha})^2}{2S^2} \}}{\sqrt{2\pi}\, S} . \, d\alpha = \tilde{\alpha}$$

so

$$n_1(f) = \frac{N_2 \log_e 10 (f-f_2+\tilde{\alpha}\Delta) S}{\Sigma \sigma^2} \exp - \{ \frac{(f-f_2)^2 \log_e 10}{2\sigma^2} + g(f) \}$$

$$= \frac{N_2 \log_e 10}{\sigma \sqrt{\sigma^2 + \Sigma^2 \Delta^2 \log_e 10}} (f-f_2+\tilde{\alpha}\Delta) . 10^{\frac{-(f-f_2+\bar{\alpha}\Delta)^2}{2(\sigma^2+\Sigma^2\Delta^2\log_e 10)}}$$

Now

$$f - f_2 + \tilde{\alpha}\Delta = f - f_2 + \left(\frac{\sigma^2 \alpha - \Sigma^2 (f-f_2)\Delta^2 \log_e 10}{\sigma^2 + \Sigma^2 \Delta^2 \log_e 10}\right).\Delta$$

$$= \frac{\sigma^2 (f-f_2+\bar{\alpha}\Delta)}{\sigma^2 + \Sigma^2 \Delta^2 \log_e 10}$$

so

$$n_{v_1}(f) = \frac{N_2 .\log_e 10 .\sigma}{\{\sigma^2 + \Sigma^2 \Delta^2 \log_e 10\}^{1.5}} (f-f_2+\bar{\alpha}\Delta).10^{\frac{-(f-f_2+\bar{\alpha}\Delta)^2}{2(\sigma^2+\Sigma^2+\Delta^2 \log_e 10)}}$$

and

$$N_{v_1}(f) = \frac{N_2}{\sqrt{1 + \Sigma^2 \Delta^2 \log_e 10/\sigma^2}} .10^{\frac{-(f-f_2-\bar{\alpha}\Delta)^2}{2(\sigma^2+\Sigma^2\Delta^2 \log_e 10)}} \qquad (32)$$

Thus if $\bar{\alpha}$ is independent of f, and if

$$\Sigma^2 \; \Delta^2 \log_e 10 \ll \quad ^2 \tag{33}$$

a change of frequency merely shifts the flux density scale by

$\bar{a} \log_{10} \nu_1 / \nu_2$.

The observed counts at 178 and 408 MHz are well respresented by

$$\log_{10} N_{178} = 1.6 - 1.89 (f + 25) - .24 (f + 25)^2$$

$$= 5.321 - \frac{(f + 28.938)^2}{2(1.44)^2} \tag{34}$$

and

$$\log_{10} N_{408} = 5.32 - \frac{(f + 28.94 + .29)^2}{2(1.44)^2}$$

The inequality (33) is satisfied if $.0225 \; ^2 \log_e 10 \ll 2.0$

i.e. if $^2 \ll 78$.

This should certainly be satisfied for $\nu_1 = 2770$ MHz,

$\nu_2 = 178$ MHz.

for which $\Delta = 1.19$.

The source-counts observed by Shimmins et al (79) do not, however, agree with those predicted by equation (32) (see Fig. 22), and it is difficult to understand Pooley's claim (97) that there is no discrepancy, unless Shimmins et al have grossly underestimated the errors involved.

One way of accounting for this change in number-count slope between 178 and 2770 MHz is to postulate a dependence of $\bar{\alpha}$ on f at 178 MHz. In fact, differentiating equation (32),

$$x_{\nu_1}(f) = \frac{-\,d \log N_{\nu_1}(f)}{df} = \frac{f - f_2 + \bar{\alpha}\,\cdot}{\cdot^2 + \Sigma^2\,\cdot^2 \log_e 10} \left\{ 1 + \cdot \cdot \frac{d\bar{\alpha}}{df} \right\}$$

$$= x_{\nu_2}(f + \bar{\alpha}\,\cdot) \cdot \frac{\left\{ 1 + \cdot \cdot \frac{d\bar{\alpha}}{df} \right\}}{1 + \Sigma^2\,\cdot^2 \log_e 10 / \cdot^2}$$

$$\simeq \left(1 + \cdot \cdot \frac{d\bar{\alpha}}{df}\right) \cdot x_{\nu_2}(f + \bar{\alpha}\,\cdot).$$

so the number-count slope will be reduced if $\frac{d\bar{\alpha}}{df} < 0$.

However, this would produce a proportional effect at intermediate frequencies, and this is not observed.

The simplest explanation is that a small proportion of the sources observed at any particular flux-level at 178 MHz have abnormally strong emission at 2770 MHz (this is known to be the case for a subset of the quasars).

The foregoing analysis can be applied to a set of sources with non power-law radio spectra to determine the relation between counts at 2 frequencies, provided α is defined by

$$\alpha = \frac{f(\nu_1) - f(\nu_2)}{\quad}$$

Thus if the spectra of the <u>whole</u> population kinked up at high frequencies in the same way, the counts would still be similar at frequencies on either side of the kink, provided that (33) holds, where Σ now describes the dispersion in the quantity defined above.

Thus for the count shape to vary with frequency, it is essential that " α " be <u>not</u> dispersed about a single mean.

The simplest departure is to suppose that the values of a are dispersed about two distinct values a_1, a_2. Then if the dispersions are small (in the sense of (33)), we can write

$$p_{\nu_2}(a) = \lambda \cdot \delta(a - a_1) + (1 - \lambda) \cdot \delta(a - a_2) \tag{35}$$

where $\delta(x)$ is the Dirac δ-function, and $a_2 > a_1$.

We shall see that λ need not be very different from zero to produce interesting effects, provide $\tau(a_2 - a_1)$ is large enough.

Then

$$N_{\nu_1}(f) = \lambda . N_{\nu_2}(f + a_1 \tau) + (1 - \lambda) . N_{\nu_2}(f + a_2 \tau)$$

$$= N_2 . 10^{\frac{-(f - f_2 + a_2 \tau)^2}{2\sigma^2}} \left\{ 1 - \lambda + \lambda . 10^{\frac{2\tau(f - f_2)(a_2 - a_1) + \tau^2 (a_2^2 - a_1^2)}{2\sigma^2}} \right\}$$

and

$$x_{\nu_1}(f) = \frac{f - f_2 + a_2 \tau}{\sigma^2} - \frac{\lambda \tau (a_2 - a_1) y}{\sigma^2 \{1 - \lambda + \lambda y\}}$$

where

$$y = 10^{\frac{2\Delta(f - f_2)(a_2 - a_1) + \Delta^2(a_2^2 - a_1^2)}{2\sigma^2}}$$

so

$$x_{\nu_1}(f) = \frac{(1 - \lambda)(f - f_2 + a_2^2 \Delta) + \lambda y (f - f_2 + a_1 \Delta)}{\sigma^2 (1 - \lambda + \lambda y)}$$

and

$$\frac{d x_{\nu_1}}{df} = \frac{1}{\sigma^2} - \frac{(1 - \lambda)\lambda y}{\sigma^2 (1 - \lambda + \lambda y)^2} \cdot \frac{\Delta^2 (a_2 - a_1)^2 \log_e 10}{\sigma^2}$$

$$= 0 \quad \text{if} \quad \frac{(1 - \lambda + \lambda y)^2}{(1 - \lambda)\lambda y} = \frac{\Delta^2 (a_2 - a_1)^2 \log_e 10}{\sigma^2}$$

The L.H.S. of this relation is a minimum when $\lambda y = 1 - \lambda$ so

$$\{ \Delta (a_2 - a_1) \}_{\min} = 2 \sqrt{\frac{\sigma^2}{\log_e 10}} .$$

The values of x_{ν_1} and N_{ν_1} corresponding to

$\frac{d x_{\nu_1}}{df} = 0$ are:

$$x_{\nu_1}\Big|_{\frac{dx}{df}=0} = \frac{f - f_2 + a_2}{\sigma^2} - \frac{1}{\sqrt{\sigma^2 \log_e 10}} \tag{36}$$

$$N_{\nu_1}\Big|_{\frac{dx}{df}=0} = 2N_2(1 - \lambda) \cdot 10^{-(f - f_2 + a_2)^2 / 2\sigma^2} \tag{37}$$

Thus using the observed fact that $x = 1.4$ over a wide range of frequencies at 2770 MHz [79] all the required parameters can be determined, assuming $\lambda \ll 1$.

Substituting (34) and (35) in (37) gives

$$N_{\nu_1}\Big|_{\frac{dx}{df}=0} = 2.03,$$

so from the observed counts at 2770 MHz we need to take $f \simeq -26$ in (36), which gives $\alpha_1 = -0.82$, $\alpha_2 = 0.78$, the latter agreeing well with the mean spectral index observed at 178 MHz. The corresponding value of λ is 2.17×10^{-3} which is indeed $\ll 1$. The predicted counts at various frequencies on the above model are shown in Fig. 22: agreement with observations is very good.

Thus if only one source in 500 at 178 MHz has an effective spectral index between 178 and 2770 MHz of -0.8, while the remainder have spectra very similar to those found in the range 38 - 1400 MHz, the counts at 2770 MHz can be understood. It is already well-known that a subset of the quasars have $\alpha < 0$ (79) and this is presumably the population required.

Clearly the relation (35) is an oversimplification, although dispersions Σ_1, Σ_2 in α about the two means α_1, α_2, would not alter the above analysis provided $\Sigma_i^2 \ll \sigma^2 \log_e 10 \ll \sigma^2$ for $i = 1,2$.

But the above arguments certainly support the suggestion of Shimmins et al [79] that the counts at 2770 MHz could be affected by a

sub-population with peculiar spectral behaviour at higher radio frequencies. There seems no reason to doubt the interpretation of the counts at 178 MHz in terms of secular evolutionary effects.

Interpretation of the counts at 2770 MHz can only proceed when the two (or more) populations involved have been separated. If the interpretation presented here is correct, each population separately will give counts similar to those at 178 MHz.

8. Luminosity function.

Detailed investigation of source counts has been conducted in the 3 asymptotic models discussed in section 1.2., the Einstein de Sitter (E), Milne (M), and de Sitter (S) models. The observed material in galaxies corresponds to $\sigma_0 = 0.035$, (30), and it is rather unlikely that $\sigma_0 > 0.5$, so the E and M models represent extreme cases if $\Lambda = 0$. Actually if $\sigma_0 \geq 1/100$, the S model is a good approximation only for $Z \ll (2\sigma_0)^{-1/3} \leq 4$. The M model, on the other hand is a good approximation to the $\Lambda = 0$ case provided $\sigma_0 Z \ll 1$, i.e., out to $Z = 10$ if $\sigma_0 = 0.035$.

In calculating the luminosity P of a source from its observed flux-density S, a factor $(c\tau_0)^2$ appears which depends on the rather uncertainly known Hubble constant. This factor plays no part in the analysis of source counts and integrated background that follows, so it will be convenient to define the luminosity in units of $(c\tau_{0/\text{metres}})^{-2}.\,\text{W(Hz)}^{-1}\text{(ster)}^{-1}$. Thus to convert $\mathcal{F} = \log_{10} P$ to the more familiar units of $\text{W (Hz)}^{-1}\text{(ster)}^{-1}$, the quantity $2\log_{10}(c\tau_{0/\text{metres}})$ must be added in what follows, i.e., $+51.9$. Similarly the source number-density will be measured in units of $(c\tau_0)^{-3}$, and must be multiplied by $10^{-77.85}$ to convert to units of m^{-3}. Below a luminosity of $\mathcal{F} = -28$ the luminosity function $\eta(\mathcal{F})$ hardly depends on model or evolutionary hypothesis, when determined from 3CR sources (compared with statistical uncertainties), so we shall use the luminosity function of Caswell and Wills[80].

From section 1.14 we saw that for 3CR radiogalaxies: for $-28 \leq \mathcal{F} < -26.5$ we may or may not have evolution, whereas for $-26.5 \leq \mathcal{F}$ evolution is definitely needed. In both cases the luminosity function depends on cosmological model and evolutionary hypothesis. Fig. 23 shows $\mathcal{F} + \log \eta(\mathcal{F})$, no evolution, E.M.S

$\mathcal{F}'$ + log $\eta(\mathcal{F}')$, exponential luminosity evolution, Z_L = 5,6

$\mathcal{F}$ + log $\eta(\mathcal{F})$, exponential density evolution, Z_D = 8,9,10

calculated from the radio-galaxy data using III (16), assuming that the identified 3CR sources cover 6 steradions of sky (see ref. 46).
The error bars represent statistical uncertainties. Where the effect of altering the magnitudes of all radio-galaxies with unknown redshift by $\pm$ 1 (see section I.14) is to give a value for $\eta(\mathcal{F})$ lying outside these error bars, these values of η are shown, and it is clear that this is a greater source of uncertainty than statistical uncertainty. At very few values of luminosity is $\log_{10} \eta$ known to better than $^{+0.1}_{-0.2}$}. The luminosity function for quasars is also shown.
The point of plotting $\mathcal{F}$ + $\log_{10} \eta(\mathcal{F})$, rather than $\log_{10} \eta(\mathcal{F})$, is that it gives an indication of the relative contribution of sources of different luminosity to the integrated radio background, since the background flux is proportional to $\int \eta(\mathcal{F}).P.d\mathcal{F}$.

The luminosity function for radio-galaxies is ill-determined for luminosity evolution if $\mathcal{F}' > -26$, in the case of luminosity evolution, or $\mathcal{F} > -25.5$ in the case of density evolution, but is consistent with the quasar luminosity function in most cases. This suggests

that most, or even all, very strong sources at large redshift are quasars, and that radio-wise there is no distinction between the 2 classes.

9. Background temperature at 178 MHz.

This can now be calculated in each model as a function of $\mathcal{F}_c$, where evolution is assumed for $\mathcal{F} \geq \mathcal{F}_c$: some examples are shown in Fig. 24 for exponential luminosity evolution. To obtain $T_{178} = 30 \pm 7^{\circ}K$, $\mathcal{F}_c$ must be

-30.5 to -28.8, -28.4 to -27.5, -26.45 to -26.1,

for the E,M,S models respectively, if $Z_L = 5$. In fact we see right away that in the de Sitter model too much background radiation will be produced even if $\mathcal{F}_c$ has its maximum value of -26.5. From Fig. 23 the most natural value for $\mathcal{F}_c$ is perhaps at the minimum in the double-humped distribution $\mathcal{F} + \log_{10} \eta(\mathcal{F})$,

i.e. $-29 \leq \mathcal{F}_c \leq -28$, which is also the point of transition from class (a) to (b) (II.1), "normal" galaxies to "radio-galaxies".

Fig. 24 demonstrates that given the form of the evolution, a strong dependence on cosmological model remains, even if only the widely different values of $\mathcal{F}_c$ required.

10. Source counts as a function of $\mathcal{F}_c$, for exponential luminosity evolution.

Using the luminosity functions calculated in III.8, source counts can be predicted as a function of $\mathcal{F}_c$, the luminosity above which luminosity evolution is assumed to apply. Since for the M and E models only one 3CR source is known with $\mathcal{F}' > -25$, the density of such sources will be assumed to be zero (and for $\mathcal{F}' > -24.5$ in the de Sitter model). Down to $f = -28$, the contribution of sources with $\mathcal{F} < -30$ is appreciably less than 1 percent, and so can be neglected to the present accuracy of the observed source-counts. For $-26 \leq \mathcal{F}' < -25$, the luminosity function is very uncertain due to the small number of sources visible in this range down to the plate limit. The radio luminosity function calculated for quasars is only a lower limit because the optical luminosity function may have a significant low-luminosity tail. The procedure we have adopted is to adjust the luminosity function for $\mathcal{F}' \geq -26$ to the condition that $\log N(-25) = 1.6$. This could, of course, be done in arbitrarily many ways: to fix the luminosity function we demand that $\frac{d \log n(\mathcal{F}')}{d \mathcal{F}'}$ be constant for $\mathcal{F}' \geq -26$, and that the function for $\mathcal{F}' \geq -26$ fit continuously onto that for $\mathcal{F}' < -26$. It will be

seen in Fig. 23 that this "normalization" is entirely consistent with the data. Note that it would be quite incorrect to "normalize" the whole luminosity function, as has been done by Petrosion[81]. This uncertainty at the high luminosity end of the radio luminosity function turns out to be unimportant at low flux levels. The counts for $Z_L = 5,6$ in the E,M,S models are shown in Fig. 25 as a function of $\mathcal{F}_c$ for $f = -24.5\ (-.25)\ -28$. An impression of the goodness of fit can be obtained by interpolating the observed values, with their uncertainties (see Table 7). If, at all flux-levels, the same value of $\mathcal{F}_c$ is required, a good model has been found.

For all 3 models $Z_L = 6$ gives too steep counts between $f = -25$ and -26.5. (The exact agreement in the M,S cases for $f \geq -25$ follows from the fact that we have already used all the information down to the 3C level; and shows only that it is consistent to assume that the unidentified 3C sources are the same kind of object as the identified, but below the plate limit). $Z_L = 5$ gives a reasonable fit in each model down to $f = -26.5$, with $\mathcal{F}_c = -28, -27.5, -26.5$ for E,M,S. Thus we can see immediately that Longair's assertion, that the data down to the Ryle-Neville survey[82] level ($f = -26.6$) required a real truncation in the distribution of sources, is incorrect, and is a consequence

of the particular kind of evolution considered by him. Moreover, down to this level ($f = -26.6$) it is not even necessary to assume evolution only for $\mathcal{F}'$ greater than some $\mathcal{F}_c$ in the E and M models: all sources could be assumed to evolve. Below this flux-level interesting differences in the models emerge. The decrease in slope is too rapid in the E model, much too slow in the S model, and exactly right in the M model (with $\mathcal{F}_c = -27.5$). This is a reflection of the different asymptotic number-count slope discussed in III.3.2.

The integrated background temperatures at 178 MHz corresponding to the optimum values of $\mathcal{F}_c$ are

	$\mathcal{F}_c$	T_{178}	
E	-28	18°K	
M	-27.5	23	observed: 30 ± 7
S	-26.5	41	

Clearly the integrated background is related to the asymptotic number-count slope, so that it is not surprising that the model which gives the best fit to the counts (the Milne model) also gives the best value for T_{178}.

This distinction in asymptotic behaviour between the cosmological models depends strongly on the fact that the exponential evolutions considered here tend towards a uniform distribution of non-evolving sources at large redshift. Two factors limit this assumption:

(i) radio-galaxies will not be found at epochs earlier than that at which galaxies first formed. While this epoch is not known, it is unlikely to correspond to redshifts greater than 1000 (83).

(ii) if the life time of the sources is limited by the life-time of the relativistic electrons, and if the microwave background radiation is cosmical black-body radiation, then when the quantity $10^{-5.65}(1+z)^2$ exceeds the magnetic field in radio-sources there will be a decline in the number-density of sources (with increasing redshift) - see sections II.6 and IV.1.

Thus our discussion of source-counts will be valid only if these two truncations are too remote to affect the counts. To investigate this, we break down the counts according to redshifts. Fig. 26 abc shows the fraction of sources out to a given redshift, down to a given flux-level, as a function of redshift, for the 3 models E,M,S (with $Z_L = 5$). A truncation at redshift 20 would have almost no effect down to $f = -28$, and a truncation at redshift 10 would affect the counts only below $f = -27$, and even then only slightly.

But a truncation at redshift 5 would have an appreciable effect, and would eliminate the possibility of distinguishing between the models on the basis of source-counts. This can be seen in Fig. 27a.,

$\log_{10} N/N_o - f$, where $\log_{10} N_0 = 1.4 + 1.5\,(-25 - f)$.

Counts are shown for the 3 models, together with the effect of a truncation at redshifts 5, 10 , 20 , compared to the observations available down to the 5C level.

Thus it matters very much whether the magnetic field in radio-galaxies is nearer 2×10^{-4} gauss (corresponding to a truncation redshift $Z^* = 10$), or 0.5×10^{-4} gauss (corresponding to $Z^* = 5$) - see (ii) above.

II. Effect of uncertainty in luminosity function.

If the distribution of sources down to different flux-levels according to luminosity is examined (Fig. 28), it is found that as f decreases, the peak contribution to sources brighter than f comes from progressively lower luminosities (as predicted in section III. 4). The number-count slope can therefore be significantly altered by increasing the number density of sources at one luminosity, while decreasing it at another. We saw in III.3 that the observed luminosity

function is rather uncertain. The question is: can the source-counts in the E and S models be brought into agreement with the observations by means of alterations to the luminosity function consistent with the present data? Unfortunately, from the point of view of distinguishing between cosmological models by means of source-counts, better agreement can be obtained by such adjustments. The adjusted luminosity functions are shown in Figs. 23 and the corresponding source-counts in Fig. 27b. The asymptotic slope is still different in the different models, but the distinction between the models does not appear until $f < -27$.

The Milne model still gives the best fit at present (and the best value for T_{178}), but the value of $\mathcal{F}_c$ required in the Einstein-de Sitter model falls nearer the transition between class (a) ("normal" galaxies) and class (b) ("radio-galaxies") sources.

12. Effect of electron scattering.

For the Einstein de Sitter model to be relevant to the observed universe, an appreciable fraction of the matter in the universe must be as yet unobserved (see III.3). If this matter is in the form of ionized hydrogen, electron scattering will modify the flux recieved from remote sources appreciably [84]. From the point of view of the present

analysis, electron scattering simply requires a modification of the luminosity distance - in fact if $\Lambda = 0$ [84],

$$\Delta \mathcal{F} = -\frac{0.13 \log_{10} e}{3q_0} \{ \sqrt{1 + 2q_0 z}\,(3q_0 + q_0 z - 1) - (3q_0 - 1) \}.$$

Fig. 29 shows the counts in the E model, with $Z_L = 5$, as a function of $\mathcal{F}_c$, including the effect of electron scattering, using the luminosity function of III.8.

The effect on the counts is appreciable, particularly at low flux-levels, and is almost sufficient to allow exponential luminosity evolution of <u>all</u> sources (though this can be ruled out, since the predicted background temperature at 178 MHz would then be 50°). The best value of $\mathcal{F}_c$ is now -28.5, and the corresponding counts, shown in Fig. 27a, agree quite well with the observations.

Thus it is not possible to distinguish between the Einstein de Sitter model, as modified by electron scattering, and the Milne model, on the basis of the present source-count data. The main distinction is in the required value of $\mathcal{F}_c$ (-28.5 and -27.5 respectively).

13. Spectral index dependent on luminosity and epoch.

In section II.2.1 we mentioned a correlation between mean spectral index and luminosity, represented by

$$\bar{\alpha} = 0.85 + 0.075\ (\mathcal{F} - 25.4),$$

where the luminosity is in units of w ster^{-1} Hz^{-1}. It has also been suggested (92) that the spectral index may increase with redshift, as a result of interaction of the relativistic electrons with the black-body radiation, e.g., $\alpha(z) = \alpha(0) + 0.5\,(1 - 1/(1+z))$. The consequence of both these effects for the source-counts are shown in Fig. 27b, for the cosmological model $q_0 = q_0 = 0.05$, with exponential luminosity evolution ($Z_L = 5$, $\mathcal{F}_c = -27.5$), including the (rather slight) effect of electron scattering.

The correlation between spectral index and luminosity has a fairly negligible effect, but a dependence of spectral index on redshift has a large effect and would require different values of Z_L, $\mathcal{F}_c$ etc.

14. Counts with exponential density evolution.

In section III.4 we saw that it was unlikely that the source counts could be explained by means of exponential density evolution, by considering a set of sources all with the same luminosity: the source-count slope changes much too slowly with flux-density to give the observed rapid change of slope below $f = -26$.

Moreoever, if $Z_D \geq 8$ (in I.14 we found $Z_D \sim 10 \pm 2$) many too many sources are predicted at low flux-levels even if $\mathcal{F}_c$ is given its maximum value of -26.5.

To see whether the additional postulate of a truncation in the density of sources beyond redshift Z^* improves the situation, we show in Fig. 30 source-counts as a function of Z^* for the E model with $Z_D = 10$, $\mathcal{F}_c = -26.5$.

For example $Z^* = 3.5$ would give a reasonable fit to the data for $f \geq -26.25$ and for $f = -27.75$, but the fit is very poor for $-26.5 \geq f \geq -27.5$ (more than twice too many sources at $f = -27$). No value of Z^* fits the counts at all flux-levels, and this conclusion applies also to power-law density evolution once the requirement $\mathcal{F}_c \leq -26.5$ is introduced (Longair's consistent model (d)[18] has $\mathcal{F}_c = -25.1$).

In IV.4 we shall consider exponential density evolution in a population of sources in which the luminosity of sources is a function of the magnetic field.

CHAPTER FOUR

Summary.

After a summary of formulae connected with synchrotron and inverse Compton radiation from relativistic electrons in a uniform magnetic field, in the presence of cosmical black-body radiation (section 1), a discussion is given of the various factors which determine the lifetime of sources (section 2). Section 3 is a rediscussion of a problem first considered by Schmidt (93), the relation between the frequency of radio events and the energy requirements of these events. The energy requirements of each parent are severer with luminosity evolution than with density evolution, but the parents need form only a small minority of the whole population of galaxies. With density evolution, cosmic rays could be accelerated in radio-galaxies, although most of the energy resources of the latter would be expended on this acceleration.

In section 4 the integrated radio and X-ray background intensities are calculated under 3 different assumptions:

(a) all sources have the same magnetic field,

(b) the magnetic field is independent of radio-luminosity, but varies with epoch,

(c) the magnetic field is a function of radio luminosity.

The observed X- ray background cannot be explained as inverse Compton radiation from radio-galaxies, if there is equipartition of magnetic field and

relativistic particle energies. Either the field in radio-galaxies is of order 10^{-6} gauss, or that in the weak radio-emitters must be of order 10^{-7} gauss. In the latter case the break in the observed X-ray spectrum below 10 kev can be understood. Perhaps the best model is where the weaker radio-galaxies have very low magnetic fields, and are the source of the X-ray background, while in the strong radio-galaxies and quasars the magnetic field is closer to the equipartition value. The source-counts can also be well interpreted in such a model.

1. Interaction of relativistic electrons in radio sources with the cosmical black body radiation.

The synchrotron power of a source in which the magnetic field is B and the energy spectrum of the electrons is given by

$E(y)\,dy = K\,y^{-1-2\alpha}\,dy$ is (65)

$$P_S(\nu) = 10^{-15.2}\ 10^{-6.1(1-\alpha)}\ .K.H^{1+\alpha}.\ \nu^{-\alpha}\ \text{erg/Hz/sec} \qquad (1)$$

If a source at redshift z is observed at frequency ν_R then $\nu = \nu_R(1+z)$ and the emission observed at frequency ν_R is due to electrons of energy

$$y = \sqrt{\frac{10^{-6.1}\,\nu_R(1+z)}{B}} \qquad (2)$$

The same electrons will interact with cosmical black-body radiation of temperature T to give inverse Compton radiation at frequency

$$\nu = 3.6\,y^2\,\frac{kT}{h} \qquad (3)$$

of power

$$P_c(\nu) = \frac{10^{-24.75}}{T} \left(\frac{h\nu}{3.6kT} \right)^{-\alpha} K U \qquad (4)$$

where $U = aT^4$ (92).

If T_0 is the black-body temperature at the present epoch, then at epoch corresponding to redshift z

$$T = T_0 (1 + z)$$

$$U = U_0 (1 + z)^4 \qquad \text{and}$$

$$\nu = \nu_c (1 + z)$$

where ν_c is the frequency of observations (in the X-ray region).

Thus

$$P_c\{\nu_c (1 + z)\} = \frac{10^{-24.75}}{T_0} \left(\frac{\nu_c}{10^{10.87} T_0} \right)^{-\alpha} K U_0 (1 + z)^3 \text{ erg/Hz/sec.} \qquad (5)$$

Inverse Compton radiation received at frequency ν_c was emitted, at epoch z, at frequency $\nu_c (1 + z)$, after interaction with photons

of energy $3.6 k T_0 (1+z)$, and so is due to electrons of energy

$$y_c = \sqrt{h \nu_c / 3.6 k T_0}, \quad \text{independent of } z.$$

Thus

$$\frac{P_c \{ \nu_c (1+z) \}}{P_S \{ \nu_R (1+z) \}} = 10^{-8.33} \left(\frac{3}{T_0} \right)^{0.2} \frac{U_0}{B^{1+a}} (1+z)^{3+a} \qquad (6)$$

if $a = 0.8$, $\nu_c = 10^{19}$ Hz, $\nu_R = 10^{8.25}$ Hz,

so this ratio is independent of P_S if B is the same in all sources.

2. Lifetime of sources.

(a) Synchrotron and inverse Compton lifetimes.

The rates at which an individual electron loses energy by synchrotron and inverse Compton radiation are (65)

$$\dot{y}_S = -10^{-7.6} \cdot B^2/_{4\pi} \cdot y^2$$

$$\dot{y}_c = -10^{-7.6} \cdot U \cdot y^2$$

so the lifetime of an electron of energy y is

$$\tau(y) = \frac{10^{7.6}}{y\,(U + B^2 / 4\pi)} \qquad (7)$$

Thus if $T_0 = 3^0$, inverse Compton losses are dominant at epochs such that the redshift is z and

$$B < B^*(z) = 10^{-5.55}(1+z)^2$$

while if

$$T_0 = 2.7^0, \quad B^*(z) = 10^{-5.65}(1+z)^2.$$

If we write $\tau(\nu, z)$ for the radiating life of electrons in a source at epoch z, whose radiation is observed at frequency ν, then

$$\frac{\tau(\nu_c, z)}{\tau(\nu_c, 0)} = \frac{1 + Z^{*4}}{Z^4 + Z^{*4}} \qquad (8)$$

where $Z = 1 + z$

$$Z^* = \sqrt{10^{5.65}\, B} \qquad (9)$$

$$\frac{\tau(\nu_R, z)}{\tau(\nu_R, 0)} = \frac{1 + Z^{*4}}{Z^4 + Z^{*4}} \cdot Z^{-1/2} \qquad (10)$$

$$\frac{\tau(\nu_c, 0)}{\tau(\nu_R, 0)} = \frac{y_S}{y_c} = \sqrt{\frac{3.6\, k\, T_0 \cdot \nu_S}{h\, \nu_c \cdot 10^{6.1} B}} \qquad (11)$$

$$= 10^{-2.74}\, B^{-1/2}$$

These relations will be needed in section 4. For compact radio-sources with dimensions of order a few light years or less, a far more serious drain on the electron energies would be inverse Compton interaction with the photons from the source itself. Interaction with radio photons might be the cause of optical emission in quasars and quasar-like objects in galaxies. Interaction with optical photons could make such sources strong X- or y-ray emitters. But we shall see that no significant part of the X-ray background is likely to be due to such sources.

(b) The life of sources determined by factors other than the synchrotron life

(i) expanding 'plasmon'

In the model of Ryle and Longair (62), discussed in II.3, the main energy losses for the majority of sources at any particular luminosity are due to the adiabatic expansion of the relativistic plasma. During such an expansion the energy of the electrons, and the magnetic field, vary with time according to

$$\gamma \propto r^{-1} \quad , \quad B \propto r^{-2} \qquad (12)$$

$$\text{so} \quad P \propto \gamma^{-2(1+2\alpha)} \nu^{-\alpha}$$

where r is the radius of the 'plasmon'.

$$\text{Thus} \quad \dot{\gamma} = - \left(\frac{\dot{r}}{\gamma_0 r_0} \right) \gamma^2 \qquad (13)$$

where suffix zero refers to the beginning of the adiabatic expansion phase (phase (iii) in ref 62). If the expansion is uniform, so that $\dot{r}$ is a constant, this electron energy loss-rate has the same form as the synchrotron and Compton radiation rates, and an "equivalent" magnetic field B_I can be defined by comparing (13) with $\dot{\gamma}_S$.

For a source at epoch z, observed at a frequency

$\nu_R = 178$ MHz,

$$y B^{1/2} = 10^{1.08} Z^{1/2}, \quad \text{from (2)}$$

$$= y_0 B_0^{1/2} (r_c/r)^2 \quad \text{by (12)}, \qquad (14)$$

Neglecting the synchrotron losses (but not inverse Compton)

$$\tau(\nu_R, z) = \left(\frac{y}{\dot{y}}\right) = \frac{1}{\left\{\frac{\dot{r}}{r_0 y_0} + 10^{-7.6} U\right\}}$$

$$= \frac{y_0}{y} \left\{ t_0^{-1} + 10^{-6.5} B_0^{-1/2} U_0 Z^{4.5} (r/r_c)^2 \right\}^{-1} \quad \text{by (14)},$$

where $t_0 = r_0/\dot{r}$, & $r/r_c = Z^{-0.17} (P/P_c)^{-0.19}$ if $\alpha = 0.8$.

Thus $$\frac{\tau(\nu_R, z)}{\tau(\nu_R, 0)} = \frac{1 + Z_*^{4.15}}{Z^{4.15} + Z_*^{4.15}} Z^{-0.17}$$

where

$$Z_* = \left\{ \frac{10^{6.5}\, B_0^{1/2}}{U_0\, t_0} \right\}^{\frac{1}{4.15}} (P/P_0)^{0.09}$$

$$= 10^{4.55} \left\{ \frac{B_0}{t_0^2} \right\}^{1/8.3} (P/P_0)^{0.09} \quad \text{if} \quad T_0 = 2.7^\circ K .$$

and these two formulae depend only slightly on P.

The parameters suggested by Ryle and Longair are

$$B_0 \sim 10^{-3} \text{ gauss}, \quad t_0 \sim 10^5 \text{ yrs} = 10^{12.5} \text{ secs}$$

(and these give $B \sim 10^{-4}$ when $r \sim 10^{5.5}$ lt yrs

if $r \sim c$, in good agreement with the mean equipartition values),

so

$$Z_* \sim 10^{4.55 - 28/8.3} (P/P_0)^{0.09} \sim 10^{1.18} (P/P_0)^{0.09}$$

i.e.

$$Z_* \sim 15 (P/P_0)^{0.09}$$

Thus inverse Compton losses do not start to dominate over adiabatic losses until a redshift sufficiently large for the analysis of Chapter III to be valid.

Actually the condition that expansion losses exceed synchrotron losses is not quite satisfied in the early part of the expansion for the parameters suggested by Ryle and Longair. However, this only increases the value of Z_* for the higher luminosity sources.

The situation is very much more complicated if $\dot{r}$ is not a constant, but if for example (as in the model suggested by Rees and Setti (85) $\dot{r} \propto r^{-2} Z^{-3/2}$ then

$$t \propto r^3 Z^{3/2}$$

$$y \propto r Z^{1/2}$$

and

$$Z_* \sim 10^{\frac{1.18 \times 4.15}{4.15 + 1.15}} \left(\frac{r_0}{r} \right)^{\frac{4}{4.15 + 1.15}}$$

$$\sim 10^{0.92} \left(P / P_0 \right)^{2/5.3(1 + 2\alpha)}$$

$$\sim 8.3 \left(P / P_0 \right)^{2/5.3(1 + 2\alpha)} \qquad (16)$$

Such a cutoff would certainly modify the counts at low flux-levels. Cut-offs of this type are discussed in section 4(c).

(ii) Continuous injection of electrons.

In this case the life of the source can be very much greater than the synchrotron life of the electrons. Suppose $n(t)$ electrons are created per sec, with life τ; then the number of electrons at time t,

$$N(t) = \int_{t-\tau}^{t} n(t)\, dt \sim n(t)\, \tau(t) \quad \text{if} \quad \tau \ll t. \tag{17}$$

The total number of electrons created

$$N_{tot} = \int_{0}^{\tau_{source}} n(t)\, dt$$

$$\sim \frac{\tau_{source}}{\tau} \cdot \bar{N}, \quad \text{where} \quad \bar{N} = \frac{1}{\tau_{source}} \int_{0}^{\tau_{source}} N(t)\, dt,$$

assuming τ independent of t.

The energy requirements are thus increased by a factor $\frac{\tau \text{ source}}{\tau}$.

If τ is the radiating life of the electrons

$$\frac{\tau(\nu_R, z)}{\tau(\nu_R, 0)} = \frac{1 + Z_*^4}{Z^4 + Z_*^4} \; Z^{-1/2}, \quad Z^* = \sqrt{10^{5.65} H}, \text{ as before,}$$

but this no longer affects the number-density of sources. Instead, it is the luminosity that is proportional to τ, because of (17). The interaction with the black-body radiation thus has the effect of a negative luminosity evolution beyond Z_* .

3. Frequency of radio-events and energy requirements.

Let $\varphi(\mathcal{F}, t)\, dt\, d$ be the number of sources per unit vol. born between $t, t + dt$ having luminosity between $\mathcal{F}, \mathcal{F} + d\mathcal{F}$. If a source has constant luminosity $\mathcal{F}$ for time $\tau(\mathcal{F}, t) \ll t_0$, the age of the universe, and we neglect the change in p, τ between $t - \tau(\mathcal{F}, t)$, t, then the number of sources alight per unit volume at time t, having luminosity between $\mathcal{F}$, $\mathcal{F} + d\mathcal{F}$:

$$\eta(t)\ \varphi(\mathcal{F}, t)\, d\mathcal{F} = p(\mathcal{F}, t) - (\mathcal{F}, t)\, d\mathcal{F}\ , \text{ where } \int_{-\infty}^{\infty} \varphi(\mathcal{F}, t)\, d\mathcal{F} = 1 .$$

(18)

If η_1 is the number density of parent objects, the number of events up to now in any one object

$$N(t_0) = \int_0^{t_0} dt \cdot \frac{1}{\eta_1} \int_{-\infty}^{\infty} p(\mathcal{F}, t)\, d\mathcal{F}$$

$$= \frac{1}{\eta_1} \int_0^{t_0} \eta(t)\, dt \int_{-\infty}^{\infty} \frac{\varphi(\mathcal{F}, t)}{\tau(\mathcal{F}, t)}\, d\mathcal{F}$$

$$= \frac{1}{\eta_1} \int_0^{t_0} \frac{\eta(t)}{\tau(t)}\, dt \quad \text{if} \quad \tau(\mathcal{F}, t) \text{ indep of } \mathcal{F} ,$$

$$= \frac{1}{\eta_1 \tau_0} \int_0^{t_0} \eta(t)\, dt \quad \text{if} \quad \tau \text{ indep } t \quad \text{also} ,$$

and if

$\eta(t) = \eta_0 \cdot j(z)$, where $j(0) = 1$ and $\eta_0 \sim 10^5$ (corresponding to $\mathcal{F} \geq -28$)

then

$$N(t_0) = \frac{\eta_0 t_0}{\eta_1 \bar{\tau}_0} \int_0^1 j(z)\, d(t/t_0) \qquad (19)$$

Any particular object is then alight for a fraction $\frac{\bar{N}_0}{t_0}$ of the time, and if the radio events in a particular parent are independent, this is also the probability that sources already alight will go off for a second time, i.e., $\bar{N}_0 / t_0$ gives the fraction of sources in which more than one event is observed. Of 82 sources for which detailed structures are given by MacDonald et al (66), 8 (33.1, 46 , 61.1, 184.1, 234, 452, 129, 465) are candidates for more than one event having occurred. Thus $\frac{\bar{N}_0}{t_0} \sim 0.1$, this value referring to radio-galaxies (i.e. sources with $\mathcal{F}_{178} \geq -28$). Equation (19) implies

$$\frac{\eta_0}{\eta_1} \int_0^1 j(z)\ d(t/t_0) \sim 0.1 \qquad (20)$$

This is valid if τ depends on $\mathcal{F}$,t, since in place of $N\tau_0/\tau_0$,

we have

$$\frac{1}{t_0} \iint \frac{d^2N}{dtd}\ \tau(\mathcal{F},t)\ d\mathcal{F}dt = \frac{1}{\eta_1} \int_0^1 \eta(t)\ d(t/t_0).$$

If there is no evolution in number-density, so $j(z) = 1$

then $\eta_1 \sim 10^6$, which is consistent with the parent population

being the set of strong elliptical galaxies, for which $\eta \sim 10^{6.6}$ (93) .

With exponential evolution, $j(z) = \exp\{ Q_D (1 - 1/z) \}$,

$\eta_1 \sim 10^6 \dfrac{(e^{Q_D} - 1)}{Q_D}$, in the Milne model

$\sim 10^{9.3}$ if $Q_D \sim 10$

i.e. all galaxies, although this could be reduced by taking $\eta_0 \sim 10^3$ (corresponding to $\mathcal{F} \geq -26.5$).

Total energy radiated per parent till now

$$E(t_0) = \int_0^{t_0} \frac{dt}{\eta_1 \beta} \int_{-\infty}^{\infty} p(\mathcal{F}, t).P.\ r(\mathcal{F}, t).d\mathcal{F}$$

where β is the efficiency factor

$$= \frac{1}{\eta_1 \beta} \int_{-\infty}^{\infty} \varphi(\mathcal{F}, t).P.\, d\mathcal{F}.$$

Now let $\varphi(\mathcal{F}, t) = \varphi_0 \{ \mathcal{F} - \log_{10} k(z) \}$,

so

$$E(t_0) = \frac{r_0}{r_1 \beta H_0} \int_{z=0}^{\infty} j(z)\, k(z)\, d(H_0 t) \int_{-\infty}^{\infty} \varphi_0(\mathcal{F}').P'.\, d\mathcal{F}'$$

$$\sim \frac{0.1 P_0 t_0}{\beta} \frac{\int_{z=0}^{\infty} j(z)\, k(z)\, d(H_0 t)}{\int_{z=0}^{\infty} j(z).d(H_0 t)}, \text{ by equation (20)}$$

where H_0 is the Hubble constant

and

$$P_0 = \int_{-\infty}^{\infty} \varphi_0 (\mathcal{F}) . P . d\mathcal{F}$$

$$\sim \frac{10^{-22}}{\eta_0} \left(\frac{c/H_0}{\text{metres}} \right) \text{ w/ster / Hz (from p.455 of Paper III).}$$

$$\sim 10^{-22-5+52+7+1} = 33 \quad \text{erg/sec/Hz , if } \eta_0 \sim 10^5$$

To convert from a monochromatic luminosity at $10^{8.25}$ Hz to an integrated luminosity, we must multiply by $\sim 10^9$,so

$$E(t_0) \sim 10^{58.5} / \beta \text{ ergs, for density evolution only} \qquad (21)$$

$$\sim 10^{58.5} \int_{z=0}^{\infty} e^{Q_L(1 - 1/Z)} d(H_0 t), \quad \text{for luminosity evolution only}$$

$\sim 10^{60} / B$ ergs if $Q_L \sim 5$, in the Milne model.

Thus the energy requirements of each parent are severer for luminosity evolution, but the parents form only a minority of the whole population of galaxies. β includes one factor due to any deviation from equipartition of energy between relativistic electrons and magnetic field, and a second factor for the energy that goes into protons.

Now the energy density of cosmic rays $\sim 10^{-12}$ erg/cc so for these to be produced universally from a set of objects whose number density is $\eta_1 (c/H_0)^{-3}$, an energy per object $\sim 10^{-12+84} / \eta_1$ ergs is required. If we take $\eta_1 \sim 10^9$, corresponding to all galaxies, this is 10^{63} ergs, the total energy available from hydrogen-burning of a typical galaxy. Thus it is reasonable, with density evolution to suppose cosmic rays are generated during the radio-galaxy phases, provided a value of $10^{-4.5}$ is taken for β. Thus a negligible fraction of the energy in these events actually appears as radiation, on this picture.

If we take $\eta_1 \sim 10^6$, corresponding to luminosity evolution, then we need $E \sim 10^{66}$ ergs to produce the cosmic rays, clearly unreasonable.

Effect of black-body radiation.

Whatever time-scale τ_0 operates within the source (not necessarily the synchrotron life) there is ultimately an epoch Z^* beyond which inverse Compton radiation, due to interaction of the relativistic electrons with the black-body radiation, is the main emission from the source. This has the effect of reducing the number density (or luminosity) of radio-sources, but provided Z^* lies beyond the observable 3C volume for Qs and RGs (need $Z^* \geq 3$, $B > 10^{-4}$) the above analysis is still correct.

The same relations also hold if all sources have the same history $P(s,t)$, where s is the time since birth, t_0 is the epoch of birth, so $P(t_0 - t, t) = P_0$, the present luminosity. If the birth function is $p(t)dt$, the number of sources having luminosity $\mathcal{F}_0$ to $\mathcal{F}_0 + d\mathcal{F}_0$ at epoch t_0:

$$\eta(t_0)\,\varphi(\mathcal{F}_0, t_0)\,d\mathcal{F}_0 = p(t)\,dt \qquad \text{where} \quad P(t_0 - t, t) = P_0$$

$$= \frac{p(t_0)}{\left(-\frac{\partial P}{\partial s}\right)_{t_0 - t, t}}\,dP \qquad \text{assuming} \quad \frac{\partial P}{\partial t} \ll \frac{\partial P}{ds}$$

so

$$\eta(t_0)\,\varphi(\mathcal{F}_0, t_0) = \frac{p(t_0)}{-\left(\frac{\partial \mathcal{F}}{\partial s}\right)_{t_0-t,t}}$$

$$= p(t_0)\,\varphi(\mathcal{F}_0, t_0) \quad \text{as before,}$$

where

$$\varphi(\mathcal{F}_0, t_0) = \frac{-1}{\left(\frac{\partial \mathcal{F}}{\partial s}\right)_{\mathcal{F}=\mathcal{F}_0,\ t=t_0}}$$

In this case

$$E = \frac{1}{\eta_1} \int_0^{t_0} p(t) \left\{ \int_0^{\tau(t)} P\,ds \right\} dt$$

Now

$$ds = \frac{\eta(t)}{p(t)}\,\varphi(\mathcal{F}, t)\,d\mathcal{F} \longrightarrow E = \frac{1}{\eta_1} \int_0^{t_0} \eta(t) \int_{-\infty}^{\infty} \eta(\mathcal{F}) \cdot P \cdot d\mathcal{F}$$

as before.

The conclusions of the previous two sections are summarized in Fig. 31, the lifetime of sources against the magnetic field, for models of type (a) , (b), [illegible] (section 2), with the ratio of the total energy required, compared to the equipartition value, shown.

4. Integrated radio and X-ray background intensities.

We shall calculate these under 3 different assumptions which cover a range of source model:

(a) All sources have the same magnetic field, B_0.

Let F_ν be the integrated background intensity at frequency ν in units of w m^{-2} Hz^{-1} $ster^{-1}$.

Then

$$F_\nu = \int_{t=0}^{t=t_0} \overline{\eta P}_\nu (z) \, . \, d(H_0 t) \qquad (22)$$

(see Paper III).

where

$$\overline{\eta P}_\nu (z) = \int_{-\infty}^{\infty} \eta(\mathcal{F}, z) \, . \, P(\nu, z) \, . \, d\mathcal{F}$$

radio bakcground, $\nu_R = 178$ MHz:

$$F_{178} = \overline{\tau_1 P}_{178}(0) \cdot \chi_s \qquad (23)$$

where

$$\chi_s = \int_{t=0}^{t_0} \frac{p(z)}{p(0)} \cdot \frac{k(z)}{k(0)} \cdot \frac{\nu_R^{(z)}}{\nu_R^{(0)}} \cdot Z^{-\alpha} \, d(H_0 t) \qquad (24)$$

where the three factors in the integral give the dependence on epoch of: the probability of a radio outbursts, the total electron energy, the lifetime of sources. If the latter is the synchrotron life of the electrons, equation (10) gives

$$\chi_s = \int_{t=0}^{t_0} \frac{p(z)}{p(0)} \cdot \frac{k(z)}{k(0)} \cdot \frac{1 + Z^{*4}}{Z^4 + Z^{*4}} \cdot Z^{-1/2-\alpha} \, d(H_0 t) \qquad (25)$$

where

$$Z^* = \sqrt{10^{5.65} B_0} \qquad (26)$$

In the case (i) of section 2(b), the $Z^{-1/2}$ term is absent and B_0 must be replaced by the "equivalent" magnetic field B_1 : in the case (ii), a similar factor is present due to the negative luminosity evolution caused by the black-body radiation.

The observed intensity is quoted as $T_{178} = 30^{\circ} \pm 7$ by Bridle (94), and $T_{178} = 10^{23.01} F_{178}$ (see paper III).

Thus given the form of evolution and $\eta(\mathcal{F}, 0)$ a strip of models consistent with the observed integrated radio background could be found in the $\sigma_0 - q_0$ plane. In practice $\eta(\mathcal{F}, 0)$ depends on cosmological model, and so also does $\mathcal{F}_c$, the critical luminosity above which evolution operates. But it is of interest to obtain a rough idea of the contribution to the radio background when evolution operates on sources with $\mathcal{F} \geq \mathcal{F}_c = -26.5$ (the maximum value of $\mathcal{F}_c$, by the arguments of I.14), and $\mathcal{F}_c = -28$ (the transition from normal spirals to radio-galaxies; see II.1). To do this we show T_{178} corresponding to (1) pk(z) = pk(0), no evolution,

(2) $pk(z) = pk(0) . \exp \{ Q (1 - 1/Z) \}$ $Q = 5$, luminosity-evolution (3) $Q = 10$, density evolution, for $\overline{\eta P}(0) = 0.5, 4$, respectively, as a function of σ_0 and q_0,

in Fig. 32a, assuming $Z^* \gg Q$.

We see that density evolution will not work without severe truncation, but that luminosity evolution of all radio-galaxies gives sensible value for T_{178}. The contribution of normal spiral galaxies will not be included in Bridle's estimate of T_{178} provided they have spectra similar to our own galaxy. The actual strip of the q_0 - q_0 plane shown shaded in Fig. 32a should not be taken seriously, since, as we show below, when we compare different cosmological models in more detail the different values of $\mathcal{F}_c$ required to give consistency with the source-counts smooth out the differences in the predicted values of T_{178}.

X-ray background, $\nu_c = 10^{19}$ Hz :

By equations (6), (11) and (22)

$$F_x = \left(\frac{T_0}{3}\right)^{1/2+\alpha} 10^{-8.33} \cdot \frac{U_0}{B_0^{1+\alpha}} \cdot 10^{-2.74} B_0^{-1/2} \cdot \eta P_{178}(0) \cdot \nu_c \qquad (26)$$

where

$$\chi_c = \int_{t=0}^{t_0} \frac{p(z)}{p(0)} \frac{k(z)}{k(0)} \cdot \frac{1 + Z^{*4}}{Z^4 + Z^{*4}} \cdot Z^3 \, d(H_o t) \qquad (27)$$

and (26) becomes

$$F_x = 10^{-10.5} \left(\frac{T_0}{3} \right)^{3/2 - \alpha} \cdot Z_*^{-3-2\alpha} \, \overline{\eta P}_{178}(0) \cdot \chi_c \qquad (28)$$

The observed flux is (95) 10^{-2} photons cm^{-2} kev^{-1} $ster^{-1}$

and 1 photon at 10^{19} Hz $= h\nu$ ergs

$$= 10^{-26.18 + 19 - 7} \text{ watts}$$

$$1 \text{ kev}^{-1} = 10^{-17.43} \text{ Hz}^{-1}$$

$$1 \text{ cm}^{-2} = 10^{4} \text{ m}^{-2}$$

finally the observed

$$F_x = 10^{-29.6} \text{ w m}^{-2} \text{ Hz}^{-1} \text{ ster}^{-1} \qquad (29)$$

The predicted quantities for the 3 cosmological models, E, M; S, with exponential luminosity evolution ($Q_L = 5$) are shown in the table below, assuming $Z^* = 10$. (see II.6), and using the values of $\mathcal{F}_c$ determined in III.10.

		E	M	S
$\mathcal{F}_c$		-28	-27.5	-26.5
$10^{23}\ \overline{\nu P}_{178}(0)$:	$\mathcal{F} \geq \mathcal{F}_c$	3.5	2.17	0.57
	$\mathcal{F} < \mathcal{F}_c$	7.8	9.2	11.2 (including normal spirals)
T_{178}, including $Z^{-1/2}$ factor	$\mathcal{F} \geq \mathcal{F}_c$	8.6	8.6	7.0
	$\mathcal{F} < \mathcal{F}_c$	3.4	5.1	14
Excluding $Z^{-1/2}$ factor	T_{178}	12	14	21
	$\mathcal{F} \geq \mathcal{F}_c$	13.5	14.5	14
	T_{178}	17	20	28
$10^{30}\ F_x$: $\mathcal{F} \geq \mathcal{F}_c$		0.00005	0.00011	0.00055

(contribution from $\mathcal{F} < \mathcal{F}_c$ still more negligible).

Other things being equal, the $Z^{-1/2}$ term in χ_s reduces the integrated radio background by about 25 percent. Now in applying the luminosity volume test in Chapter I, and in interpreting the source-counts in Chapter III, this terms was not included. The effect would be to increase Q_L slightly and presumably to increase T_{178} slightly. The relevant numbers for comparison with the results of Chapter III are those calculated excluding the $Z^{-1/2}$ term. It will be seen that the $\Lambda = 0$ models give a value for T_{178} rather on the low side, the best prediction now being that of the de Sitter model.

This may be seen another way. If we suppose that below the 5C flux-level the source counts are represented by $N(S) \propto S^{-x}$ with $0 \leq x < 1$ (to give a finite integrated background), then the value of x which leads to $T_{178} = 30^\circ$ is $x = 0.8$, close to the asymptotic value for the de Sitter model (see III.3.2). The deduction of the observed value of 30° for extragalactic sources is a difficult matter (94), but if correct, suggests a non-zero asymptotic number-count slope, and this implies (i) a model with q_0 close to zero (III.3.2) (ii) the black-body radiation is not affecting source-counts until flux-levels appreciably below the 5C level are reached.

It is probably incorrect to attribute the rapid change in number-count slope below 1 flux unit (at 178 MHz) to the effects of black-body radiation on sources (96).

Turning to the X-ray background, the predicted intensity falls below that observed by a factor 5×10^{-5} to 5×10^{-4}. F_x is very dependent on the value of Z^*, so in Fig. 32b, the dependence on Z^* of $10^{23} \cdot \chi_s$ and $10^{-3.5} Z^{*-4.6} \cdot \chi_c$ is shown for the 3 models E,M,S. The former quantity is T_{178} (observed value 30 ± 7) and the latter quantity is F_x in units of 10^{-30} wm^{-2}Hz^{-1}ster^{-1} (observed value 2.5, from equation (29)), in both case if $\overline{\eta P}_{178}(0) = 10^{-23}$. The box corresponds to

$$10^{-6} \leq B_0 \leq 10^{-3.7}, \quad 0.5 \leq 10^{23} \overline{\eta P}_{178}(0) \leq 10;$$

for satisfactory models the intersections of radio and X-ray loci (marked with circles) should lie in the box. The dependence on cosmological model is illustrated by Figs. 32 c,d, which show the same quantities for ranges of models with $\sigma_0 = 0.05$, $\sigma_0 = 0.15$ (and $Q = 0,5,10$).

For no cosmological model does luminosity evolution ($Q = 5$) admit a value of Z^* which would give the correct radio and X-ray background. Models with $\Omega_0 \leq 0.05$ could give the right backgrounds with density evolution and $B_0 \sim 10^{-6}$ gauss($Z^* \sim 0.7 - 0.8$) But if $Z^* < 1$ steeper evolutionary rates than those obtained in Chapter I would be necessary to give the same apparent evolution, and by different amounts for quasars and radio-galaxies. Magnetic fields as low as a microgauss seem implausible for strong radio-galaxies, since the energy requirements would be increased by $10^3 - 10^4$ above the equipartition values. Such fields are not unreasonable for weaker radio-galaxies: in paragraph (c) below, the case where the magnetic field varies with source luminosity will be discussed.

An alternative possibility is that the X-ray background is produced in normal spiral galaxies which are weak radio-emitters. If there is no evolution in this population, and $Z^* \ll 1$,

$$\chi_s \simeq \int_{t=0}^{t_0} Z^{-4.5-\alpha}\, d(H_0 t) = \frac{1}{6+\alpha} \quad , \quad \frac{1}{5.5+\alpha} \quad , \quad \frac{1}{3.5+\alpha}$$

$$\chi_c \simeq \int_{t=0}^{t_0} Z^{-1}\, d(H_0 t) = \frac{1}{2.5}\ ,\ \frac{1}{2}\ ,\ 1$$

in the E, M , S models.*

To get $F_x = 10^{-29.6}$ with $\eta\, P_{178}(0) = 10$

need

$\log_{10} Z^*$ =	-0.72,	-0.70,	-0.60
$\log_{10} B_0$ =	-7.1,	-7.05,	-6.85
for	E	M	S.

These magnetic fields are appreciably smaller than the estimate for our own galaxy ($1 - 3 \times 10^{-6}$ gauss).

---

*

Note that the main contribution to the X-ray background, when there is no evolution, comes from nearby regions of space, and not from far out as suggested by Longair (96).

Thus the observed X-ray background requires, if all sources of a particular class have the same magnetic field, either that this field is of order 10^{-6} gauss in the strong sources, or is of order 10^{-7} gauss in the weak sources.

We now show how the change in slope of the X-ray background spectrum below about 10 kev (102) helps to discriminate between the two models. To explain this rather sharp change in slope below 10 kev, it is necessary that a substantial fraction of the X-radiation comes from sources with similar redshifts. This is indeed the case if the radiation comes from weak radio-emitters since, as we have remarked above, most of the X-radiation then comes from nearby parts of space. Moreover if we calculate the radio-frequency at which the relativistic electrons responsible for the 10 kev inverse Compton radiation are producing synchrotron radiation, assuming a magnetic field, B , of 10^{-7} gauss, we find a frequency of about 1 MHz ($\nu_s \sim 10^{6.1} . B . h \nu_c / 3.6 kT .$). This is just the kind of frequency at which the spectra of radio-sources may turn over (103). Thus if the relativistic electrons in the weak radio-sources associated with normal spiral galaxies are the source of the X-ray background, a natural explanation is provided of the flattening of the X-ray background

spectrum below 10 kev. It is just a reflection of the flattening of radio spectra below about 1MHz.

No such explanation can be provided if the X-radiation arises from radio-galaxies with $B \sim 10^{-6}$. With exponential evolution, the fraction of the X-radiation which comes from sources beyond the epoch corresponding to redshift z is in fact $\gamma(s, Q/(1+z))/\gamma(s,Q)$, where γ is the incomplete Γ-function (see Paper III), and $s = 2.5, 2, 1$, for the E, M, S models, respectively. For example, in the de Sitter model, with $Q = 5$,

percent of background	90	80	70	60	50	10
comes from redshift	> 1.17	2.1	3.15	4.4	6.25	42.4.

The X-radiation comes from a very wide range of redshifts, and there is no possibility of achieving a sharp break in the integrated X-ray spectrum. With power-law evolution, a divergent integral has to be truncated at some redshift z^* so that in fact most of the radiation does come from a small range of redshifts close to z^*. Quite apart from the unsatisfactory nature of such a hypothesis, the radio-frequency corresponding to the break becomes about $10(1+z^*)^2$ MHz, or 100 MHz if $z^* \sim 2$ as suggested by Longair (96). Most radio-spectra are <u>not</u> curved at 100 MHz (50),

and no explanation of the break can be given.

Note that even if the X-ray background comes mainly from spiral galaxies, the strength of individual sources in the Virgo cluster would still be well below the present limit of detectability.

(b) B indep of P, but a function of epoch.

In this case

$$\frac{\tau_{\nu_R}(z)}{\tau_{\nu_R}(0)} = \sqrt{\frac{B/B_0}{1+z}} \cdot \frac{U_0 + B_0^2 / 4\pi}{U_0 Z^4 + B^2 / 4\pi} .$$

The case of greatest interest is $B = B_0 (1+z)^2$, which arises if the magnetic field in radio sources were a universal turbulent field, behaving like a pressure as the universe expands.

Then

$$\chi_s = \int_{t=0}^{t=t_0} \frac{k(z)}{k(0)} \frac{p(z)}{p(0)} Z^{\alpha - 3/2} \, d(H_0 t)$$

$$\chi_c = \int_{t=0}^{t=t_0} \frac{k(z)}{k(0)} \frac{p(z)}{p(0)} Z^{-1} \, d(H_0 t)$$

so

$\chi_s \sim \chi_c$ if $a = 0.8$ ($\chi_s = \chi_c$ if $a = 0.5$).

Thus

$T_0 = 2.7$, $T_{178} = 25$: $Z_*^{4.6} = 10^{-2.5}$, $B_0 = 10^{-6.75}$,

so the energy density of the magnetic field is $\sim$ 1 percent of that of the black-body radiation at all epochs.

The distribution of sources would be affected by luminosity evolution, with $P(z) \propto k(z) \cdot (1+z)^{2(1+a)}$ and density evolution, with $\eta(z) \propto p(z) \cdot (1+z)^{-3.5}$. The argument of section III.3.5 would then require

$(Q_D - 3.5) + 2(Q_L + 3.5) \sim 10$, or $Q_D + 2Q_L \sim 6.5$

(c) Luminosity dependent on magnetic field.

There are 3 cases of interest: the first two have been discussed in III.1 and IV.2, (i) K = constant, so $P \propto B^{1+a}$, (ii) adiabatic expansion of a "plasma",

$K \propto r^{-\alpha} \propto B^{\alpha}$, so $P \propto B^{1+2\alpha}$. The third case, equipartition of magnetic and particle energies in sources of constant volume, hardly corresponds with the wide range of source volumes observed (II.2.3), but is of some theoretical interest; $K \propto B^{2}$, so $P \propto B^{3+\alpha}$. These can be summarized by:

$K \propto B^{x}$, $P \propto B^{1+\alpha+x}$, with $x = 0, \alpha, 2$ for cases (i) (ii) and (iii).

Let B_0, P_0 be the magnetic field and corresponding luminosity at the present epoch, and let P_{cr} be the luminosity such that $B_0 = 10^{-5}.65$ gauss (so that $B_0^{2} = 4\pi U_0$ in such sources).

Then by equations (3),(22)

$$10^{-23} T_{178} = \int_{-\infty}^{\infty} \eta_0(\mathcal{F}_0).P_0.d\mathcal{F}_0 \int_{t=0}^{t_0} \frac{p(z)k(z)}{p(0)k(0)} \left(\frac{B}{B_0}\right)^{1+\alpha+x} \sqrt{\frac{B}{B_0 Z}}$$

$$\times \frac{1 + (B_0 / 10^{-5.65})^2}{Z^4 + (B / 10^{-5.65})^2} Z^{-\alpha} \, d(H_0 t)$$

$$= \int_{-\infty}^{\infty} n_0(\mathcal{F}_0) \cdot P_0 \cdot d\mathcal{F}_0 \int_{t=0}^{t_0} \frac{p(z)k(z)}{p(0)k(0)} \left(\frac{B}{B_0}\right)^{3/2 + a + x}$$

$$\cdot \frac{1 + (P_0 / P_{cr})^{\frac{2}{1+a+x}}}{Z^4 + (B/B_0)^2 (P_0/P_{cr})^{\frac{2}{1+a+x}}} \; Z^{-a-\frac{1}{2}} \cdot d(H_0 t)$$

and by equation (6)

$$P_c(10^{19}.Z) = 10^{-8.33} U_0 P_{cr} (P_0/P_{cr})^{\frac{x}{1+a+x}} (B/B_0)^x \cdot \frac{k(z)}{k(0)} \cdot Z^3 \cdot 10^{5.65(1+a)}$$

so

$$F_x = 10^{1.9} U_0 P_{cr} \int_{-\infty}^{\infty} n_0(\mathcal{F}_0)(P_0/P_{cr})^{\frac{x-\frac{1}{2}}{1+a+x}} d\mathcal{F}_0 \int_{t=0}^{t_0} \frac{p(z)k(z)}{p(0)k(0)} \left(\frac{B}{B_0}\right)^x$$

$$\cdot \frac{1 + (P_0/P_{cr})^{\frac{2}{1+a+x}}}{Z^4 + (B/B_0)^2 (P_0/P_{cr})^{\frac{2}{1+a+x}}} \cdot Z^3 \cdot d(H_0 t)$$

If we now take $k(z) \doteq k(0)$, $p(z) \doteq p(0) . \exp \{ 10 (1 - 1/Z) \}$ for sources with $\mathcal{F} \geq \mathcal{F}_{min}$, to give the right distribution in space for 3C radiogalaxies and quasars, then ideally, $\mathcal{F}_{cr} \sim -27$ (to correspond to the transition from increasing to decreasing number-density with epoch) and $\mathcal{F}_{min} \sim -28$ to -29 (to correspond to the transition from ellipticals to spirals). As we saw in IV.3, density evolution cannot affect the distribution in space of <u>all</u> radio-sources.

The source-counts to low flux-level hardly depend at all on $\mathcal{F}_{min}$, and can be used to determine $\mathcal{F}_{cr}$ as a function of model and the parameter x, in those cases where consistency with the observed counts can be obtained. Fig. 33a, b, c shows the source counts as a function of $\mathcal{F}_{cr}$ for the Milne model and $x = 0$, 0.8, 2. The most satisfactory case is $x = 0$, $\mathcal{F}_{cr} = -26.75$, and the case $x = 2$ is certainly inconsistent with the observed counts. The dependence of T_{178} and F_x on $\mathcal{F}_{min}$ for the case $x = 0$ is shown in Fig. 34. F_x is highly dependent on $\mathcal{F}_{min}$ and to get the observed flux we need $\mathcal{F}_{min} \sim -28.5$ (the corresponding minimum magnetic field is $10^{-6.65}$ gauss).

This type of model thus seems the most satisfactory of those investigated to date. Although, as in cases (a) and (b), the main contribution to the X-rays comes from sources with magnetic fields of a microgauss or less (and this seems quite unavoidable, if the X-rays are to come from interaction of relativistic electrons in radio-sources with the black-body radiation), the class of sources in which we are requiring these weak fields, namely the weaker of the radio-galaxies, is the only one for which we do not have arguments against this situation. It need not be surprising that the magnetic fields in normal spiral galaxies are somewhat stronger than those in the weaker radio galaxies (which are much stronger radio-emitters), since the structure of the 2 classes of source is quite different. In spiral galaxies the source has small dimensions and is centred on the galaxy: in radio-galaxies, the source is almost always double, and the components are large and far from the parent galaxy.

Finally we should remark that other explanations of the X-ray background have been suggested: these have been discussed recently by Silk and McCray (98).

TABLE 1 QUASAR DATA

3c	z	F178	V	KV	VCORR	ALPHA	RLUME	OLUME	VOLE	L	B
273.	0.158	-24.14	12.80	-0.64	12.16	0.35	-25.75	-28.84	9.433E-3	290.	64.
323.1	0.260	-25.02	16.69	-0.45	16.24	0.64	-26.18	-30.02	3.466E-2	34.	49.
249.1	0.311	-24.91	15.72	-0.36	15.36	0.87	-25.88	-29.50	5.415E-2	130.	38.
277.1	0.320	-24.89	17.93	-0.35	17.58	0.92	-25.83	-30.36	5.806E-2	123.	60.
48.	0.367	-24.30	16.20	-0.28	15.92	0.50	-25.17	-29.57	8.080E-2	134.	-29.
351.	0.371	-24.93	15.28	-0.27	15.01	0.60	-25.78	-29.20	8.291E-2	90.	36.
215.	0.411	-24.97	18.27	-0.22	18.05	1.00	-25.67	-30.32	1.055E-1	212.	37.
47.	0.425	-24.67	18.10	-0.21	17.89	0.89	-25.36	-30.23	1.140E-1	137.	-41.
279.	0.536	-24.70	17.75	-0.13	17.62	0.54	-25.24	-29.90	1.921E-1	305.	57.
147.	0.545	-24.21	17.80	-0.12	17.68	0.45	-24.75	-29.91	1.992E-1	162.	10.
334.	0.555	-24.97	16.41	-0.12	16.29	0.78	-25.43	-29.34	2.072E-1	33.	41.
275.1	0.557	-24.77	19.00	-0.12	18.88	0.88	-25.21	-30.37	2.088E-1	293.	79.
345.	0.594	-24.97	15.96	-0.10	15.86	0.24	-25.48	-29.10	2.398E-1	63.	41.
263.	0.652	-24.86	16.32	-0.06	16.26	0.88	-25.16	-29.17	2.917E-1	134.	50.
380.	0.691	-24.21	16.81	-0.04	16.77	0.77	-24.48	-29.32	3.287E-1	77.	24.
254.	0.734	-24.69	17.98	-0.02	17.96	0.93	-24.86	-29.74	3.714E-1	173.	66.
138.	0.754	-24.70	18.84	0.00	18.84	0.38	-24.98	-30.07	3.918E-1	187.	-11.
286.	0.846	-24.65	17.30	0.02	17.32	0.15	-24.90	-29.35	4.906E-1	57.	81.
196.	0.872	-24.20	17.60	0.02	17.62	0.70	-24.28	-29.44	5.198E-1	171.	33.
309.1	0.903	-24.74	16.78	0.02	16.80	0.45	-24.85	-29.08	5.552E-1	111.	41.
336.	0.927	-24.84	17.47	0.02	17.49	0.87	-24.81	-29.33	5.830E-1	41.	42.
288.1	0.960	-24.99	18.12	0.01	18.13	0.93	-24.91	-29.55	6.220E-1	112.	56.
245.	1.029	-24.99	17.25	0.00	17.25	0.61	-24.94	-29.14	7.054E-1	233.	56.
287.	1.054	-24.82	17.67	-0.01	17.66	0.48	-24.79	-29.28	7.363E-1	23.	81.
186.	1.063	-24.84	17.60	-0.01	17.59	1.18	-24.59	-29.24	7.475E-1	182.	26.
204.	1.112	-24.99	18.21	-0.02	18.19	1.05	-24.73	-29.44	8.091E-1	150.	36.
208.	1.112	-24.77	17.42	-0.02	17.40	0.98	-24.54	-29.12	8.091E-1	214.	33.
181.	1.382	-24.86	18.92	-0.10	18.82	0.94	-24.43	-29.48	1.164	204.	15.
268.4	1.400	-25.02	18.42	-0.10	18.32	0.69	-24.68	-29.27	1.188	147.	71.
446.	1.403	-24.74	18.39	-0.10	18.29	0.53	-24.46	-29.25	1.192	59.	-49.
298.	1.436	-24.33	16.79	-0.11	16.68	0.98	-23.85	-28.59	1.237	352.	61.
270.1	1.519	-24.89	18.61	-0.13	18.48	0.69	-24.47	-29.25	1.350	167.	81.
280.1	1.659	-24.83	19.44	-0.15	19.39	1.09	-24.17	-29.53	1.543	115.	77.
454.	1.756	-25.02	18.40	-0.14	18.26	0.73	-24.46	-29.02	1.677	87.	-36.
432.	1.804	-24.91	17.96	-0.14	17.82	1.04	-24.18	-28.82	1.743	68.	-23.
191.	1.946	-24.95	18.40	-0.12	18.28	0.98	-24.18	-28.93	1.939	212.	21.
9.	2.012	-24.77	18.21	-0.09	18.12	1.02	-23.95	-28.83	2.030	112.	-47.
NEW DATA NOT INCLUDED IN PAPER 1											
207.	0.683	-24.97	18.15	-0.04	18.11	0.70	-25.26	-29.87	3.210E-1	214.	30.
175.	0.768	-24.77	16.60	0.00	16.60	0.93	-24.89	-29.15	4.064E-1	205.	10.
454.3	0.860	-24.79	16.10	0.02	16.12	0.16	-25.02	-28.85	5.062E-1	86.	-39.
94.	0.962	-24.81	16.49	0.01	16.50	0.69	-24.80	-28.90	6.243E-1	197.	-43.
2.	1.037	-24.79	19.35	-0.01	19.34	0.73	-24.69	-29.96	7.153E-1	99.	-61.

NOTES

1 REDSHIFTS AND OPTICAL MAGNITUDES FROM REFS 7,41,42,104

2 RADIO FLUXES,F178, FROM 3CR,REF 38, EXCEPT 3C279,446, WHICH ARE FROM 3C, REF??

3 KV TAKEN FROM REF 52

4 3C 47,279,334,345,380,254,138,309.1,245,287,208,446,298,191 ARE CLASSIFIED BY KELLERMANN,REF 50, AS HAVING STRAIGHT RADIO SPECTRA. ALPHA FOR REST OF SOURCES CALCULATED AS IN APPENDIX 1,

5 RLUME,OLUME,VOLE ARE RADIO AND OPTICAL LUMINOSITIES, AND COMOVING COORDINATE VOLUME IN THE EINSTEIN DE SITTER MODEL

Table 2.

Distribution of radio-luminosities of strong radio-galaxies in two equivalent volumes of space, for 4 cosmological models.

(a) nearer half, (b) further half, of the observable volume.

range of $\log_{10}P$	cosmological models (A = 20.5, B = 5)							
(w/(c/s)ster)	Einstein-de Sitter		Milne		de Sitter		steady-state	
	(a)	(b)	(a)	(b)	(a)	(b)	(a)	(b)
27.4 - 27.9	0	0	0	0	0	1	0	0
26.9 - 27.4	2	1	2	1	3	0	2	1
26.4 - 26.9	1	0	1	2	1	3	1	3
25.9 - 26.4	13	22	13	25	14	33	13	34
25.4 - 25.9	8	33	8	30	6	23	5	24
24.9 - 25.4	10	15	10	13	11	13	11	13
24.4 - 24.9	9	7	9	7	8	5	8	5
23.9 - 24.4	9	5	9	5	10	5	10	5
23.4 - 23.9	5	2	5	2	4	2	4	2
totals								
$\log_{10}P > 23$	57	85	57	85	57	85	54	87
$\log_{10}P > 24.9$	34	71	34	71	35	73	32	75

Table 3.

Maximum effect of errors of ± 2 in estimated visual magnitudes, and of varying various parameters on the totals in Table 2.

optical magnitudes all reduced by 1
(A = 20.5, B = 5)

	Einstein-de Sitter		Milne		de Sitter		Steady-state	
	(a)	(b)	(a)	(b)	(a)	(b)	(a)	(b)
$\log_{10} P > 23$	60	82	60	82	61	81	55	85
$\log_{10} P > 24.9$	35	60	35	61	36	62	31	66

optical magnitudes all reduced by 2
(A = 20.5, B = 5)

$\log_{10} P > 23$	65	77	65	77	65	77	63	79
$\log_{10} P > 24.9$	36	53	36	53	36	54	35	55

Table 3. cont'd....

Milne model, A = 20.5				Milne model (A = 20.5, B = 5) galaxies with V ≤ 19 only.	
B = 4		B = 6			
(a)	(b)	(a)	(b)	(a)	(b)
58	84	58	84	50	71
37	69	35	70	27	57

Table 4.

Radio-galaxies with $\mathcal{F} < -27$

3C	V			
15	15.5	*	277.3	15.5 †
29	13		278	13.2
31	12		285	15.5
35	14.5		296	12
40	12		305	13.5
66	12.3		317	12.5
75	13		338	12
76.1	14		356	15.3 †
78	13.2		371	14.2
83.1	12.5		382	14.5
84	12		403	14.5
88	13.1		442	13
98	14		445	15.3
177	15.5		449	12.5
192	15		435	13.3
227	14.5	†	465	12.2
236	15			
253	15.5			
264	13			
274	10.8			

* $\mathcal{F} \geq -27$ in Eddington-Lemaître model with $Z_m = 2.95$

† . . . . . and in de Sitter model.

Table 5.

Evolutionary parameters for radio-galaxies and quasars

		luminosity evolution		density evolution	
		Q_L	z_L	Q_D	z_D
Einstein-de Sitter	RGs	4 ± 1	4 ± 2	9 ± 2	9 ± 3
	Qs	not consistent	4.5 ± 1	5 ± 1.5	10 ± 3
Milne	RGs	4 ± 1	4 ± 2	9 ± 2	9 ± 3
	Qs	2.5 ± 0.5	5 ± 1	5 ± 1.5	10 ± 3
de Sitter	RGs	4 ± 1	4 ± 1	9 ± 1	9 ± 1
	Qs	3 ± 1	5 ± 1.5	3.5 ± 1.5	10 ± 4

TABLE 6 RADIO GALAXY DATA

3C	Z PRED	Z OBS	F178	V	ALPHA	RLUME	VOLE	Y
14.	1.3527	1.	-24.99	20.0	1.05	-25.83	7.346E-3	0.926
15.	1.0827	1.073	-24.82	15.5	0.65	-27.09	1.106E-4	0.523
17.	1.2329	1.2201	-24.65	18.5	0.70	-25.95	2.263E-3	0.350
18.	1.2329	1.	-24.61	18.5	0.75	-25.85	2.618E-3	0.320
26.	1.2329	1.2106	-24.87	18.5	1.01	-26.18	2.018E-3	0.654
28.	1.1699	1.1959	-24.82	17.5	1.20	-26.18	1.671E-3	0.570
29.	1.0295	1.045	-24.79	13.0	0.59	-27.48	2.751E-5	0.466
31.	1.0191	1.017	-24.78	12.0	0.79	-28.32	1.577E-6	0.442
33.	1.0679	1.060	-24.28	15.0	0.71	-26.72	6.313E-5	0.093
35.	1.0555	1.	-24.87	14.5	0.95	-27.37	5.051E-5	0.613
40.	1.0191	1.0177	-24.59	12.0	1.13	-28.09	1.777E-6	0.234
46.	1.3094	1.	-24.99	19.5	1.10	-25.94	5.348E-3	0.924
52.	1.2329	1.	-24.97	18.5	0.64	-26.22	2.618E-3	0.864
61.1	1.2329	1.	-24.97	18.5	0.50	-26.24	2.618E-3	0.863
63.	1.2329	1.	-24.79	18.5	1.05	-26.01	2.618E-3	0.531
66.	1.0218	1.0215	-24.45	12.3	0.74	-27.78	3.158E-6	0.147
67.	1.2399	1.	-24.97	18.6	0.72	-26.19	2.825E-3	0.866
68.1	1.3094	1.	-24.74	19.5	0.91	-25.71	5.348E-3	0.540
75.	1.0295	1.0241	-24.61	13.0	0.68	-27.84	4.422E-6	0.251
76.1	1.0452	1.0326	-24.99	14.0	0.87	-27.96	1.074E-5	0.904
78.	1.0322	1.0289	-24.79	13.2	0.53	-27.87	7.546E-6	0.460
79.	1.1997	1.2561	-24.59	18.0	1.02	-25.72	3.336E-3	0.337
83.1	1.0238	1.0180	-24.52	12.5	0.64	-28.01	1.867E-6	0.184
84.	1.0191	1.0180	-24.21	12.0	0.77	-27.70	1.867E-6	0.065
88.	1.0308	1.0302	-24.77	13.1	0.66	-27.81	8.586E-6	0.432
89.	1.0827	1.	-24.70	15.5	1.02	-26.85	1.574E-4	0.365
93.1	1.2695	1.	-24.97	19.0	0.84	-26.08	3.793E-3	0.870
98.	1.0452	1.0306	-24.36	14.0	0.87	-27.38	8.924E-6	0.112
99.	1.1997	1.	-24.97	18.0	0.74	-26.35	1.756E-3	0.863
107.	1.1077	1.	-24.93	16.2	0.92	-26.85	3.306E-4	0.755
109.	1.1434	1.3056	-24.68	17.0	0.84	-25.67	5.186E-3	0.524
114.	1.2329	1.	-24.97	18.5	1.09	-26.18	2.618E-3	0.870
123.	1.3094	1.	-23.73	19.5	0.78	-24.72	5.348E-3	0.540
124.	1.2329	1.	-24.99	18.5	0.89	-26.22	2.618E-3	0.918
129.	1.2695	1.	-24.65	19.0	0.78	-25.76	3.793E-3	0.383
130.	1.1202	1.	-24.87	16.5	0.84	-26.69	4.477E-4	0.629
132.	1.2329	1.	-24.87	18.5	0.85	-26.11	2.618E-3	0.654
135.	1.1202	1.1270	-24.77	16.5	0.53	-26.56	5.210E-4	0.459
136.1	1.1434	1.	-24.86	17.0	0.94	-26.52	7.261E-4	0.618
153.	1.1997	1.	-24.73	18.0	0.71	-26.11	1.756E-3	0.431
166.	1.3094	1.	-24.86	19.5	0.89	-25.84	5.348E-3	0.653
171.	1.2545	1.2387	-24.61	18.8	0.75	-25.83	2.789E-3	0.321
173.	1.1997	1.	-24.97	18.0	0.92	-26.34	1.756E-3	0.865
173.1	1.2329	1.	-24.89	18.5	0.85	-26.13	2.618E-3	0.692
177.	1.0827	1.	-24.99	15.5	0.69	-27.15	1.574E-4	0.908
180.	1.2695	1.	-24.82	19.0	0.97	-25.91	3.793E-3	0.582
184.1	1.1434	1.	-24.89	17.0	0.71	-26.57	7.261E-4	0.671
187.	1.3094	1.	-24.93	19.5	0.79	-25.92	5.348E-3	0.783
192.	1.0679	1.0596	-24.68	15.0	0.82	-27.12	6.193E-5	0.332
196.1	1.1700	1.	-24.81	17.5	1.10	-26.31	1.145E-3	0.544
197.1	1.1202	1.	-24.99	16.5	0.80	-26.82	4.477E-4	0.911
198.	1.1434	1.0809	-24.75	17.0	0.93	-26.92	1.481E-4	0.425
200.	1.3527	1.	-24.86	20.0	0.96	-25.71	7.346E-3	0.742
210.	1.3527	1.	-24.95	20.0	1.00	-25.79	7.346E-3	0.835
212.	1.2695	1.	-24.78	19.0	0.90	-25.88	3.793E-3	0.521
213.1	1.2695	1.	-24.93	19.0	0.73	-26.05	3.793E-3	0.777
218.	1.0452	1.0533	-23.57	14.0	0.96	-26.11	4.490E-5	0.012
219.	1.1699	1.1745	-24.33	17.5	0.91	-25.82	1.230E-3	0.145
220.1	1.3094	1.	-24.89	19.5	1.09	-25.84	5.348E-3	0.712
220.2	1.2125	1.	-24.99	18.2	0.86	-26.31	2.067E-3	0.917
220.3	1.2329	1.	-24.81	18.5	1.10	-26.02	2.618E-3	0.562
222.	1.3527	1.	-25.02	20.0	1.26	-25.83	7.346E-3	1.000
223.	1.1202	1.1367	-24.81	16.5	0.95	-26.51	6.373E-4	0.531
223.1	1.1000	1.1075	-24.99	16.0	0.62	-26.92	3.288E-4	0.909
226.	1.3094	1.	-24.84	19.5	1.22	-25.78	5.348E-3	0.631

226.	1.3094	1.	-24.84	19.5	1.22	-25.78	5.348E-3	0.631
227.	1.0555	1.0855	-24.52	14.5	0.85	-26.64	1.731E-4	0.209
234.	1.1699	1.1846	-24.51	17.5	1.02	-25.94	1.428E-3	0.24
236.	1.0679	1.0988	-25.02	15.0	0.40	-27.04	2.598E-4	1.000
244.1	1.2695	1.	-24.69	19.0	0.95	-25.78	3.793E-3	0.414
255.	1.0827	1.0238	-24.75	15.5	1.35	-27.99	4.262E-6	0.405
256.	1.1434	1.	-24.99	17.0	1.05	-26.65	7.261E-4	0.913
258.	1.3094	1.	-25.02	19.5	0.55	-26.04	5.348E-3	1.000
263.1	1.3527	1.	-24.73	20.0	1.02	-25.57	7.346E-3	0.742
264.	1.0295	1.0206	-24.59	13.0	0.78	-27.96	2.783E-6	0.234
265.	1.3527	1.	-24.71	20.0	0.99	-25.55	7.346E-3	0.742
266.	1.2260	1.	-25.02	18.4	0.95	-26.27	2.422E-3	1.000
268.2	1.2695	1.	-25.02	19.0	0.78	-26.13	3.793E-3	1.000
274.	1.0112	1.0038	-22.98	10.8	0.85	-27.82	1.814E-8	0.001
274.1	1.3527	1.	-24.79	20.0	0.54	-25.69	7.346E-3	0.742
277.3	1.0827	1.0857	-24.91	15.5	0.75	-27.04	1.743E-4	0.703
278.	1.0322	1.0143	-24.47	13.2	0.73	-28.16	9.441E-7	0.154
284.	1.2329	1.	-24.95	18.5	0.75	-26.19	2.618E-3	0.818
285.	1.0827	1.0797	-24.95	15.5	0.53	-27.15	1.419E-4	0.796
287.1	1.2329	1.2156	-24.91	18.5	0.45	-26.25	2.145E-3	0.720
288.	1.1202	1.	-24.81	16.5	0.87	-26.63	4.477E-4	0.524
293.	1.0295	1.0454	-24.89	13.0	0.75	-27.57	2.822E-5	0.650
293.1	1.2695	1.	-24.99	19.0	1.15	-26.06	3.793E-3	0.922
295.	1.3527	1.4600	-24.11	20.0	0.75	-24.75	1.366E-2	
296.	1.0191	1.0237	-24.87	12.0	0.34	-28.12	4.209E-6	0.600
299.	1.3527	1.	-24.93	20.0	0.90	-25.79	7.346E-3	0.791
300.	1.1997	1.	-24.77	18.0	0.93	-26.14	1.756E-3	0.490
300.1	1.2695	1.	-24.95	19.0	0.79	-26.06	3.793E-3	0.822
303.	1.1000	1.	-24.87	16.0	0.90	-26.85	2.688E-4	0.625
303.1	1.1997	1.	-24.91	18.0	0.65	-26.30	1.756E-3	0.722
305.	1.0366	1.0416	-24.84	13.5	0.72	-27.60	2.189E-5	0.550
306.1	1.2695	1.	-24.87	19.0	1.15	-25.94	3.793E-3	0.670
310.	1.0555	1.0543	-24.26	14.5	1.14	-26.78	4.737E-5	0.090
313.	1.2695	1.	-24.52	19.0	0.96	-25.61	3.793E-3	0.383
314.1	1.1434	1.	-25.02	17.0	0.91	-26.68	7.261E-4	1.000
315.	1.1077	1.1086	-24.73	16.2	0.92	-26.64	3.382E-4	0.409
317.	1.0238	1.0351	-24.34	12.5	1.23	-27.24	1.334E-5	0.109
318.	1.3094	1.	-24.97	19.5	0.85	-25.95	5.348E-3	0.873
319.	1.2329	1.	-24.70	18.5	0.99	-25.92	2.618E-3	0.416
320.	1.1997	1.	-24.91	18.0	0.97	-26.27	1.756E-3	0.728
322.	1.2695	1.	-24.99	19.0	0.86	-26.09	3.793E-3	0.920
323.	1.2329	1.	-24.99	18.5	1.07	-26.21	2.618E-3	0.919
326.	1.2329	1.	-24.97	18.5	0.80	-26.21	2.618E-3	0.866
327.	1.0679	1.1041	-24.37	15.0	0.83	-26.32	3.007E-4	0.138
327.1	1.2329	1.	-24.59	18.5	0.98	-25.81	2.618E-3	0.312
332.	1.1000	1.	-24.95	16.0	0.84	-26.94	2.688E-4	0.802
338.	1.0191	1.0303	-24.36	12.0	1.51	-27.38	8.670E-6	0.115
341.	1.3094	1.	-24.95	19.5	0.81	-25.94	5.348E-3	0.827
346.	1.1000	1.	-24.93	16.0	0.69	-26.92	2.688E-4	0.751
348.	1.1997	1.1540	-23.46	18.0	1.05	-25.05	8.803E-4	0.089
349.	1.2695	1.	-24.89	19.0	0.68	-26.01	3.793E-3	0.694
353.	1.0679	1.0307	-23.67	15.0	0.69	-26.69	9.010E-6	0.012
356.	1.0765	1.	-24.81	15.3	1.07	-27.03	1.262E-4	0.513
357.	1.0827	1.	-24.02	15.5	0.78	-26.18	1.574E-4	0.047
371.	1.0491	1.0508	-24.99	14.2	0.90	-27.57	3.908E-5	0.906
381.	1.1434	1.1614	-24.87	17.0	0.63	-26.45	9.988E-4	0.634
382.	1.0555	1.0586	-24.67	14.5	0.77	-27.13	5.899E-5	0.321
388.	1.0555	1.0917	-24.63	14.5	0.87	-26.69	2.108E-4	0.295
390.3	1.0415	1.0569	-24.33	13.8	0.57	-26.82	5.420E-5	0.107
401.	1.1997	1.	-24.69	18.0	0.81	-26.07	1.756E-3	0.389
403.	1.0555	1.0590	-24.55	14.5	0.77	-27.00	6.016E-5	0.219
403.1	1.1077	1.	-24.87	16.2	0.73	-26.80	3.306E-4	0.624
405.	1.0679	1.0570	-22.06	15.0	0.80	-24.54	5.448E-5	0.006
424.	1.1997	1.	-24.87	18.0	1.23	-26.21	1.756E-3	0.656
430.	1.0679	1.	-24.51	15.0	0.78	-26.84	9.009E-5	0.196
433.	1.1000	1.1025	-24.25	16.0	0.90	-26.21	2.879E-4	0.099
436.	1.2695	1.2154	-24.79	19.0	0.87	-26.09	2.140E-3	0.521
441.	1.3012	1.	-24.86	19.4	0.81	-25.87	5.003E-3	0.649
442.	1.0295	1.0262	-24.67	13.0	1.05	-27.83	5.656E-6	0.310
445.	1.0765	1.0568	-24.61	15.3	0.86	-27.09	5.393E-5	0.265
449.	1.0238	1.0181	-24.84	12.5	0.60	-28.32	1.898E-6	0.542
452.	1.1000	1.0820	-24.28	16.0	0.94	-26.44	1.538E-4	0.102

452.	1.1000	1.0820	-24.28	16.0	0.94	-26.44	1.538E-4	0.102
455.	1.0336	1.0331	-24.86	13.3	0.82	-27.82	1.123E-5	0.585
456.	1.2695	1.2377	-24.86	19.0	0.77	-26.08	2.759E-3	0.635
458.	1.3527	1.	-24.97	20.0	0.86	-25.83	7.346E-3	0.877
459.	1.1814	1.2205	-24.63	17.7	1.02	-25.90	2.274E-3	0.343
465.	1.0218	1.0301	-24.43	12.2	0.96	-27.47	8.503E-6	0.141
470.	1.3094	1.	-25.02	19.5	1.19	-25.96	5.348E-3	1.000

NOTES

1 SEE NOTE 5 TO TABLE 1

2 Y IS THE RATIO OF VOLE TO THE MAXIMUM OBSERVABLE VOLUME

3 THE IDENTIFICATION FOR 3C356 IS PROBABLY A STAR, REF66

TABLE 6A DOUBLE SOURCES

3C	IDN	ANG SEP	VEL	S1	S2
33.		244 230	0.10	9.9	3.3
47.		63 240	0.03	1.59	1.01
103.	A	88 120	0.14	3.7	1.8
103.	B	88 260	0.04	1.8	3.7
103.	C	88 240	0.45	1.8	3.7
109.		81 260	0.12	2.3	2.6
219.		138 300	0.03	4.2	3.9
223.1		71 107	0.44	1.06	0.78
250.		42 140	0.35	0.52	0.50
252.		55 180	0.39	0.54	0.97
			-0.0		
313.		122 360	0.17	2.17	1.52
332.		54 76	0.13	1.92	1.50
340.		34 95	0.84	1.67	0.75
356.	B	69 320	0.74	0.64	1.12
381.		60 125	0.08	2.63	1.36
390.3		205 180	0.20	4.0	4.7
405.		106 90	0.12	1000	800
46.	A	145 460	0.10	0.58	0.5
46.	B	145 350	0.14	0.58	0.5
52.	A	54 150	0.19	1.48	3.2
79.		60 170	0.02	1.92	3.2
76.1	A	45 24	0.11	1.2	1.3
114.	A	45 120	0.03	0.56	0.56
177.		75 160	0.48	1.97	1.58
244.1	A	44 130	0.15	1.82	2.11
263.		46 210	0.47	3.4	1.1
268.2	A	77 230	0.18	0.65	0.71
274.1	A	142 470	0.02	1.07	0.93
274.1	B	142 680	0.40	1.07	0.93
284.		161 430	0.21	1.27	0.43
285.		134 160	0.06	1.27	1.03
300.		75 180	0.63	3.2	0.58
319.		64 170	0.06	2.17	1.52
323.1	A	65 190	0.08	0.82	1.56
323.1	B	65 190	0.33	1.56	0.82
334.		41 170	0.52	0.78	1.00
338.		41 20	0.06	2.0	2.0
341.		54 170	0.05	0.84	1.63
349.	A	70 210	0.08	1.94	1.32
349.	B	70 340	0.04	1.32	1.94
357.		74 90	0.08	1.32	0.92
379.1		68 160	0.21	1.59	0.83
382.		152 130	0.10	4.0	1.6
			-0.0		
402.	A	340 230	0.02	1.08	0.16
430.		57 57	0.09	4.9	4.5

NOTES

1 COLUMN 2 INDICATES WHICH IDENTIFICATION IN REF.66 IS REFERRED TO, WHERE THERE IS MORE THAN ONE IDENTIFICATION

2 COLUMN 3 GIVES THE ANGULAR SEPARATION OF THE 2 COMPONENTS, IN SECONDS OF ARC

4 COLUMN 4 GIVES THE PROJECTED LINEAR SEPARATION, IN KPC.

5 COLUMN 5 GIVES THE LINE OF SIGHT COMPONENT OF THE VELOCITY OF THE COMPONENTS ON THE RYLE - LONGAIR MODEL, IN UNITS IN WHICH THE VELOCITY OF LIGHT IS 1.

6 S1 AND S2 ARE THE FLUXES AT 1407 MHZ OF THE INNER AND OUTER COMPONENTS, RESPECTIVELY, IN FLUX-UNITS.

Table 7.

log N - log S data

$f = \log_{10} S_{178}$	$\log_{10} N$	log N - 1.4 + 1.5 (+25 + f)
-24.455	0.60 ± .09	+.02
-24.67	1.00 ± .06	+.095
-24.79	1.23 ± .05	+.145
-24.97	1.56 ± .03	+.205
-25.00	1.61 ± .03	+.21
-25.15	1.83 ± .025	+.205
-25.30	2.10 ± .025	+.25
-25.40	2.265 ± .015	+.265
-25.53	2.48 ± .03	+.285
-25.71	2.79 ± .015	+.325
-25.92 +	3.13 + .10, -.12	+.33
-26.00 *	3.27 ± .05	+.37
-26.03 *	3.34 + .14, -.20	+.395
-26.12 +	3.45 + .08, -.10	+.37
-26.25 *	3.57 + .10, -.13	+.295
-26.30 +	3.65 + .06, -.08	+.40
-26.43 *	3.83 + .07, -.10	+.285
-26.00 +	4.02 ± .05	+.32
-26.73 *	4.08 ± .06	+.105
-26.97 *	4.32 ± .04	-.035
-27.07 *	4.42 ± .04	-.085
-27.27 *	4.63 ± .04	-.175
-27.45 *	4.73 ± .045	-.345
-27.62 *	4.85 + .05	-.48
-27.73 *	4.96 ∓ .07	-.535

Table 7 cont'd....

Interpolated values

f	log N
-24.5	0.68 ± .09
-24.75	1.13 ± .06
-25	1.60 ± .03
-25.25	2.00 ± .03
-25.5	2.425 ± .025
-25.75	2.85 ± .02
-26	3.26 ± .05
126.25	3.58 ± .10
-26.5	3.90 ± .07
-26.75	4.12 ± .06
-27	4.36 ± .04
-27.25	4.61 ± .04
-27.5	4.76 ± .05
-27.75	5.00 ± .07

\+ N. Polar Survey (101)

* counts at 408 MHz, assuming $f_{178} = f_{408} + 0.27$ (i.e., $\bar{\alpha} = 0.75$) (106)

rest from 3C and 4C (17).

Table 8.

Predicted luminosity distributions at 4C and 5C flux-levels.

models:	E1	Einstein-de Sitter,	$Z_L = 5$, $\mathcal{F}_c = -28$
	M1	Milne	$Z_L = 5$, $\mathcal{F}_c = -27.5$
	S1	de Sitter	$Z_L = 5$, $\mathcal{F}_c = -26.5$
	E2	Einstein-de Sitter	$Z_D = 10$, $\mathcal{F}_c = -26.5$, $Z^* = 3.5$
	E3	Einstein-de Sitter	$Z_L = 5$, $\mathcal{F}_c = -30$, including effect of electron scattering.
	M2	Milne	$Q_D = 10$, $P \propto H^{1+\alpha}$, $\mathcal{F}_c = -26.5$
	M3	Milne	$Q_D = 10$, $P \propto H^{1+2\alpha}$, $\mathcal{F}_c = -27$.

Table 6 cont'd....

4C, f = -25.75

	-30	-29.5	-29	-28.5	-28	-27.5	-27	-26.5	-26	-25.5	-25	
E1	2.05	1.8	2.4	7.2	37.7	94.6	304.6	278.5	38.1	2.5		
M1	2.05	1.8	2.4	7.2	20.6	79.9	186.5	247.3	103.0	24.6	4.0	
S1	2.05	1.8	2.4	7.3	20.9	22.5	37.5	283.2	180.7	82.3	30.3	
E2	2.0	1.8	2.4	7.2	20.5	27.2	36.4	182.4	175.6	151.5	73.7	7.4
E3	2.2	2.0	3.1	11.1	42.6	73.5	272.6	248.4	17.6	3.9		
M2	2.1	1.9	2.8	8.0	29.8	32.4	69.3	106.8	104.1	151.3	80.8	29.6
M3	2.1	1.9	2.8	8.1	31.1	36.2	75.1	116.5	110.0	130.4	68.7	22.4

5C, f = -27.75

E1	1631	1216	1292	2654	50,270	20,210	6390	1318	100	5		
M1	1637	1228	1324	2816	5816	57,590	24,490	11,830	2658	461	62	
S1	1657	1267	1426	3297	6956	5364	6371	97,990	29,180	8230	2237	
E2	1632	1216	1292	2653	4556	3227	1904	75,380	7366	737	74	7
E3	3543	5087	14,980	40,280	42,100	11,270	4357	946	38	6		
M2	2342	2185	3177	8580	25,220	17,390	19,220	13,670	6041	4232	1212	271
M3	2347	2199	3247	9140	29,500	23,830	27,370	19,240	7300	3476	814	137

Table 8 cont'd....

Predicted numbers of sources with $z \leq 0.25$

	f = -25.75 (4C)		f = -26.75 (NPS)		f = -27.75 (5C)	
	$\mathcal{F} \geq$ -28	$\mathcal{F} \geq$ -29	$\mathcal{F} \geq$ -28	$\mathcal{F} \geq$ -29	$\mathcal{F} \geq$ -28	$\mathcal{F} \geq$ -29
EI	112	122	305	542	305	1651
MI	107	116	413	651	413	2027
SI	90	94	770	883	2622	5546
M2	126	137	960	1330	960	4480
M3	135	146	1060	1440	1060	4680

For comparison the number of identifications of 5C sources to date (108), when converted to number/ster, is

$\mathcal{F} \geq$ -28	$\mathcal{F} \geq$ -29
2400	4800

but the redshifts of these objects have not been measured.

Table 9.
Median redshift at different flux-levels (see Table 8 for description of models.)

		E1	M1	S1	M3
f =	-25	0.31	0.38	0.44	0.30
	-25.5	0.70	0.66	0.81	0.46
	-26	1.09	0.95	1.32	0.60
	-26.5	1.38	1.34	2.20	0.74
	-27	1.77	2.00	3.45	0.81
	-27.5	2.89	3.12	4.98	0.90
	-28	4.16	4.56	7.00	0.96
4C	-25.7	0.85	0.77	1.00	0.52
NPS	-26.6	1.46	1.45	2.42	0.75
5C	-27.75	3.5	3.8	6.0	0.93
at 4C level, 1% of sources have z >		6.8	3.4	4.9	2.35

Table 10

Local theory for quasars

V_{lim}	19.5	19	18.5	18	17.5
number of quasars	54	51	48	35	25
$\bar{x}$	0.58	0.57	0.61	0.61	0.70
t	3.0	2.5	3.7	2.6	3.5
probability %	0.5	1.5	0.1	1	0.2
α(s.t. $\propto \alpha S^{-\alpha}$)	2	2	2.5	2.5	3
R.A. < 11h., $\bar{x}$ =		0.56	0.62	0.60	0.80
R.A. $\geq$ 11h.		0.58	0.59	0.61	0.62
dec. $\geq 30^{\circ}$		0.54	0.59	0.56	0.60
dec $< 30^{\circ}$		0.60	0.62	0.64	0.77

Appendix 1.

Radio and optical K-corrections:

We write $f_{rad} = \log_{10} S_{178}$ where S_{178} is theflux-density at 178 Mc/s in units of watts $(c/s)^{-1} m^{-2}$, taken from the 3CR catalogue increased by 8 percent (38), and take the radio K-correction to be

$$-0.4K = (\alpha - 1) \log_{10} (1 + z)$$

where α is the spectral index in the range 178 - 750 Mc/s.

α is taken from Kellerman (50) in the case of those sources classified by him as having straight spectra: for the remainder of the sources α is calculated from the relation

$$\alpha = \frac{\log_{10} S_{178} - \log_{10} S_{750}}{\log_{10} 750 - \log_{10} 178}$$

where S_{750} is taken from Pauliny-Toth, Wade and Heeschen (51).

This procedure is exact for sources having spectra of the form $F(\nu) \propto \nu^{-\alpha}$, and is reasonably accurate even for sources with curved spectra, since the curvatures are not very great.

In order to convert the optical magnitudes to approximately the same absolute scale as the radio flux-densities, we write

$$f_{opt} = -22.4 - 0.4\ V$$

where V is the apparent visual magnitude. We use the optical K-correction calculated by Sandage (52).

Appendix 2.

Calculation of $\mathcal{F}$ and $\mathcal{Y}$.

By definition $\mathcal{Y}(z) = \int_0^{r_0(z)} \frac{4\pi r^2 \, dr}{(1 + \frac{1}{4} k r^2)^3}$

and $\mathcal{F} - f + 0.4 K = 2 \log_{10} \{ \frac{r_0 R_0 Z}{1 + \frac{1}{4} k r_0^2} \}$ where $Z = 1 + z$

$= 2 \log_{10} (R_0 v Z)$ where $v = \frac{r_0}{1 + \frac{1}{4} k r_c^2}$.

From equations 2, 4, and 5 we find $\int_0^{r_0(z)} \frac{dr}{1 + \frac{1}{4} k r^2} = \frac{c}{R_0 H_0} \mathcal{X}(z)$

<u>k = + 1 :</u> $R_0 = c/H_0 . (3 \Omega_0 - 1 - q_0)^{1/2}$

$v = \sin \{ \mathcal{X} . (3 \Omega_0 - 1 - q_0)^{1/2} \}$

$\mathcal{Y}(z) = 2\pi \{ \sin^{-1} v - v (1 - v^2)^{1/2} \}$

$k = 0$:

$$R_0 = c/H_0$$

$$v = \chi$$

$$\nu(z) = 4\pi v^3 / 3$$

$k = -1$:

$$R_0 = c / H_0 . (1 + q_0 - 3 q_0)^{1/2}$$

$$v = \sinh \{ \chi . (1 + q_0 - 3 q_0)^{1/2} \}$$

$$\nu(z) = 2\pi \{ v (1 + v^2)^{1/2} + \sinh^{-1} v \}$$

The cases where χ can be evaluated exactly are

$q_0 = 0$ $(q_0 \neq 0)$

$$\frac{R_0 H_0 v}{c} = \frac{q_0 z + (q_0 - 1) . (\sqrt{1 + 2 q_0 z} - 1)}{q_0^2 (1 + z)}$$

$q_0 = 0$ $(q_0 \neq -1)$

$$\frac{R_0 H_0 v}{c} = \frac{\sqrt{(1 + q_0) Z^2 - q_0} - Z}{q_0}$$

The 3 asymptotic models are:

$\sigma_0 = q_0 = 0$ (Milne) : $v = (Z^2 - 1) / 2Z$

$\sigma_0 = q_0 = \frac{1}{2}$ (Einstein de Sitter) : $v = 2(1 - Z^{-1/2})$

$\sigma_0 = 0$, $q_0 = -1$ (de Sitter) : $v = z$

Appendix 3.

Discussion of recent data, and of Schmidt's version of the luminosity-volume test.

In this appendix the luminosity-volume test is applied to the latest data on quasars and radio-galaxies (April, 1969), in a slightly modified form.

Quasars.

Redshifts are available for 5 new 3C quasars (104). The distribution of quasars on the sky for

$V \leq 18$, $18 < V \leq 18.5$, $18.5 < V$, is shown in Fig. 35, sin b - ℓ. Any anisotropy in this distribution is confined to the faintest sources, confirming the suggestion of Penston and Rowan-Robinson (3) that this is an effect of selection. It seems reasonable to assume the data is complete down to $V = 18.5$.

Schmidt (90) has independently confirmed the conclusion of Chapter I that evolution must affect the distribution in space of the quasars, using a slightly different version of the luminosity-volume test. Like Kafka (32), Schmidt defines $x = \mathcal{S} / \hat{\mathcal{S}}(\mathcal{F})$, and argues that if the quasars are uniformly distributed, the mean value of $x = \max \{ x_{rad}, x_{opt} \}$, $\bar{x}$, should be 0.5. The Kafka-Schmidt

test can be quantified by using Student's t-test. If x is uniformly distributed in $(0,1)$, the expected standard deviation is given by

$$\sigma^2 = \int_0^1 (x - \mu)^2 \, dx = 1/12$$

and then $t = (\bar{x} - \mu) \sqrt{N} / \sigma$, where $\bar{x}$ is the mean for N sources.

Contours of equal probability using this version of the luminosity-volume test are shown in Fig. 36a, $q_0 = q_0$ (no evolution). Also shown are the results using the test of section I.4, modified slightly as follows:

for strong sources ($\mathcal{F}_{rad} \geq -25$, $\mathcal{F}_{opt} \geq -29$), we use

$z_{max} = \mathcal{V}^{-1}(\frac{1}{2}\mathcal{V}(2.3))$, and for weak sources,

$z_{max} = \mathcal{V}^{-1}(\frac{1}{2}\mathcal{V}(1.2))$. The number of sources of all classes (radio and optical, weak and strong) in the near half of observable space is compared with the number in the far half, using the X^2 - test.

The results are similar for the ? tests:

the Kafka-Schmidt test assigns a lower probability to models near the

de Sitter model and the model with $\Omega_0 = 1$, $q_0 = 0$, and a higher probability elsewhere. But both versions agree that evolution is necessary in all models with $q_0 \geq -1$.

Schmidt states that $\bar{x}$ is not very dependent on optical or radio luminosity and therefore rejects luminosity evolution as an interesting possibility. However evolution of this type gave good consistency with the source-counts in Chapter III. The correct scientific question is: can evolution of this kind be ruled out yet? A lower limit to the rate of luminosity evolution can be set by using the modified luminosity-volume test of section I.7., incorporating the changes described above. To obtain an upper limit, we set $z_{max} = 2.2$ for strong sources (which we have taken as $\mathcal{F}'_{rad} \geq -27$, $\mathcal{F}'_{opt} \geq -31$) and $z_{max} = 1.2$ for weak sources. The results are shown for a number of cases in Figs. 36 b,c, and d.

Power-law luminosity evolution can be ruled out for $\Omega_0 = q_0 \geq 0.17$, and exponential luminosity evolution for $\Omega_0 = q_0 \geq 0.2$, and for $\Omega_0 = 0$, $q_0 \geq 2$, for example. The Kafka-Schmidt test rules out luminosity evolution in no

models. It is a weaker test because it automatically throws away half the information available, in taking $x = \max \{ x_{rad} , x_{opt} \}$.

Radio-galaxies.

Redshifts are available for a further 10 3C radio-galaxies and mostly agree well with those predicted by equation (21) of section 1.14 (see table 6). Applying the luminosity-volume test to the ranges of radio-luminosity

$$-28.5 + 0.5\,n \leq \mathcal{F} \leq -28 + 0.5\,n \quad , \quad \text{for } n = 0, 1, \ldots, 7,$$

and comparing

$$\sum_{n=0}^{7} \frac{(N_{near} - N_{far})^2}{total}$$ with the

χ^2 variable with 8 degrees of freedom, gives the very low probabilities shown in the table below, for the E, M and S models. The effects of changing all optical magnitudes by ± 1 are also shown: also of confining attention to $V \leq 19$. The final effect on table 5 of the latest data is slight.

Finally we note the probability of mistaken identifications. Wyndham (60) gives this as 5 percent for a galaxy with $V = 19$, and 20 percent for $V = 20$.

	E	M	S
$V_{lim} = 20$	0.4 %	1 %	0.5 %
all mags + 1	0.01%	0.01%	0.1%
all mags - 1	0.2 %	0.1%	2.5 %
$V_{lim} = 19$	0.4 %	0.3 %	1 %

Appendix 4

Remarks on a suggestion of Jauncy.

Jauncy (105) has suggested that $\frac{dN}{df}$, = - x N ,

should be used in place of $x = -\frac{d \log N}{d \log f}$, when comparing the observed source-counts with theoretical models. This is because $N(f_1)$ is not independent of $N(f_2)$ if $f_1 < f_2$, so that the quoted statistical uncertainties are not independent and a least squares fit is no longer valid. This does not affect the analysis of Chapter III, where we have been more concerned with the dependence of the theoretical number-count relation on the various cosmological and evolutionary parameters, but it is worth pointing out a serious drawback to Jauncy's suggestion.

The point is that N(f) is the only observable quantity which is a precisely defined function of flux-density. To observe $\frac{dN}{df}$ (and $\frac{dN}{dS^{-3/2}}$ would seem a more convenient choice), the number of sources between two flux-levels f_1 and f_2 must be counted: the number $\Delta N / \Delta f$ then applies to the whole range of flux-density (f_1, f_2). In practice the uncertainty in $\frac{dN}{df}$ caused

by this uncertainty in f, $\pm \Delta f/2$, is generally much greater than that due to statistical uncertainty in ΔN. Fortunately the error introduced by the non-independence of $N(f_1)$ and $N(f_2)$ is very slight, since for reasonable steps in f, $N(f_1) \gg N(f_2)$, so $\Delta N \sim N(f_1)$.

Jauncy's criticism is just if applied to counts of different classes of 3C source (e.g. (46)), where the range of flux-density covered by the sources is small. Very little weight should be attached to such counts, since it is impossible to predict theoretical quantities without full knowledge of optical and radio luminosity functions for each class of source. The luminosity-volume test is a much sound approach, though requiring more information.

However, for interest we show the source-counts that would be obtained for a number of different cases considered in Chapters 3 and 4 if all sources beyond $z = 0.5$ were invisible (Fig. 37). This gives a crude indication of the number of galaxies brighter than the plate limit of the Palomar Sky Survey that should be identifiable with radio-sources at different flux-levels. For comparison with Fig. 13, the counts of sources with $\mathcal{F} \geq -27$ are also shown.

Appendix 5.

The local theory for quasars.

Pooley and Ryle (106) have shown that if the quasars are the cause of the steep radio-source counts then it is extremely unlikely that the quasars form a 'local' population. The question remains: can a uniformly distributed local population form a significant fraction of the observed sources?

Suppose we have a set of sources distributed locally such that the number having luminosity between $\mathcal{F}$ and $\mathcal{F} + d\mathcal{F}$ out to distance r is

$$M(r, \mathcal{F})\, d\mathcal{F} = n_0 r^{2x} \varphi(\mathcal{F})\, d\mathcal{F}$$

where

$$\int_{\mathcal{F}_1}^{\mathcal{F}_2} \varphi(\mathcal{F})\, d\mathcal{F} = 1$$

and

$$\varphi(\mathcal{F}) = 0 \quad \text{outside} \quad (\mathcal{F}_1, \mathcal{F}_2).$$

Then the number observed down to flux-level

$$S, \quad N(S) = \int_{-\infty}^{\infty} n_S(\mathcal{F})\, d\mathcal{F}$$

where

$$n_S(\mathcal{F}) = n_0 S^{-x} P^x \varphi(\mathcal{F}) = M(P/S, \mathcal{F})$$

since

$$S = P/r^2 .$$

$$N(S) = n_0 P_2^{-x} S^{-x} \int_{\mathcal{F}_1}^{\mathcal{F}_2} (P/P_2) \varphi(\mathcal{F}) \, d\mathcal{F} = 10^{-x(f-f_0)}$$

where

$$xf_0 = \log_{10} \{ n_0 P_2^x \int_{\mathcal{F}_1}^{\mathcal{F}_2} (P/P_2)^x \varphi(\mathcal{F}) \, d\mathcal{F} \} \qquad (1)$$

The integrated flux out to R, the nearest edge of the distribution.

$$F = \int_0^R \int_{\mathcal{F}_1}^{\mathcal{F}_2} \frac{P}{r^2} \, dM \, d\mathcal{F}$$

$$= 2x \, n_0 \int_{\mathcal{F}_1}^{\mathcal{F}_2} P \varphi(\mathcal{F}) \, d\mathcal{F} \int_0^R r^{2x-3} \cdot dr$$

$$= \eta_0 P_2 \cdot \frac{2x R^{2x-2}}{2x-2} \int_{\mathcal{F}_1}^{\mathcal{F}_2} (P/P_2)\, \varphi(\mathcal{F})\, d\mathcal{F} \qquad (2)$$

To get no more than 30° at 178 MHz we need

$$10^{23} F \leq 30 \qquad (3)$$

where r is measured in metres.

Then equations (1) (2) and (3) imply

$$\frac{P_2}{R^2} \geq \left[\frac{x}{x-1} \, 10^{21.5 + x} f_0 \left\{ \frac{\int_{\mathcal{F}_1}^{\mathcal{F}_2} (P/P_2)\, \varphi(\mathcal{F})\, d\mathcal{F}}{\int_{\mathcal{F}_1}^{\mathcal{F}_2} (P/P_2)^x\, \varphi(\mathcal{F})\, d\mathcal{F}} \right\} \right]^{\frac{1}{x-1}} \qquad (4)$$

Now the condition that the edge be unobservable down flux-level S, (and hence, assuming we are not at the centre of the distribution, the condition that the source counts be isotropic at all flux-levels down to S) is

$$\frac{P_2}{R^2} \leq S_1 \quad \ldots \qquad (5)$$

This is consistent with (4) if

$$\log_{10}\left\{\frac{\int_{\mathcal{F}_1}^{\mathcal{F}_2} (P/P_2)\,\varphi(\mathcal{F})\,d\mathcal{F}}{\int_{\mathcal{F}_1}^{\mathcal{F}_2} (P/P_2)^x\,\varphi(\mathcal{F})\,d\mathcal{F}}\right\} \leq (x-1)f_1 - 21.5 - xf_0 + \log_{10}\left(\frac{x-1}{x}\right) \qquad (6)$$

$$= \frac{f_1}{2} - 21.5 - \frac{3f_0}{2} - .48 \quad \text{if} \quad x = 1.5$$

$$= 0.75 \quad \text{if} \quad f_0 = -24.4\,, \quad f_1 = -27.75$$

corresponding to 22.5 percent of 3C sources

$$= 0.45 \quad \text{if} \quad f_0 = -24.2\,, \quad f_1 = -27.75$$

corresponding to 45 percent of 3C sources

(or alternatively to $T \leq 15^{\circ}$ K).

The dependence of the expression on the L.H.S. of (6) on the form of $\varphi(\mathcal{F})$ can be seen by taking $\log_{10}\varphi(\mathcal{F}) = \text{const} + a(\mathcal{F}_2 - \mathcal{F})$

and estimating the maximum value of $(\mathcal{F}_2 - \mathcal{F}_1)$ consistent with the R.H.S. of (6) for different values of a.

$\log_{10}\{\ \} \leq$	a = ∞	2.5	2	1.75	1.5	1.25	1	0.9	0.8	0.7
0.75	1.5	1.8	2.0	2.2	2.5	3.0	5.0	∞		
0.45	0.9	1.2	1.3	1.4	1.6	1.8	2.3	2.6	3.2	∞

$\mathcal{F}_2 - \mathcal{F}_1$

Thus a local population cannot be ruled out at all if its luminosity function $\varphi(\mathcal{F})$ is flat enough, or if the spread in luminosities, $(\mathcal{F}_2 - \mathcal{F}_1)$, is not too great, < 1 say.

The above argument is essentially that of Ryle and Clarke (15), except that they have a different expression in place of (5). They were considering the case $f_1 = -26.6$ (corresponding to the Ryle-Neville survey limit (82)) and $f_0 = -23.9$ (corresponding to all 3C sources), which makes the R.H.S. of (6) 0.55. In retrospect it is difficult to see how they were able to conclude that the radio-sources could not be galactic.

A second possibility is that most of the 3C quasars are local objects, but part of a population which extends uniformly throughout space. If the 3C quasars are very local, say $z_c \leq .003$, then the number down to the 5C level will be given by

$$N(S) \propto S^{-3/2}, \quad \text{i.e.}$$

$$\log_{10} N = 0.95 + 1.5\,(2.75) = 5.075$$

since there are 9 quasars per steradian at the 3C level. The actual number of sources per ster at the 5C level is given by $\log_{10} N = 4.96 \pm 0.07$, so all sources at this level would have to be quasars. Moreover, the number-count slope at this level is closer to 1.0 than 1.5, so on both these grounds we must have

$$z_c > 0.003 \qquad (7)$$

The contribution to the integrated background, in the steady-state cosmology, is given by

$$T_{178} \sim \frac{0.07}{z_c} \qquad \text{for these objects,}$$

so to get 30^{o} or less, we need

$$z_c > 0.0023 \qquad (8)$$

If the redshifts of quasars are gravitational, then the model of Fowler and Hoyle (107) requires the masses to be $\geq 10^{13}$ solar masses, so for the 3C quasars to contribute no more than 2×10^{-29} gm/cc we again find

$$z_c \geq 0.003 \qquad (9)$$

However 4 quasars, including 3C 191, have emission time redshifts $1.9555 \pm .0005$, presumably an intrinsic redshift (on the local model). For one object out of 54 to have a cosmological redshift ≤ 0.001, we need

$$z_c \leq 0.001\,(54)^{1/3} \sim 0.004 \qquad (10)$$

The inequalities (7) - (10) imply that $z_c \sim 0.004$, i.e. that most of the 3C quasars are as close as the Virgo cluster, or closer.

Thus, although implausible, neither a local uniform irregularity, nor a uniform distribution of quasars with gravitational redshifts, can be ruled out by arguments using isotropy etc. We now show that provided the redshifts of 3C quasars are independent of distance, their distribution in space cannot be uniform.

Let the distance of a source of luminosity P be $D \ll c\,t_0$, where t_0 is the Hubble time, and let the observed flux-density be S. The inverse square law gives

$$SD^2 = \frac{P}{J(z)} \qquad (I)$$

where $J(z)$ takes account of the shift of the emitted spectrum across the waveband of the observer, and any other dimming caused by the redshift.

Now the R.H.S. of equation (I) depends only on intrinsic properties of the source, and so is constant for any particular class of source (i.e. of given P and z). This applies even if the luminosity is a function of redshift, as suggested by Hoyle and Burbidge (53).

Thus if S_{min} is the limiting flux-level, down to which we have a complete sample of sources, then the maximum distance at which this class of source is observable, D_{max} is given by

$$SD^2 = S_{min} D^2_{max} \qquad (2)$$

If the distribution of the sources is uniform in space , the probability of finding a source at any particular distance is found by considering the corresponding volume of space, $\mathcal{V}(D)$. If we define

$$x = \mathcal{V}(D) / \mathcal{V}(D_{max}) \qquad (3)$$

for any particular class of source, then x should be uniformly distributed in $(0,1)$.

Now if $D \ll c_0$, $\mathcal{V}(D) = 4\pi D^3/3$

so

$$\left(\frac{D}{D_{max}}\right)^3 = \left(\frac{S_{min}}{S}\right)^{3/2}, \quad \text{from (2) and (3)} \qquad (4)$$

As in Appendix 3, the quantity which should be uniformly distributed in $(0,1)$ for quasars is in fact

$$x = \max \{ x_{rad}, x_{opt} \}$$

$$= \max \left\{ \left(\frac{S_{min}}{S}\right)^{3/2}_{rad}, \left(\frac{S_{min}}{S}\right)^{3/2}_{opt} \right\},$$

and we compare $\sqrt{12N}\,(\bar{x} - 0.5)$ with Student's t.

We apply this to 54 quasars identified with 3C sources (104), for which $S_{min} = 9$ f.u., and take

$$\left(\frac{S_{min}}{S}\right)^{3/2}_{opt} = 10^{0.6\,(V - V_{lim})}$$

with

$$V_{lim} = 19.5\ (0.5)\ 17.5.$$

Table 10 gives $N, \bar{x}, t$ and the corresponding probability for the different values of V_{lim}. With a high degree of confidence we can assert that the quasars are <u>not</u> uniformly distributed locally. For each value of V_{lim}, $\bar{x}$ is significantly greater than 0.5

If we take $\propto a\, S^{-a}$ instead of $S^{-3/2}$, then

$$\bar{x} = \int_0^1 \frac{2a}{3}\, x^{2a/3}\, dx = \frac{2a}{2a+3}$$

$$\bar{x}^2 = \int_0^1 \frac{2a}{3}\, x^{2a/3+1}\, dx \qquad \sigma^2 = \frac{2a}{2(3+a)} - \left(\frac{2a}{2a+3}\right)^2$$

The identifications are probably complete down to $V = 18.5$ (Appendix 3), so $\mu = 0.6$ and $a = 2.25$.

The uncertainty in a is $\dfrac{\sigma}{\sqrt{N}\ \frac{dM}{dx}} \sim 0.3$.

Thus even if the quasars are "local", they show a strong departure from a uniform distribution in space, ressembling the radio-galaxies (1 .14) in this respect.

Since the number of sources is not very large it is not possible to test in detail to what extent this effect depends on direction in the sky. But when the area of sky covered by the 3C catalogue is divided into two ranges of declination, and two ranges of hour angle, the values pf $\bar{x}$ are ~~similar~~ >0.5 for each portion of the sky , as shown in the table.

If we are in a "local" cluster of quasars then we are in a special position, at the bottom of a ~~isotropic~~ density-well. The more natural inference is that the number-density or luminosity of these objects was greater in the past, ruling out the steady-state cosmology.

REFERENCES

(1) Greenstein, J.L., and Schmidt, M., 1964. Astrophys. J., 140, 1.

(2) Strittmatter, P., Faulkner, J. and Walmesley, M., 1966. Nature, Lond., 212, 1441.

(3) Penston, M.V., and Rowan-Robinson, M., 1967. Nature, Lond., 213, 375.

(4) Burbidge, G.R., and Burbidge, E.M., 1967. Astrophys. J., 148, 107.

(5) Arp, H., 1966. Science, 151, 1214.

(6) Arp, H., 1967. Astrophys. J., 148, 321.

(7) Sandage, A.R., 1966. Astrophys. J., 146, 13.

(8) Terrell, J., 1964. Science, 145, 918.

(9) Hoyle, F., and Burbidge, G.R., 1966. Astrophys. J., 144, 534.

(10) Faulkner, J., Gunn, J.E., and Peterson, B.A., 1966. Nature, Lond., 211, 502

(11) Noedlinger, P.D., Jokipii, J.R. and Woltjer, L., 1966. Astrophys. J., 146, 523.

(12) Hughes, R.G., and Longair, M.S., 1967. Mon. Not. R. astr. Soc., 135, 131.

(13) Hoyle, F., and Burbidge, G.R., 1966. Nature, Lond., 210, 1346.

(14) Kafka, P., 1967. Nature, Lond., 213, 346.

(15) Ryle, M., and Clarke, R.W., 1961. Mon. Not. R. astr. Soc., 122, 349.

(16) Davidson, W., 1962. Mon. Not. R. astr. Soc., 123, 425.

(17) Gower, J.F.R., 1966. Mon. Not. R. astr. Soc., 133, 151.

(18) Longair, M.S., 1966. Mon. Not. R. astr. Soc., 133, 421

(19) Davidson, W., 1962. Mon. Not. R. astr. Soc., 124, 79.

(20) Davidson, W. and Davies, M., 1964. Mon. Not. R. astr. Soc., 127, 421.

(21) Davidson, W., and Davies, M., 1966. Mon. Not. R. astr. Soc., 134, 405

(22) Longair, M.S., 1966. Nature, Lond., 211, 949.

(23) Roeder, R.C., and Mitchell, G.F., 1966. Nature, Lond., 212, 165.

(24) Rowan-Robinson, M., 1966. Nature, Lond., 212, 1556.

(25) Robertson, H.P., 1933. Rev. mod. Phys., 5, 62.

(26) McCrea, W.H., 1935. Z. Astrophys., 15, 69.

(27) McVittie, G.C., 1956. General Relativity and Cosmology, Chapman and Hall, London.

(28) Refsdal, S. and Stabell, R., 1966. Mon. Not. R. astr. Soc., 132, 379.

(29) Solheim, J., 1966. Mon. Not. R. astr. Soc., 133, 321.

(30) Oort, J.H., 1958. Solvay Conference on La Structure et l'Evolution de l'Univers, p. 163.

(31) Humason, M.L., Mayall, N.U., and Sandage, A. R., 1956. Astr. J., 61, 97.

(32) Baum, W. A., 1962. I. A. U. Symposium No. 15, Problems of Extragalactic Research, ed. by G. C. McVittie, p. 390.

(33) Sandage, A. R., 1961. Astrophys. J., 134, 916.

(34) McCrea, W.H., 1966. Astrophys. J., 144, 516.

(35) McVittie, G.C., and Stabell, R., 1967. Nature, Lond., 213, 133.

(36) Rees, M.J., and Sciama, D.W., 1966. Nature, Lond., 211, 1283.

(37) Edge, D.O., et at., 1959. Mem. R. astr. Soc., 68, 37.

(38) Bennett, A.S., 1962. Mem. R. astr. Soc., 68, 163.

(39) Rees, M.J., and Sciama, D.W., 1967. Nature, Lond., 213, 374.

(40) Petrosian, V., Saltpeter, E., and Szekeres, P., 1967. Astrophys. J., 147, 1222.

(41) Sandage, A. R., 1965. Astrophys. J., 141, 1560.

(42) Burbidge, G.R., Burbidge, E.M., Hoyle, F., and Lynds, C.R., 1966. Nature, Lond., 210, 774.

(43) Lynden-Bell, D., 1967. Herstmonceux Conference on the Helium Problem.

(44) Bahcall, J.N., and Sargent, L.W., 1967. Astrophys. J., 148, 165.

(45) Wills, D. and Parker, E. A., 1966. Mon. Not. R. astr. Soc., 131, 503.

(46) Veron, P., 1966. Ann. Astrophys., 29, 231.

(47) Brans, C. and Dicke, R. H., 1961. Phys. Rev., 124, 925.

(48) Dicke, R.H., 1967. Phys. Rev. Lett., 18, 313.

(49) Braccesi, A., 1967. Nuovo Cim. (B), 49, 148.

(50) Kellerman, K. I , 1964, Astrophys. J., 140, 969.

(51) Pauliny-Toth, I. I. K., Wade, C.M. and Heeschen, D. S., 1966. Astrophys. J., Suppl. Ser., 13, No. 116.

(52) Kafka, P., 1967. Personal communication.

(53) Burbidge, G.R. and Hoyle, F., 1967. Nature, Lond., 216, 351.

(54) Rowan-Robinson, M., 1968. Mon. Not. R. astr. Soc., 138, 445.

(55) Maltby, P., Matthews, T.A., and Moffet, A.T., 1963. Astrophys., J., 137, 153.

(56) Matthews, T.A., Morgan, W.W., and Schmidt M., 1964. Astrophys. J., 140, 35.

(57) Schmidt, M., 1965. Astrophys. J., 141, 1.

(58) Sandage, A.R., 1966. Astrophys. J., 145, 1.

(59) Burbidge, E.M., 1967. Astrophys. J. 149, L51.

(60) Wyndham, J.P., 1966. Astrophys. J., 144, 459.

(61) Sciama, D.W., and Saslaw, W.C., 1966. Nature, Lond., 210, 348.

(62) Ryle, Sir M., and Langair, M.S., 1967. Mon. Not. R. astr. Soc., 136, 123

(63) Sandage, A.R., 1967. Astrophys. J., 150, L.9; Oke J.B., 1967. Astrophys. J., 150, L.5.

(64) Kellermann, K.I., Pauliny-Toth I.I.K., Davis, M.N., 1968. Astrophys. J., Letters 2 .105.

(65) Ginzburg, V.L., and Syrovatskii, S.I., 1965. Ann. Rev. Astra. Astrophys. 3.

(66) MacDonald, G.H., Kenderdine S., Neville, A.C., 1968 Mon. Not. R. astr. Soc. 138, 259.

(67) Allen, L.R. Hanbury Brown, R., Palmer, H.P., 1962. Mon. Not. R. astr. Soc. 125, 57.

(68) Williams, P.J.S., 1966. Nature, Lond., 210, 285.

(69) Scheuer, P.A.G., 1966. Rendiconti della Scuola Internazionale di Fisica, 'E.Fermi', Varenna.

(70) Rees, M. and Sciana, D.W., 1966. Astrophys. J., 145, 1.

(71) Colgate, S.A., and Johnson, M.H., 1960. Phys. Rev. Letters, 5, 235.

(72) Burbidge, G.R., 1961. Nature, Lond., 190, 1053.

(73) Gold, T., Axford, W.I., Ray, E.C., 1965. Proceedings of 1st Texas Symposium on Relativistic Astrophysics, ed. I. Robinson, p. 93.

(74) Hoyle, F., and Fowler, W.A., 1963. Mon. Not. R. astr. Soc., 125, 169.

(75) Sandage, A.R., 1961. Hubble Atlas of Galaxies (Carnegie Institution of Washington).

(76) Taylor, Sir G.i., 1950. Proc. Roy. Soc., 201, A 159.

(77) Hoyle, F., Burbidge, G.R., and Sargent, W.L.W., 1966. Nature, Lond., 209, 751.

(78) Rees, M.J., 1966. Nature, Lond., 211, 805.

(79) Shimmins, A.J., Bolton, J.G., and Wall, J., 1968. Nature, Lond., 217, 818.

(80) Caswell, J.L., and Wills, D., 1967. Mon. Not. R. astr. Soc., 135, 231.

(81) Petrosian, V., 1969. Astrophys. J.

(82) Ryle M., and Neville, A.C., 1961. Mon. Not. R. astr. Soc., 125, 39.

(83) Peebles, P.J.E., 1965. Astrophys. J., 142, 1317.

(84) Bahcall, J.N., and May, R.M., 1968. Astrophys. J., 152, 37.

(85) Rees, M.J., and Setti, G., 1968. Nature, Lond., 219, 127.

(86) Sandage, A.R., 1968. Halley lecture, Ohs. 88, 91.

(87) Braccesi, P., 1968. 3rd Texas Symposium

(88) Shklovsky, I., 1967. Astrophys. J., 150, L1.

(89) Kardashev, N., 1967. Astrophys. J., 150, L 135.

(90) Schmidt, M., 1968. Astrophys. J., 151, 393.

(91) Schmidt, M., private communication quoted in ref (66).

(92) Bergamini R.; Londrillo, P., and Setti, R., 1967. Nuova Cimento 52, B, 495.

(93) Schmidt, M., 1967, Astrophys. J., 149 L 39.

(94) Bridle, A.H., 1967, Mon. Not. R. astr. Soc. 136, 219.

(95) Felten, J.E., and Morrison, P., 1966. Astrophys. J., 146, 686.

(96) Longair, M.S., 1968. 12th Herstmonceux Conference on Structure of Galaxies, Obs: 88, 199.

(97) Pooley, G.G., 1968. Nature, Lond., 218, 154.

(98) Silk, J., and McCray, R., 1969. preprint.

(99) Mattig, W., 1959. Astron. Nach., 285, 1.

(100) Longair, M.S., and Scott, P.F., 1965, Mon. Not. R. astr. Soc., 130, 379

(101) Ryle, M., and Neville, A.C., 1961, Mon. Not. R. astr. Soc., 125, 39.

(102) see Fig. 2 of Ref. (98).

(103) Braude, S. Ya., etal, 1969, Mon. Not. R. astr. Soc., 143, 289

(104) Burbidge, G.R., and Burbidge, E.M., 1967. Quasi-stellar objects (W.H. Freeman and Co.).

(105) Jauncey, D.L., 1967. Nature, Lond., 216, 877.

(106) Pooley, G.G. and Ryle, Sir M., 1968. Mon. Not. R astr. Soc. 139, 515.

(107) Hoyle, F. and Fowler, W.A., 1967. Nature, Lond., 213, 373.

(108) Kenderdine, S., Ryle, M., Pooley, G.G., 1966. Mon. Not. R. astr. Soc., 134, 189.

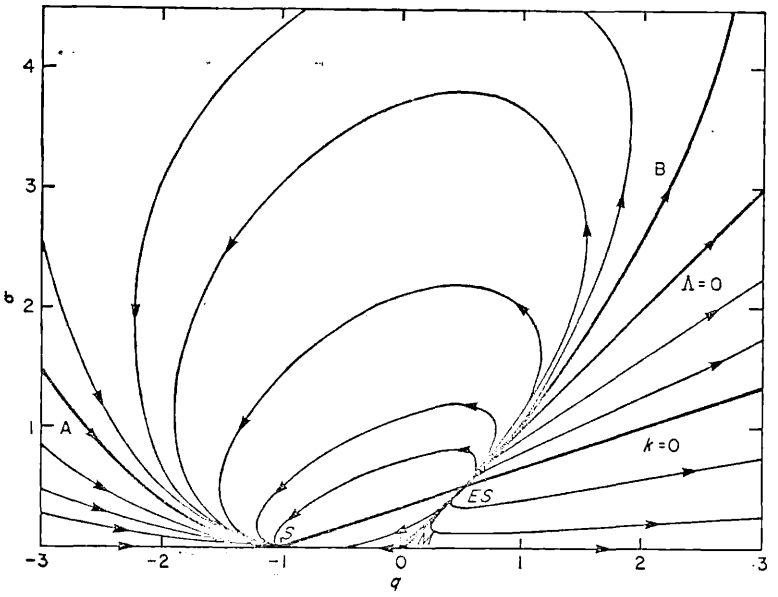

FIG. 1.—*Flow diagram for the models. Loci to the right of B are oscillating models; those to the left of A have 'bounced' under the action of cosmological repulsion; those between A and B are monotonic expanding models. The three fixed points are the Einstein–de Sitter (ES), Milne (M), and de Sitter (S) models. The directions indicated by the arrows correspond to expansion of the Universe.*

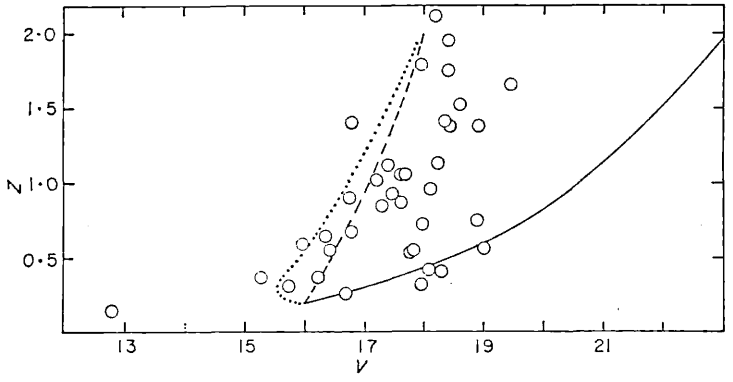

FIG. 2.—*Magnitude (V)–redshift (z) diagram for quasars showing 'volume effect'. The continuous line is the theoretical magnitude–redshift curve for the de Sitter model. The other two curves show the* shapes *of the predicted loci of brightest sources in this model for simple luminosity functions: dotted curve, Gaussian with dispersion of two magnitudes; broken curve, exponential dependence on luminosity, F(νν), with index −1·5 (to base 10). These forms are chosen only to give a similar shape to the upper envelope for the observational points (circles), and are not necessarily consistent with the data.*

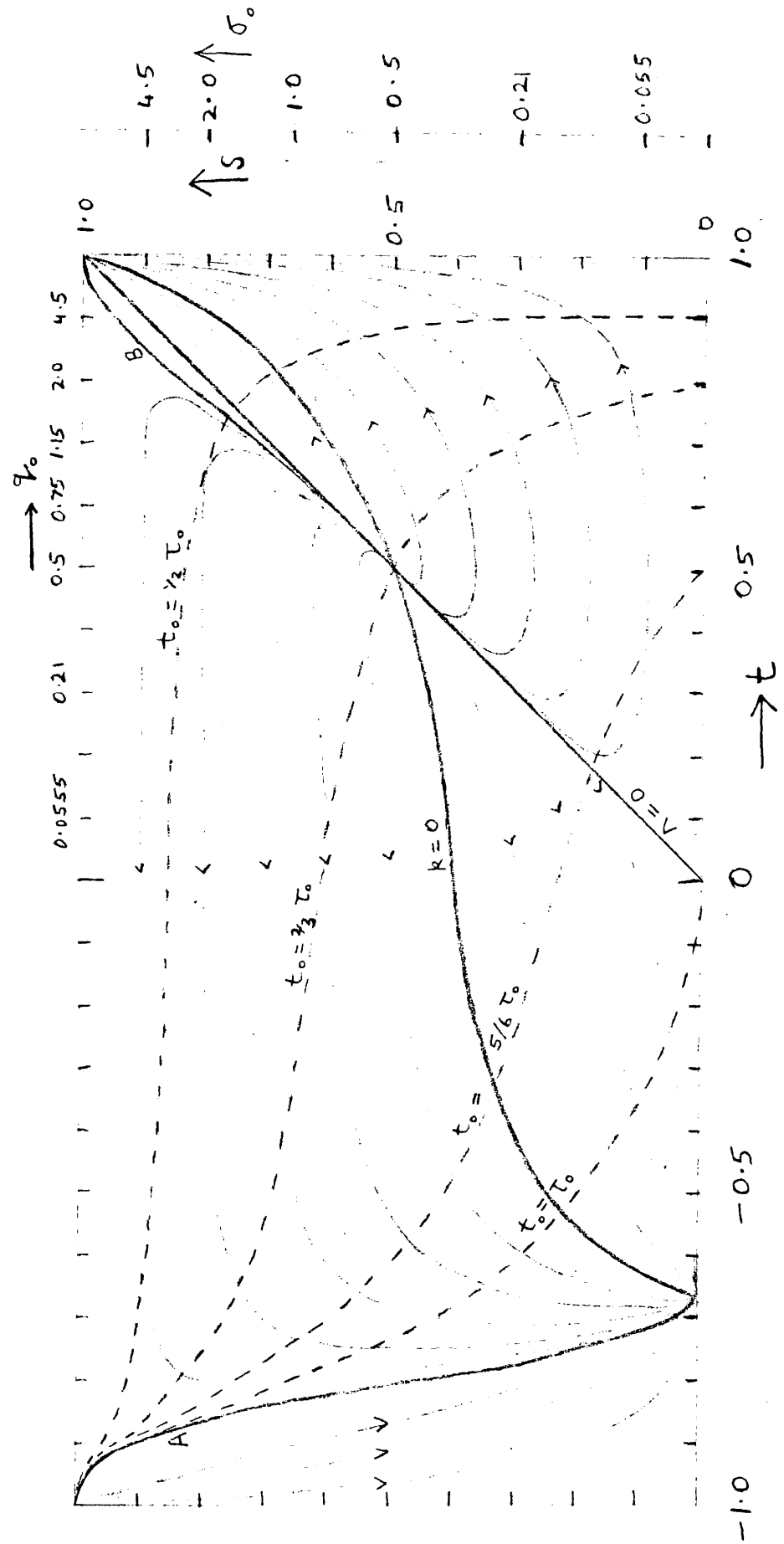
σ_0
S
q_0
t
B
A
$t_0 = \frac{1}{2}\tau_0$
$t_0 = \frac{2}{3}\tau_0$
$t_0 = \frac{5}{6}\tau_0$
$t_0 = \tau_0$
k=0
0=V
4.5
2.0
1.0
0.5
0.21
0.0555
0.75
1.15
-4.5
-2.0
-1.0
-0.5
-0.21
-0.055
-1.0
-0.5
0
0.5
1.0

Fig. 1b

Fig 20 The volume-effect test, steady-state cinematology.

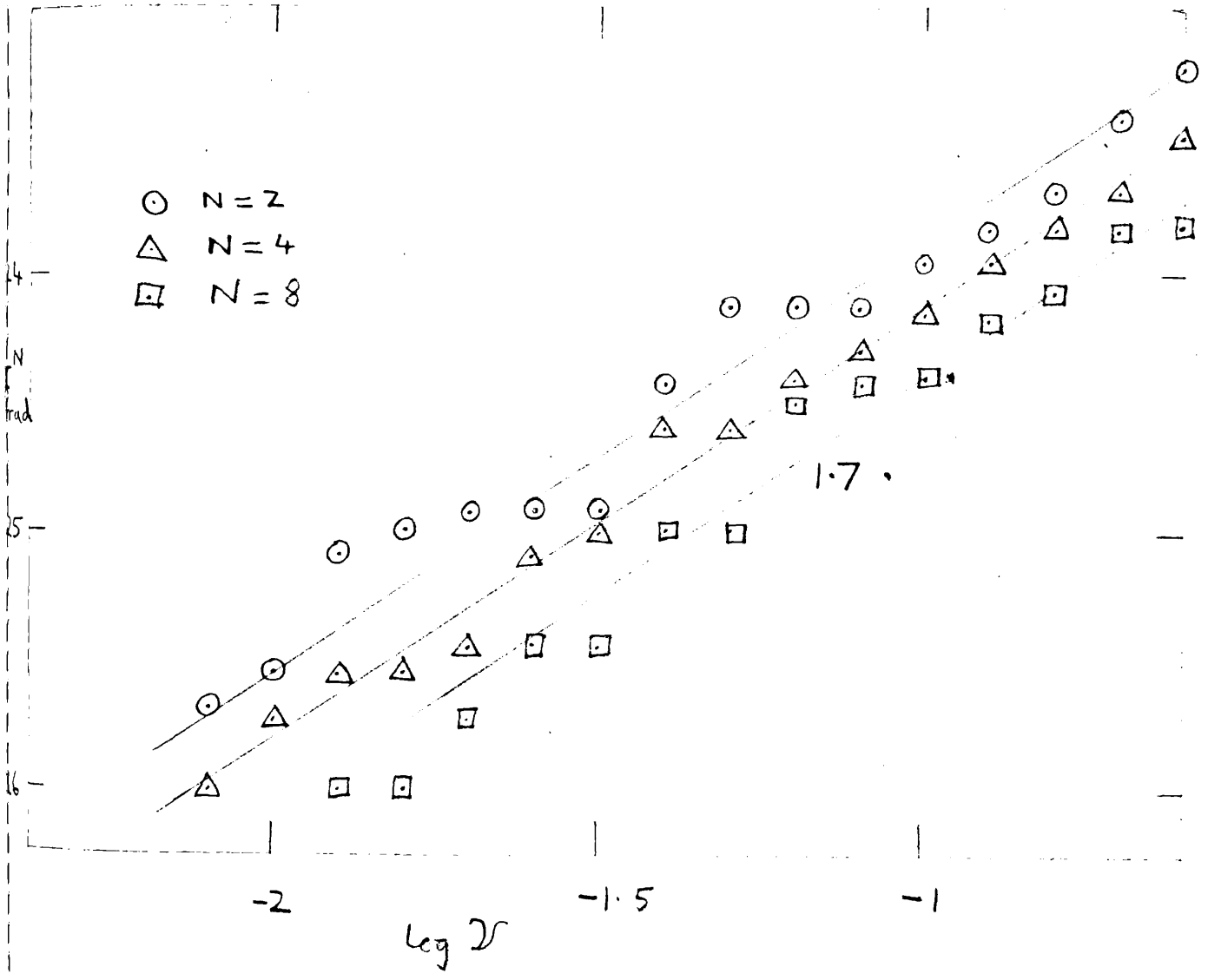

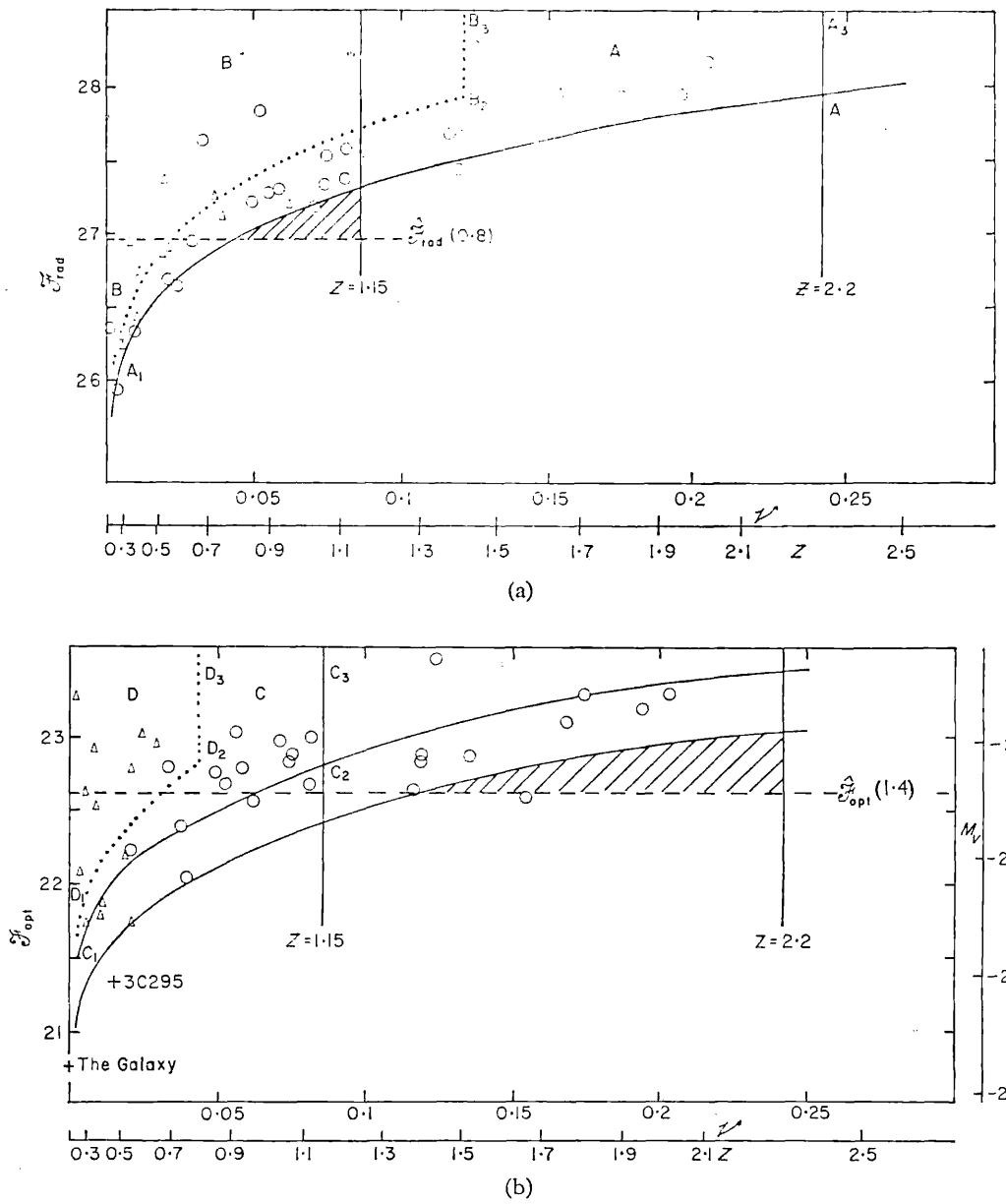

FIG. 3. *Radio* (a) *and optical* (b) *' luminosity-volume ' diagrams for quasars in the Einstein–de Sitter model.* A_1A_2 *corresponds to the* 3*C cutoff of nine flux-units,* C_1C_2 *to a visual magnitude of* 18. *In* (a) *circles/triangles are those quasars with* $\mathcal{F}_{opt} \gtrless \hat{\mathcal{F}}_{opt}(0{\cdot}8)$ *respectively: in* (b) *circles/triangles are those quasars with* $\mathcal{F}_{rad} \gtrless \hat{\mathcal{F}}_{rad}(1{\cdot}4)$. *Units of* $\mathcal{F}$ *are* $\log_{10}$ *watts/ster/(c/s).*

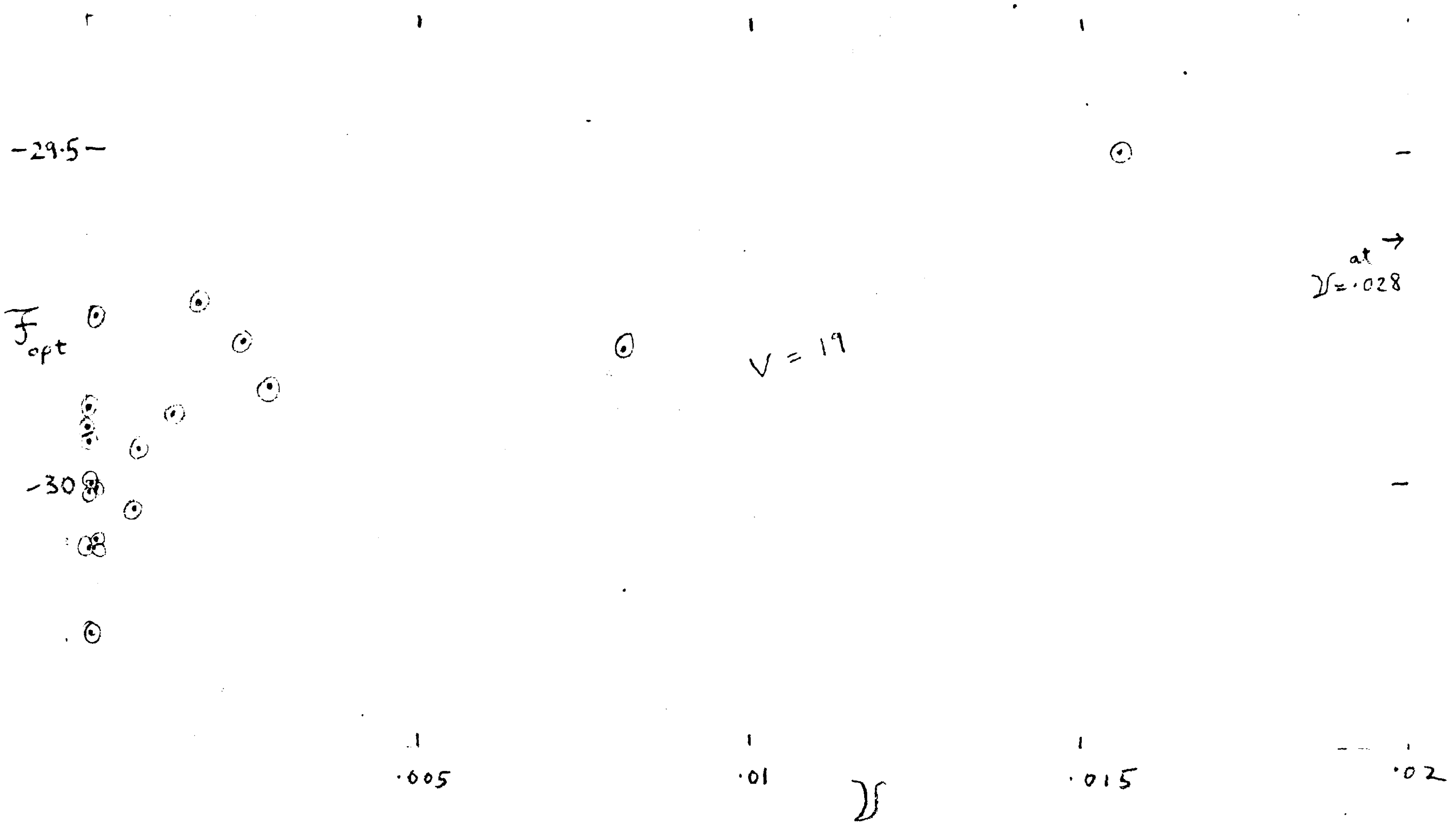

Fig. 3[illegible] Optical [illegible] for the brightest [illegible] in [illegible]
in the de Sitter [illegible].

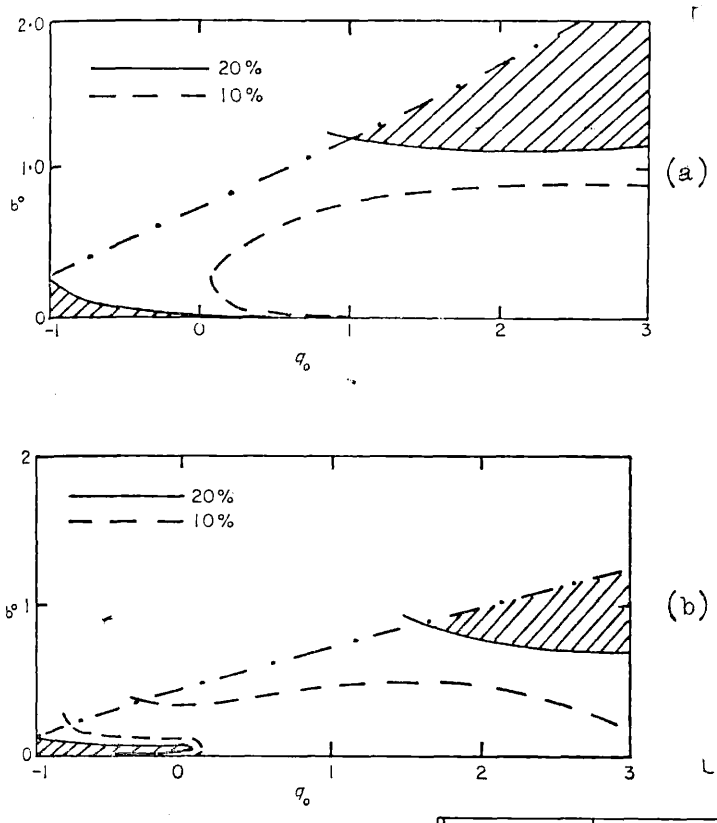

Fig 4 Model diagram, $\sigma_0 - q_0$: (a) power-law luminosity evolution, Q_L=2.5, combined optical and radio tests; (b) as in (a), but Q_L=3. Dash-dotted lines in Figs 4,7-10, correspond to the maximum rate of luminosity evolution discussed in section 8. The contours join models with an equal probability of being correct.

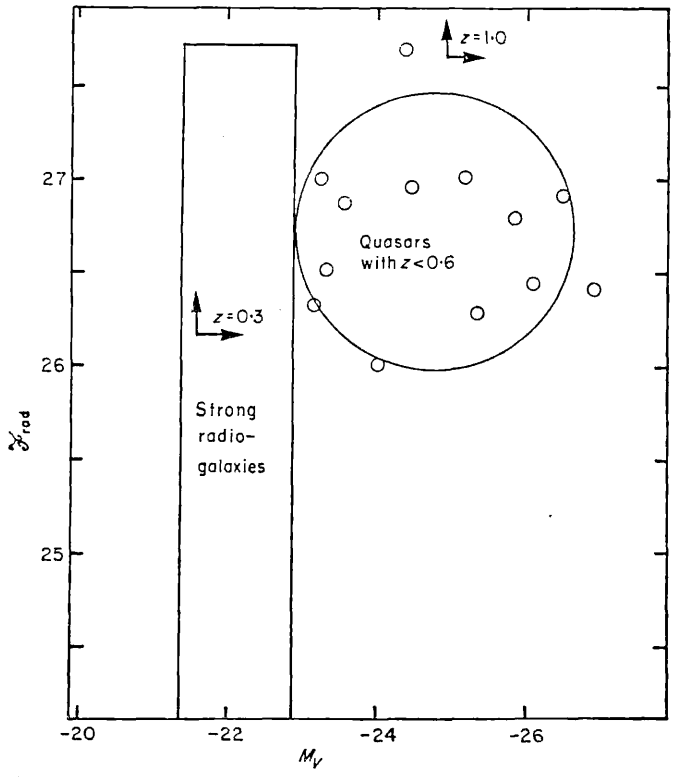

FIG. 5. *Radio vs optical luminosity for quasars with redshift less than 0·6 (circles), calculated in the Milne model, showing absence of detailed correlation. The region of this diagram occupied by the strong radio-galaxies is indicated, as also are the cutoffs imposed by limiting optical and radio flux-levels of 19 m and 9 f.u. respectively on quasars with redshifts 0·3 and 1·0 respectively (a quasar with redshift 1·0, for example, must be above and to the right of the point of intersection of the arrows labelled 'z = 1·0').*

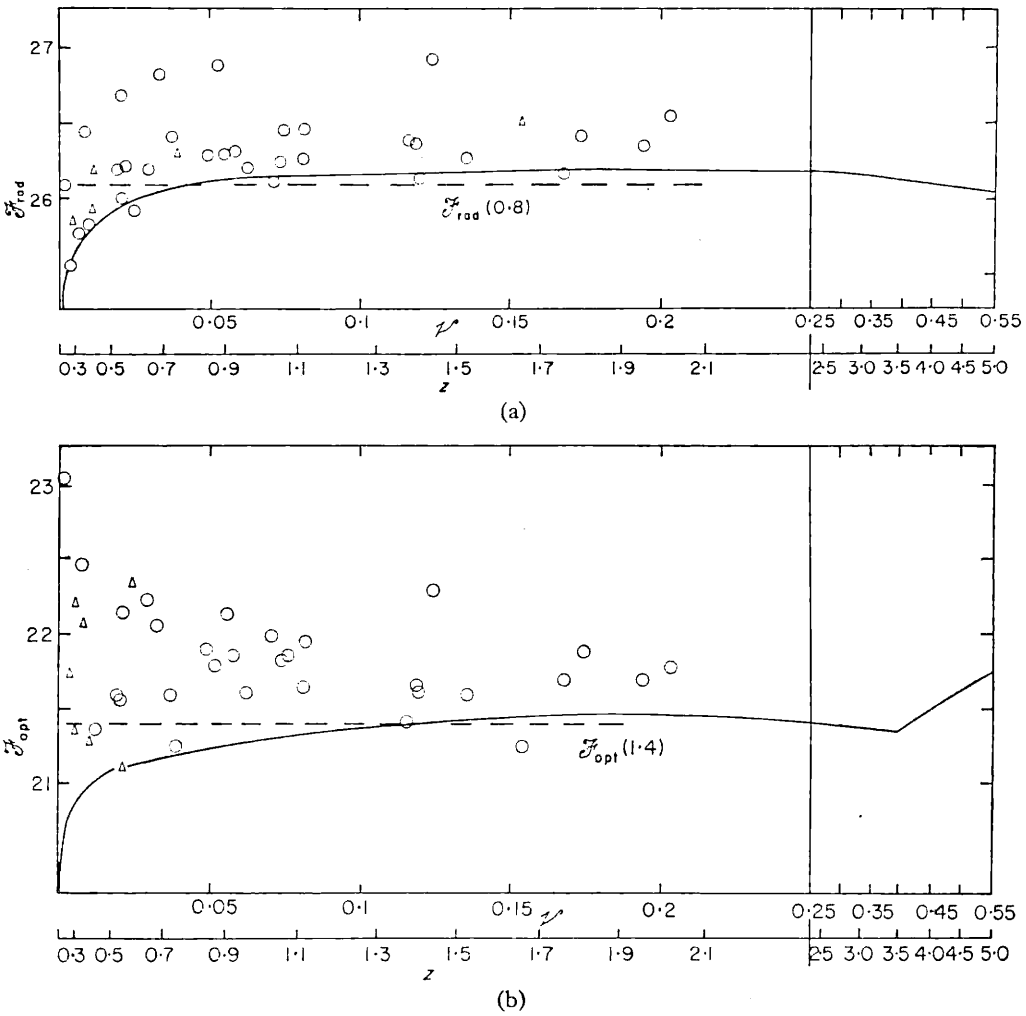

FIG. 6. *As in Fig.* 3, *but the luminosities corrected for power-law luminosity evolution with* $Q_L = 3{\cdot}07$. *The solid lines show cutoffs at nine flux-units and* 19 *magnitudes respectively, except that the effect of a sharp decline in the optical continuum beyond Lyman* α *is indicated in* (b). *Note that the volume scale is compressed beyond* $V = 0{\cdot}25$.

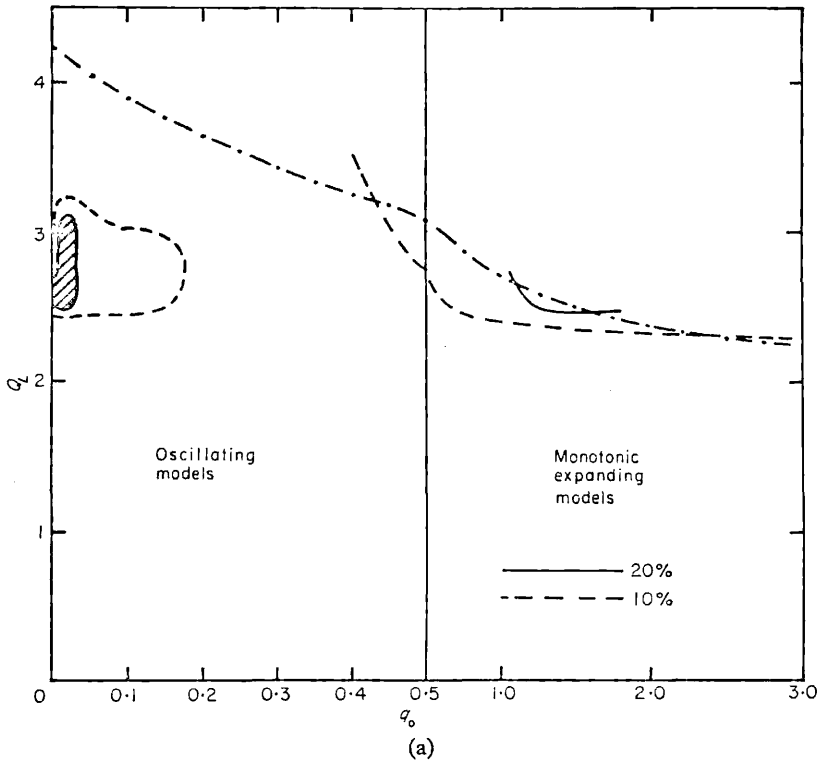

FIG. 7. *Results of tests of models with power-law luminosity evolutions:* (a) $\Lambda = 0$, $Q_L - q_0$; (b) $k = 0$, $Q_L - \sigma_0$; (c) $\sigma_0 = 0$, $Q_L - q_0$. *Shaded regions correspond to models giving probabilities greater than 20 per cent of being correct.*

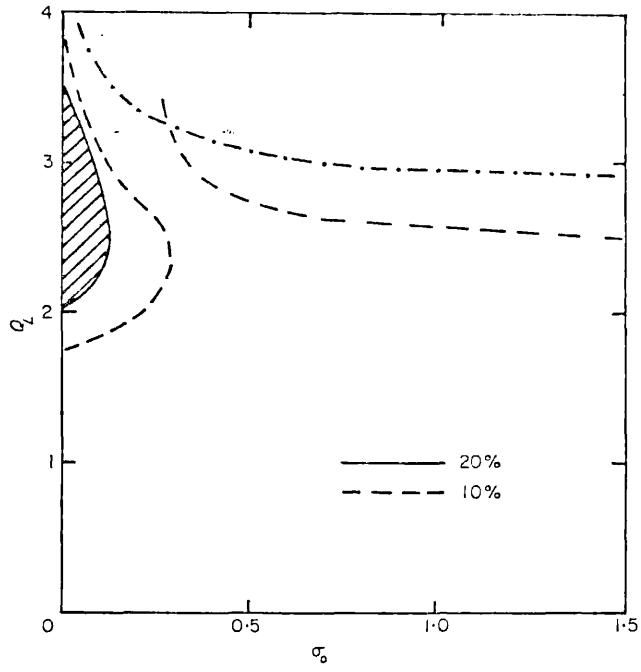
4
3
2
1
0
q_L
0·5
1·0
1·5
σ_0
20%
10%

(b)

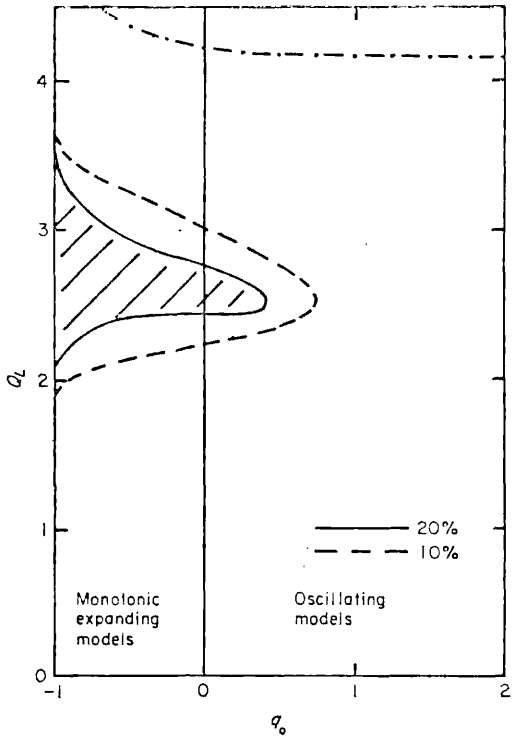
4
3
2
1
0
q_L
−1
0
1
2
q_0
20%
10%
Monotonic expanding models
Oscillating models

(c)

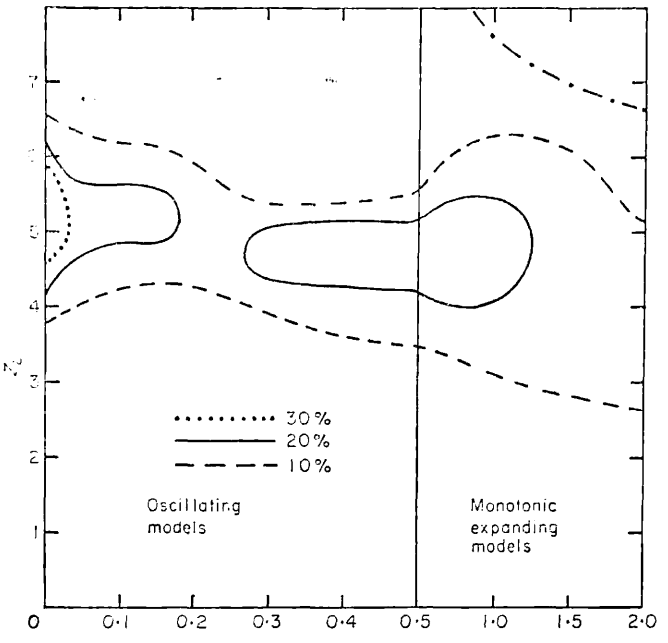

(a)

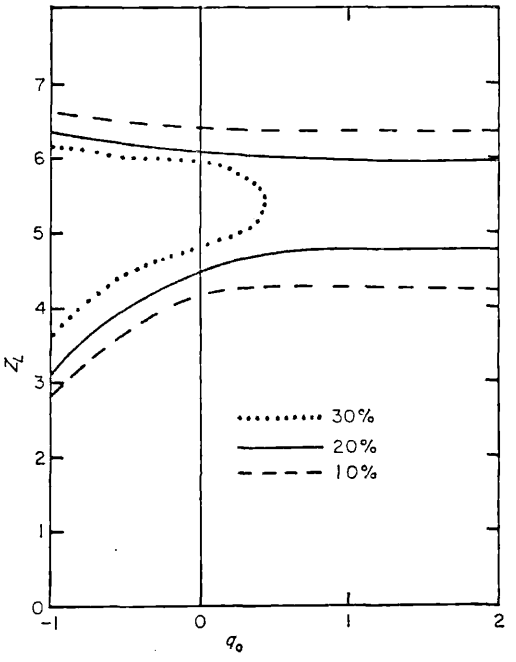

(b)

FIG. 8. *Test of exponential luminosity evolution,* $z_L - q_0$: (a) $\Lambda = 0$ *(scale expanded for* $q_0 < \frac{1}{2}$*);* (b) $\sigma_0 = 0$.

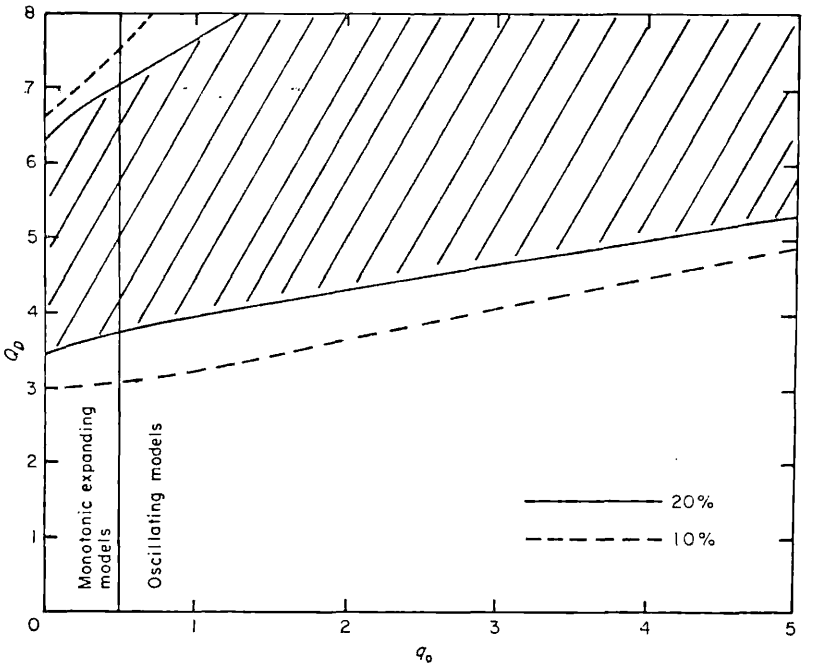

(a)

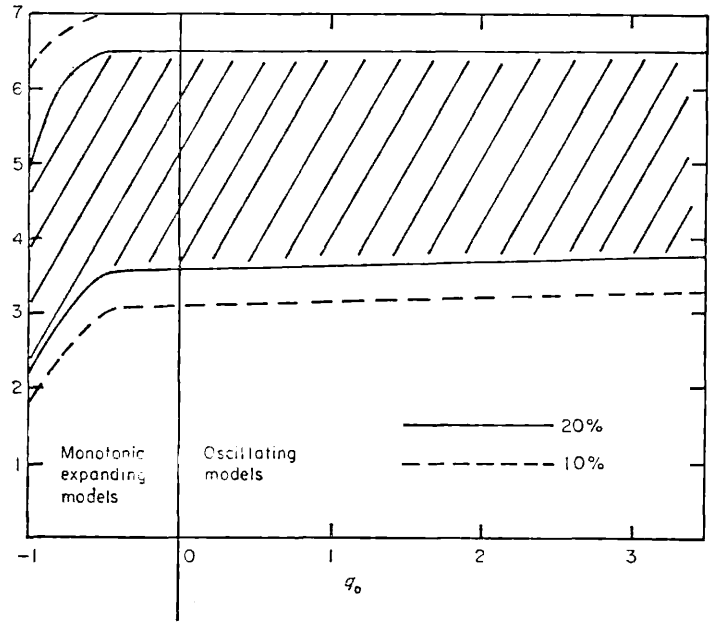

(b)

FIG. 9. *Test of power-law density-evolutions,* $Q_D - q_0$: (a) $\Lambda = 0$; (b) $\sigma_0 = 0$.

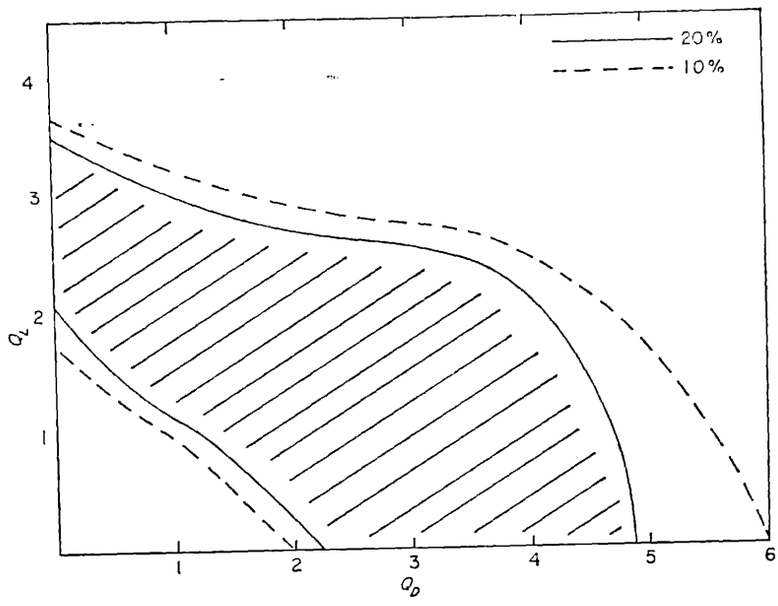

Fig 10 (c)

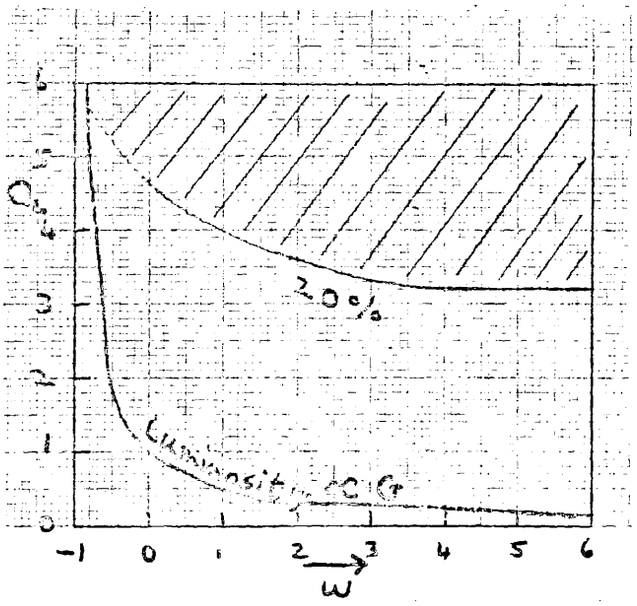

Fig 11

$Q_L - \omega$, Brans-Dicke models with zero curvature.

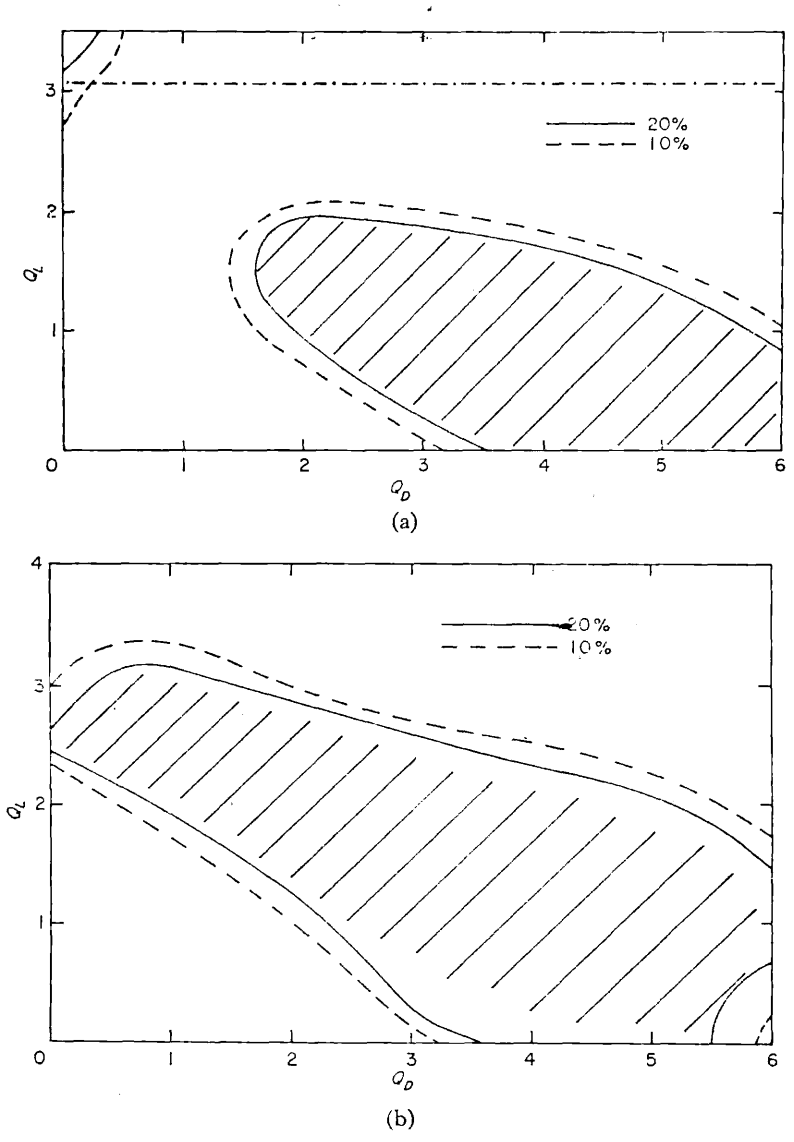

FIG. 10. *Test of combined power-law luminosity and density evolutions,* $Q_L - Q_D$: (a) *Einstein–de Sitter,* (b) *Milne and* (c) *de Sitter models.*

Fig 1[illegible] redshift-magnitude diagram for radio-galaxies
(crosses denote more recent data - A.R.Sandage 19[illegible] ApJ 1[illegible] L1[illegible])

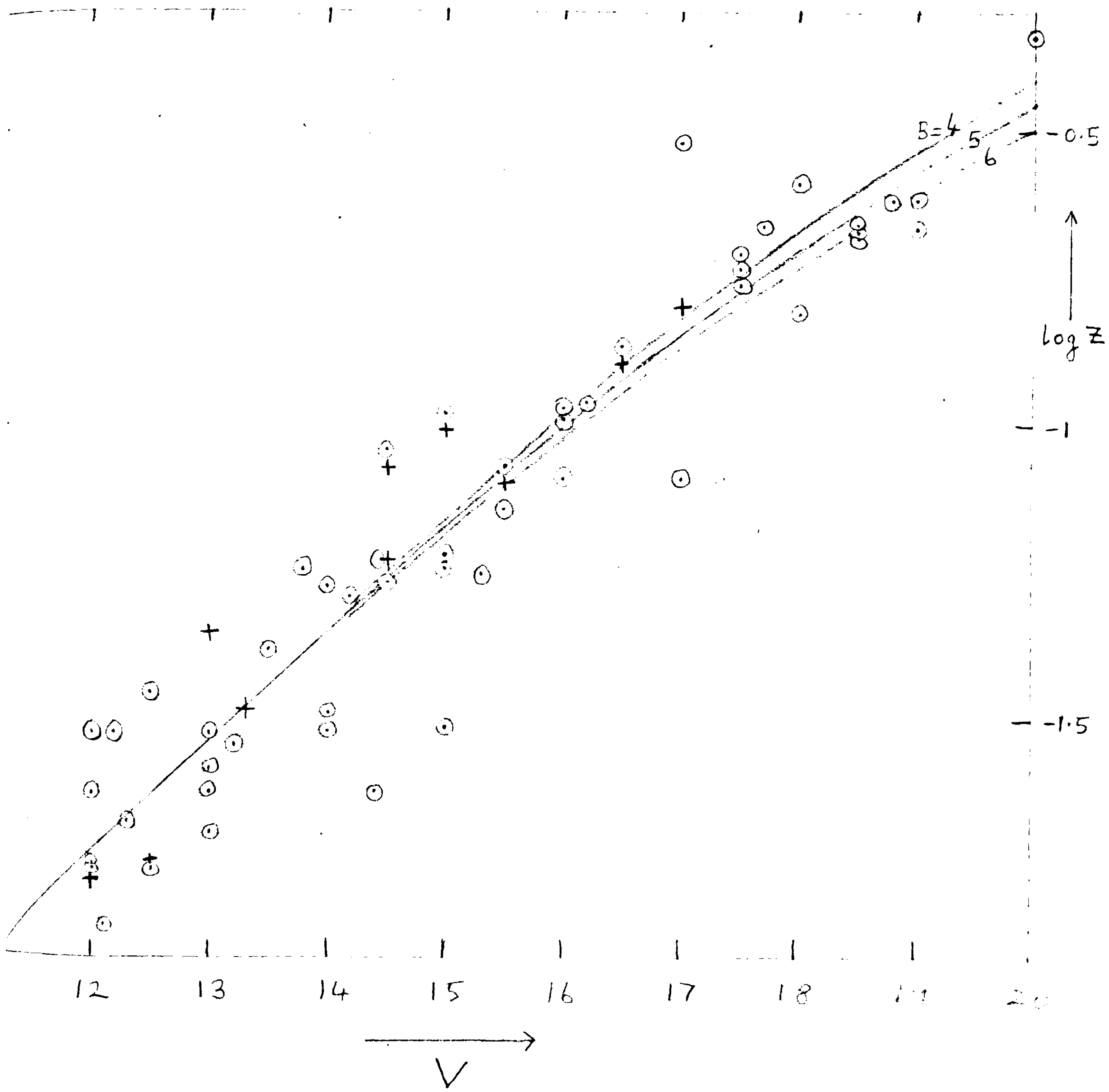

Fig 13 Radio source-counts at 178 MHz for
□ all radio-galaxies (upper curve)
⊙ strong radio-galaxies ($\mathcal{F}_{178} \geqslant -27$)
△ weak radio-galaxies (lower curve).

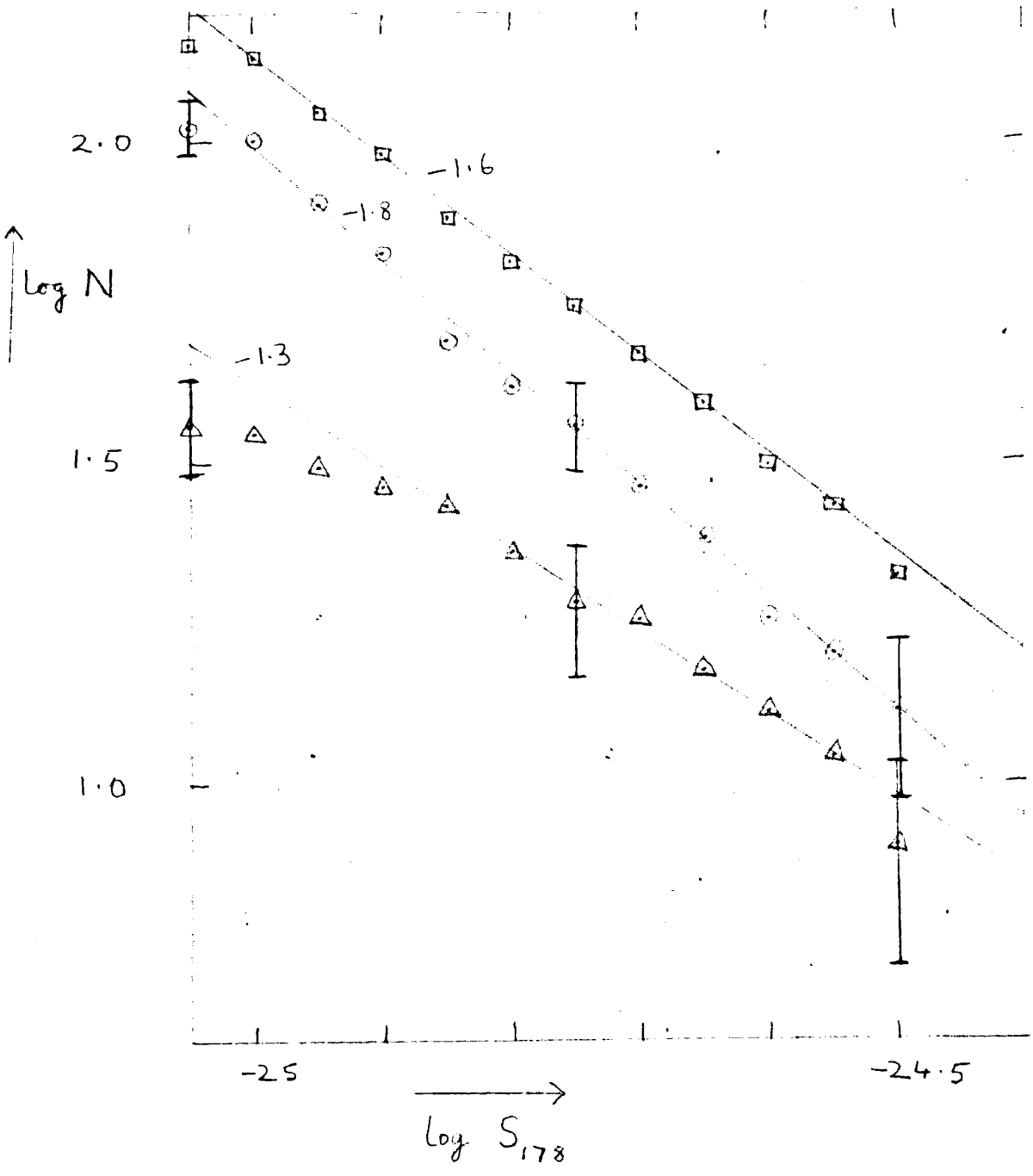

Fig. 14 Radio luminosity (17) vs. Hubble (or Stibbe count) against spectral index for radio-galaxies(circles) and quasars(crosses). The mean line, $\alpha = 0.5 \pm 0.075(F + 26.5)$, refers to radio-galaxies.

Fig 1ba Radio luminosity against component separation in double sources

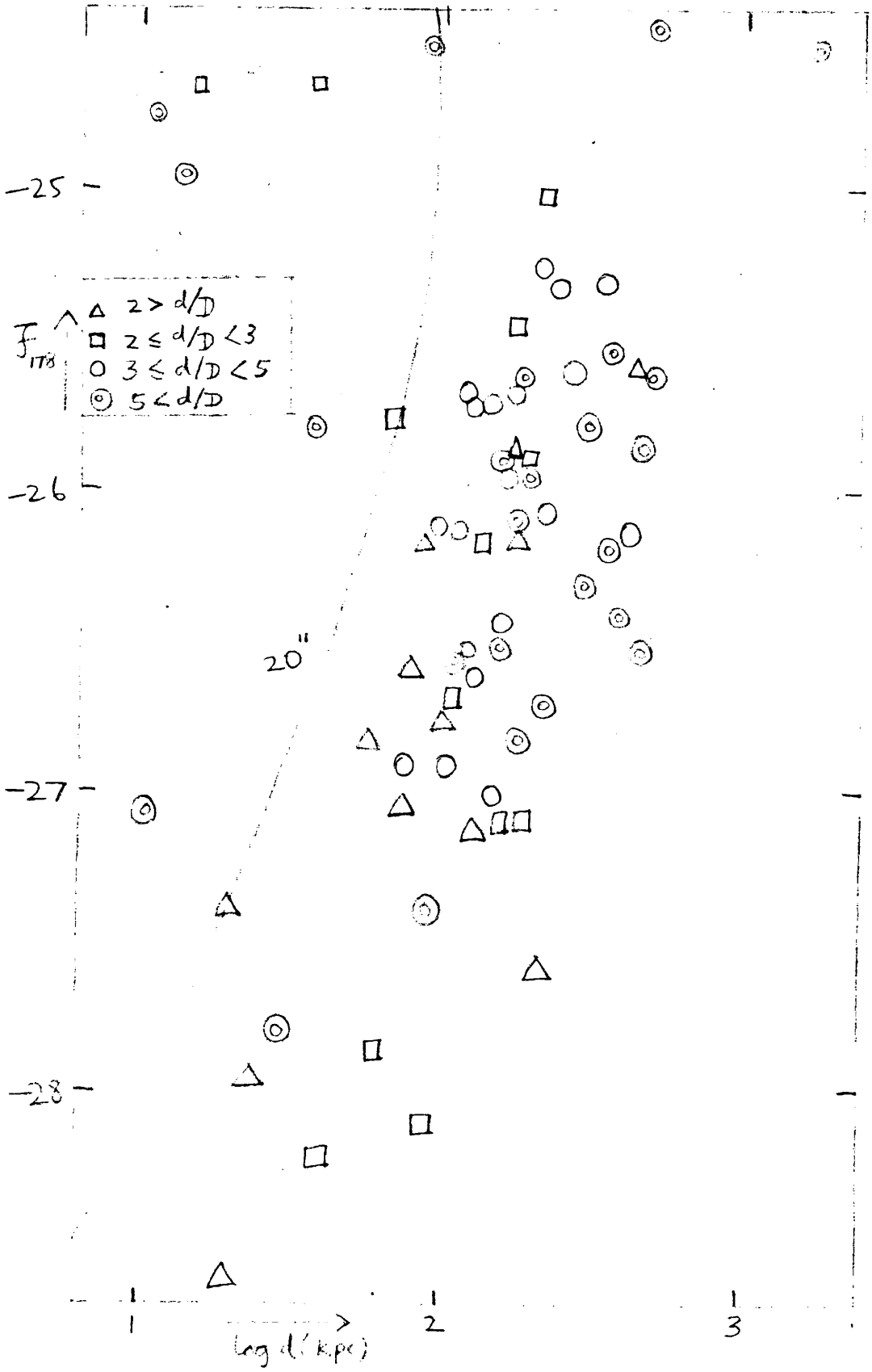

Fig 15b Radio luminosity against component diameter in double sources

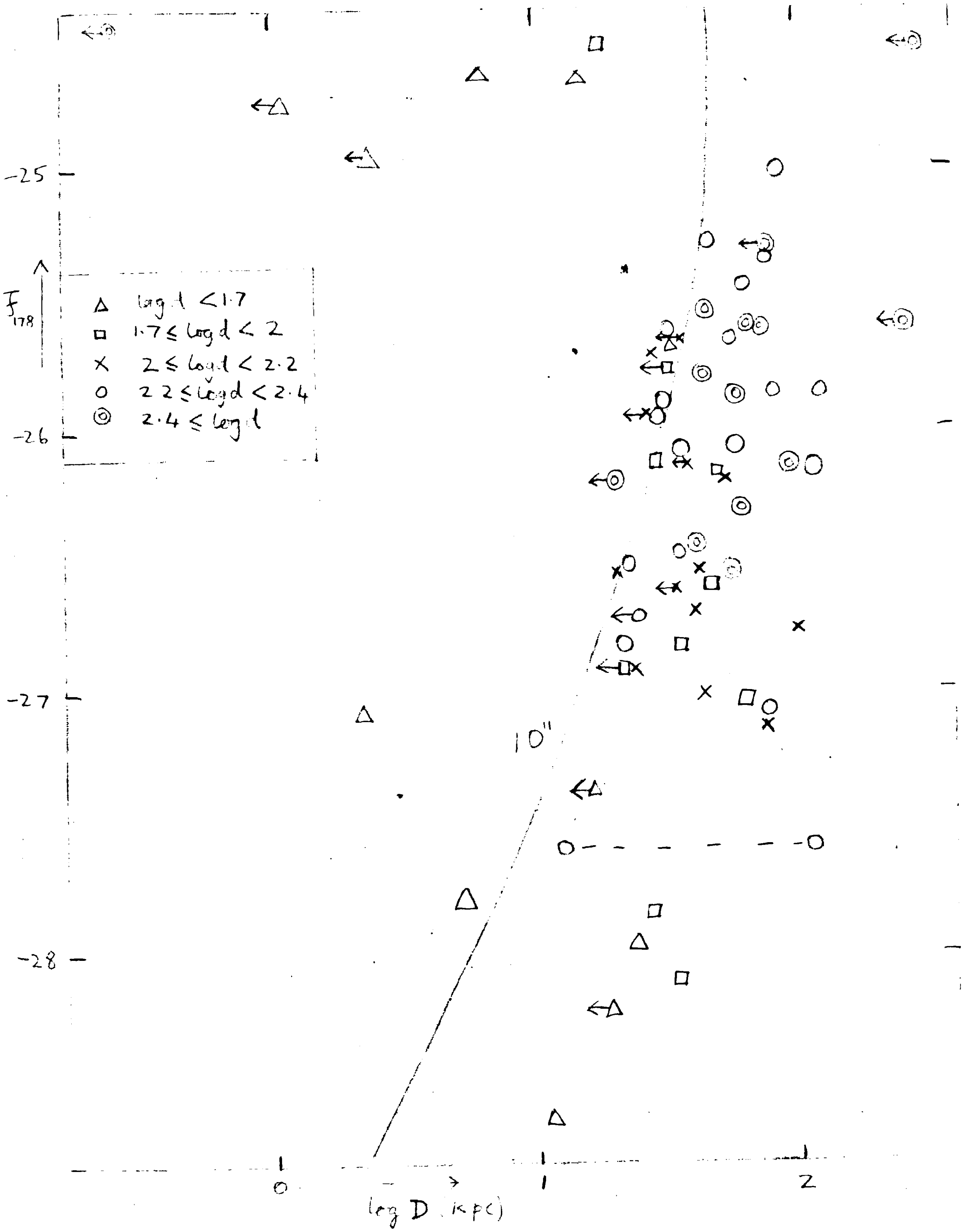

Fig 15c Component separation against diameter in double sources

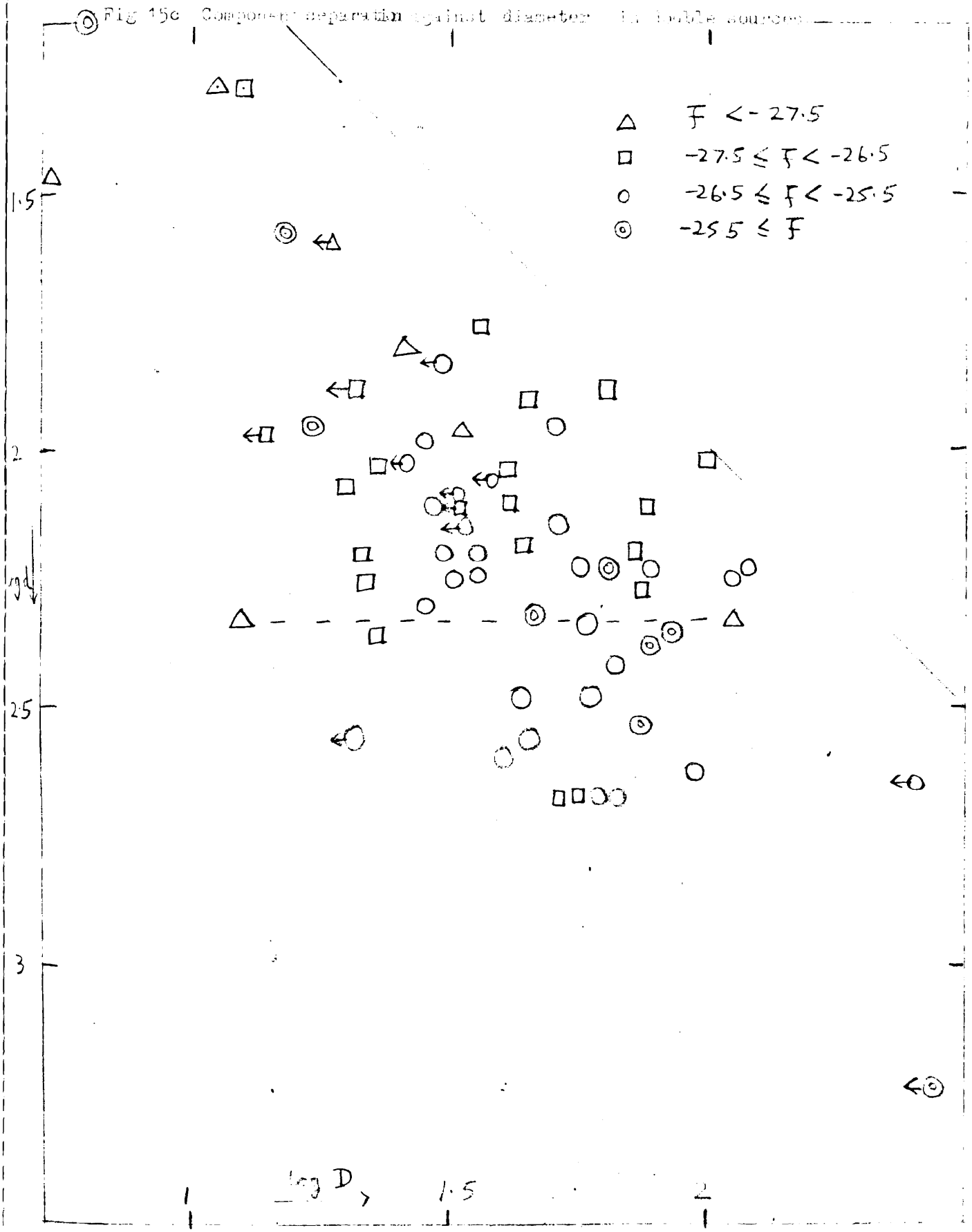

Fig 1a Dependence of equipartition magnetic field strength and total particle energies on spectral index, and on the parameters x, γ_1, γ_2.

	x	$\log_{10}(\gamma_1 H^{-x})$	$\log_{10}(\gamma_2 H^{-x})$	ν_1	ν_2
①	$-\frac{1}{2}$	0.7	1.7	7	10
②	$-\frac{1}{2}$	-0.3	0.7	6	12
③	0	2	4	$6.6+\log(10^4 H)$	$10.6+\log(10^4 H)$
④	$\frac{1}{2}$	4	6	$6.6+2\log(10^4 H)$	$10.6+2\log(10^4 H)$

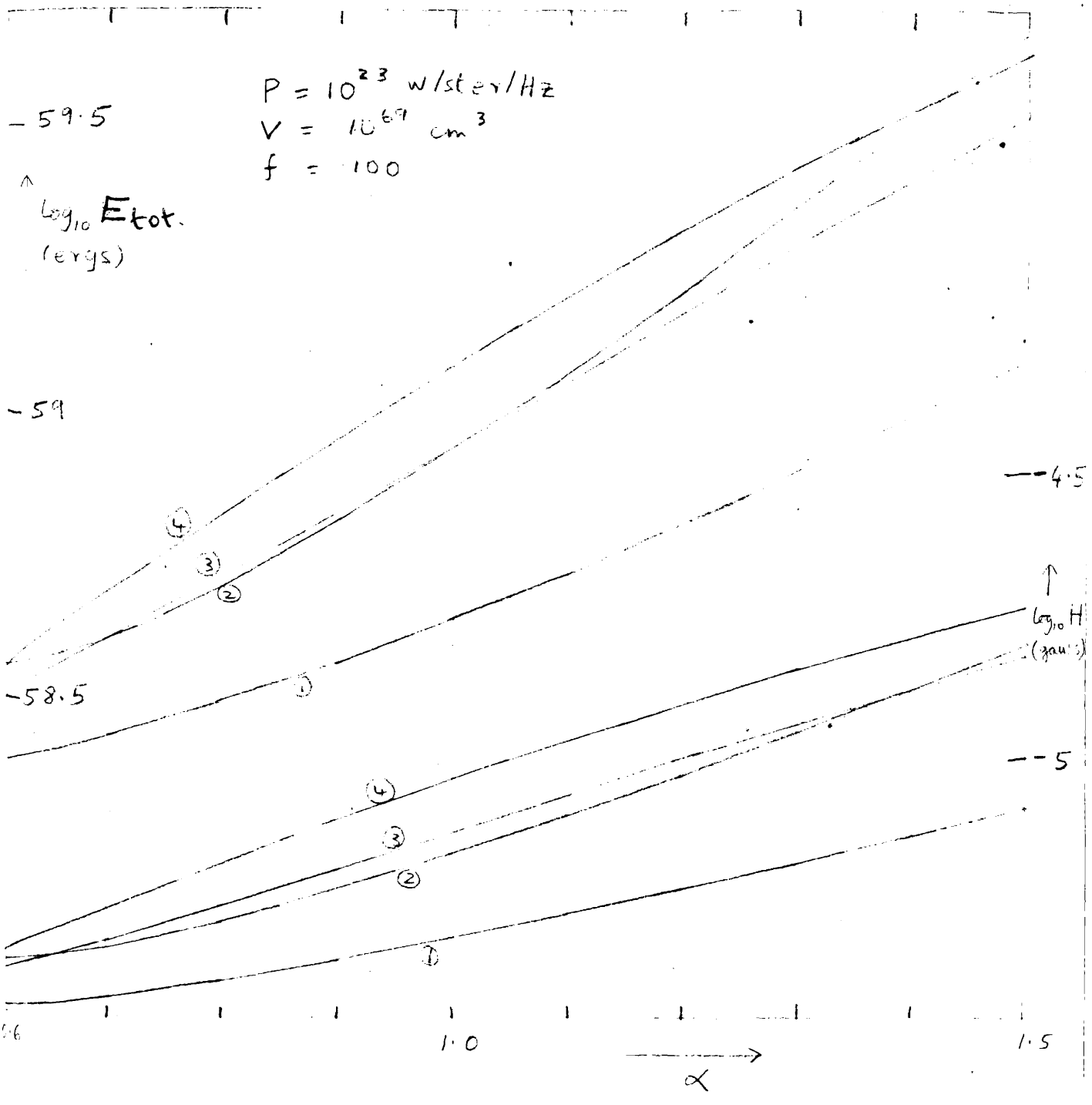

Fig 16b Radio luminosity - volume of emitting component
(1400 MHz, Einstein de Sitter model, data from ref 66)

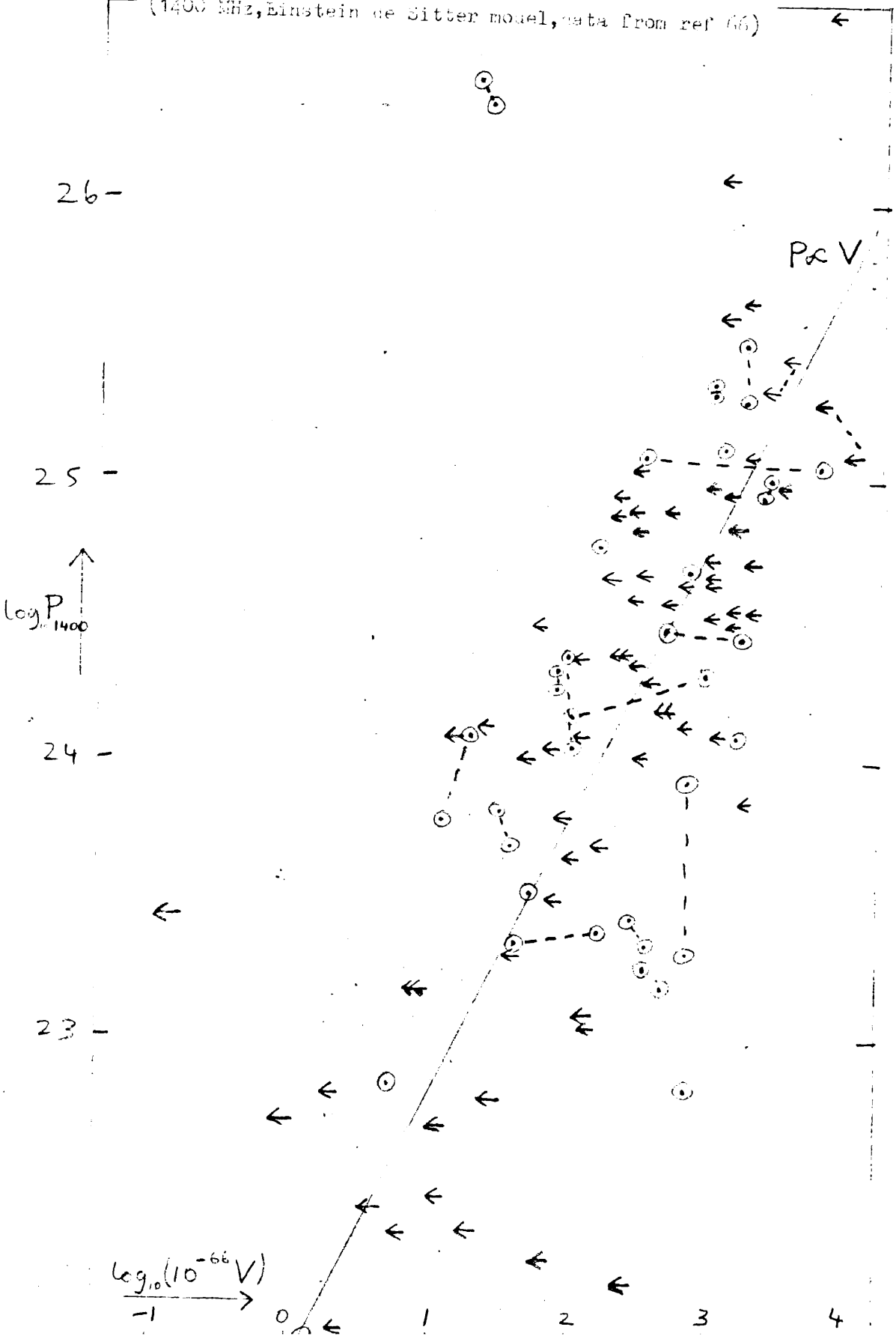

Fig 16c Radio luminosity - equipartition magnetic field

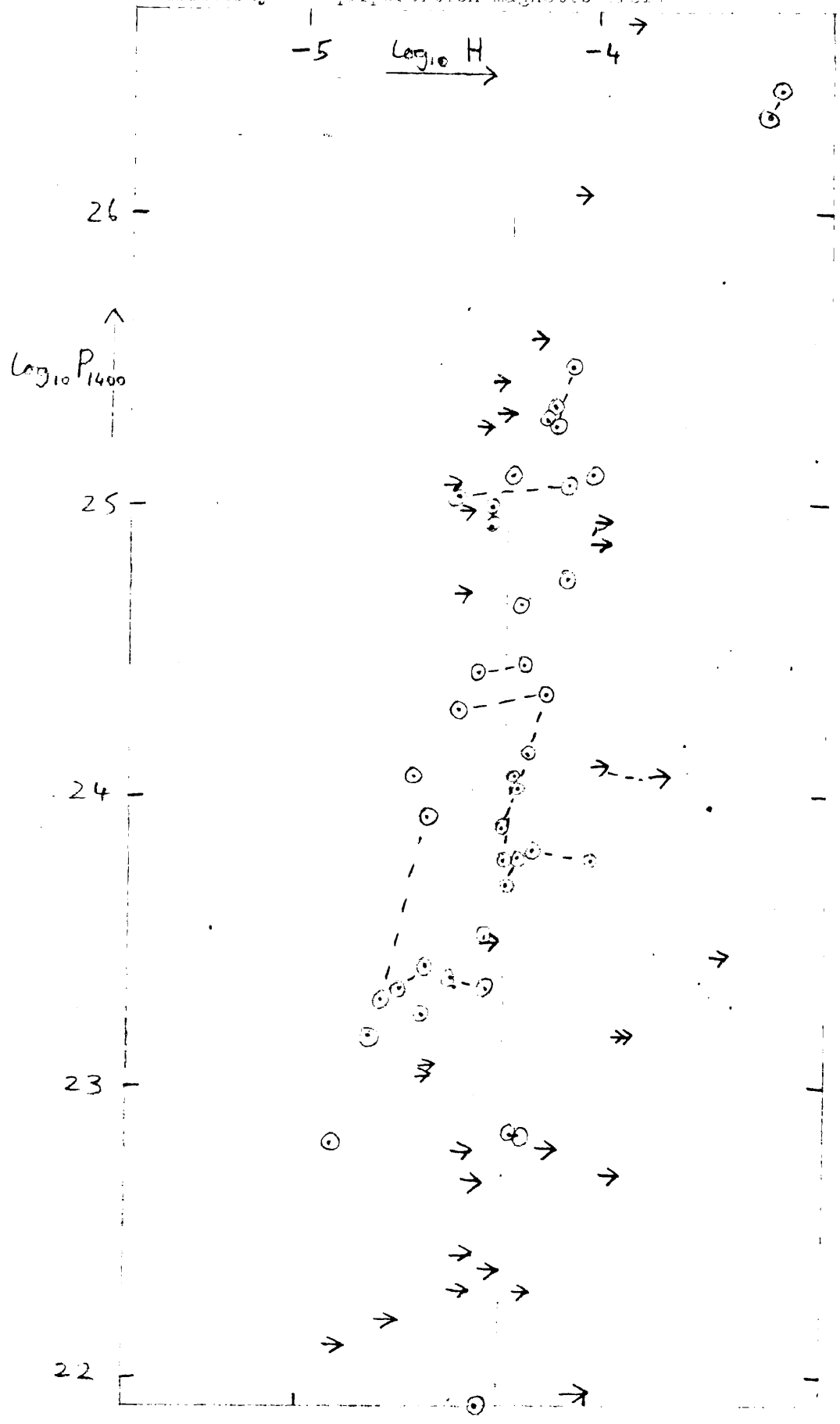

Fig 16d Radio luminosity - total energy in particles(assuming equipartition)

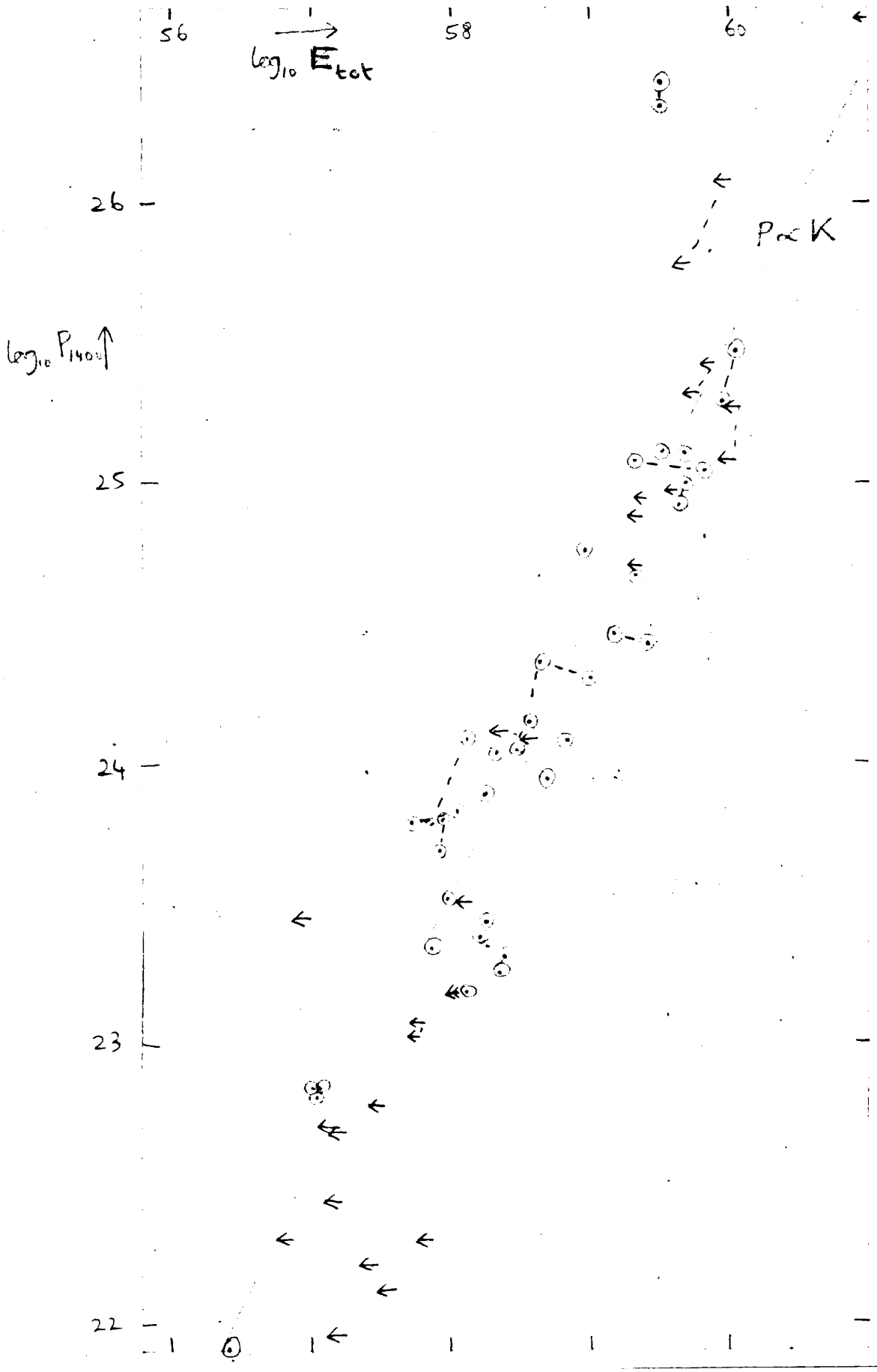

Fig 17 Separation ($d \sin\phi$) against velocity ($\bar{v} \cos\phi/c \simeq (\theta_a - \theta_r)/(\theta_a + \theta_r)$)

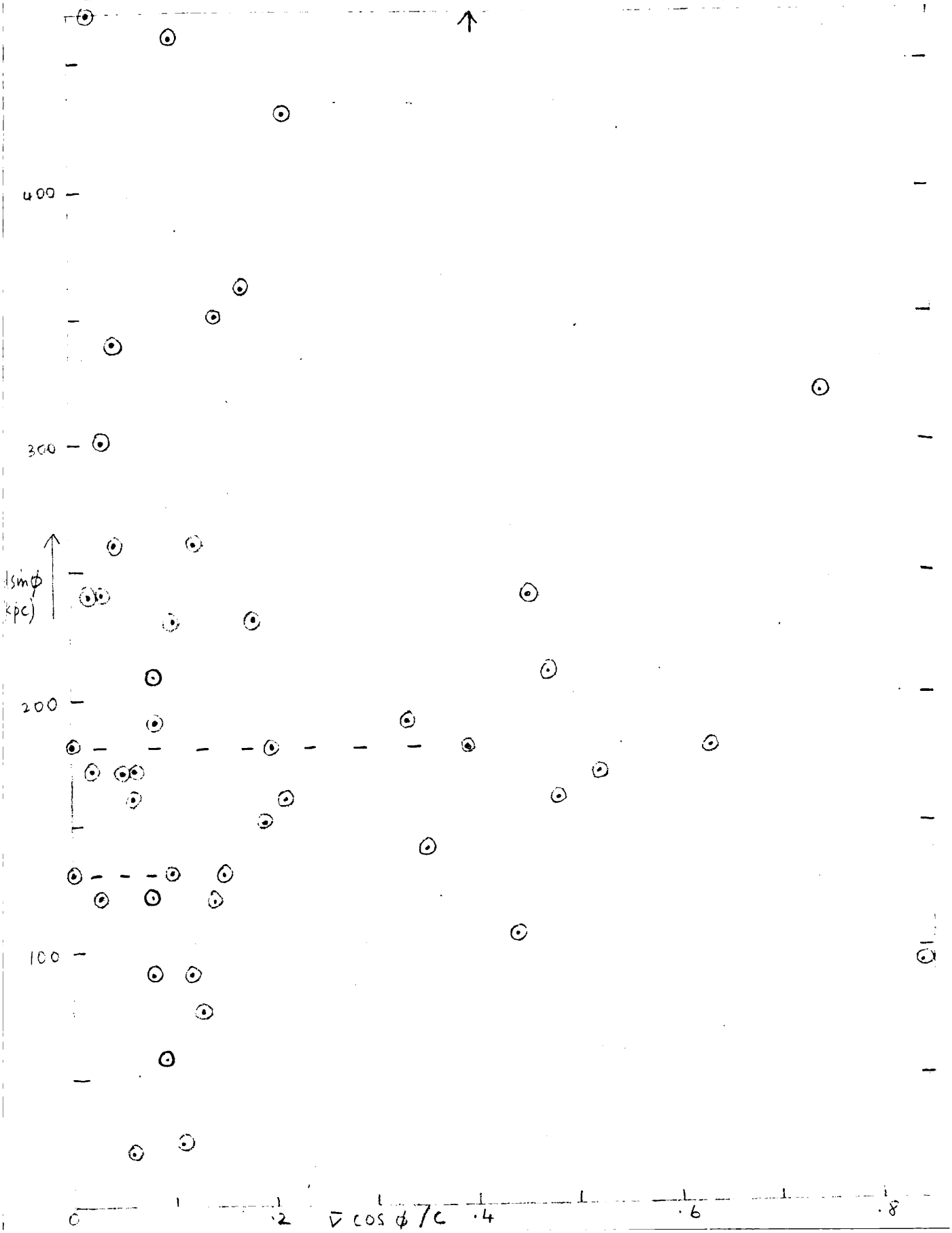

Fig 18 log N - log S for population of sources with the same luminosity and spectral index(α=0.75) is shown, with the effects of altering by $\pm$ 0.25),(i) no evolution,(ii) exponential luminosity evolution, Z_L = 6 ,(iii) exponential density evolution, Z_D = 10, in (a) Einstein-de Sitter (b) Milne (c) de Sitter models.

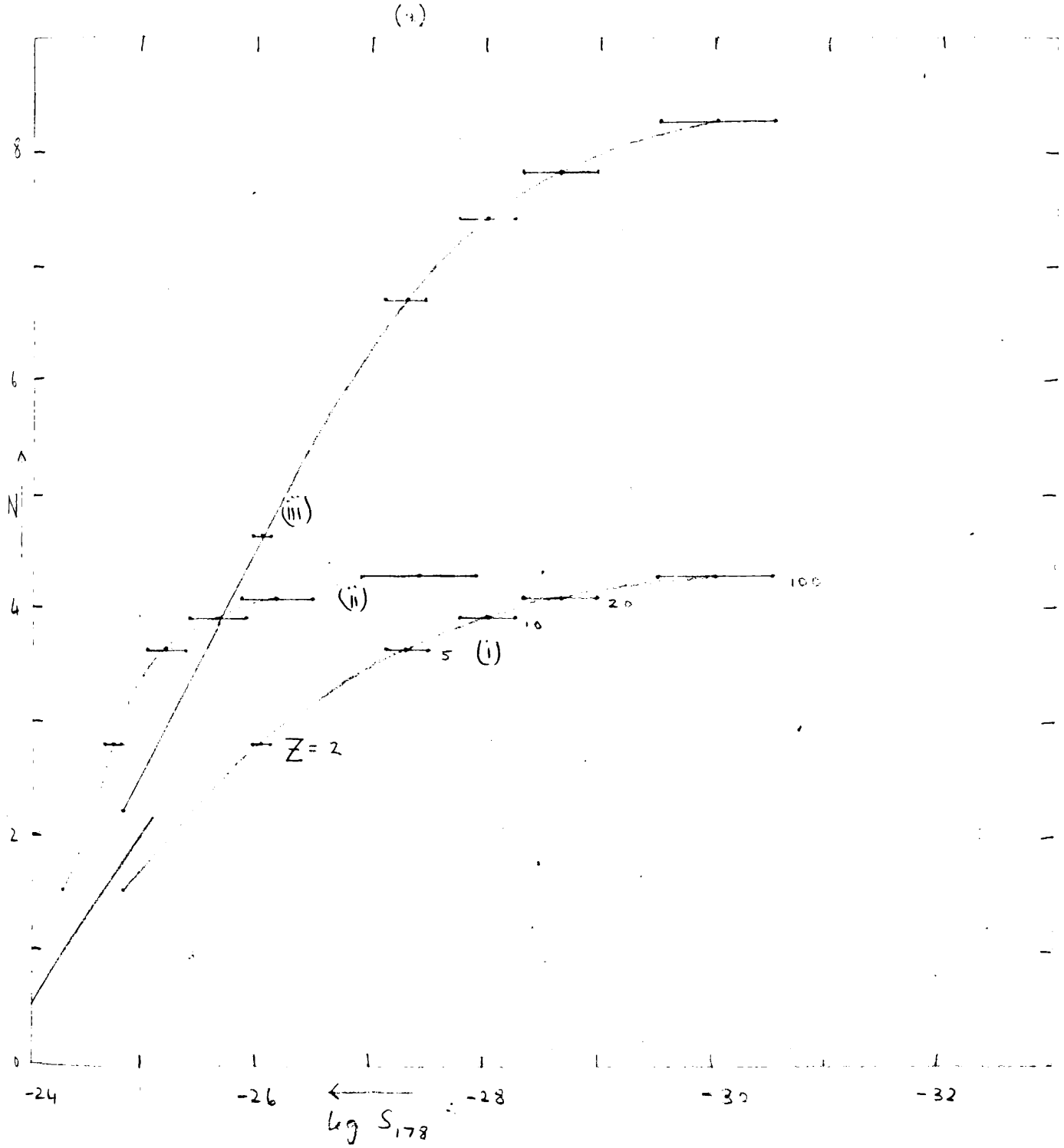

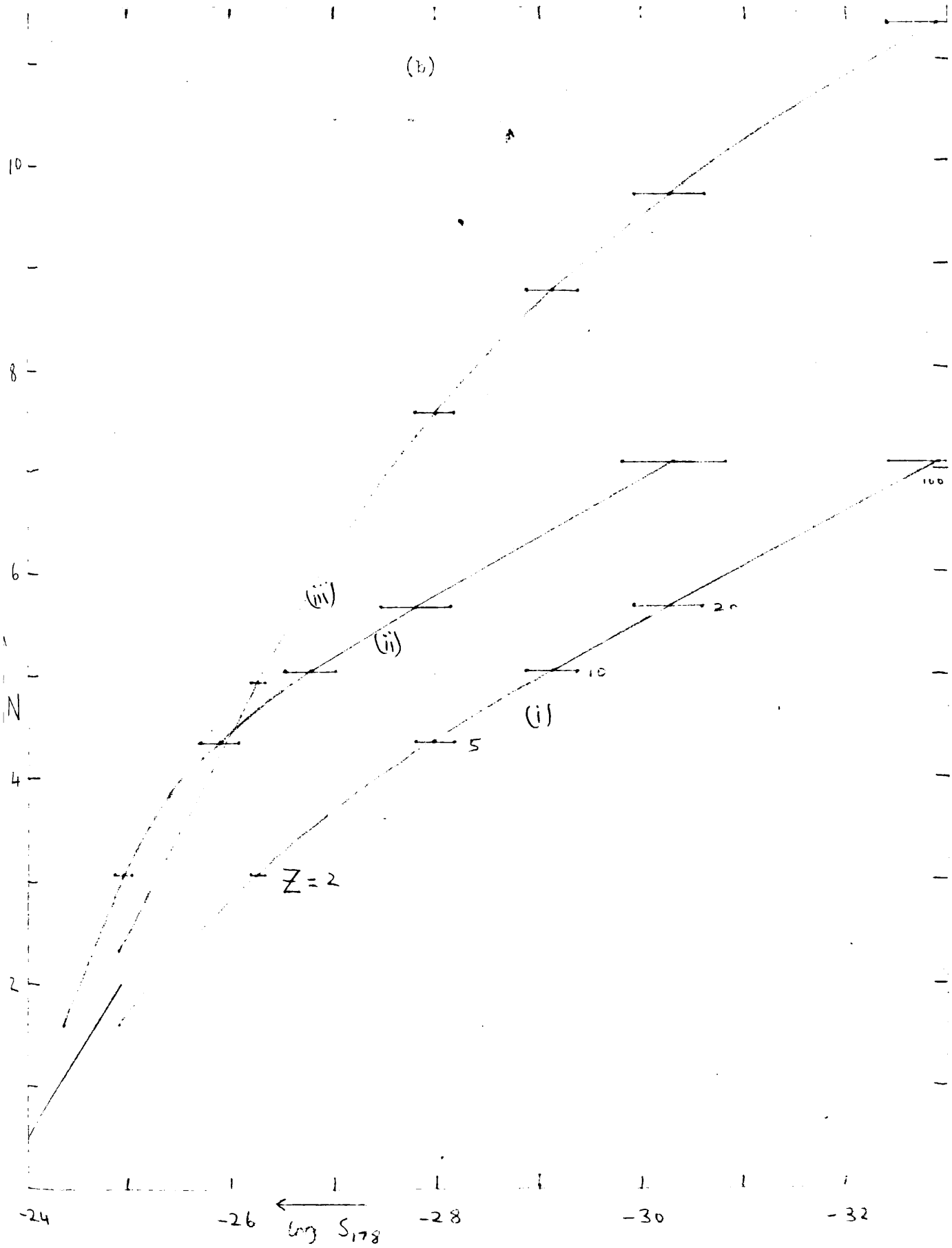
(b)
10
8
6
4
2
N
(iii)
(ii)
(i)
100
20
10
5
Z = 2
-24
-26
-28
-30
-32
log S_{178}

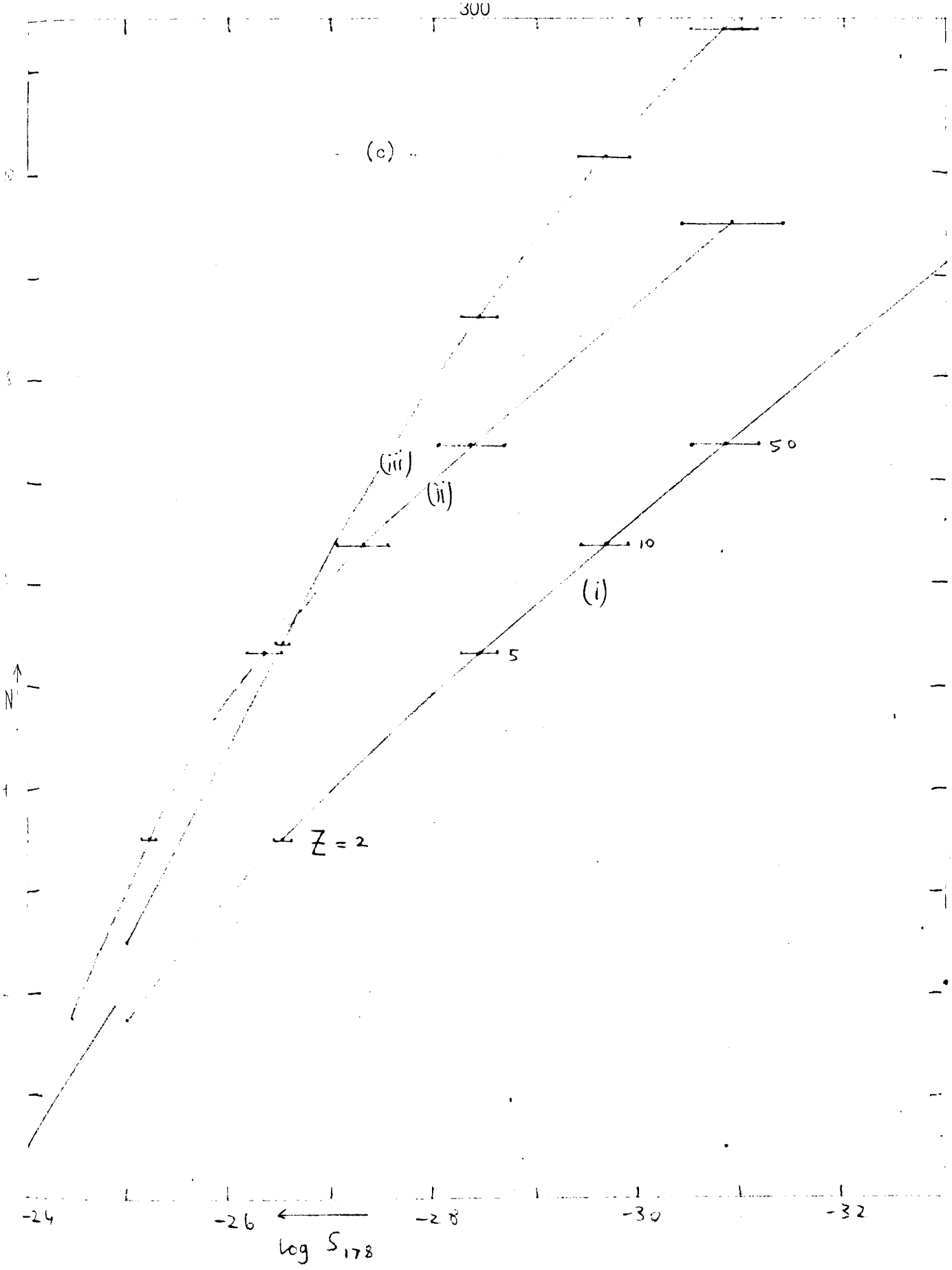
(c)
(iii)
(ii)
(i)
50
10
5
N
Z = 2
-24
-26
-28
-30
-32
log S_{178}

Fig 19 Number-count slope as a function of redshift in different cosmological models(E: Einstein-de Sitter, M: Milne, S: de Sitter, L: Edington-Lemaître model with Z_0=?.??), and histogram of V for (i) all 3C radio-galaxies (ii) those with known redshift.

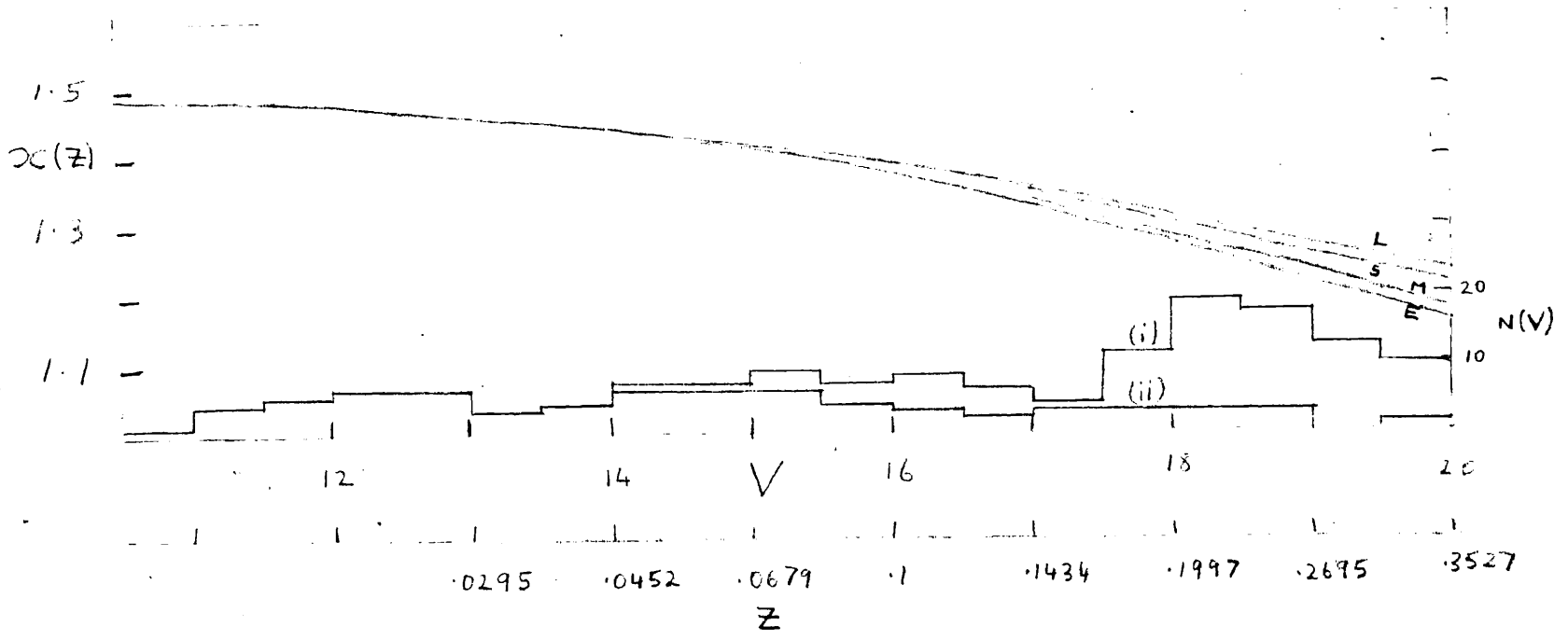

Fig 20 Comparison with observations(see Table 7) of predicted log N - log S relations, using the convolution relation (section III.4). See p.145 for parameters describing models shown.

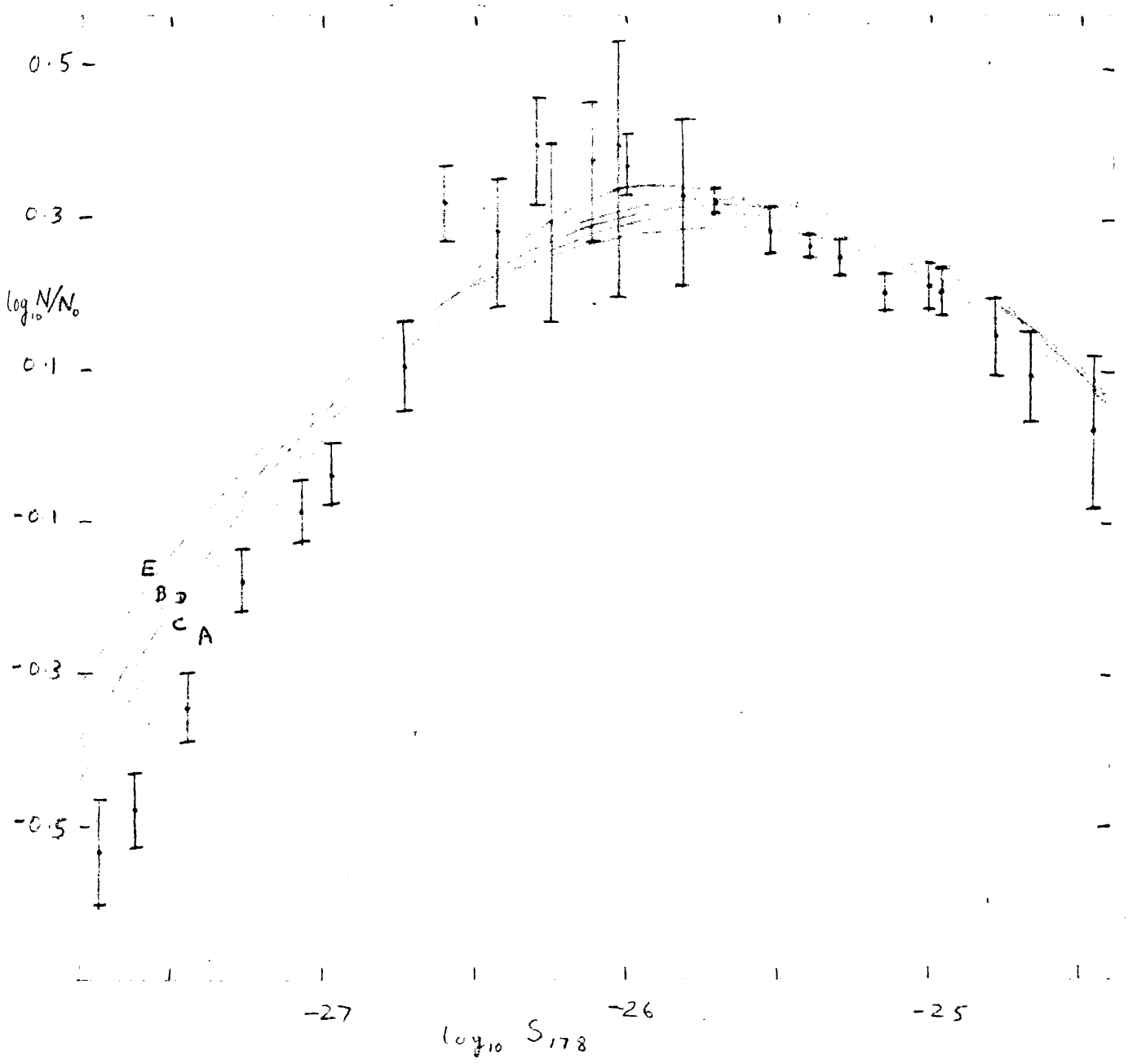

Fig 21 Effect of dispersion in spectral index on log-counts: $E = \log_{10}(1+\frac{1}{2}\sigma^2 \frac{d^2}{d\alpha^2})\Big|_{x=\alpha}$ against $\log_{10} S$.

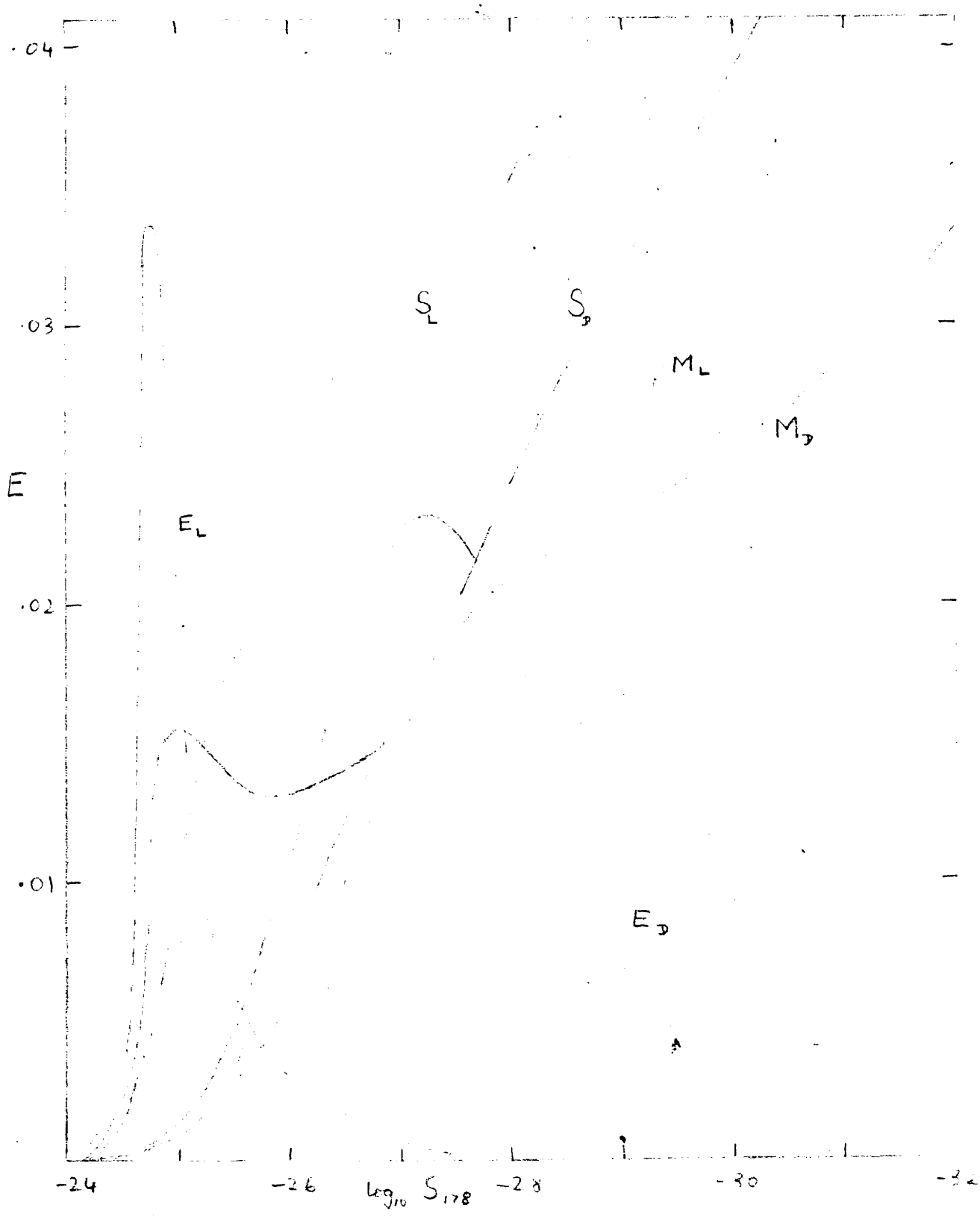

Fig 22 Radio source-counts at 178,408 & 2772 MHz, assuming α=0.8 (broken line) and a two-population model (section III.7)

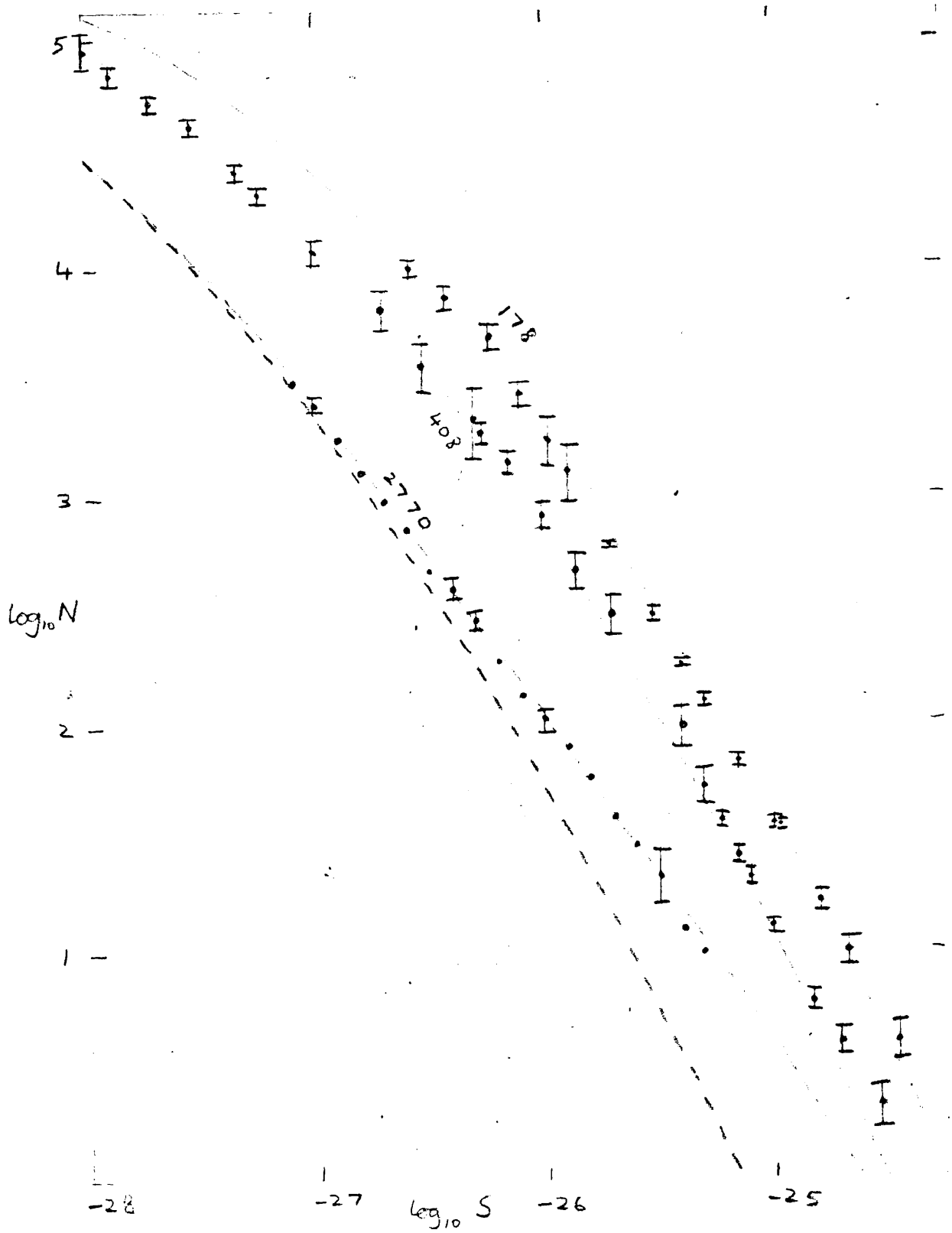

Fig 23 Luminosity function for radio-galaxies (⊥) and quasars (↕) in Einstein-de Sitter (E), Milne (M), and de Sitter (S) models with exponential luminosity ($_L$) and density ($_D$) evolutions.

solid line: normalized to give log N(-25) = 1.6 (see section III.10)

broken line: adjusted to give best fit to counts (see section III.11)

dotted line: luminosity function in absence of evolution.

⊕ and ⊖ indicate where the effect of changing the V-magnitudes of radio-galaxies, whose redshifts are unknown, by ± 1 (see section I.14) is greater than the statistical uncertainty.

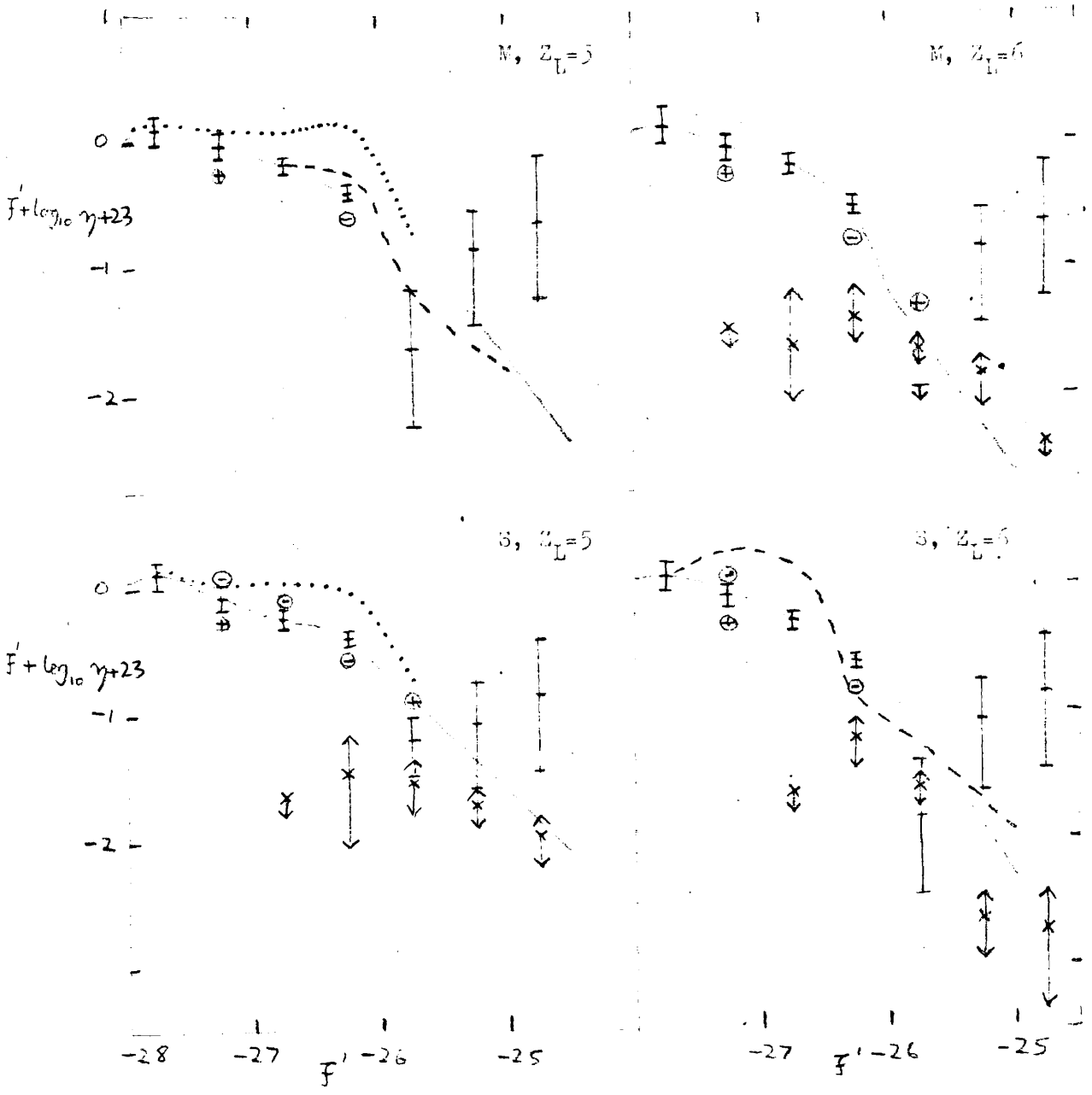

Fig 23 (continued)

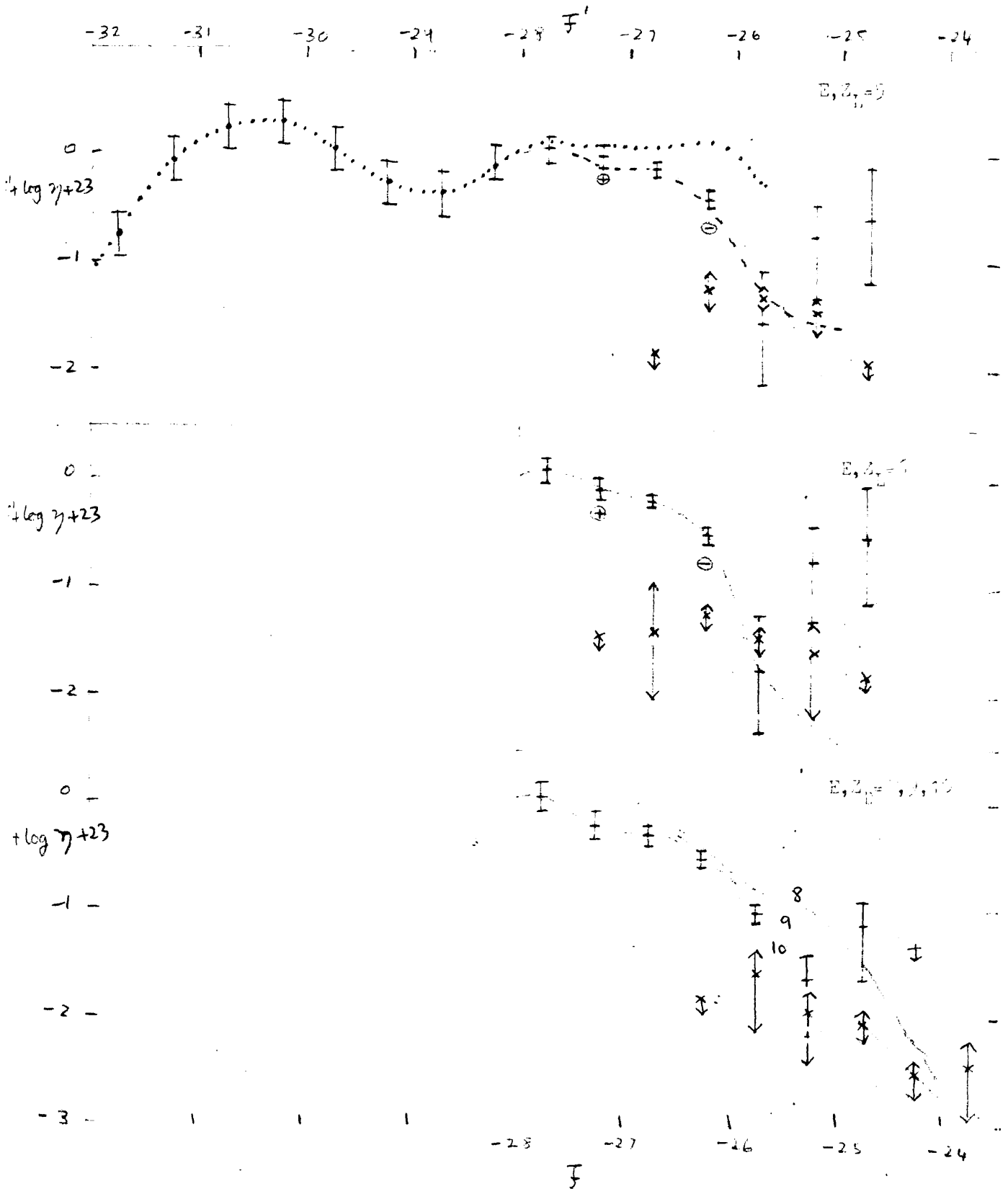

Fig 24 Integrated background temperature at 178 MHz as a function of $\mathcal{F}_c$

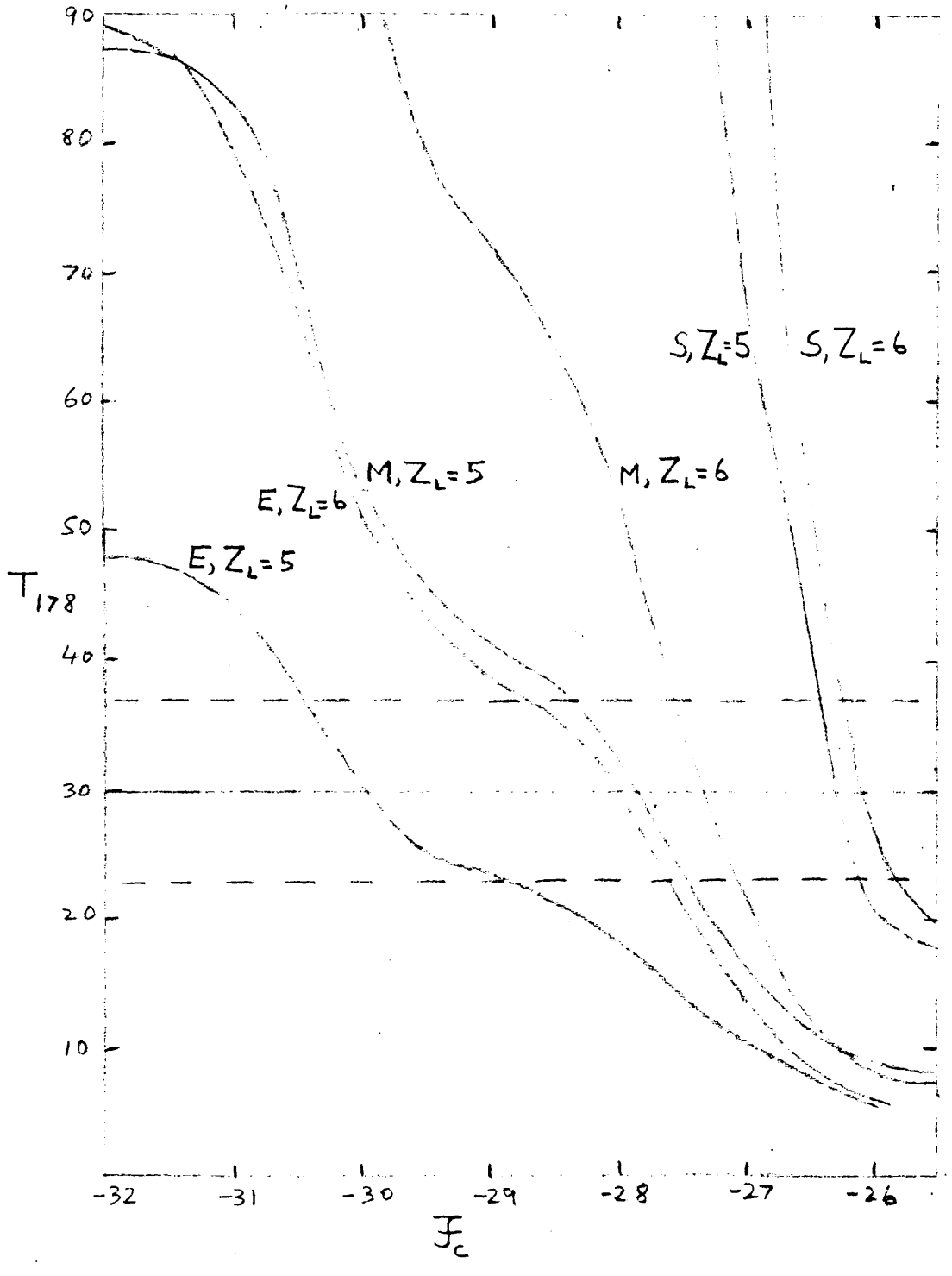

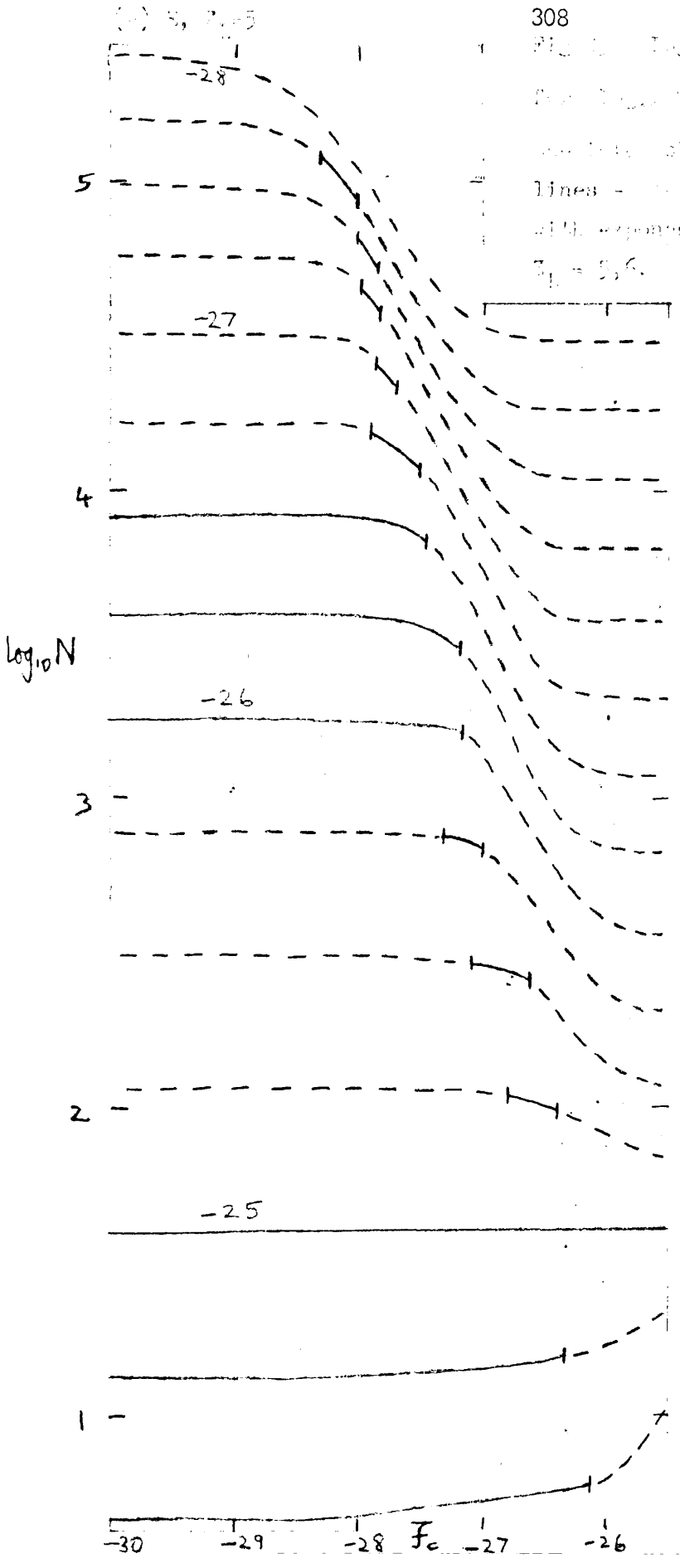
-28
-27
-26
-25
5
4
3
2
1
$\log_{10}N$
-30
-29
-28
$\mathcal{F}_c$
-27
-26

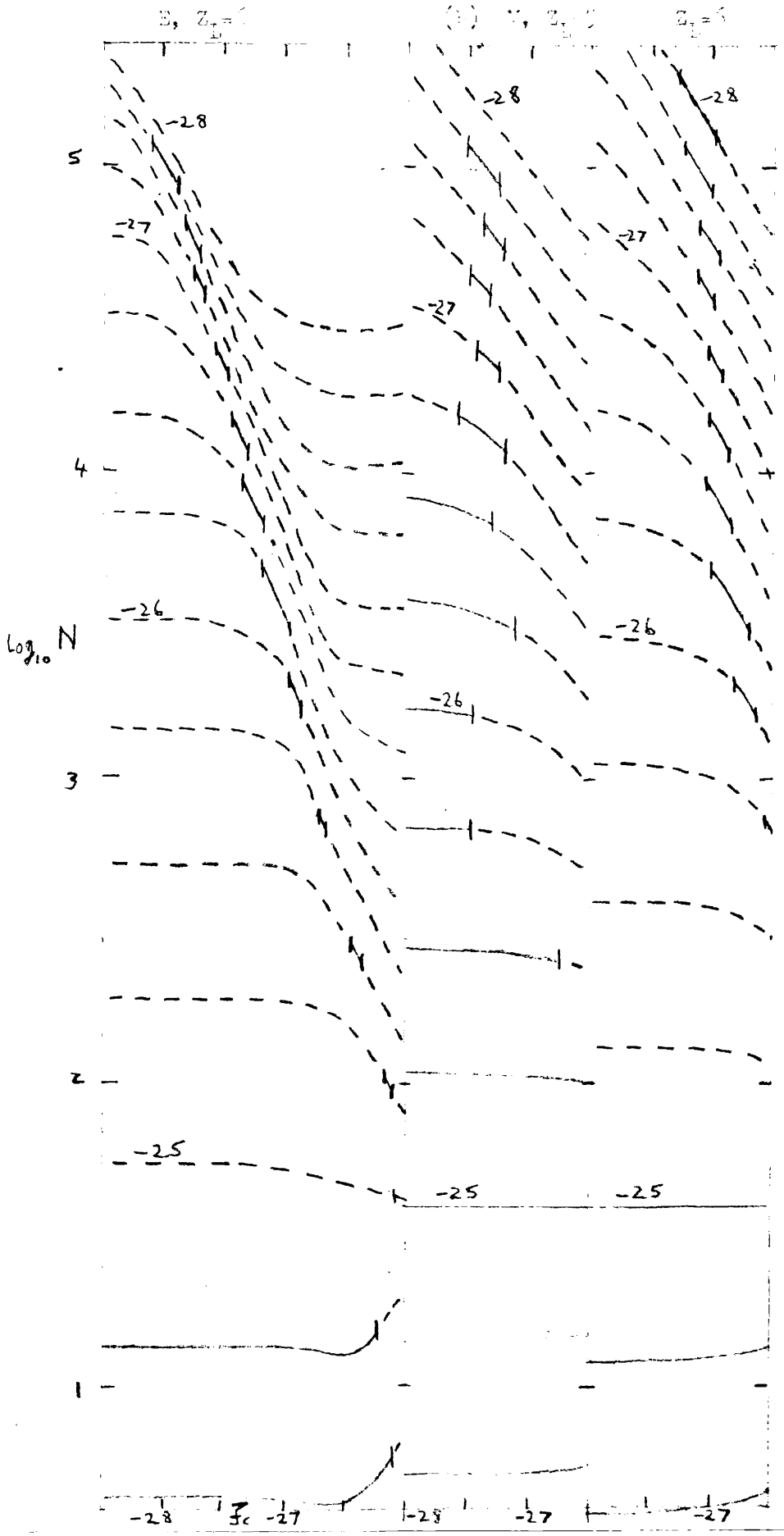
-28
-27
-26
-25
5
4
3
2
1
$\log_{10} N$
$\frac{1}{-28}$
$\frac{1}{-27}$
$\frac{1}{-28}$
$\frac{1}{-27}$
$\frac{1}{-27}$

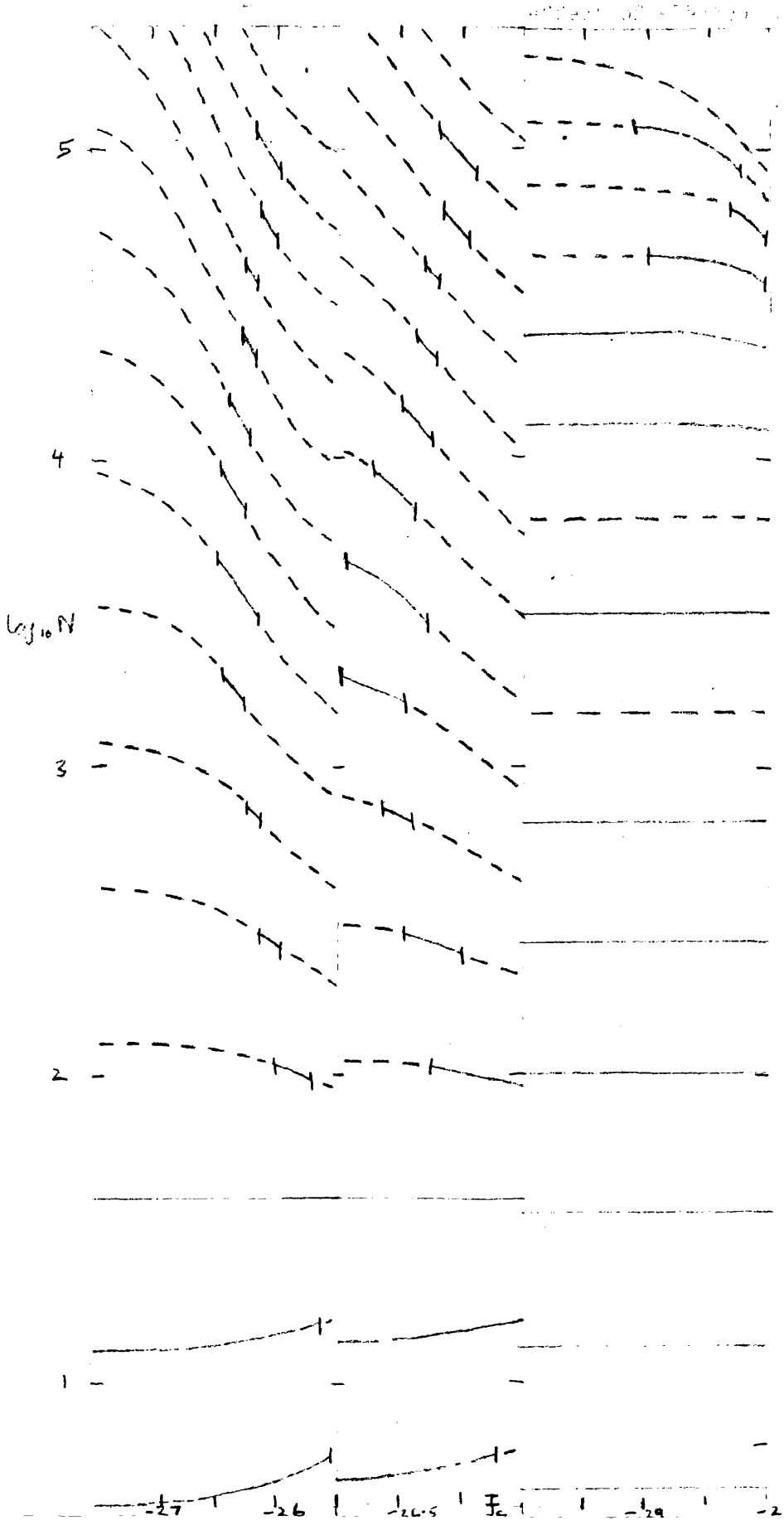
5
4
$\log_{10} N$
3
2
1
-27
-26
-25.5
-25
-24
-23
-22

Fig. [illegible] Fraction of [illegible]
($\log_{10}$ [illegible]) in (a) [illegible] (b) [illegible] (c) [illegible], with
exponential luminosity evolution, Z_f = [illegible], (d) [illegible] with
exponential density evolution, Z_f = 1[illegible], [illegible] $I \propto F$ [illegible] ([illegible] IV.)

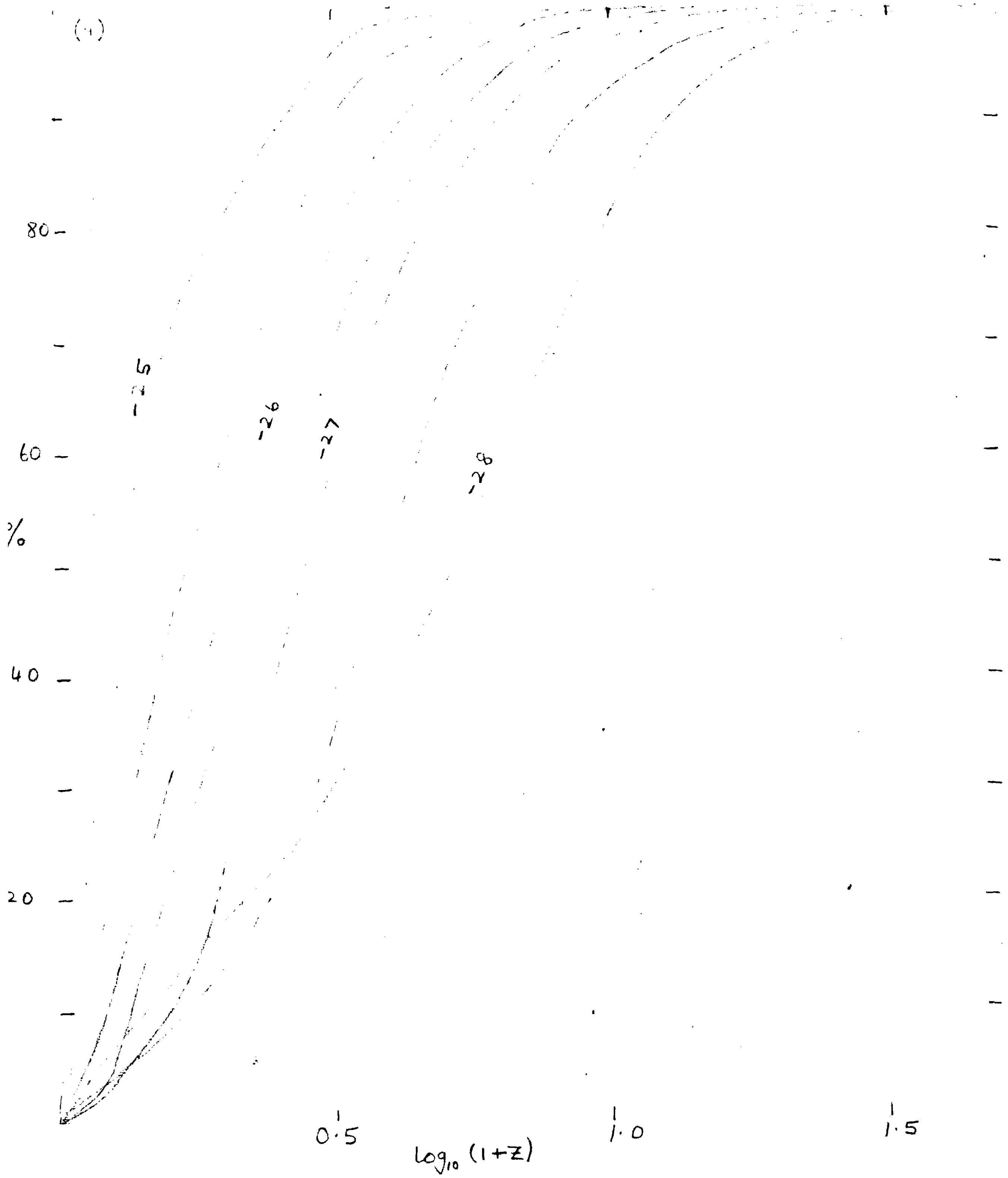

Fig 2.6

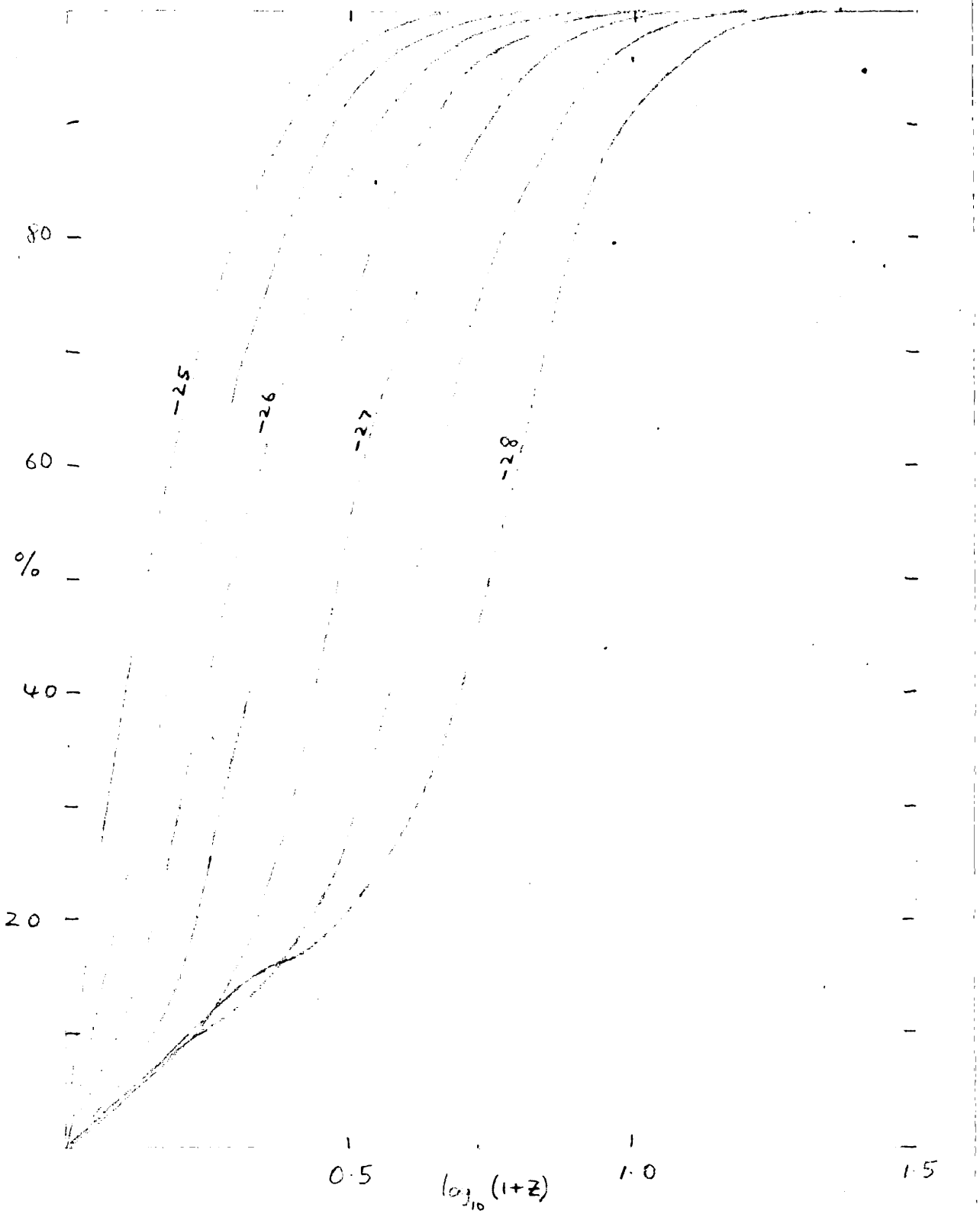

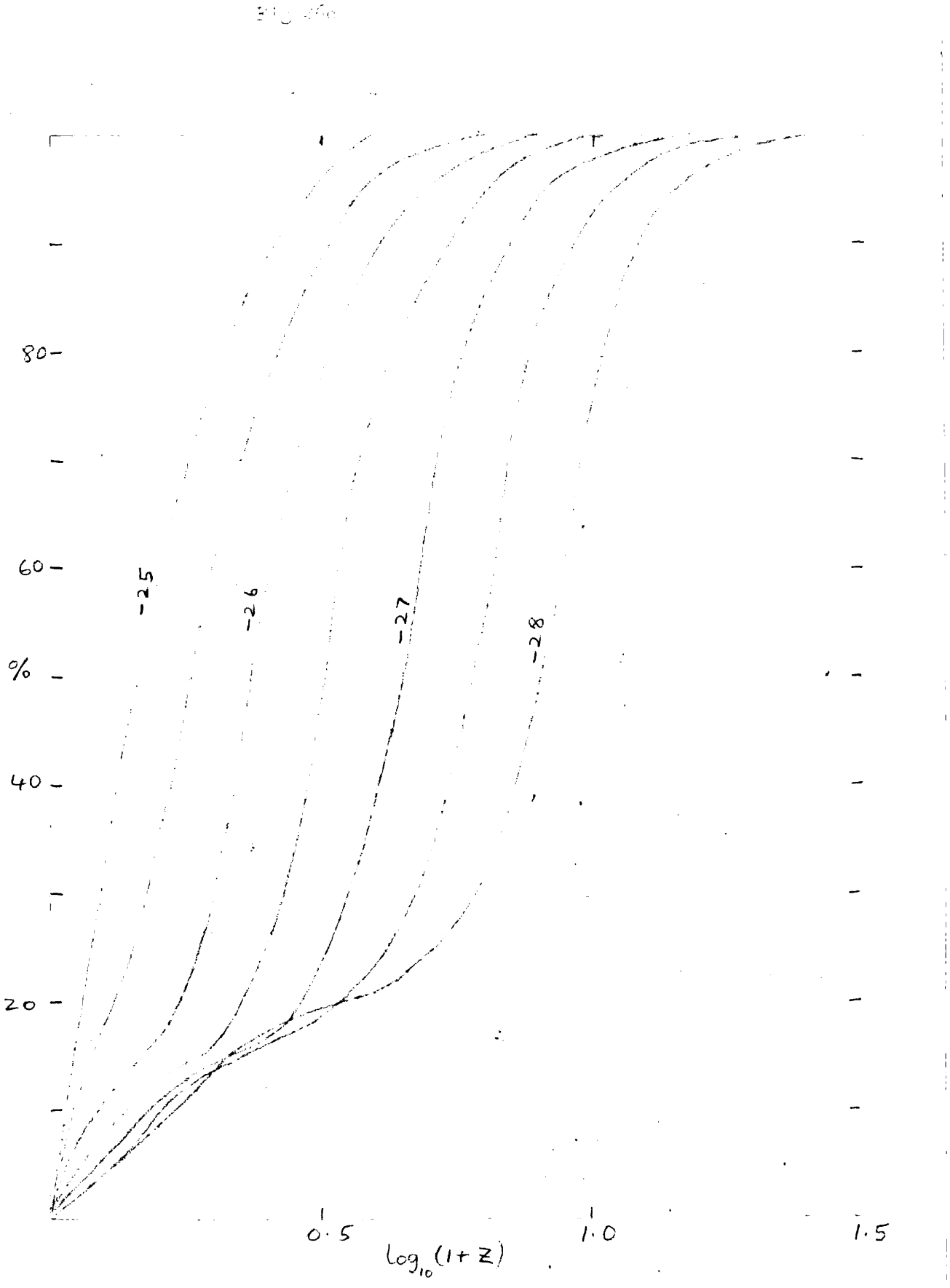
80
60
%
40
20
-25
-26
-27
-28
0·5
1·0
1·5
log10(1+z)

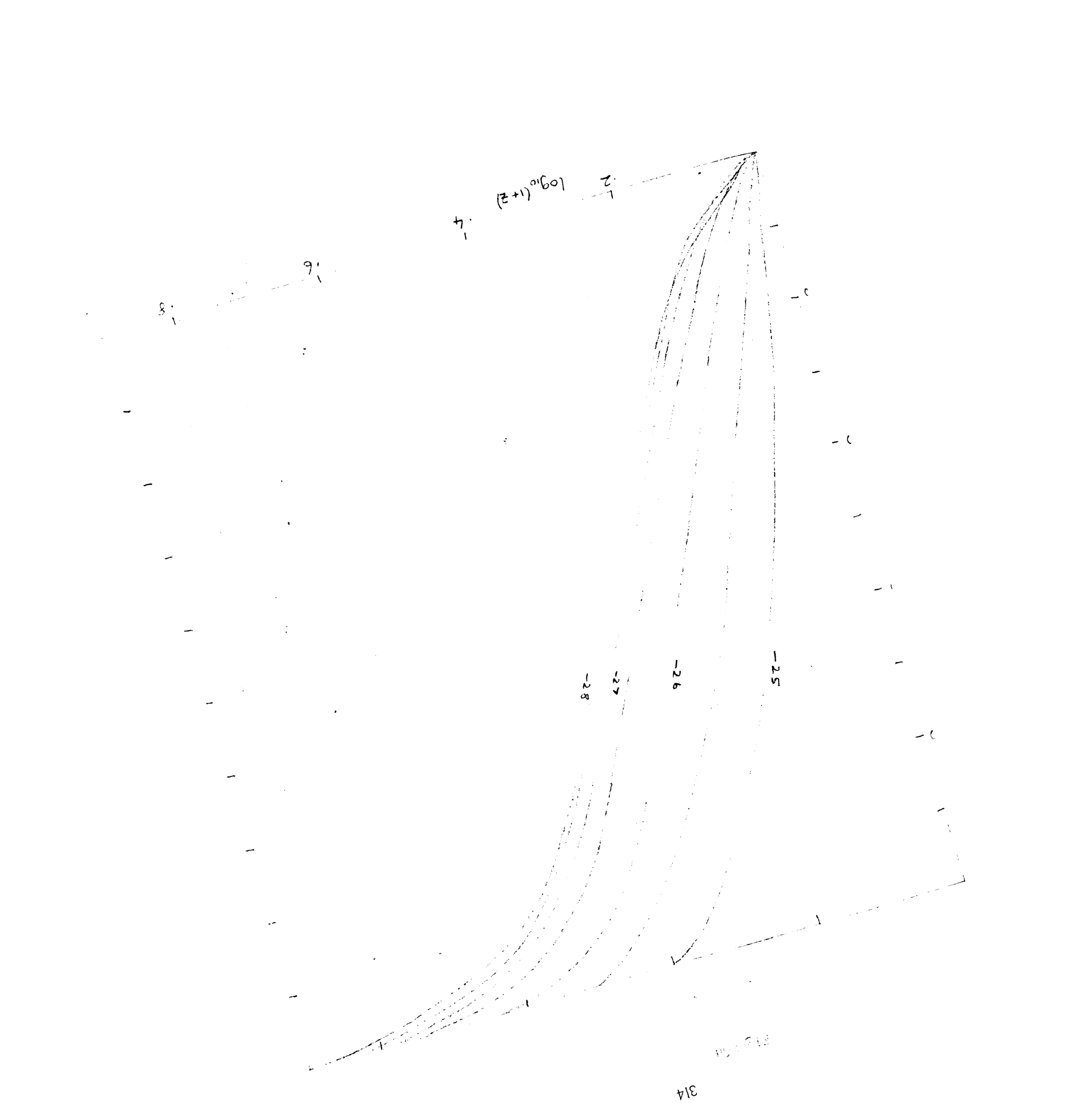
$\log_{10}(1+z)$

Fig. 7a. Source-counts as a function of flux-level at 178 MHz (see text, Table 7)

(a) E, S, M models, Z_1=5, including effect of a truncation at redshift z_t = 10 (dash-dotted line), 10 (broken line), = 5 (solid line, following page)

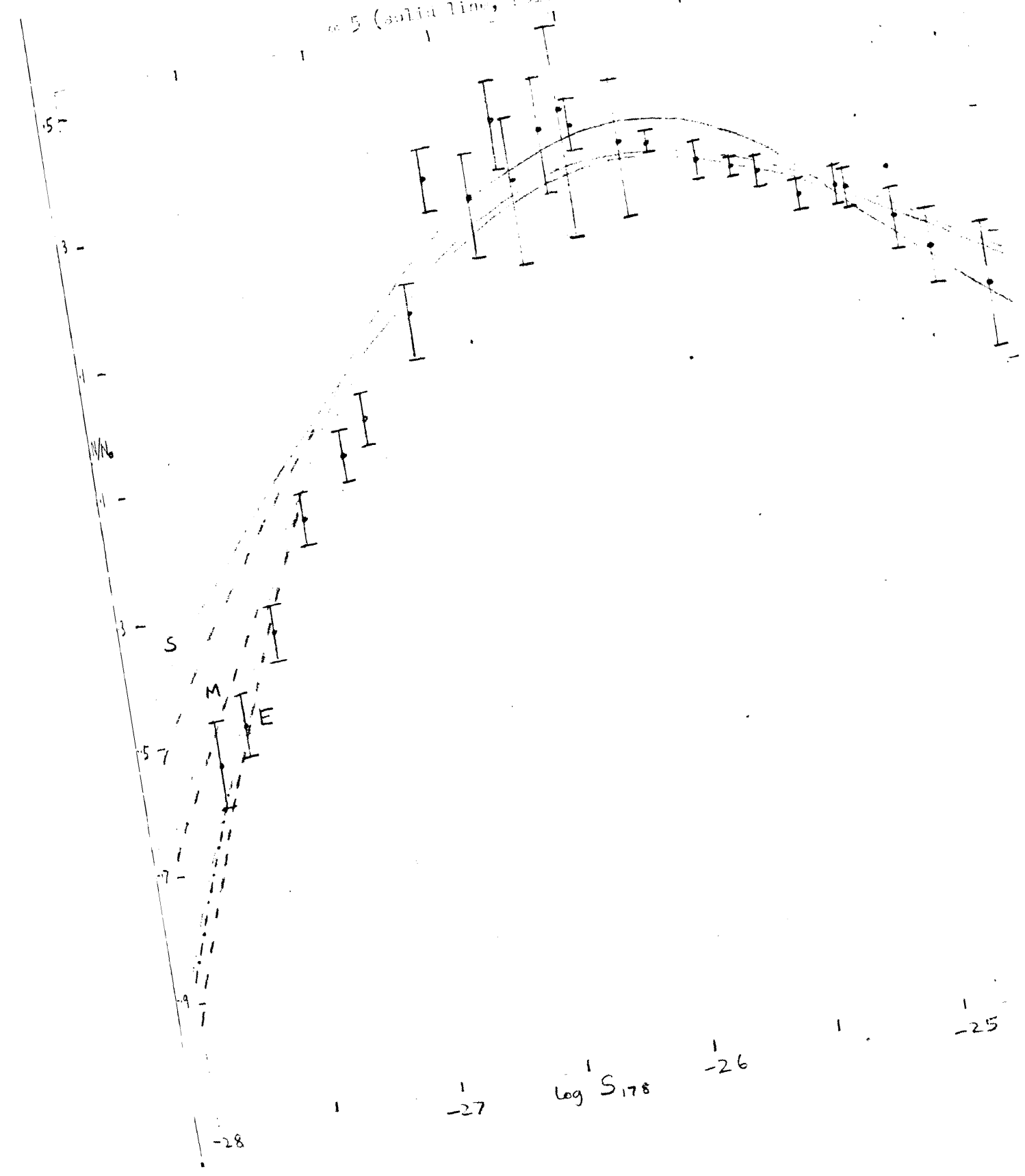

Fig 27a (cont.) [illegible], Z_L=[illegible]; with effect of electron screening (broken line)
(see previous caption for legend to solid lines)

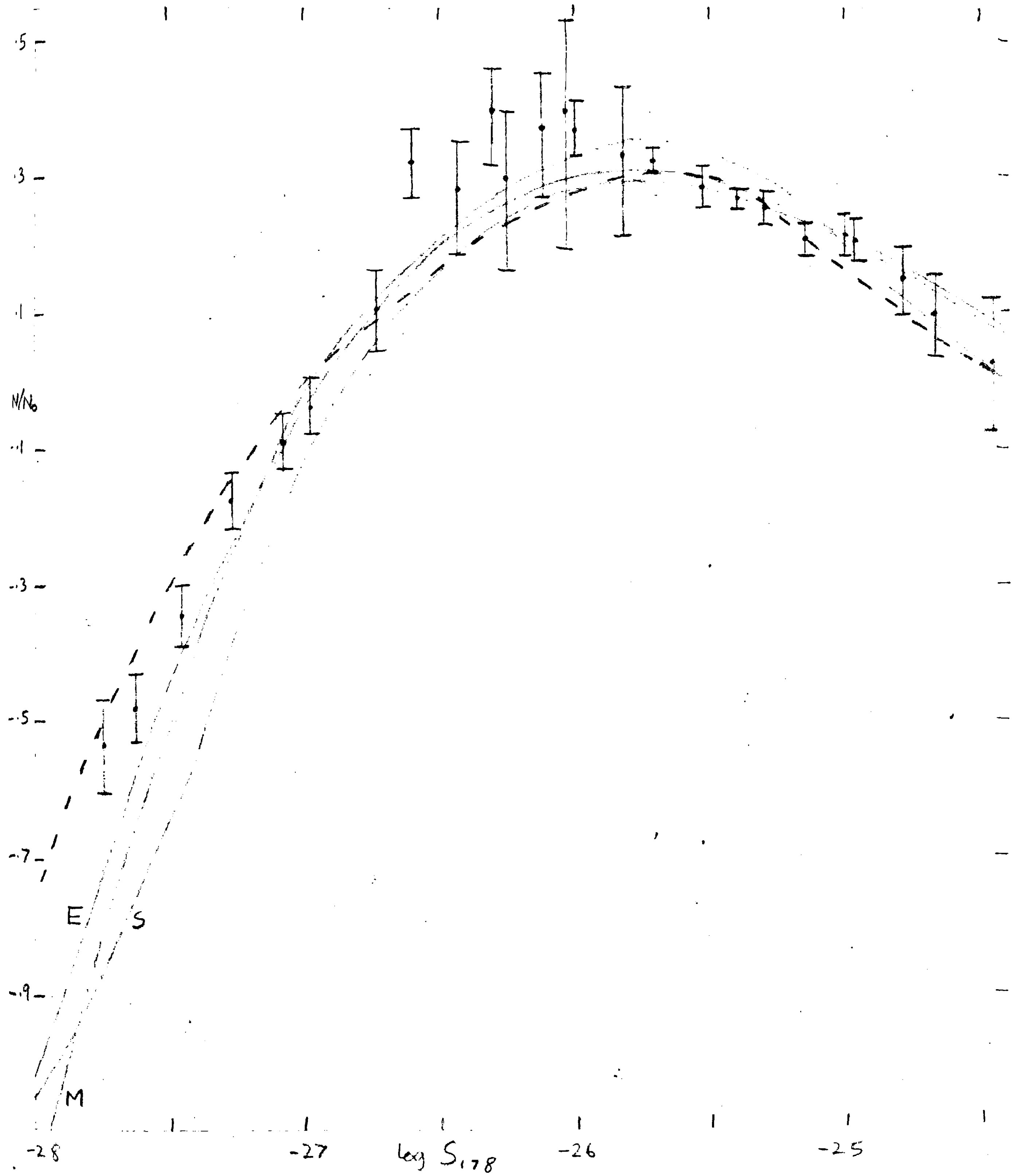

Fig. 7c α_1', α_1=3, & S, α_1=4, with weighted intensity functions (see Fig. 2)

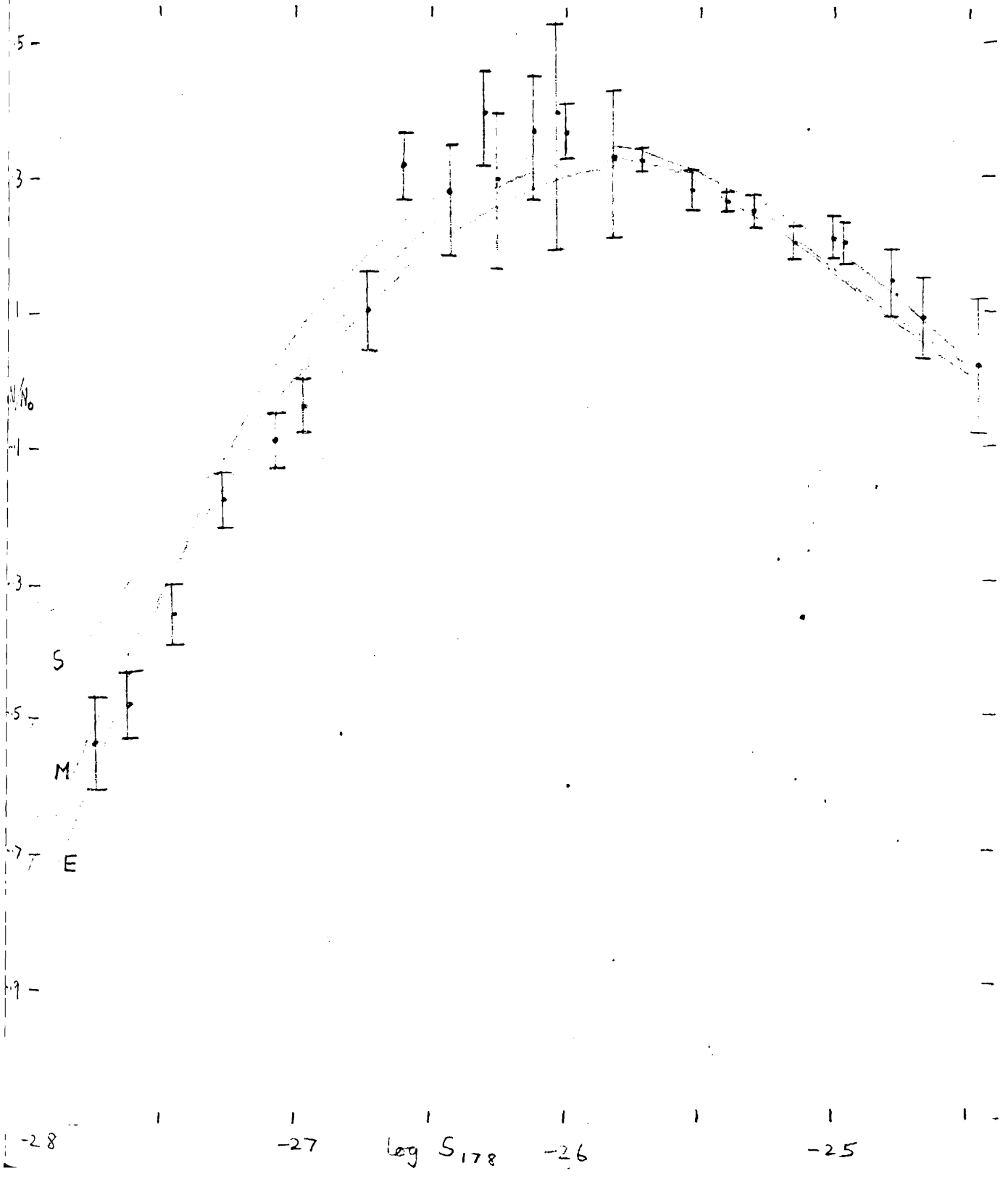

Fig 7b(cont.) Effect of spectral index dependent on luminosity (middle curve), and on epoch (lower curve), on source-counts in model with $\Lambda=0$, $q_0=0.05$.

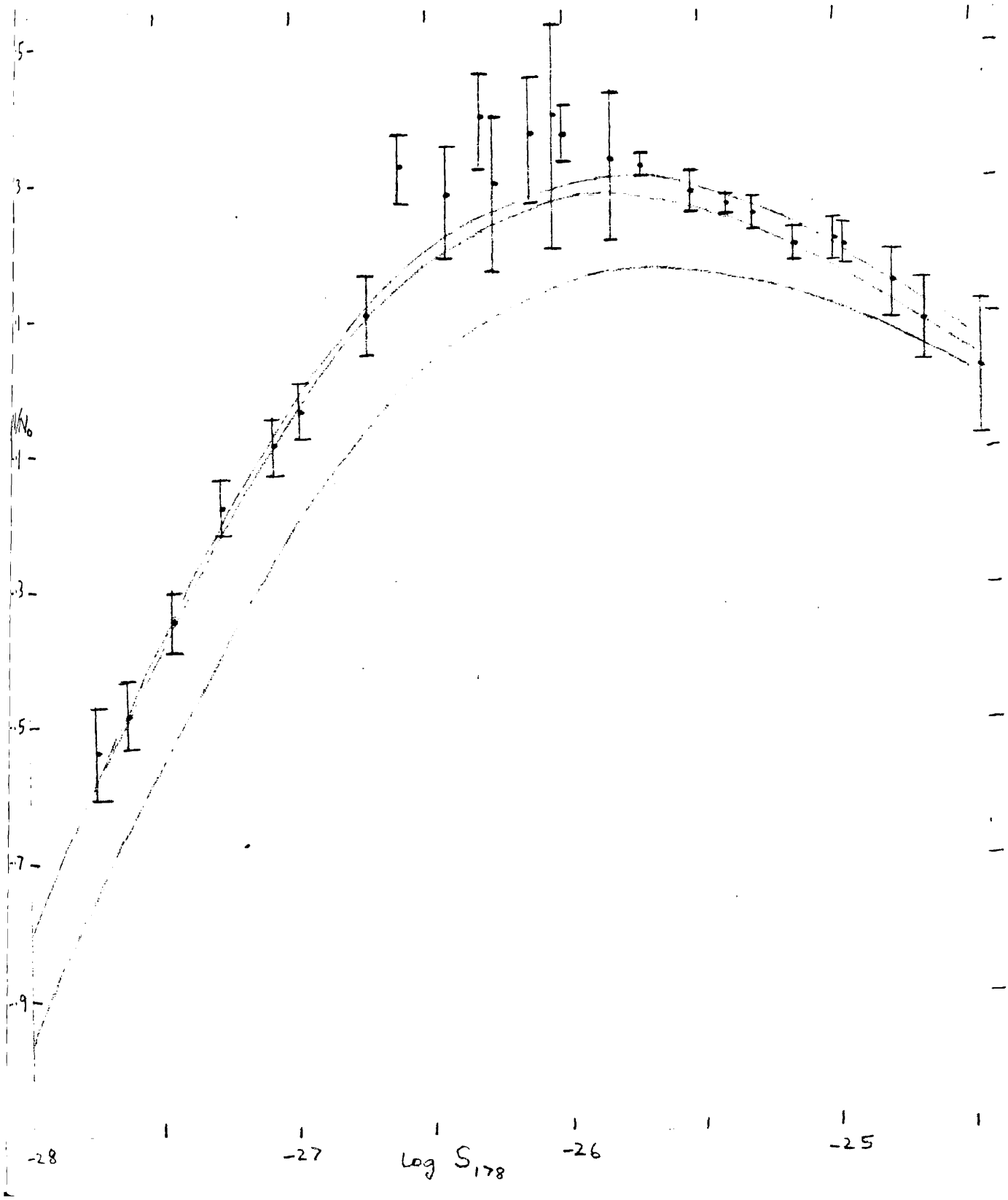

Fig 23 Luminosity distribution at different flux-levels ($\log_{10} S_{175}$ = -23(-1)-28) in S,E,M models, with Z_L=5.

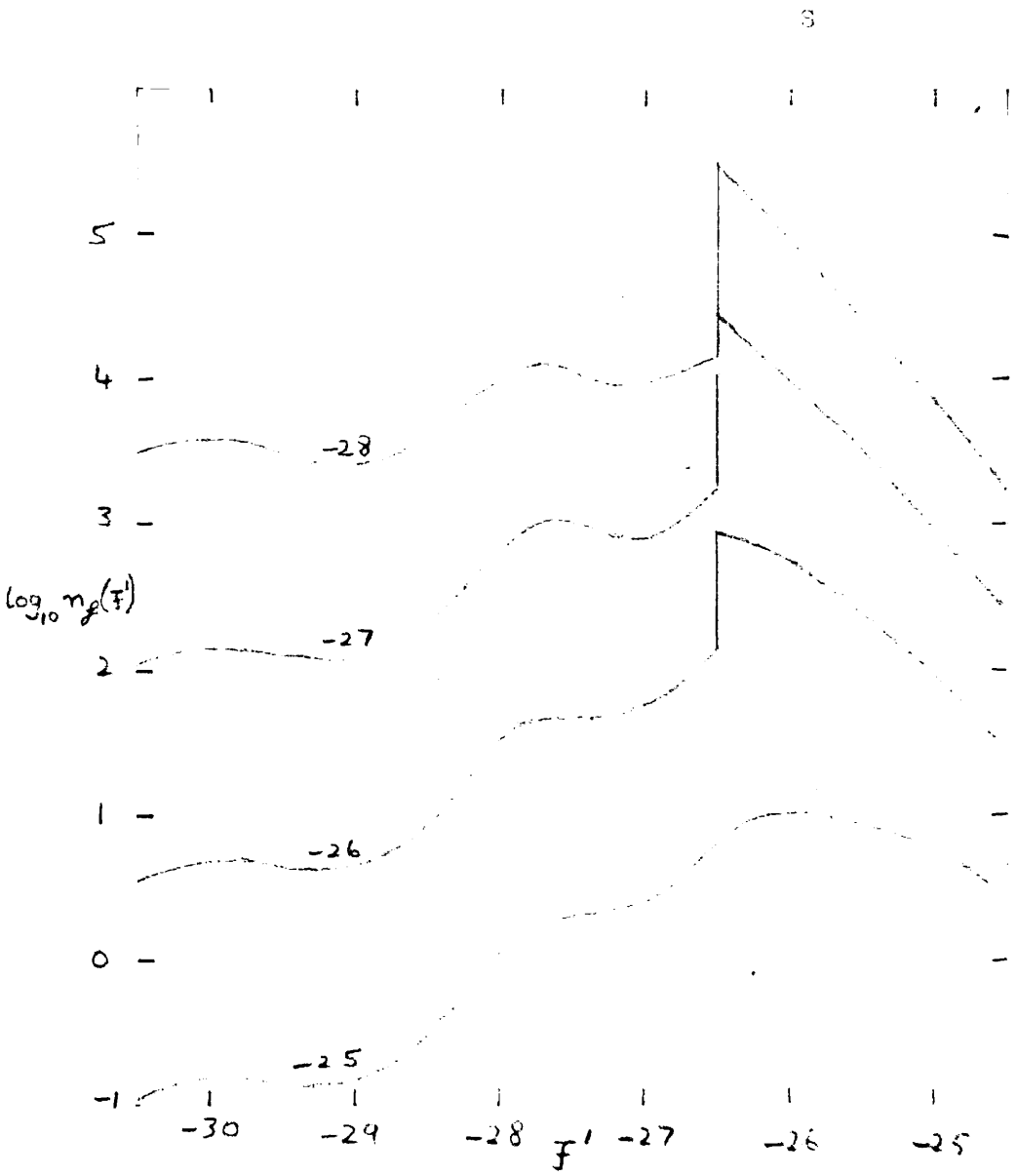

Fig 20(cont.)

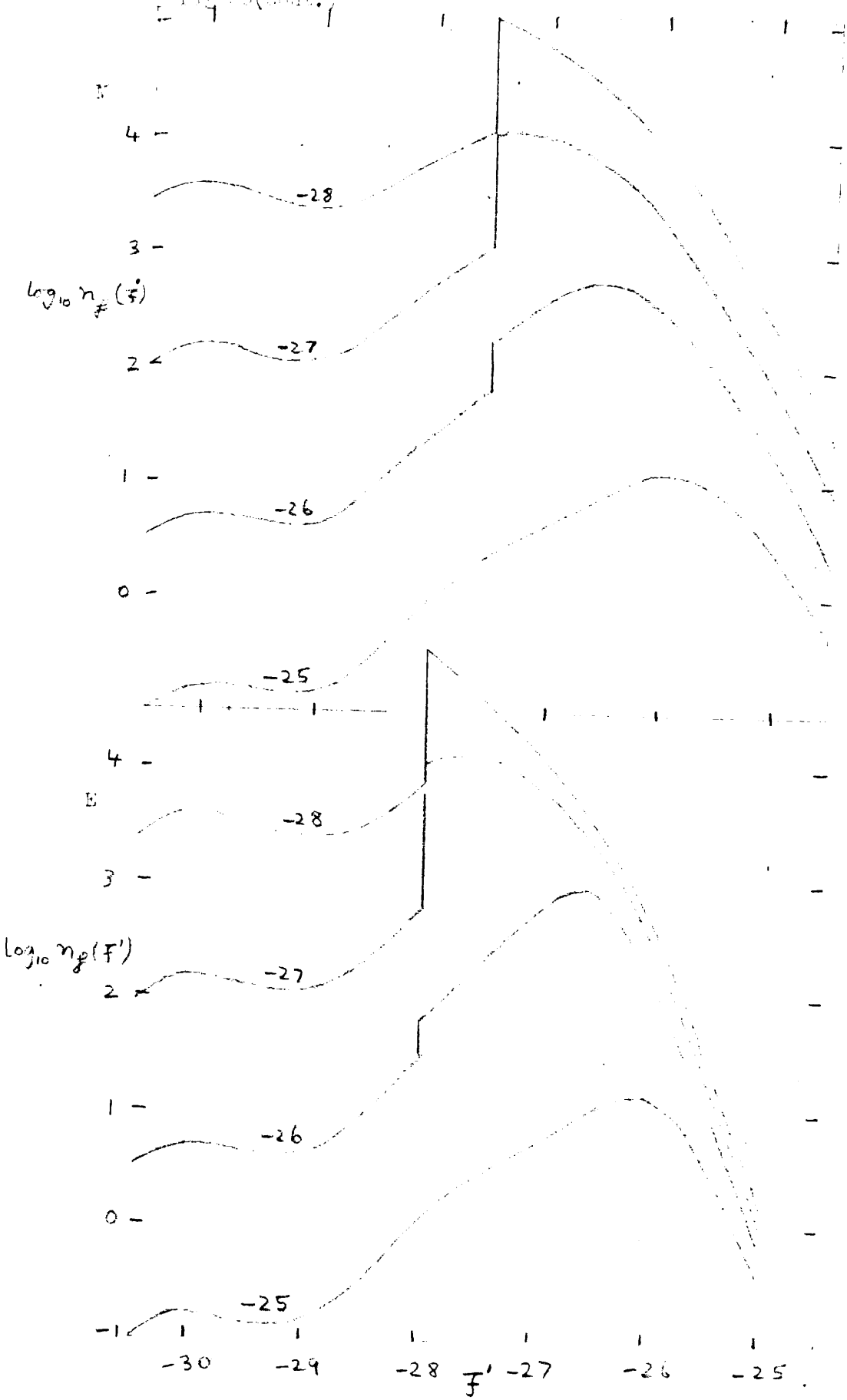
E
4
3
2
1
0
-1
-28
-27
-26
-25
$\log_{10} n_e(F')$
E
4
3
2
1
0
-1
-28
-27
-26
-25
$\log_{10} n_g(F')$
-30
-29
-28
-27
-26
-25
F'

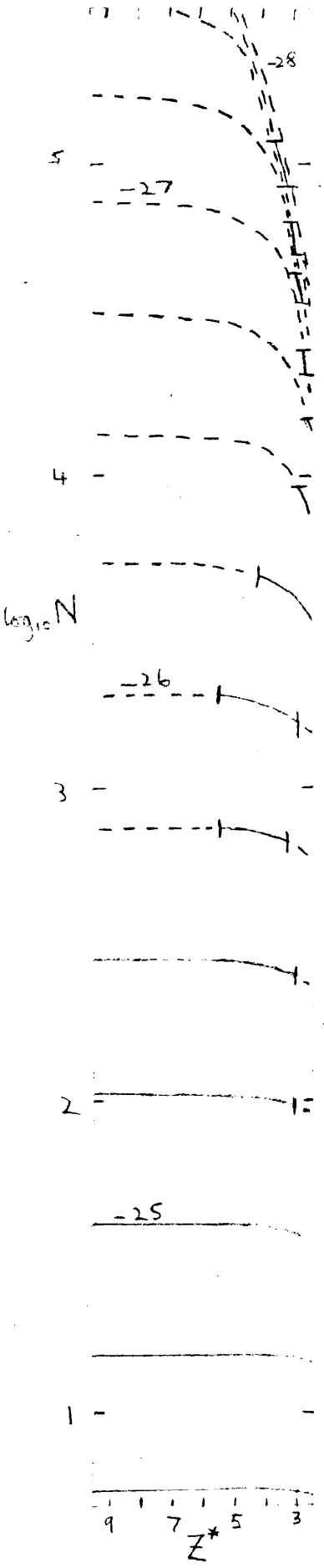

Fig 20 Effect of luminosity evolution at different redshifts on source-counts at different flux-levels in the Einstein-de Sitter model, with exponential density evolution, $Z_c = 10$.

Fig 31 Magnetic field against age in double sources.

A denotes the minimum age of about 3.10^5 yrs, obtained if the components are ejected from the parent galaxy at velocity ~ c.

B corresponds to the synchrotron life-, $\tau_s(F)$, of electrons radiating at 408 MHz. Models of type (a) of section IV.2 lie on this line: models of type (bi) and (bii) lie below and above this line, respectively.

C corresponds to the equipartition magnetic field in sources,

$$\log B_e = -4 \pm 0.3 \ .$$

If $B \neq B_e$, total energy requirements are increased by χ, where

$$\log \chi = 1.3 \left| \log B/B_e \right| \ .$$

If also there is continuous injection of electrons, the energy requirements are increased by a further factor $\beta = \tau/\tau_s$.

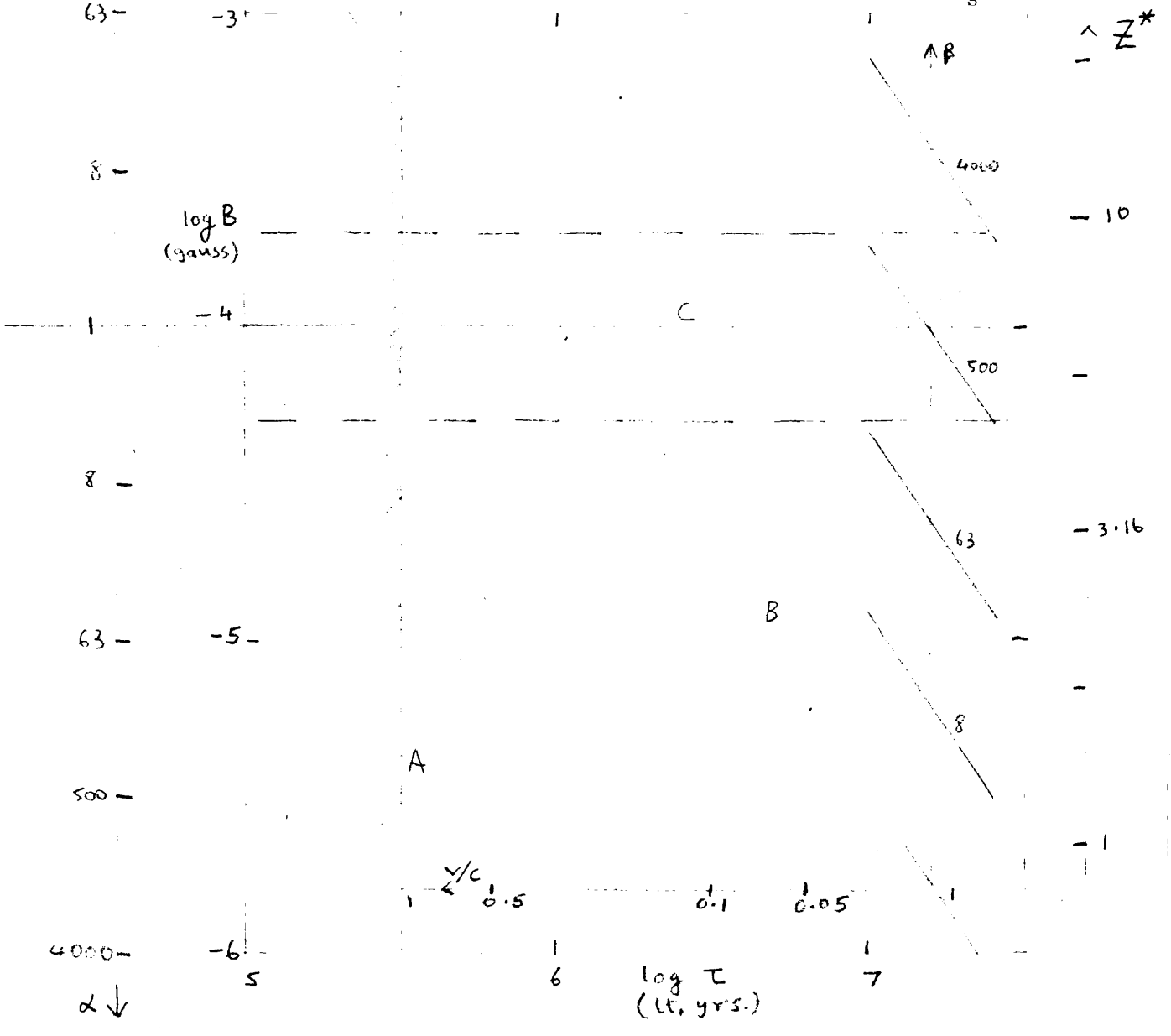

Fig. 5.a. Background temperature at 178 MHz, as a function of cosine of zenith angle for 3 models: (1) no evolution, $\overline{\eta P} = 4$ (2) exponential luminosity evolution, $Z_L = 5$, $\overline{\eta P(0)} = 4$ (3) exponential density evolution, $Z_L = 10$, $\overline{\eta P(0)} = 1.5$.

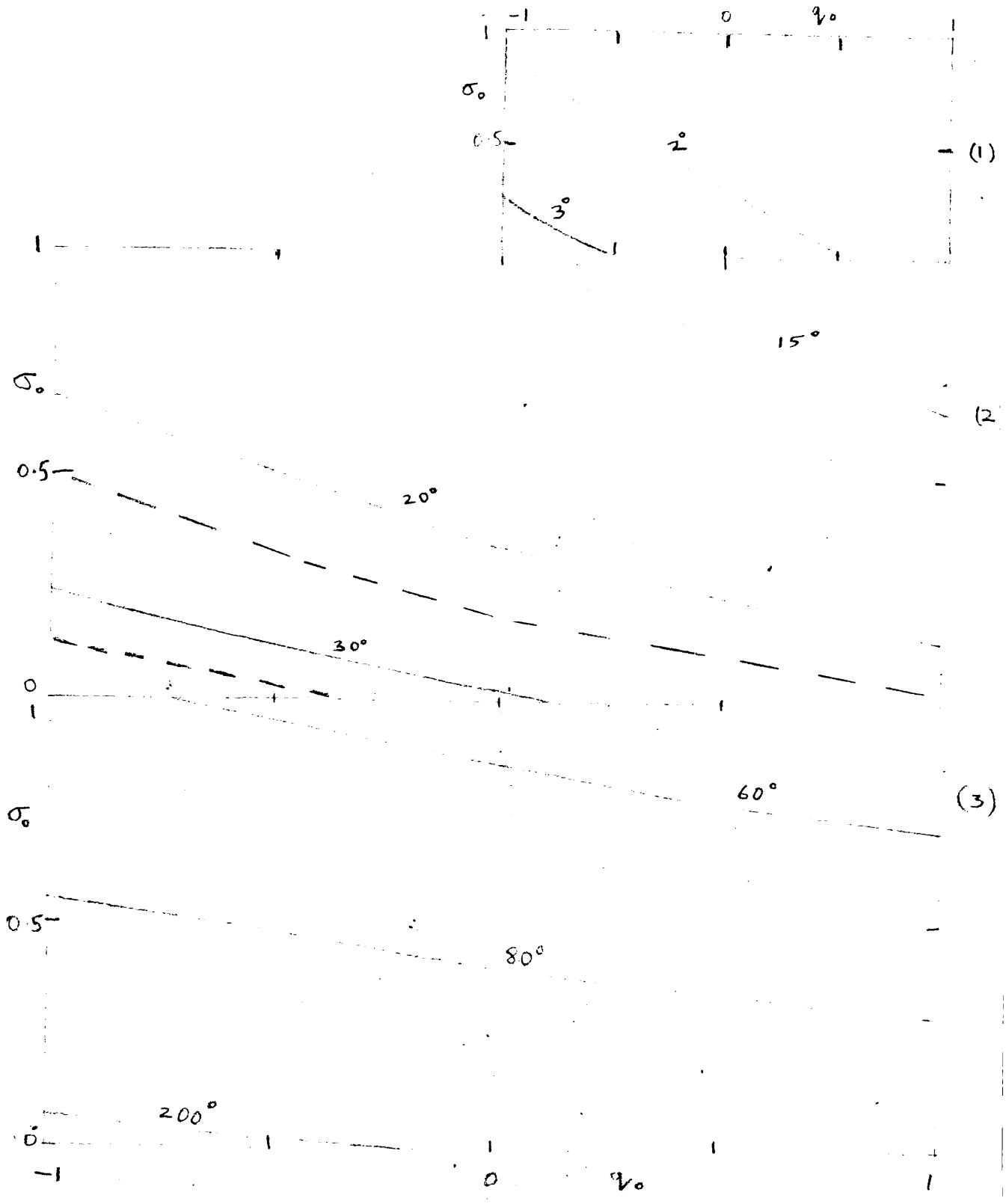

Fig 32b Th[illegible] [illegible] of T_{178} (right-h[illegible] scale) and F_x on Z^*([illegible] B.the [illegible]) for E,M,S [illegible], with $Z_D=10$, $Z_L=5$, [illegible] evolution.

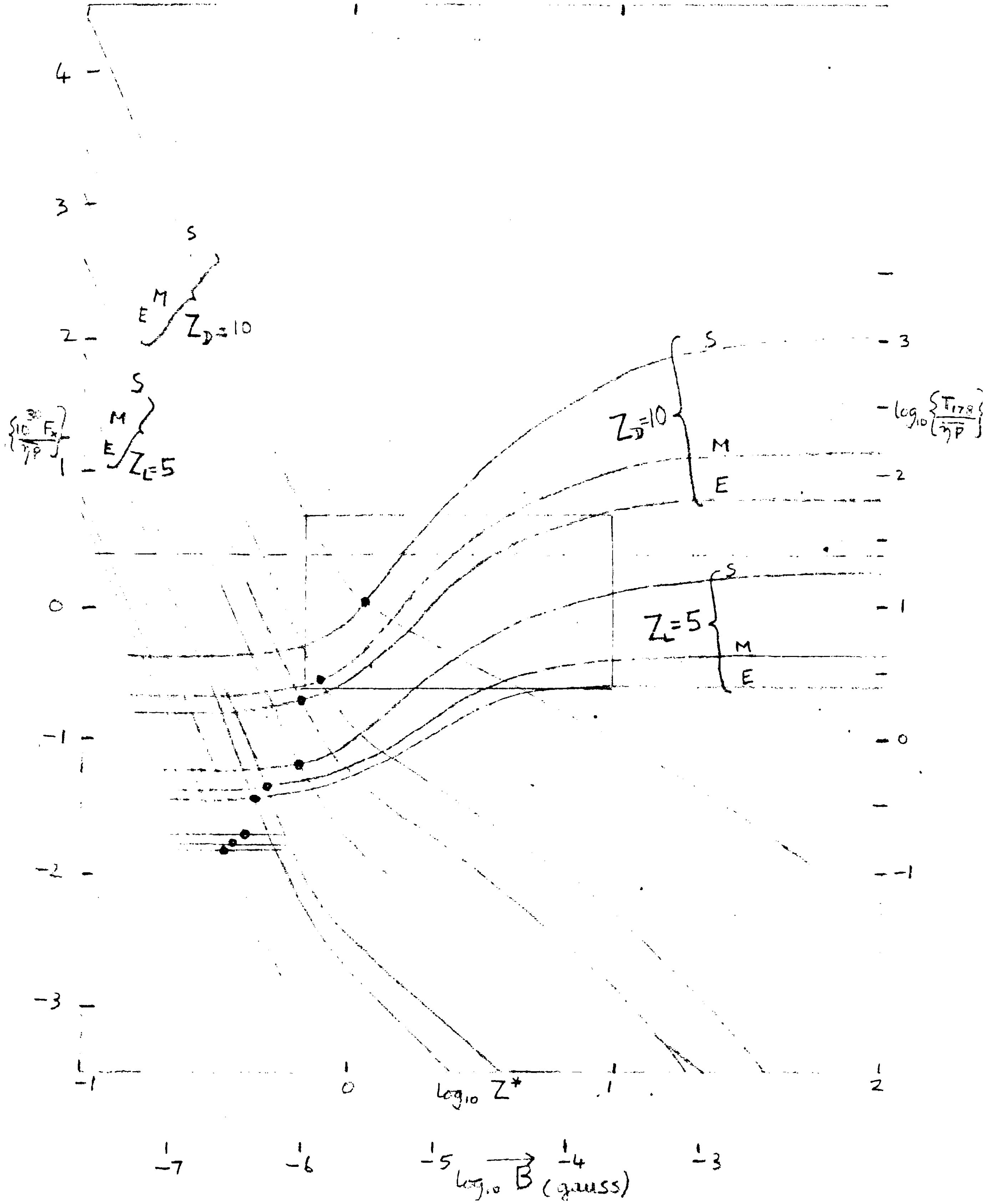

Fig. 32a ... and 1.5?? ( ).

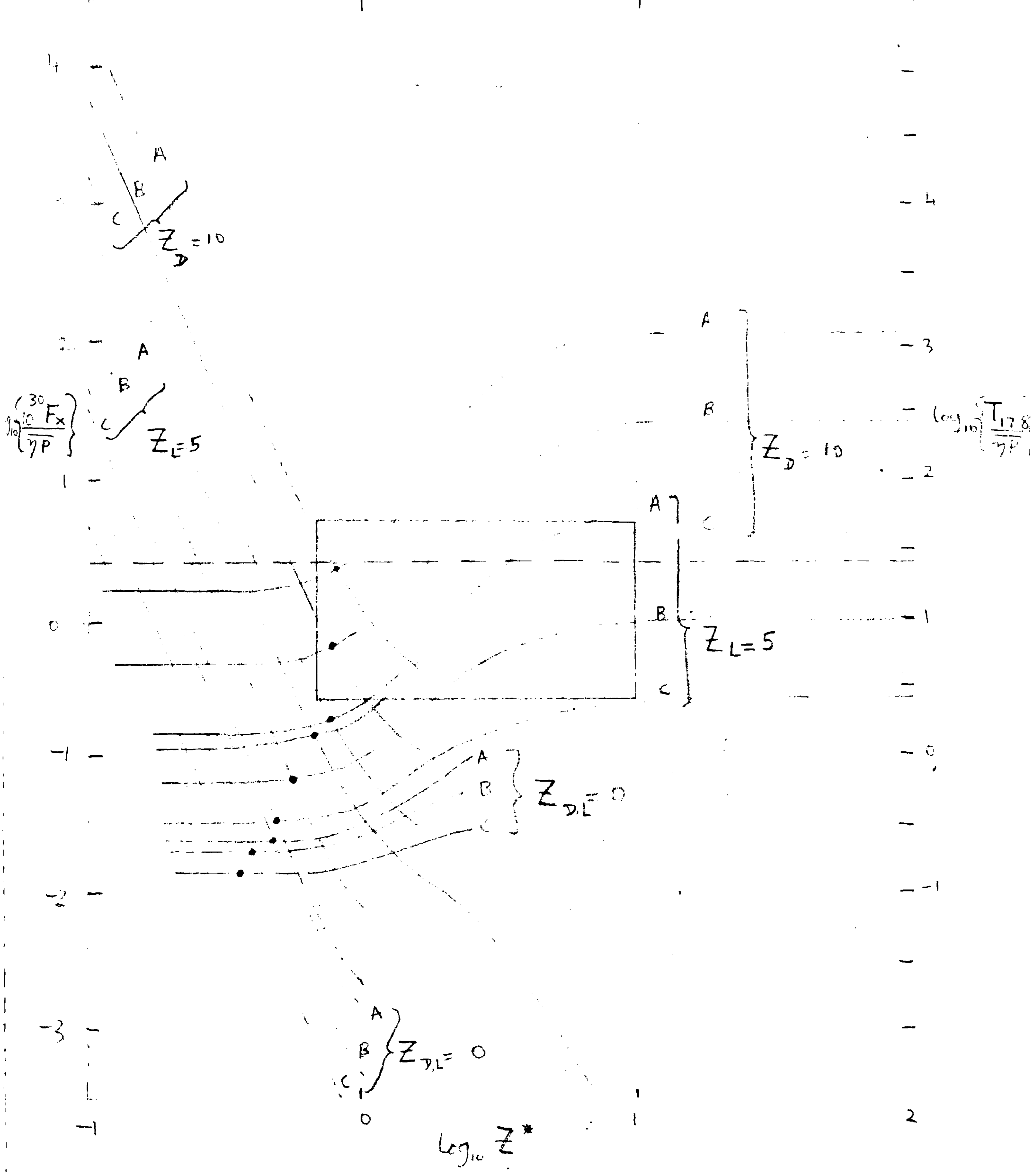

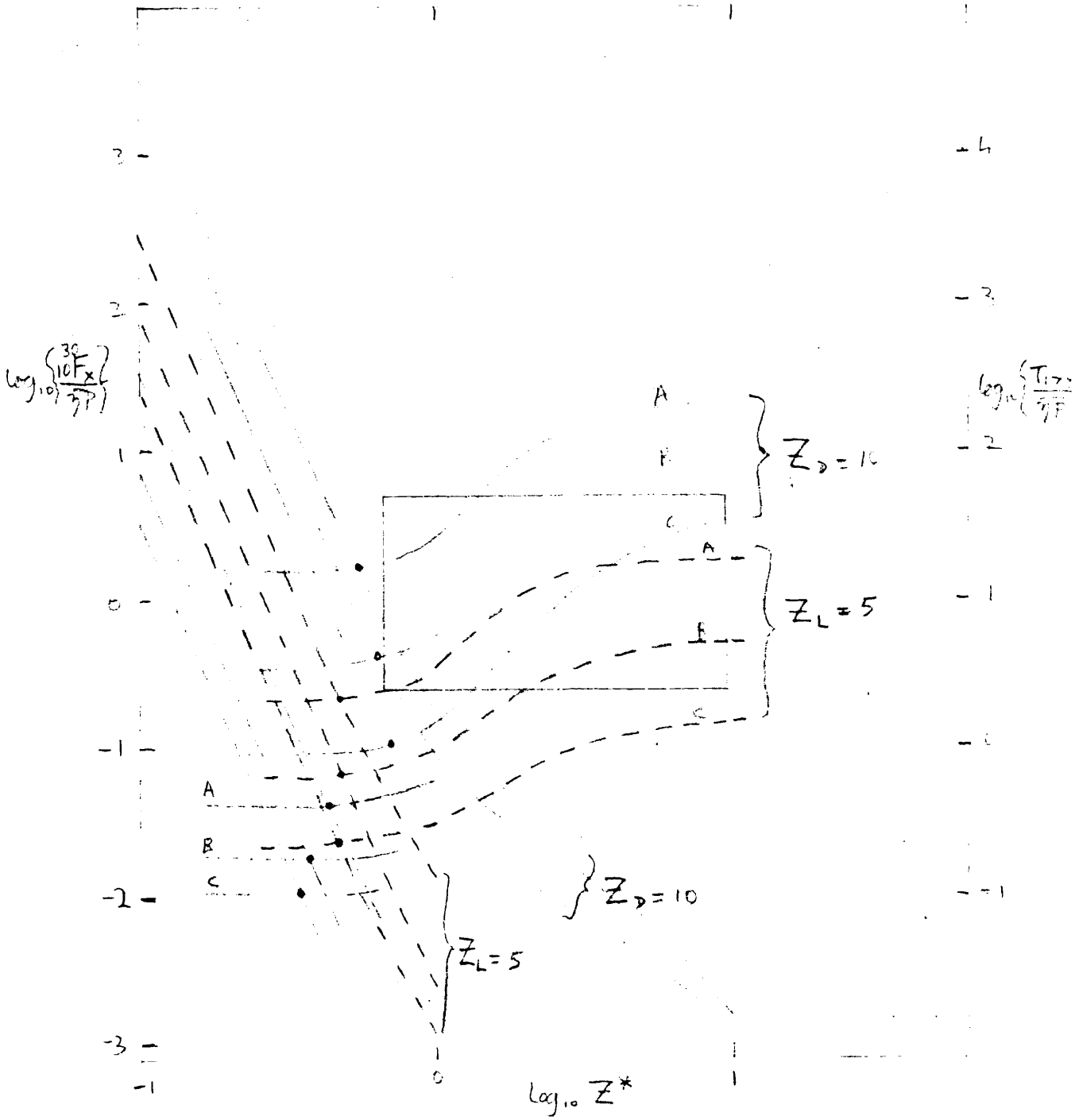
$\log_{10}\left\{\frac{3\sigma}{16F_x}\right\}$
$\log_{10}\left\{\frac{T_{12}}{\gamma F}\right\}$
$Z_D = 10$
$Z_L = 5$
$Z_D = 10$
$Z_L = 5$
A
B
C
$\log_{10} Z^*$

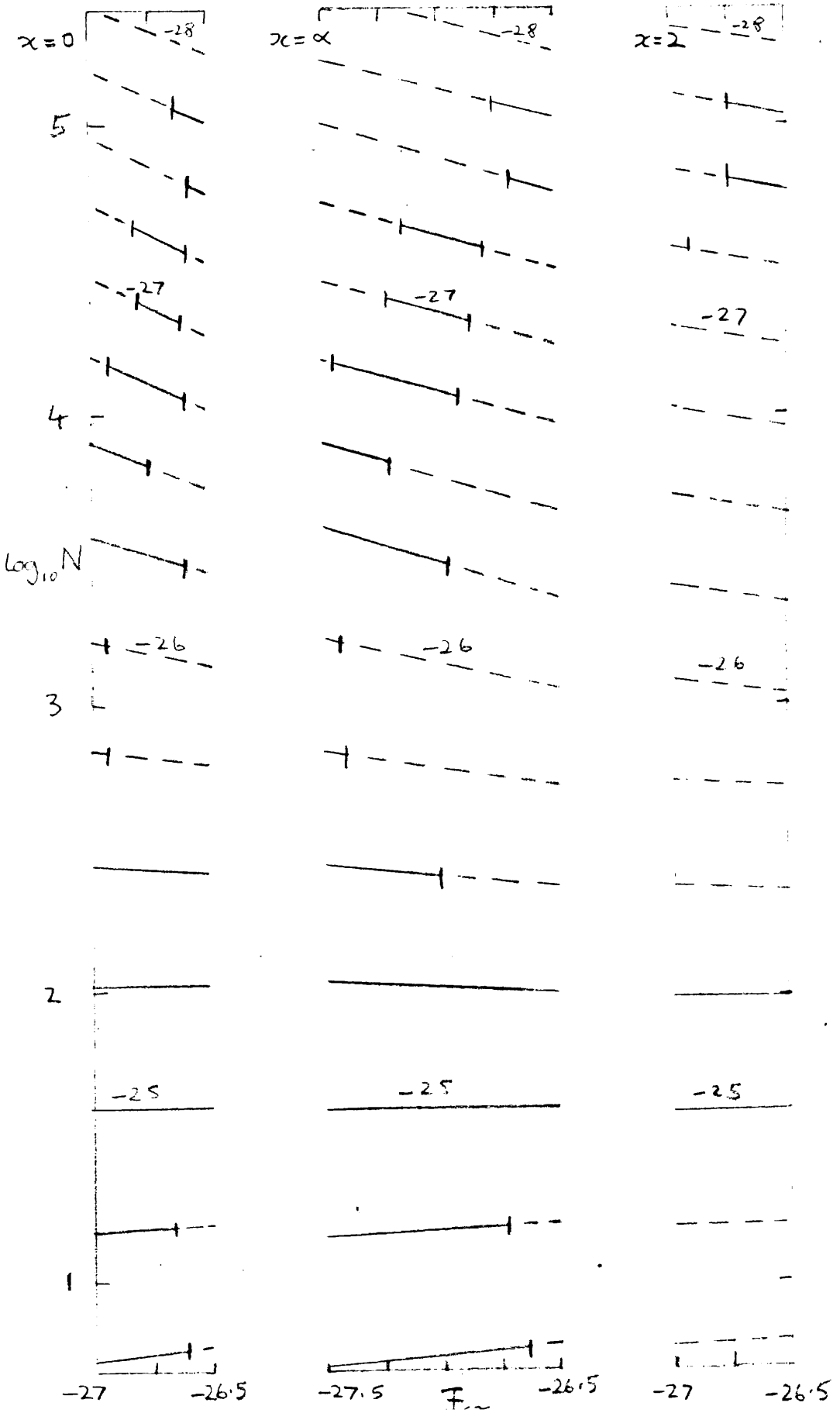
x = 0
x = α
x = 2
-28
-27
-26
-25
5
4
3
2
1
log10 N
-27
-26·5
-27·5
-26·5
-27
-26·5

Fig 24 T_{178} and F_X as a function of ζ_{min}, [illegible]

exponential density evolution, $z_0 = 10$, [illegible] $P \propto P^{-\alpha}$.

(contribution from $\zeta \geqslant \zeta_{min}$ only)

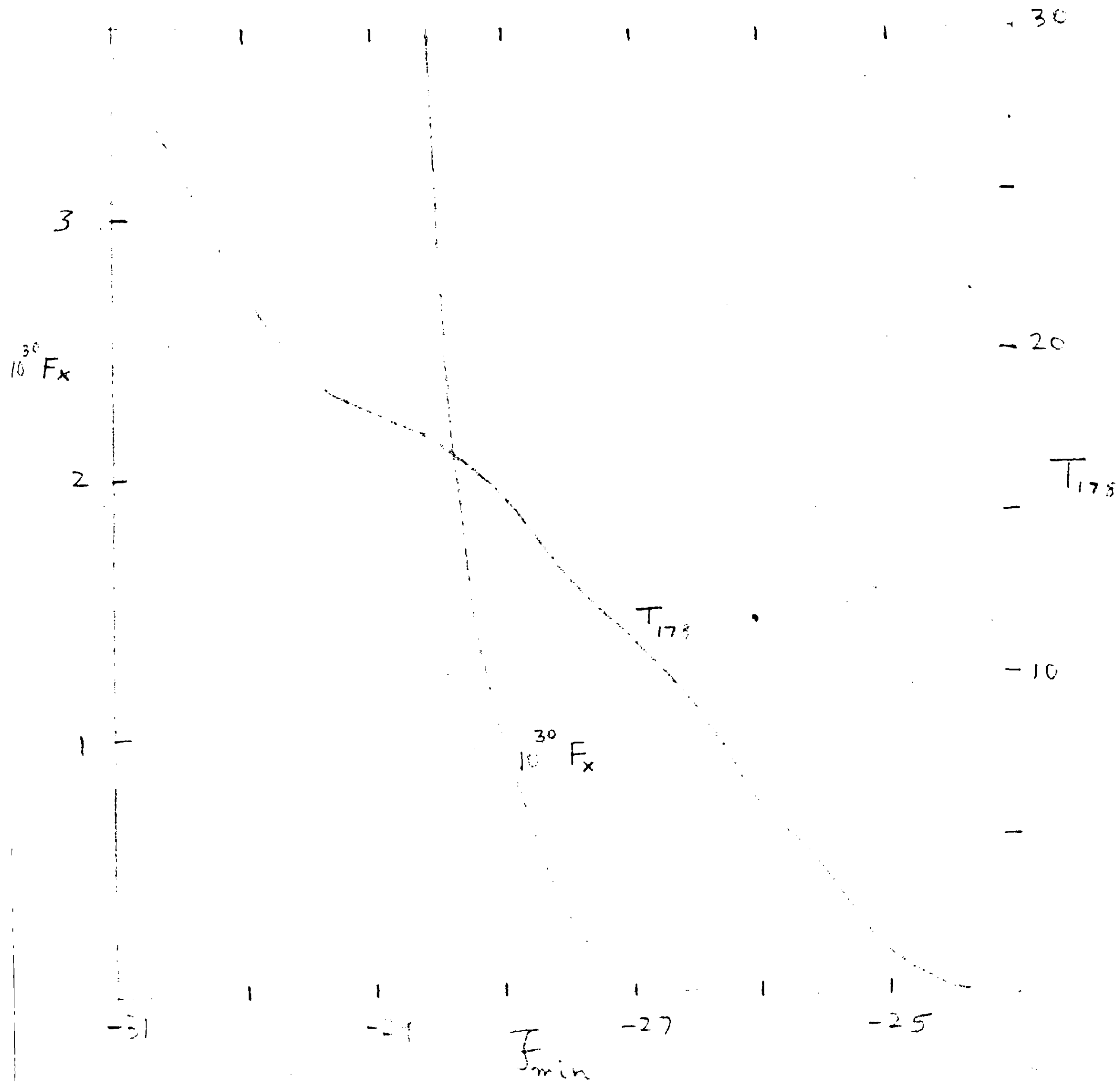

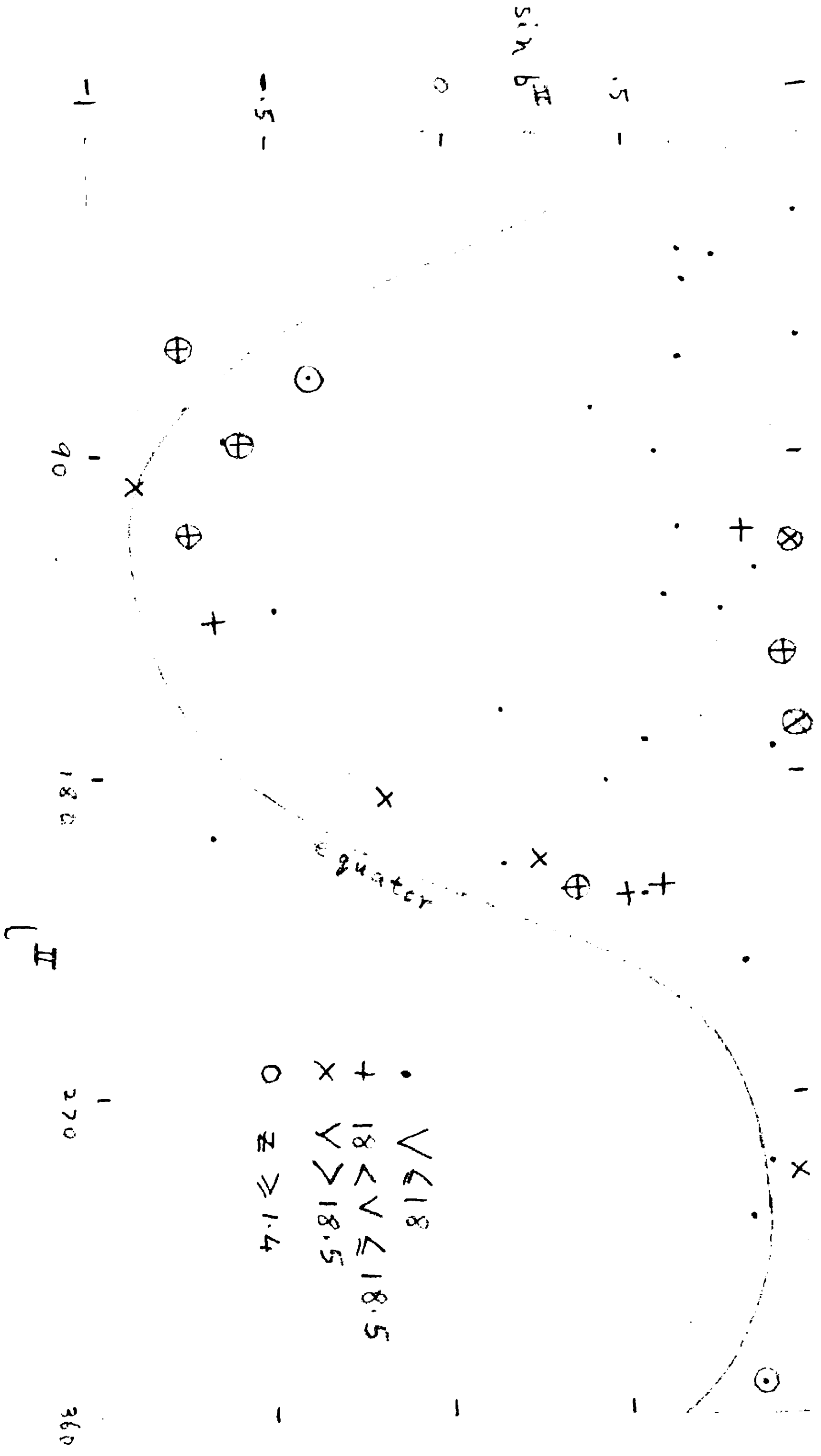
sin b^{II}
1
.5
0
-.5
-1
90
180
270
360
l^{II}
equator
• V ≤ 18
+ 18 < V ≤ 18.5
× V > 18.5
○ z ≥ 1.4

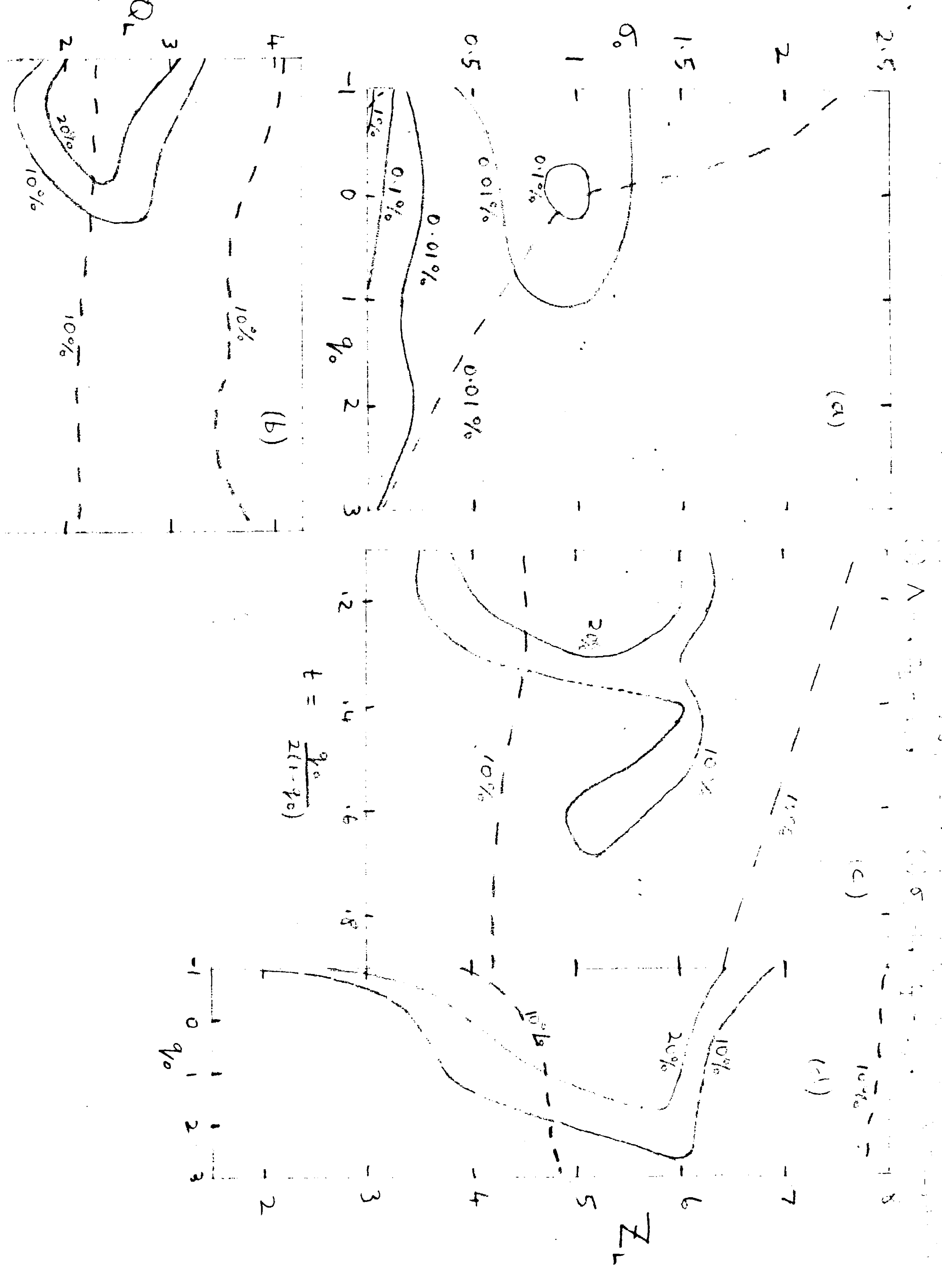
(a)
(b)
(c)
(d)
Q_L
Z_L
q_0
20%
10%
0.1%
0.01%

Fig 37 [illegible] 178 MHz [illegible] > [illegible] M and S model with exponential luminosity evolution, $Z_L=5$, M model with exponential density evolution, $Z_L=10$, and $P \propto B^{1+\alpha}$. (a) all luminosities, (b) $\xi \geq -27$ only.

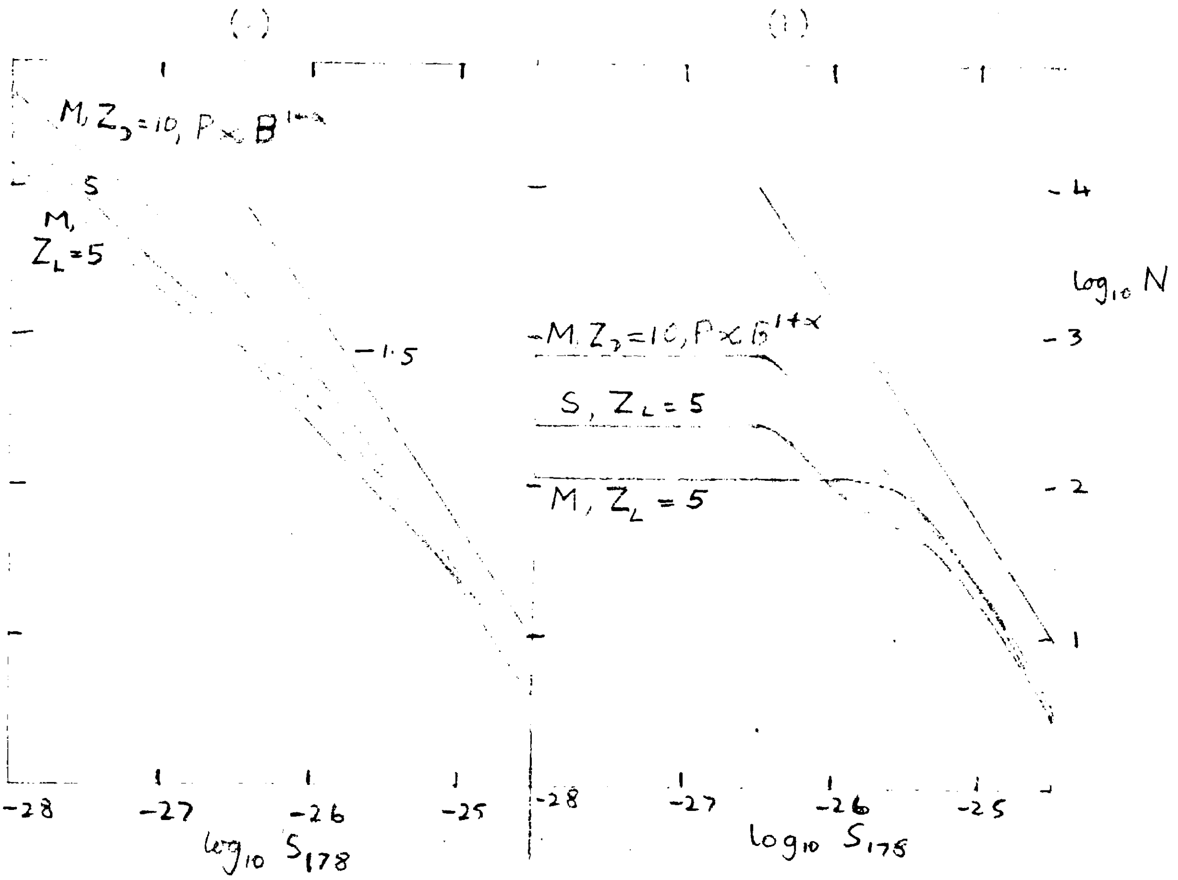

THE DETERMINATION OF THE EVOLUTIONARY PROPERTIES OF QUASARS BY MEANS OF THE LUMINOSITY-VOLUME TEST

M. Rowan-Robinson

REPRINTED FROM

Mon. Not. R. astr. Soc. (1968) **138**, 445–475

PUBLISHED BY

BLACKWELL SCIENTIFIC PUBLICATIONS · OXFORD AND EDINBURGH

PRINTED IN ENGLAND BY

ADLARD AND SON LTD, DORKING

Mon. Not. R. astr. Soc. (1968) **138**, 445–475.

THE DETERMINATION OF THE EVOLUTIONARY PROPERTIES OF QUASARS BY MEANS OF THE LUMINOSITY-VOLUME TEST

*M. Rowan-Robinson**

(Communicated by W. H. McCrea)

(Received 1967 August 3)

Summary

A cosmological test suitable for sources with a large dispersion in luminosity, the luminosity-volume test, is described.

Application to both the optical and radio data for quasars, assuming their redshifts to be cosmological, shows that none of the relativistic models can apply without some evolutionary factor that affects both radio *and* optical properties. Simple evolutionary hypotheses are tested, and it is found that only relatively empty models ($4\pi G\rho_0 \ll H_0^2$) with $-1 \leqslant q_0 \leqslant 0{\cdot}5$ are consistent with power-law luminosity-evolution, whereas all models are consistent with density-evolution. Evolutions with a negative exponential dependence on the scale-factor, which do not require a truncation of the evolving population at finite redshift to give a finite integrated background radiation, represent the data well.

The test should be applicable to radio-galaxies when the data is more complete.

1. *Introduction.* Throughout this work we take the conventional view that the redshifts of quasars are cosmological (**1**). Although we recognize that severe difficulties exist for this view (**2**), (**4**)–(**6**), the other possible explanations that have been presented in detail to date (**8**), (**9**) pose more difficulties than they solve (**10**)–(**12**).

Pessimism has been expressed whether, even if quasars are at cosmological distances, they are of much value to cosmology (**13**), (**14**). The two classical tests, the magnitude–redshift test and the number-counts of sources, are only effective in distinguishing between cosmological models in situations where the dispersion in luminosity is small. While this is the case for the optical luminosities of galaxies, it is certainly not true for the radio-luminosities of radio-galaxies, or for either the optical or radio luminosities of quasars (we shall drop the qualification ' if the redshifts of quasars are cosmological ' in the remainder of this paper). We aim to show that this pessimism is unjustified, since the additional factor of completeness down to a limiting flux-level enables a far more powerful test, the ' luminosity-volume ' test, to be applied. This test combines the essential features of both the redshift–magnitude and number-count tests, and uses more information than either. A simple extension enables evolutionary hypotheses to be tested.

Radio number-counts of *all* sources provide clear evidence that evolutionary factors are affecting at least a sub-population of the sources (**15**)–(**18**). Two kinds of evolution have been considered in some detail in earlier interpretations of the radio number-counts (**18**)–(**20**):

* Present address: Department of Mathematics, Queen Mary College, London E.1.

(a) *Density evolution.* The fraction of material in the form of active sources is a function of epoch.

(b) *Radio luminosity evolution.* The typical luminosity of sources is a function of epoch, while the fraction of material in the form of active sources and the form of the dispersion of luminosities are independent of epoch.

Longair (**18**) has shown that to obtain consistency with number-counts to low flux-levels and the extragalactic contribution to the integrated background radio emission *all* classes of source can not be supposed to evolve. If the evolution is then due to an *indistinguishable* sub-population of the sources, the distinction between hypotheses (a) and (b) disappears (**18**). However if the evolution takes place in a recognizable sub-population (e.g. the quasars) then we are dealing with distinct hypotheses and can hope to test between them. Earlier suggestions that the magnitude–redshift diagram for quasars supported luminosity rather than density evolution (**22**), (**23**) were shown to be incorrect (**24**). The present results are still stronger: luminosity evolution of the form considered in (**18**)–(**20**), (**22**), (**23**) is inconsistent with a wide range of cosmological models, whereas consistency with all models can be obtained using density evolution.

However, it is important to consider whether results obtained using a particular mathematically simple form of evolution may not depend rather strongly on that mathematical form. The truncation of the evolving population beyond a redshift of about four (**18**) may fall in this category. In this paper we consider other forms of evolution which do not require such a truncation. It is a matter for subsequent investigation to decide whether such forms of evolution could give consistency with radio number-counts to low flux-levels and with the integrated extragalactic background.

The cosmological models we have tested are the familiar relativistic models. We include the possibility of a non-zero cosmological constant Λ: purists who dislike the cosmological constant may simply examine our results for $\Lambda = 0$.

In Section 12 we also describe the results of testing the steady-state cosmology and a class of Brans–Dicke models.

2. *The models*

(i) *Summary of properties.* The properties of the relativistic cosmological models are discussed in many standard references, e.g. (**25**)–(**27**), but for completeness we summarize here the relations we need.

The observed flux in the frequency range ν_0 to $\nu_0+d\nu_0$, from a source emitting $F(\nu_e)d\nu_e$ in the corresponding range of emitted frequency ν_e to $\nu_e+d\nu_e$, is given by

$$f(\nu_0)d\nu_0 = \frac{F(\nu_e)d\nu_e(1+kr_0^2/4)^2}{R_0^2 r_0^2 Z^2} \tag{1}$$

where

$$\frac{\nu_0}{\nu_e} = 1+z = Z$$

and

$$\int_{t_e}^{t_0} \frac{dt}{R} = \int_0^{r_0} \frac{dr}{1+kr^2/4} \tag{2}$$

Writing $\mathscr{F} = \log_{10} F(\nu_0)$, $\mathscr{f} = \log_{10} f(\nu_0)$, equation (1) becomes

$$\mathscr{F} = \mathscr{f} + \log_{10} \frac{R_0^2 r_0^2 Z^2}{(1+kr_0^2/4)^2} - 0{\cdot}4\,K \tag{3}$$

where the K-correction takes account of the selectivity of the atmosphere and the apparatus, and of the shift of the spectrum across the observed frequency band. The forms we have used for optical and radio K-corrections are presented in Appendix I.

From Einstein's equations for uniform, pressure-free universes, the scale-factor $R(t)$ satisfies the equations

$$\ddot{R} = -4\pi G\rho R/3 + \Lambda R/3 \tag{4}$$

$$(\dot{R})^2 = 8\pi G\rho R^2/3 + \Lambda R^2/3 - kc^2 \tag{5}$$

where Λ is the cosmological constant and the density, ρ, satisfies the equation

$$\rho R^3 = \rho_0 R_0{}^3,$$

subscripts zero referring to the present epoch.

Then if we write

$$\mathrm{H} = \dot{R}/R, \qquad q = -\ddot{R}R/\dot{R}^2, \tag{6}$$

and

$$\sigma = 4\pi G\rho/3\mathrm{H}^2, \tag{7}$$

equations (4) and (5) become

$$\Lambda/3 = (\sigma - q)\mathrm{H}^2 = (\sigma_0 - q_0)\mathrm{H}_0{}^2 \tag{8}$$

and

$$\begin{aligned} kc^2 &= (3\sigma - q - 1)\mathrm{H}^2R^2 \\ &= (3\sigma_0 - q_0 - 1)\mathrm{H}_0{}^2R_0{}^2. \end{aligned} \tag{9}$$

(ii) *Flow diagram for the models.* Writing $Z = R_0/R$, we can use equations (5) (8), (9) to obtain

$$\begin{aligned} \mathrm{H}^2(t) &= \mathrm{H}_0{}^2\{\sigma_0 - q_0 + (1 + q_0 - 3\sigma_0)Z^2 + 2\sigma_0 Z^3\} = \mathrm{H}_0{}^2 . Y(Z) \\ \sigma(t) &= \sigma_0 Z^3/Y(Z) \\ q(t) &= \{\sigma_0(Z^3 - 1) + q_0\}/Y(Z). \end{aligned}$$

Thus if H_0, σ_0, q_0 are known at the present epoch, then H, σ, q are known for all epochs, past and future. The behaviour of the models can be illustrated by a flow diagram (Fig. 1). This diagram, and an illuminating discussion of the σ–q representation, can be found in Refsdal & Stabell (**28**). For our purposes the interesting feature to note is that there are just three fixed points in this diagram: the Einstein–de Sitter model ($\sigma = q = 1/2$), the de Sitter model ($\sigma = 0$, $q = -1$), and the Milne model ($\sigma = q = 0$). These represent asymptotic states of the Universe: the Einstein–de Sitter model is the initial state of all non-empty models except those to the left of the curve A, while the Milne and de Sitter models are the final states of monotonic expanding models (all those to the left of the curve B) with $\Lambda = 0$ and $\Lambda \neq 0$, respectively. Oscillating models are those to the right of the curve B. A and B correspond to those models which approach the Einstein static universe as $t \to \pm\infty$ respectively (i.e. A is the Eddington–Lemaitre model).

The loci to the left of the curve A correspond to those models which ' bounce ' under the action of cosmological repulsion. As Solheim (**29**) has remarked, most of these models are ruled out if the redshifts of quasars are cosmological, since they give upper limits to Z which are inconsistent with values already obtained for

quasars. In fact for these models to be correct we must be indistinguishably close to the de Sitter model at the present epoch. Their philosophical attraction is that they are the only non-empty models which do not possess a singularity.

From the point of view of the testing of models, the most interesting situations arise if (σ_0, q_0) are *not* near any of the three fixed points. For then we know the future of the Universe and its past history (at least back to the epoch where the pressure becomes significant). But if (σ_0, q_0) are near to one of the fixed points in the σ–q plane, we cannot tell whether the Universe has always had these values of σ and q, or whether it is in an asymptotic state.

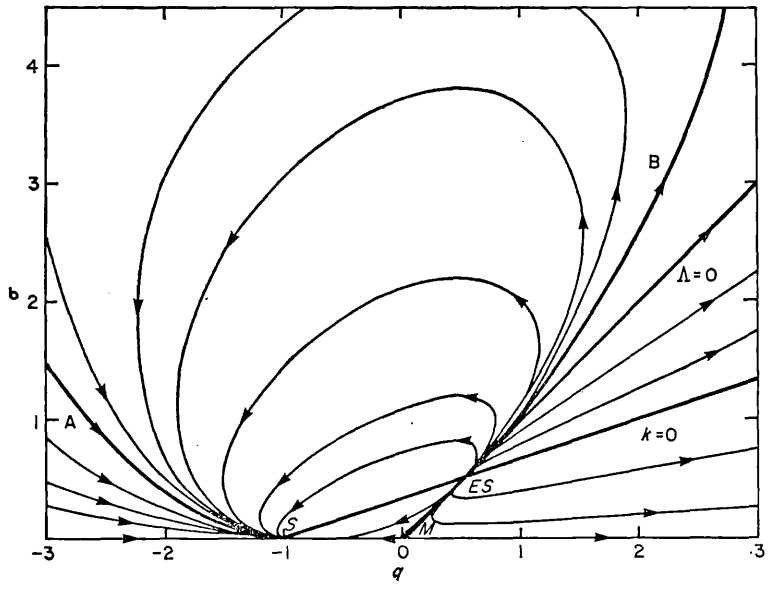

FIG. 1. *Flow diagram for the models. Loci to the right of B are oscillating models; those to the left of A have 'bounced' under the action of cosmological repulsion; those between A and B are monotonic expanding models. The three fixed points are the Einstein–de Sitter (ES), Milne (M), and de Sitter (S) models. The directions indicated by the arrows correspond to expansion of the Universe.*

The smoothed-out density of the material actually observed to date (7×10^{-31} g cm^{-3}) (**30**), and the present value of the Hubble constant ($H_0^{-1} = 1{\cdot}2 \times 10^{10}$ years), suggest that our present position in the σ–q plane may be rather close to the $\sigma = 0$ axis. Difficulties in reconciling the ages of the oldest stars with the age of the Universe may force us to the left of the point M and perhaps rather near to the point S. But considerations of this kind are subject to enormous uncertainty.

3. *Influence of volume effect on magnitude–redshift test*

(i) *Magnitude–redshift test.* The results of attempts to distinguish between these models using the magnitude–redshift test for the brightest galaxies in clusters have been reviewed and extended by Solheim (**29**), who has computed exact theoretical relations instead of the power-series expansions used in earlier work (**31**), (**32**). His best values for the cosmological parameters are

$$q_0 = -0{\cdot}06, \qquad \sigma_0 = 4{\cdot}53,$$

though these values are appreciably modified if the galaxies are assumed to change their luminosity with epoch (29), (33).

The acceptable models appear as a region of the $\sigma_0 - q_0$ plane (the 'model' diagram). He also applies this procedure to optical data for fifteen quasars. However it is necessary to take account of the severe selection effect imposed by the limiting radio magnitude for these objects (nine flux-units if we confine our attention to identifications from the 3C catalogue (37), (38)), and also of the 'volume effect' discussed below. In the present work we have rather more data available (37 redshifts), we take account of these selection effects, and we also perform the test in a different and more powerful way.

A number of other authors have discussed the observational data for quasars with respect to particular cosmological models. McCrea (34) plotted the absolute optical magnitudes of quasars against redshift for three models: the Milne model ($\sigma_0 = q_0 = 0$), the de Sitter model ($\sigma_0 = 0$, $q_0 = -1$; the steady-state model gives the same diagram), and a particular model used by Schmidt for which $\sigma_0 = q_0 = 1$. McCrea pointed out that the luminosity, $F_1(z)$ say, of the most luminous source out to redshift z should be an increasing function of z, simply as a probability effect. The Schmidt model then seemed to be rendered improbable by the fact that the nearest quasars, 3C273, would be intrinsically the most luminous, in this model. The rate of increase of $F_1(z)$ appeared improbably steep in the steady-state model, on the other hand.

(ii) *The volume effect.* Some quantitative estimate of the importance of the effect may be made as follows. We assume that the proper number-density of quasars at any epoch, $\zeta(t)$, is proportional to the smoothed-out cosmological density, $\rho(t)$, and that the luminosity-function (18) for quasars is independent of epoch. That is, at epoch t let the number of sources per unit proper volume having $\log_{10} F$ in the range

$$\mathscr{F} \text{ to } \mathscr{F} + d\mathscr{F} \text{ be } \zeta(t).\phi(\mathscr{F})d\mathscr{F}$$

where

$$\int_{-\infty}^{+\infty} \phi(\mathscr{F})d\mathscr{F} = 1.$$

Define the coordinate number-density,

$$\eta(t) = \zeta(t).\frac{R^3(t)}{R_0{}^3}:$$

thus if $\zeta(t) \propto \rho(t)$, then $\eta(t) = \text{const} = \eta(t_0) = \eta_0$, say. The element of proper volume is

$$\frac{R^3(t)\, r^2\, dr \sin\theta\, d\theta\, d\phi}{(1 + k\, r^2/4)^3}$$

so the total number of sources in the range of luminosity $\mathscr{F}$ to $\mathscr{F} + d\mathscr{F}$ out to redshift z is

$$N(\mathscr{F}, z)d\mathscr{F} = \eta_0 R_0{}^3.V(z).\phi(\mathscr{F})d\mathscr{F}$$

where

$$V(z) = \int_0^{r_0(z)} \frac{4\pi r^3\, dr}{(1 + k\, r^2/4)^3}$$

Then the expected luminosity, $F_N(z)$, of the Nth most luminous source out to

redshift z will be roughly the solution of the equation

$$\eta_0 R_0^3 . V(z) . y \int_{\mathscr{F}_N(z)}^{\infty} \phi(\mathscr{F})\, d\mathscr{F} = N,$$

where $\mathscr{F}_N(z) = \log_{10} F_N(z)$, and y is the fraction of the sky covered by the sources.

Let

$$\Phi(x) = \int_{-\infty}^{\infty} \phi(\mathscr{F})\, d\mathscr{F}$$

Then

$$\mathscr{F}_N(z) = \Phi^{-1}\left\{1 - \frac{N}{\eta_0 R_0^3 . V(z) . y}\right\},$$

where

$$\Phi^{-1}\{\Phi(x)\} = x. \tag{10}$$

For example if (a)

$$\phi(\mathscr{F}) = \frac{1}{\sqrt{2\pi}a} . \exp\{-(\mathscr{F}-\mathscr{F}_0)^2/2a^2\}$$

Then

$$\mathscr{F}_N(z) = \mathscr{F}_0 + a\ \mathrm{erf}^{-1}\left\{1 - \frac{N}{\eta_0 R_0^3\, V(z) y}\right\}$$

and if (b)

$$\phi(\mathscr{F}) = b\ (\log_e 10)\ 10^{-b(\mathscr{F}-\mathscr{F}_1)} \quad \text{for } \mathscr{F} \geqslant \mathscr{F}_1$$
$$\text{for } \mathscr{F} < \mathscr{F}_1$$

then

$$\Phi(\mathscr{F}) = 1 - 10^{-b(\mathscr{F}-\mathscr{F}_1)},$$

and

$$\mathscr{F}_N(z) = \mathscr{F}_1 + \frac{1}{b} \log_{10}\left\{\frac{R_0^3 y \eta_0 V(z)}{N}\right\}$$

$$= \text{const.} + \frac{1}{b} \log_{10} V(z).$$

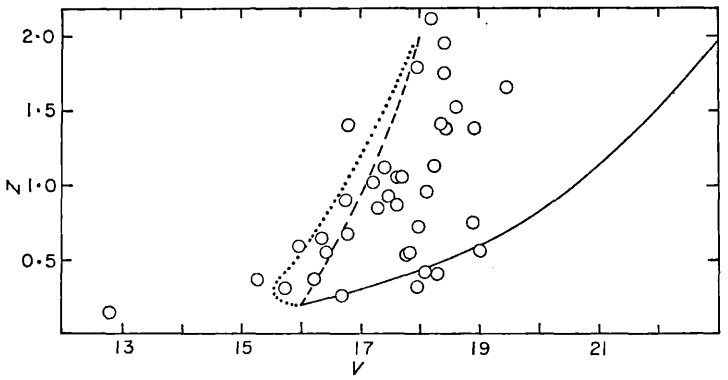

FIG. 2. *Magnitude (V)–redshift (z) diagram for quasars showing 'volume effect'. The continuous line is the theoretical magnitude–redshift curve for the de Sitter model. The other two curves show the* shapes *of the predicted loci of brightest sources in this model for simple luminosity functions: dotted curve, Gaussian with dispersion of two magnitudes; broken curve, exponential dependence on luminosity, $F(vv)$, with index $-1{\cdot}5$ (to base 10). These forms are chosen only to give a similar shape to the upper envelope for the observational points (circles), and are not necessarily consistent with the data.*

Some idea of the importance of the volume effect for the optical redshift–magnitude diagram for quasars may be gained from Fig. 2, which shows $F_1(z)$ for two simple luminosity functions of type (a) and (b), in the de Sitter model. The parameters chosen are $a = 0{\cdot}8$, $b = 1{\cdot}5$, $4\pi\eta_0 y = 10^{-3}$ per $(c/H_0)^3$.

We are not claiming that the optical luminosity function for quasars is actually of either of these forms, but merely demonstrating how severe the effect of a large dispersion in luminosity can be. Clearly a large part of the divergence of the data from the normal de Sitter m–z curve could be ascribed to this effect, so that analysis of the kind performed by Solheim (**29**) is unlikely to give accurate results for quasars. However if from counts and from identifications we can obtain information about η_0 and the form of $\phi(\mathscr{F})$, then it is in principle possible to test cosmological models by comparing equation (10) with the observed locus of the Nth most luminous source out to redshift z, for different values of N. In practice this is unsatisfactory, since η_0 and $\phi(\mathscr{F})$ cannot be at all accurately determined. The test we shall describe in section takes full account of the volume effect, but does not require knowledge of η_0 or $\phi(\mathscr{F})$.

McVittie & Stabell (**35**) have also considered plots of the optical luminosity of quasars against redshift in several models and argue that although evolution would be necessary in models with $q_0 = \sigma_0 = 0$ and $q_0 = \sigma_0 = 1$, this is not the case for the model $q_0 = 1$, $\sigma_0 = 3$, for example. In Section 5 we show that *none* of the relativistic models are consistent with the present data for quasars, without some kind of evolutionary factors.

McVittie & Stabell (**35**), and Kafka (**14**) have allowed for the volume effect in a rather different manner from that described above. Confining their attention to a fixed range of optical luminosity they compare the number of sources out to redshift z with $V(z)$. This is equivalent to the 'luminosity-volume' test we describe in the next section, but is limited in two ways. Firstly it does not take account of the serious selection effect imposed by the 3C limiting flux-level.* And secondly it uses the available information in such an inefficient way that, as Kafka admits, no conclusions of real statistical significance can be drawn with the present data.

Rees & Sciama (**36**) showed that in different ranges of radio luminosity in the steady-state model there was an excess of quasars at large redshift. The inconsistency is even more striking when correction is made for the effect of optical selection, and when the optical luminosities are also considered.

4. *Luminosity-volume test.* The central suggestion of this paper is that for quasars the magnitude–redshift test be replaced by the 'luminosity-volume' test. Suppose that (i) the number of quasars per unit proper volume, $\zeta(t)$, is proportional to the smoothed-out cosmical density at that epoch; (ii) the distribution of luminosities of quasars (i.e. the form of $\phi(\mathscr{F})$) is the same at all epochs.

Then the total number of sources out to the epoch corresponding to redshift z is

$$N(z) = \int_{-\infty}^{+\infty} N(\mathscr{F}, z)d\mathscr{F} = \eta_0 R_0{}^3 . V(z) \qquad (11)$$

$V(z)$ is the comoving coordinate volume of the sphere bounded by sources whose light is redshifted by z.

* In more recent work Kafka (**54**) now takes account of the selection effect but still does not combine the information in an efficient enough way to obtain significant results.

Then in any particular model that we wish to test we consider the distribution of luminosity $\mathscr{L}$ (see equation (3)) with respect to volume U: that is, we transform the magnitude–redshift diagram to a luminosity-volume diagram. If assumptions (i) and (ii) hold, we should expect to find, in any given range of luminosity, equal numbers of sources in any two equal volumes of comoving coordinate space. However as a result of the limitations of our telescopes, not all quasars are visible. Confining our attention to 3C quasars, only those brighter than the limiting flux-level are visible. An optical identification can then only be made if the quasars is brighter than the limiting optical magnitude. Moreover the degree of complete-

TABLE I

3C	z	f_{rad}	V	K_v	$V+K_v$	α
273	0·158	−24·14	12·80	−0·64	12·16	0·35
323·1	0·260	−25·02	16·69	−0·45	16·24	0·64
249·1	0·311	−24·91	15·72	−0·36	15·36	0·87
277·1	0·320	−24·89	17·93	−0·35	17·58	0·92
48	0·367	−24·30	16·20	−0·28	15·92	0·50
351	0·371	−24·93	15·28	−0·27	15·01	0·60
215	0·411	−24·97	18·27	−0·22	18·05	1·00
47	0·425	−24·67	18·10	−0·21	17·89	0·89 (K)
279	0·536	−24·70 (3C)	17·75	−0·13	17·62	0·54 (K)
147	0·545	−24·21	17·80	−0·12	17·68	0·45
334	0·555	−24·97	16·41	−0·12	16·29	0·78 (K)
275·1	0·557	−24·77	19·00	−0·12	18·88	0·88
345	0·594	−24·97	15·96	−0·10	15·86	0·24 (K)
263	0·652	−24·86	16·32	−0·06	16·26	0·88
380	0·691	−24·21	16·81	−0·04	16·77	0·77 (K)
254	0·734	−24·69	17·98	−0·02	17·96	0·93 (K)
138	0·754	−24·70	18·84	0·00	18·84	0·38 (K)
286	0·846	−24·65	17·30	+0·02	17·32	0·15
196	0·872	−24·20	17·60	+0·02	17·62	0·70
309·1	0·903	−24·74	16·78	+0·02	16·80	0·45 (K)
336	0·927	−24·84	17·47	+0·02	17·49	0·87
288·1	0·960	−24·99	18·12	+0·01	18·13	0·93
245	1·029	−24·99	17·25	0·00	17·25	0·61 (K)
287	1·054	−24·82	17·67	−0·01	17·66	0·48 (K)
186	1·063	−24·84	17·60	−0·01	17·59	1·18
204	1·112	−24·99	18·21	−0·02	18·19	1·05
208	1·112	−24·77	17·42	−0·02	17·40	0·98 (K)
181	1·382	−24·86	18·92	−0·10	18·82	0·94
268·4	1·400	−25·02	18·42	−0·10	18·32	0·69
446	1·403	−24·74 (3C)	18·39	−0·10	18·29	0·53 (K)
298	1·436	−24·33	16·79	−0·11	16·68	0·98 (K)
270·1	1·519	−24·89	18·61	−0·13	18·48	0·69
280·1	1·659	−24·83	19·44	−0·15	19·29	1·09
454	1·756	−25·02	18·40	−0·14	18·26	0·73
432	1·804	−24·91	17·96	−0·14	17·82	1·04
191	1·946	−24·95	18·40	−0·12	18·28	0·98 (K)
9	2·012	−24·77	18·21	−0·09	18·12	1·02

Notes: (i) Redshifts and optical magnitudes from Refs (7), (41) and (42).
(ii) Radio fluxes from 3CR (38), except those marked (3C), which are from 3C (37).
(iii) K_v taken from Sandage (52).
(iv) Sources classified by Kellerman (50) as having straight spectra marked (K). The rest calculated as in Appendix I.

ness of the identifications may be different in different ranges of magnitude, an effect which could be reinforced by non-random selection of objects for redshift measurements. However, although such effects may well be present, it is not necessary that the set of quasars with known redshift at our disposal be complete, but only that it be representative down to the limiting flux-levels. Throughout this work we assume that the set of 37 quasars listed in Table I are representative down to the 3C limiting flux-level of nine flux-units, and down to the 18th visual magnitude.

Penston & Rowan-Robinson (3) have suggested that the 3C quasars with visual magnitudes fainter than 18 are not distributed isotropically on the sky. Preferring to suppose that this is some effect of observational selection that the Universe is inhomogeneous on the large scale (39), we shall make a correction for this effect at a later stage. For the moment we treat our set of quasars as if it were representative down to the 19th magnitude, which, since there are only two quasars with $V > 19$ in our set, we shall regard as the limiting magnitude for quasars.

Fig. 3 shows optical and radio luminosity-volume diagrams for a particular cosmological model (the Einstein–de Sitter model). The cutoffs imposed by the limiting flux-levels are calculated by eliminating z between

$$\hat{\mathscr{F}} = \hat{f} + \log_{10} \frac{R_0^2 r_0^2 (1+z)^2}{(1+k r^2/4)^2} - 0{\cdot}4\, K(z) \tag{12}$$

and

$$\hat{V} = V(z) \tag{13}$$

where $\hat{f}$ is the limiting flux-level and K the appropriate K-correction (see Appendix I: the radio cut-off is shown for sources with spectral index $\alpha = 0{\cdot}8$).

Clearly, a source with luminosity $\mathscr{F}$ and redshift z will only be observable if $V(z) \leqslant \hat{V}(\mathscr{F})$. A difficulty here is that in the radio case, $\hat{V}(\mathscr{F})$ is different for sources with different spectral indices. But the error introduced by taking the radio cutoff to be that appropriate to sources with the mean spectral index (about 0·8) is not very great: a few sources with steep spectra might be missed.

The vertical lines to the right of the two diagrams correspond to a redshift of 2·2, beyond which no quasar has yet been observed. Thus in the radio diagram the line $A_1A_2A_3$ bounds the observable region of the luminosity-volume plane. If we define the line $B_1B_2B_3$ by the relations

$$V = V(2{\cdot}2)/2 \text{ for } \mathscr{F} \geqslant \hat{\mathscr{F}}(2{\cdot}2)$$

and

$$V = \hat{V}(\mathscr{F})/2 \quad \text{for } \mathscr{F} < \mathscr{F}(2{\cdot}2),$$

then $B_1B_2B_3$ divides $A_1A_2A_3$ into two regions in which, under assumptions (i) and (ii), we should expect to find equal numbers of sources.

Before we compare the numbers of quasars actually found in such equivalent regions, we have to allow for the fact that the set of quasars in $A_1A_2A_3$ is affected by optical selection. Sources which are intrinsically faint optically can only be found at small redshifts on account of the *optical* cutoff. Similarly the optical diagram is affected by radio selection, since sources intrinsically faint radio-wise can only be found at small redshifts on account of the *radio* cutoff.

For a set of sources free from optical selection out to redshift z_1 we should

confine our attention to sources with $\mathscr{F}_{\rm opt} \geqslant \hat{\mathscr{F}}_{\rm opt}(z_1)$. For $z_1 = 2{\cdot}2$ this would be very restrictive, but we can relax this requirement considerably without much loss of accuracy. In Fig. 3(b) we show $\mathscr{F}_{\rm opt} = \hat{\mathscr{F}}_{\rm opt}(1{\cdot}4)$, for example (the broken line). Optical selection operates against sources falling in the shaded region in

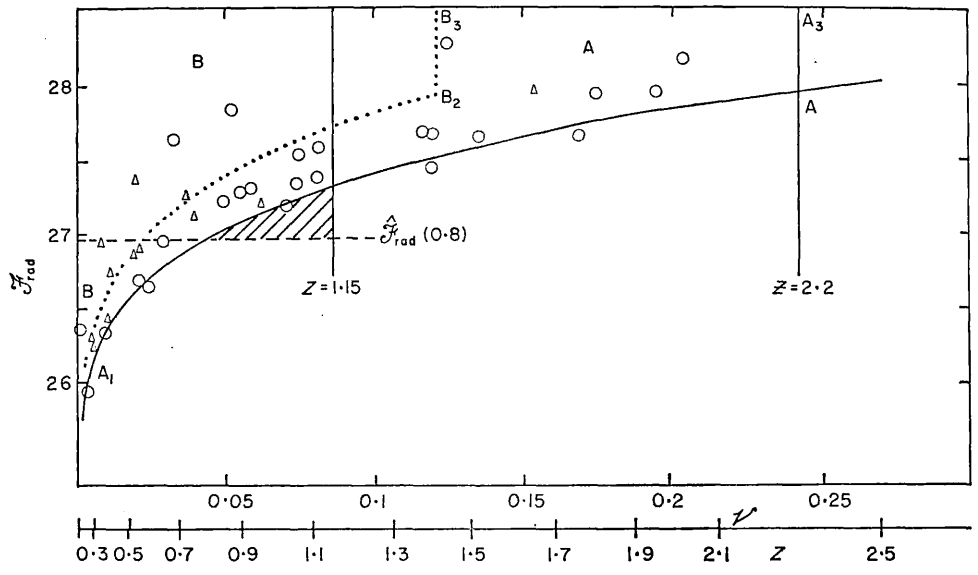

(a)

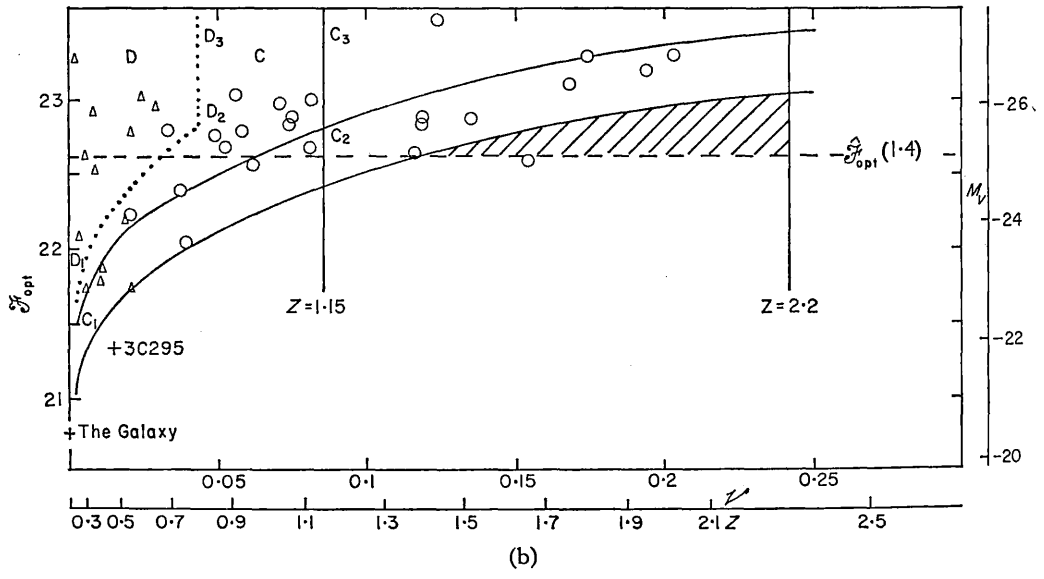

(b)

FIG. 3. *Radio* (a) *and optical* (b) *' luminosity-volume ' diagrams for quasars in the Einstein–de Sitter model.* A_1A_2 *corresponds to the* 3*C cutoff of nine flux-units,* C_1C_2 *to a visual magnitude of* 18. *In* (a) *circles/triangles are those quasars with* $\mathscr{F}_{\rm opt} \gtrless \hat{\mathscr{F}}_{\rm opt}(0{\cdot}8)$ *respectively: in* (b) *circles/triangles are those quasars with* $\mathscr{F}_{\rm rad} \gtrless \hat{\mathscr{F}}_{\rm rad}(1{\cdot}4)$. *Units of* $\mathscr{F}$ *are* $\log_{10}$ *watts/ster/(c/s).*

Fig. 3(b), since they would have $V > 19$. It seems unlikely that very many sources are 'missing': moreover these would all fall in the farther of the two regions of space described above. Since it transpires that there are significantly more quasars in this further region for all the relativistic cosmologies, our conclusions are merely reinforced.

Similarly, for a set of quasars free from radio selection out to z_2 we should confine our attention to sources with $\mathscr{F}_{\text{rad}} \geqslant \mathscr{F}_{\text{rad}}(z_2)$. In view of the probable incompleteness of the identifications for $18 < V \leqslant 19$, we shall apply the optical luminosity-volume test to sources with $V \leqslant 18$ only.* Since only two out of our 37 sources have $V \leqslant 18$ and $z > 1{\cdot}15$, presumably due to radio selection, we take $z_2 = 1{\cdot}15$. The line $C_1C_2C_3$ now bounds the region of interest in Fig. 3(b). A set of quasars mainly free from radio selection out to redshift $1{\cdot}15$ can be obtained by demanding $\mathscr{F}_{\text{rad}} \geqslant \mathscr{F}_{\text{rad}}(0{\cdot}8)$: a few sources in the shaded region of Fig. 3(a) would be missed. The point of this procedure is that for the price of a small remaining effect of selection we more than double the number of quasars available for testing. The conclusions have been found to be insensitive to the actual parameters chosen.

Finally, the line $D_1D_2D_3$ in Fig. 3(b) is defined by

$$V = \hat{V}(\mathscr{F})/2 \quad \text{for } \mathscr{F} < \mathscr{F}_{\text{opt}}(1{\cdot}15)$$

and

$$V = V(1{\cdot}15)/2 \text{ for } \mathscr{F} \geqslant \mathscr{F}_{\text{opt}}(1{\cdot}15).$$

Then if n_A, n_B, n_C, n_D are the numbers of quasars found in the regions A, B of Fig. 3(a) and C, D of Fig. 3(b), respectively, we expect $n_A = n_B$, $n_C = n_D$, if hypotheses (i) and (ii) are satisfied. To test whether the numbers obtained are consistent with these expectations, we compare the quantity

$$\frac{(n_A - n_B)^2}{(n_A + n_B)} + \frac{(n_C - n_D)^2}{(n_C + n_D)}$$

with the χ^2 variable with two degrees of freedom. A probability can then be assigned, from this combined radio and optical luminosity-volume test, to the chosen cosmological model under assumptions (i) and (ii).

5. *Relativistic cosmological models without evolutionary effects.* The procedure described above has been applied, with the aid of a computer, to a grid of cosmological models in the range: $-1 \leqslant q_0 \leqslant 3$, $0 \leqslant \sigma_0 \leqslant 3$, which includes most of the region of interest in the $\sigma_0 - q_0$ plane.

Recently Lemaitre's models have been re-advocated (**40**): these lie to the right of but close to curve A in Fig. 1, and have the possibility of an antipole. Whereas $\hat{\mathscr{F}}(z)$ is monotonic increasing for most models, in certain models it can reach a maximum and then start to decrease, eventually tending to zero at the antipole.

* It may seem logically unsatisfactory to take the optical limiting magnitude as 19 when correcting the radio-data for optical selection, and as 18 when performing the optical luminosity-volume test. However in the latter case it is necessary only that we choose some magnitude brighter than or equal to the actual limiting magnitude, so our procedure is certainly consistent if the data is representative in the range $18 < V \leqslant 19$ (though wasteful of information). On the other hand if our set of quasars is incomplete in the range $18 < V \leqslant 19$, then the effect is much severer for the optical luminosity-volume test than for the correction of the radio-data for optical selection, since many of the 'missing' sources would be excluded anyway from the radio test by the condition $\mathscr{F}_{\text{opt}} \geqslant \mathscr{F}_{\text{opt}}(1{\cdot}4)$.

Although these exotic models have to be considered individually and are not immediately amenable to the procedure described in the previous section, it may well be that the range of parameters we have considered includes all the serious possibilities. Actually we have tested models with larger values of σ_0 and q_0, but these give no new results and anyway imply unreasonable values for the average density of the Universe and the total age of the Universe.

The formulae used are summarized in Appendix II: a detailed discussion can be found in Solheim's paper (**29**). Our results are presented in Fig. 4(a), which

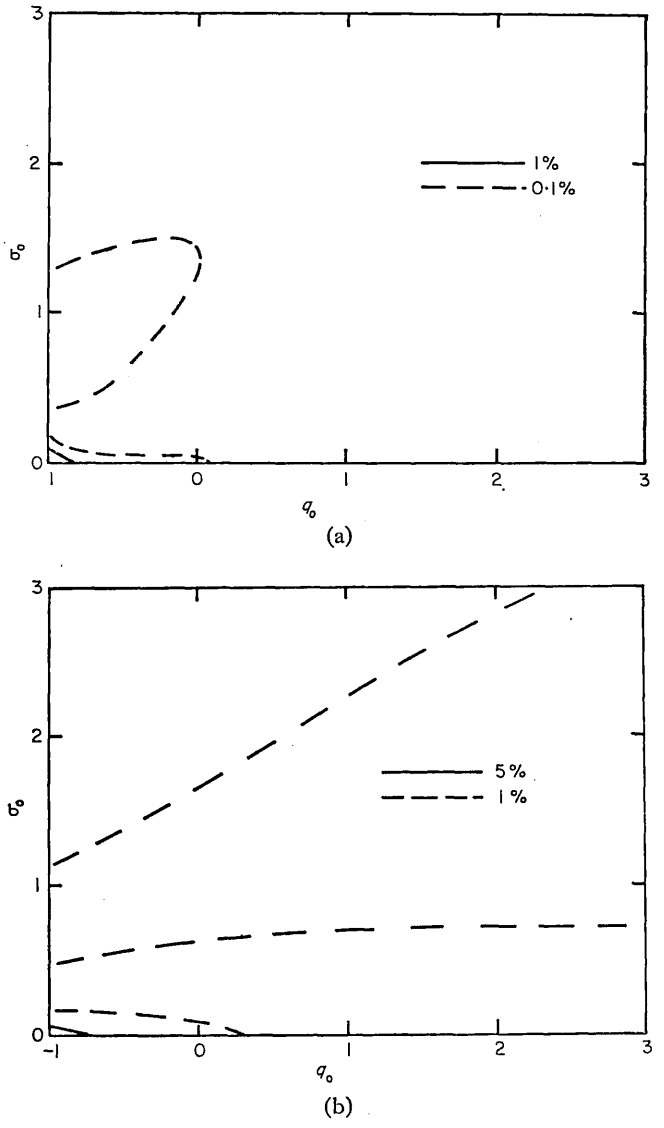

FIG. 4. *Model diagram:* $\sigma_0 - q_0$*:* (a) *no evolution, optical and radio luminosity-volume tests combined;* (b) *no evolution, optical test only;* (c) *power-law luminosity evolution,* $Q_L = 2{\cdot}5$*, combined optical and radio tests;* (d) *as in* (c) *but with* $Q_L = 3{\cdot}0$*. Dash-dotted lines in* (c), (d) *and Figs* 7–10 *correspond to the maximum rate of luminosity evolution discussed in Section* 8. *The contours join models with equal probability of being correct.*

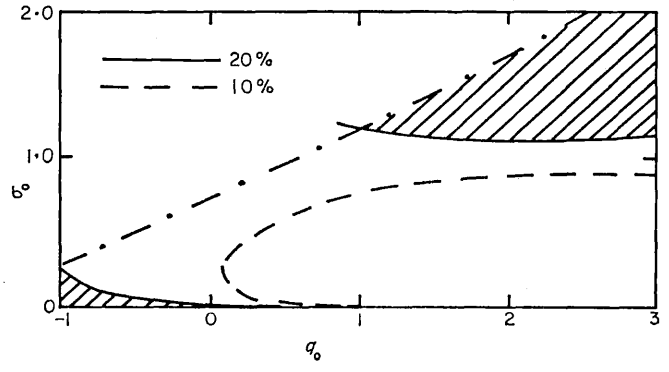

(c)

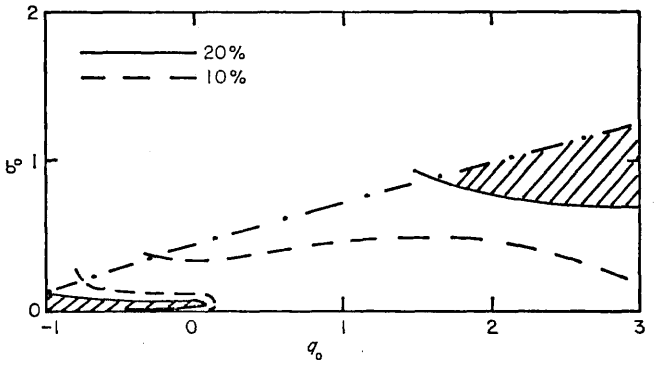

(d)

shows interpolated contours of equal probability in the $\sigma_0 - q_0$ plane. No model gives a probability above a few per cent, so we may conclude with some confidence that none of these models are consistent with the present data for quasars. Here we are at odds with McVittie & Stabell (**35**), who consider that the model with $q_0 = 0$, $\sigma_0 = 3$ is acceptable. Our procedure assigns a probability of less than 0·01 per cent to this model. Evolutionary factors must be affecting the distribution of quasars if *any* of the relativistic models are to apply.

In Fig. 4(b) we plot the contours of equal probability if the optical luminosity-volume alone is applied (suitably corrected for the effects of radio-selection). Although the probabilities are rather higher from this weaker test, all the models are ruled out at the 10 per cent level of significance. The least inconsistent models are those near to the de Sitter model ($\sigma_0 = 0$, $q_0 = -1$). These results should be compared with those of Solheim from applying the magnitude–redshift test to the cluster data of Baum (**32**) and Humason, Mayall & Sandage (**31**). His outermost contour includes an area of the $\sigma_0 - q_0$ plane very much larger than the whole of that which we have considered, yet corresponds to a probability of nearly 40 per cent. Such a comparison demonstrates the great power of the luminosity-volume test, given a set of objects like the quasars to which it can be applied.

The fact that the optical data alone is inconsistent with all the models considered demonstrates that the evolutionary factors required cannot be such as to affect the radio-emission alone. Thus the simplest form of the luminosity-evolution

hypothesis is insufficient, namely that the fraction of cosmical material in the form of quasars is the same at each epoch but the typical radio luminosity was greater in the past. Our analysis demonstrates that if the number-density of quasars at any epoch is proportional to the smoothed out cosmological density at that epoch, then *the typical optical luminosity must also have been greater in the past*, for the relativistic models to apply. Presumably the optical and radio emissions would then have to arise from a common mechanism. The evidence for a relationship between optical and radio luminosity is discussed in Section 7.

An alternative, and perhaps simpler, explanation is that the fraction of material in the form of quasars is a decreasing function of the cosmical time. In either case, we may predict that if optical counts can be performed on a complete set of quasars, free from radio selection (e.g. if optical or infrared (**49**) searches of the sky are performed), then those counts will give a log N–log S slope steeper than $-1{\cdot}5$. Since optical counts by Sandage (**41**) down to $18{\cdot}5$ magnitudes of the Haro-Luyten catalogues of blue objects give a slope rather less steep than $-1{\cdot}0$ ($d \log N/dm_{pg} = 0{\cdot}38$), we may deduce that these quasars do not make a *dominant* contribution to those catalogues at $18{\cdot}5$ m. But a *substantial* contribution is, of course, not ruled out by this argument. Or putting the argument another way, if the quasars *do* make a dominant contribution to the Haro-Luyten catalogues at faint magnitudes, then we have to rule out either the cosmological interpretation of the redshifts of quasars, or the relativistic cosmologies.

Before attempting to set some limits on the evolutionary parameters required to obtain consistency with relativistic models, we discuss some of the physical factors which might give rise to evolutionary effects. Some unrealistic assumptions made for reasons of mathematical simplicity may well vitiate some of the conclusions of earlier investigations.

6. *Possible evolutionary factors affecting the distribution of quasars.* Since only a small fraction of the available material at any epoch appears to be in the form of active quasars, it is quite uncertain that this fraction should be the same at different epochs. However we may distinguish two situations of particular interest:

6.1 *Quasars are violent outbursts in pre-existing agglomerations of matter.* Such a view links them with the strong radio-galaxies, which they resemble in total radio power, in radio spectra, and in certain cases, in radio structure (e.g. 3C47). It is then reasonable to suppose that the fraction of matter in the form of active quasars at any (recent) epoch is independent of epoch. But this is certainly not necessary, for evolution in number-density $\eta(t)$ may arise if the probability that an object has an outburst between epochs t and $t+dt$, $p(t)\,dt$, is a function of epoch, or if the typical lifetime of a source is a functon of epoch.

Luminosity evolution may also occur, that is, the typical luminosity of a source may be a function of epoch.

The objects undergoing the outbursts must then have some knowledge of the cosmical epoch. Either they were all born simultaneously and are aware of their age (through some internal evolution), or the outbursts (and/or the associated radiation) are the results of interaction with uncondensed material whose properties change with epoch. Theories of the latter kind might be suitable for radio-galaxies, if it transpires that they too must evolve, since their radio-emission is often centred far from the optical galaxy. But they do not seem very likely for the very compact

quasars, particularly as we have shown that the typical optical luminosity is required to be greater in the past if there is no evolution in number-density.

We shall investigate two simple mathematical forms of luminosity evolution:

(a) $\bar{F}(t) \propto R(t)^{-Q_L}$, which we can write $\bar{F}(z) \propto (1+z)^{Q_L}$

(b) $\bar{F}(t) \propto \exp(-\text{const. } R(t))$, which we can write

$$\bar{F}(z) \propto \exp\left\{(1+z_L).\left(1-\frac{1}{1+z}\right)\right\}.$$

For the cosmological models considered by Davidson & Davies (**20**), (**21**) in which $R(t)$ has a power law dependence on the cosmical time t, our form of evolution (a) is equivalent to that considered by Davidson & Davies, namely a power law dependence of luminosity on cosmical time. Of the relativistic cosmological models, only the Einstein–de Sitter model, with $R(t) \propto t^{2/3}$, is of the form considered by Davidson & Davies, so that only their results for this model can be compared with this work.

The disadvantage of evolutions of the form (a) is that they must be truncated at some finite value of z, z^* say, in order that a finite background radiation be obtained. Davidson & Davies (**20**) choose for z^* the point at which

$$\frac{d}{dz}\{\hat{\mathscr{F}}(z) - Q_L \log_{10}(l+z)\} = 0,$$

which seems a completely arbitrary assumption and may strongly influence their conclusions. Longair (**18**) takes z^* as a parameter to be fitted to the observations, and requires a value for z^* of about three to obtain consistency with the source-counts and the integrated background in the Einstein–de Sitter model.

But unless there are strong physical grounds for considering evolutions of the form (a), it seems rather premature to conclude that there is a real dearth of sources beyond $z = 3-4$ (**18**). An example of a form of evolution that does not require such a truncation is provided by form (b), where the typical luminosity at any epoch declines exponentially with epoch. We investigate this form in order to demonstrate that definitive conclusions can not be obtained by confining attention to form (a) only, rather than for any special merit in an exponential evolution. The actual form of evolution can not really be determined until the structure of the sources has been settled. But as an illustration of the way different models for the emission might give rise to different evolutionary parameters, we note that:

$Q_L = 3$ corresponds to $\bar{F}(t) \propto \rho(t)$, which could arise if the emission were the result of the interaction of high-velocity shocks or ejected material with intergalactic material;

$Q_L = 3{\cdot}5$ corresponds to $\bar{F}(t) \propto \mathrm{H}(t)^{(1+y)/2}$, $\mathrm{H}(t) \propto R(t)^{-2}$, $y = 2{\cdot}5$, which could arise if the emission were the synchroton radiation of electrons with a power-law energy spectrum of index $2{\cdot}5$, in a universal magnetic field: as the Universe expands the magnetic pressure is supposed to expand adiabatically ($\mathrm{H}^2 R^4 = \text{constant}$).

6.2 *Quasars correspond to the formation of galaxies.* If galaxies burn up some 20 per cent of their hydrogen during the final stages of their formation, perhaps inside massive objects, then objects emitting energy at about the rate found in quasars would be expected (**43**). If this stage is short compared with cosmological

time-scales, then the number-density of quasars would be proportional to the rate of galaxy formation. In this case it would be extremely unreasonable to suppose that the number-density of quasars is independent of epoch. For comparison, the rate of star-formation is often taken to have a power-law dependence on the gas density. Or perhaps an exponential dependence would be more appropriate. We have tested both of the forms:

(c) $\eta(t) \propto (1+z)^{Q_D}$

(d) $\eta(t) \propto \exp\{(1+z_D)(1-1/(1+z))\}$, where Q_D, z_D are parameters.

Evolution (c) has to be truncated at some z^*, but not form (d).

7. *Modified luminosity-volume test.* In order to test cosmological models when evolutionary effects of the kind discussed in the preceding section are present, we modify the luminosity-volume diagrams in a simple way, described in Ref. (24). We consider the distribution of ' corrected ' luminosity, $\mathscr{F}'$, with respect to ' weighted ' volume, V'. Assuming that the increase of luminosity with redshift is the same for all classes of quasars, we divide out this increase and compare the distribution of the luminosities as they would be at the present epoch in different ranges of volume weighted by the postulated increase in number-density with redshift. Thus for the four types of evolution suggested in the previous section:

(a) $\mathscr{F}' = \mathscr{F} - Q_L \cdot \log_{10}(1+z)$

(b) $\mathscr{F}' = \mathscr{F} - (1+z_L)\left(1-\frac{1}{1+z}\right)\log_{10} e$

(c) $V' = \int_0^{r_0} \frac{4\pi r^2 (1+z)^{Q_L}\, dr}{(1+k r^2/4)^3}$

(d) $V' = \int_0^{r_0} \frac{4\pi r^2 . \exp\left\{(1+z_D).\left(1-\frac{1}{1+z}\right)\right\} dr}{(1+k r^2/4)^3}.$

Now it is an assumption underlying our analysis that the radio and optical luminosities are independent. Since we are requiring radio and optical luminosities to be influenced by the same evolutionary factors in cases (a) and (b), we need to consider whether there is a detailed correlation between radio and optical luminosities. Such a correlation might appear if the optical and radio emissions were produced by the same mechanism, and would invalidate results obtained by the modified luminosity-volume test. In Fig. 5 we have plotted the optical against radio luminosity for quasars with $z \leqslant 0{\cdot}6$. Quasars with large redshift can only be observed if they are intrisically powerful both optically and radio-wise : thus a spurious correlation between optical and radio luminosity is introduced if *all* quasars are plotted in this diagram. Moreover for quasars with large redshifts the effects of cosmological model and evolutionary hypothesis are very large. Fig. 5 shows luminosities as calculated in the Milne model, but the results are not very different for other models.

Fig. 5 shows clearly that there is no detailed correlation between optical and radio luminosities, so that the procedure described in Section 4 will be valid.

8. *An upper limit to the rate of luminosity evolution.* Before we proceed to test evolutions of the form (a)–(d), it is advisable to consider whether arbitrarily large

values of the parameters Q_L and z_L are acceptable. The effect of correcting the luminosities of all the sources is to reduce the value of $\hat{\mathscr{F}}(z)$ for any given value of z, by an amount which increases with z. In fact there is a value of z for which $\hat{\mathscr{F}}(z)$ reaches a maximum, decreasing for larger values of z. The consequence of this redshift falling within the range of redshift covered by our set of quasars can be seen from Fig. 6(a), (b), which show the optical and radio luminosity-

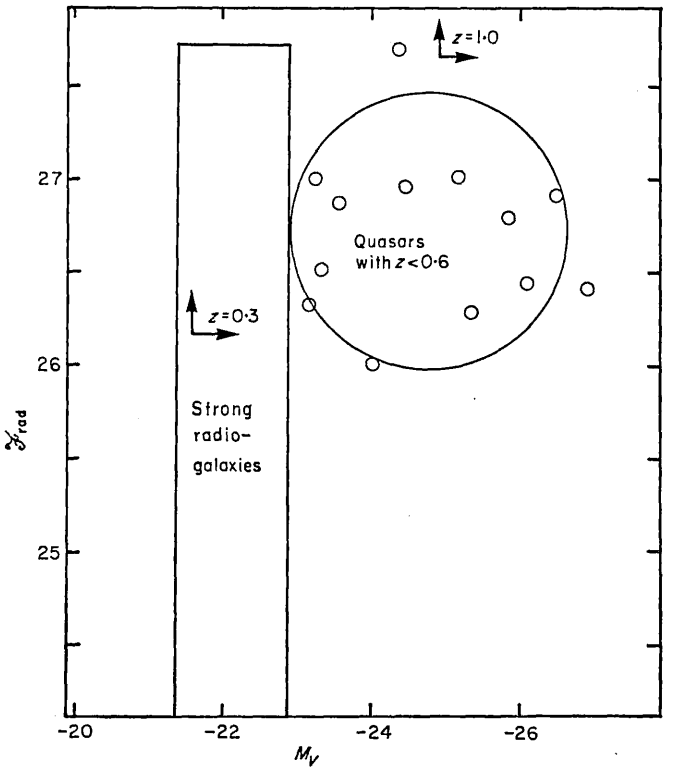

FIG. 5. *Radio vs optical luminosity for quasars with redshift less than* 0·6 (*circles*), *calculated in the Milne model, showing absence of detailed correlation. The region of this diagram occupied by the strong radio-galaxies is indicated, as also are the cutoffs imposed by limiting optical and radio flux-levels of* 19 *m and* 9 *f.u. respectively on quasars with redshifts* 0·3 *and* 1·0 *respectively* (*a quasar with redshift* 1·0, *for example, must be above and to the right of the point of intersection of the arrows labelled* 'z = 1·0').

volume diagrams for the Einstein–de Sitter model, corrected for luminosity evolution of form (a) with $Q_L = 3{\cdot}07$. In this case $\hat{\mathscr{F}}(z)$ has a maximum at redshift 2·2, and if this form of evolution is correct then we should expect large numbers of quasars with redshifts greater than 2·2 and fluxes above the 3C limiting flux-level. Now although a sharp decline in the optical continuum emission beyond Lyman α (44) could explain the absence of such objects amongst those 3C sources identified with *blue* quasi-stellar objects, they should be visible as *red* stellar objects. Fig. 6(b) shows the effect of such a sharp cutoff (arbitrarily taken as $F(\nu) \propto \nu^{-5}$) on the distribution of visual luminosities. Clearly very many objects should be found in 3C with redshifts between 2·2 and 3·5 (note that the scale has been compressed beyond $U = 0{\cdot}25$). Beyond $z = 3{\cdot}5$, the radio-sources

would correspond to empty fields down to 19 magnitudes. Now although there are one or two tentative identifications of 3C sources with red stellar objects (45), and about 30 sources associated with empty fields (46), many of the latter are likely to be distant radio-galaxies. Thus the identifications of 3C do not permit large numbers of quasars beyond redshift 2·2, and evolutions so extreme as to

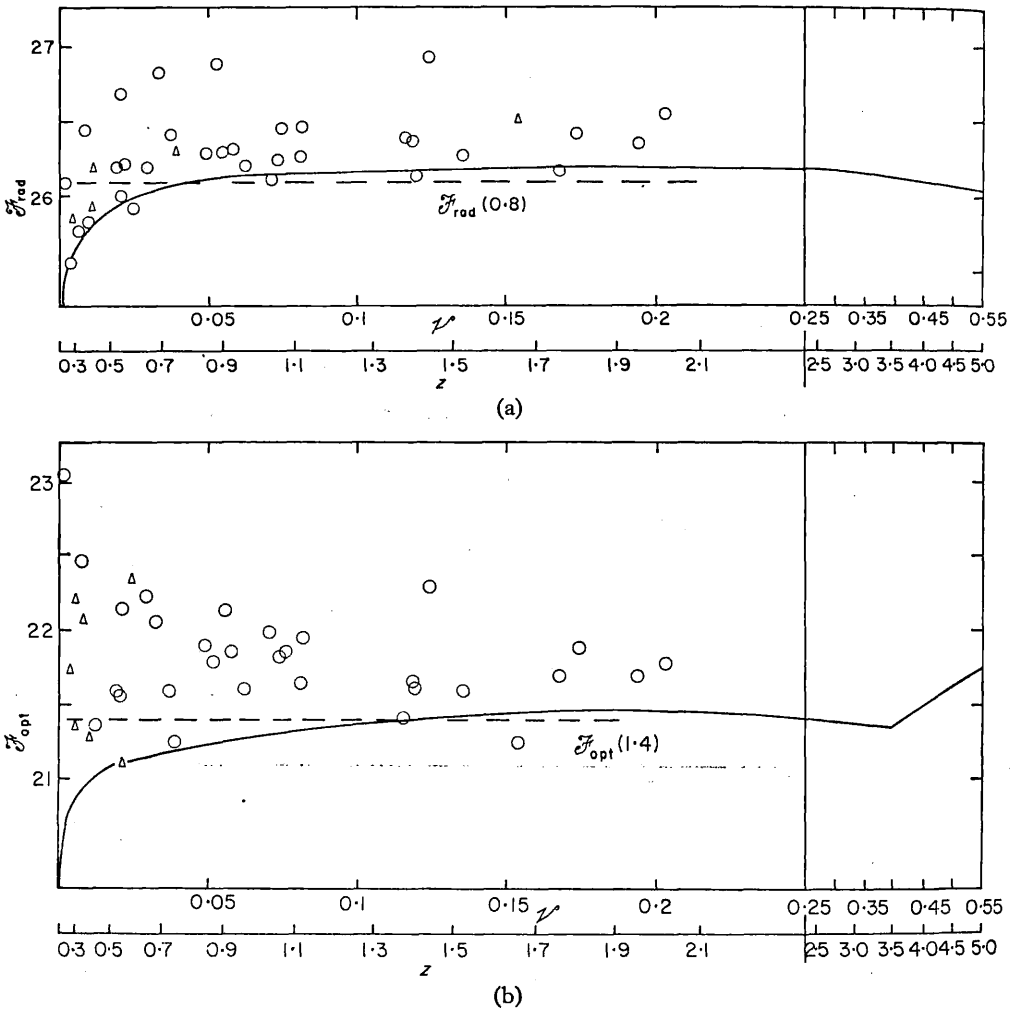

FIG. 6. *As in Fig.* 3, *but the luminosities corrected for power-law luminosity evolution with* $Q_L = 3{\cdot}07$. *The solid lines show cutoffs at nine flux-units and* 19 *magnitudes respectively, except that the effect of a sharp decline in the optical continuum beyond Lyman* α *is indicated in* (b). *Note that the volume scale is compressed beyond* $V = 0{\cdot}25$.

produce the situation illustrated in Fig. 6 can be ruled out. We are loath to introduce some *ad hoc* cutoff in the distribution of quasars beyond $z = 2{\cdot}2$ until the less extreme models, where the radio cutoff provides a fairly natural explanation of the absence of 3C quaxsars beyond $z = 2{\cdot}2$, have been eliminated.

Thus in any model we restrict our attention to values of Q_L and z_L for which the maximum in $\hat{\mathcal{F}}(z)$ occurs at $z > 2{\cdot}2$. This limitation is indicated by a dash-dotted line in Figs 4, 7–10.

Models which require Q_L or z_L less than but close to this limiting value are clearly unsatisfactory, by the same argument. For this reason the models in the top right-hand corners of Fig. 4(c), (d) are probably ruled out, even though they give consistency with the modified luminosity-volume test.

Finally, we may remark that it is a peculiarity of all models with luminosity evolution that the corrected luminosity of 3C273, the quasar with the smallest redshift in our set, is the largest of all: this peculiarity also applies to some cosmological models even without luminosity evolution (**34**).

9. *Correction for the incompleteness of the data for* $V > 18$. We can not hope to obtain accurate values for the evolutionary parameters if the selection effect postulated by Penston & Rowan-Robinson (**3**) is present. Without some such effect we have to admit that the quasars with large redshift are distributed anisotropically, so that analysis of the present kind is invalid. Since the quasars with $V > 18$ cover about half as much of the sky as those with $V \leqslant 18$, the simplest correction is to include each of the sources with $V > 18$ twice. Such a correction influences the radio luminosity-volume test only: the general effect is to increase the values of the evolutionary parameters slightly, though the results are not changed much qualitatively.

10. *Evolutionary parameters in the relativistic models.* Some of our results are summarized in Figs 4, 7–10. The models we have tested are as follows:

(i) a grid of models in the range: $-1 \leqslant q_0 \leqslant 3$, $0 \leqslant \sigma_0 \leqslant 3$; luminosity evolution (a) with $Q_L = 2{\cdot}5$, 3 (Fig. 4(c), (d)),

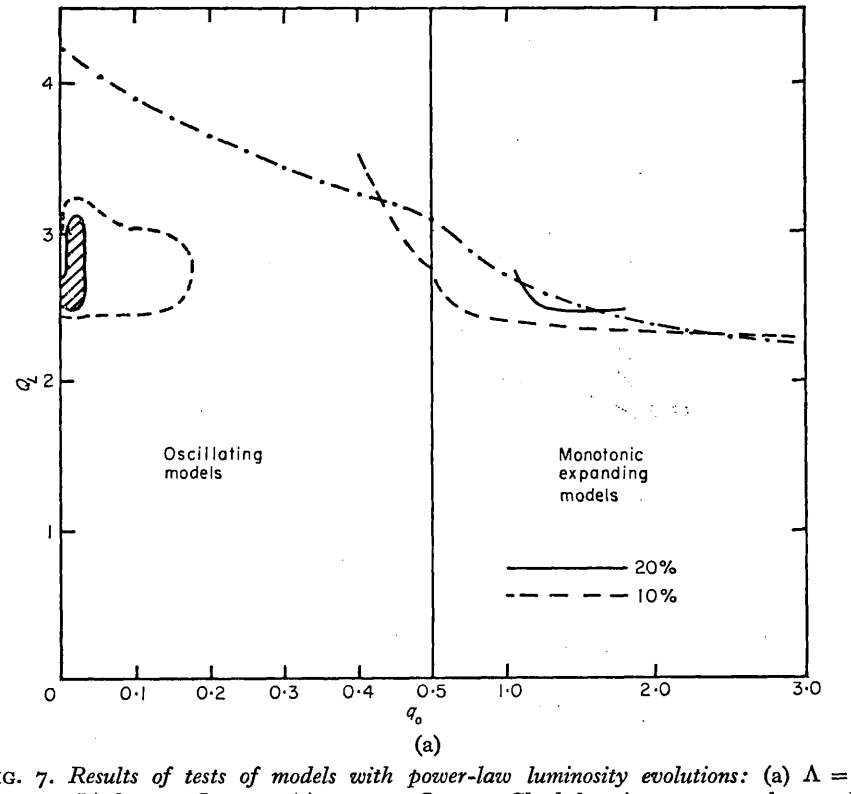

(a)

FIG. 7. *Results of tests of models with power-law luminosity evolutions:* (a) $\Lambda = 0$, $Q_L - q_0$; (b) $k = 0$, $Q_L - \sigma_0$; (c) $\sigma_0 = 0$, $Q_L - q_0$. *Shaded regions correspond to models giving probabilities greater than* 20 *per cent of being correct.*

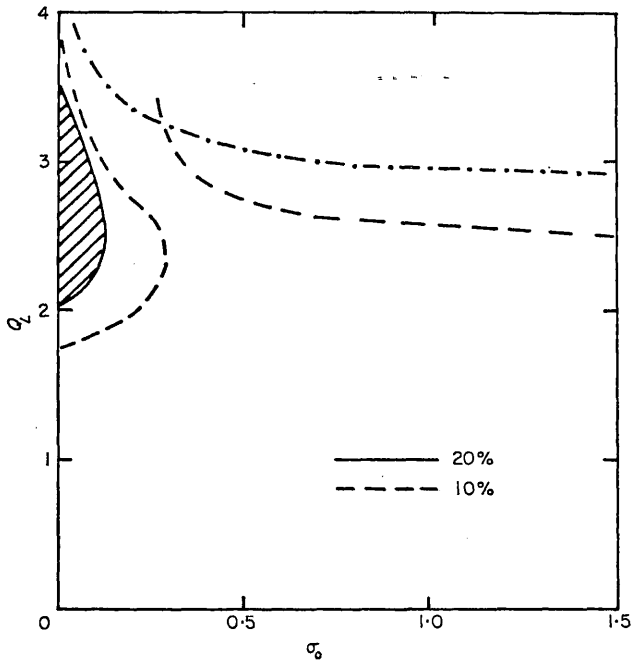
4
3
2
1
0
Q_2
0·5
1·0
1·5
σ_0
20%
10%

(b)

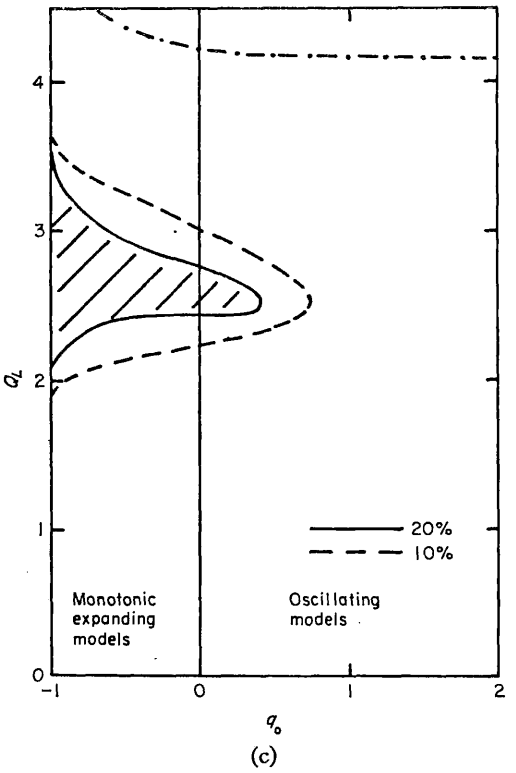
4
3
2
1
0
Q_2
−1
0
1
2
q_0
20%
10%
Monotonic expanding models
Oscillating models

(c)

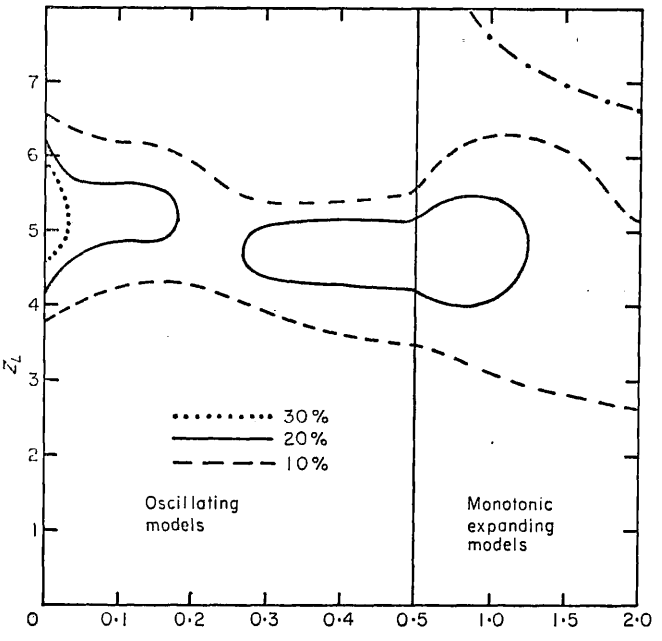

(a)

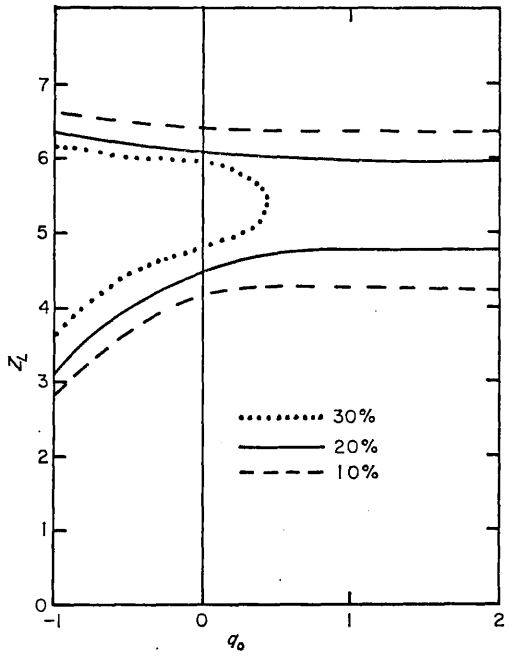

(b)

FIG. 8. *Test of exponential luminosity evolution,* $z_L - q_0$*:* (a) $\Lambda = 0$ *(scale expanded for* $q_0 < \frac{1}{2}$*);* (b) $\sigma_0 = 0$.

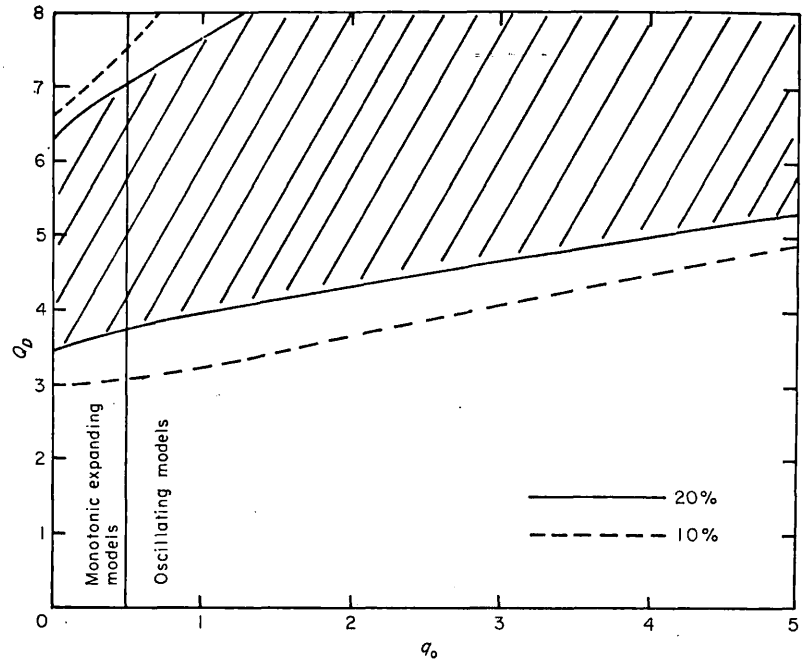

(a)

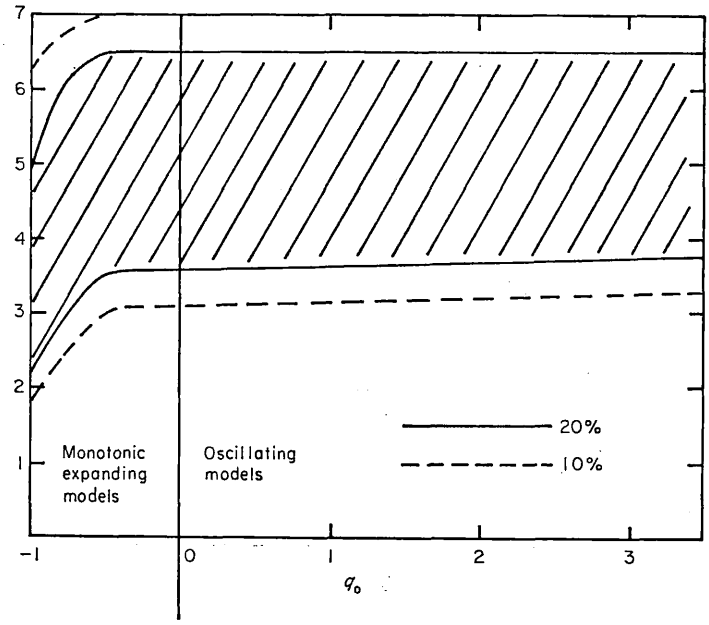

(b)

FIG. 9. *Test of power-law density-evolutions, $Q_D - q_0$:* (a) $\Lambda = 0$; (b) $\sigma_0 = 0$.

(ii) models with $\Lambda = 0$, $k = 0$, and $\sigma_0 = 0$ respectively; luminosity evolution (a) for a range of Q_L (Fig. 7(a), (b), (c)),

(iii) models with $\Lambda = 0$ and $\sigma_0 = 0$; luminosity evolution (b), and density evolutions (c) and (d) for ranges of the respective parameters z_L, Q_D, z_D (Figs 8(a), (b); 9(a), (b)),

(iv) de Sitter, Milne & Einstein–de Sitter models; combined evolutions of type (a) and (c) (Fig. 10(a), (b), (c)).

In each figure we show interpolated contours of 10 and 20 per cent probabilities that the present available data is consistent with the given model. Models giving probabilities below 10 per cent can probably be ruled out, even when the limitations

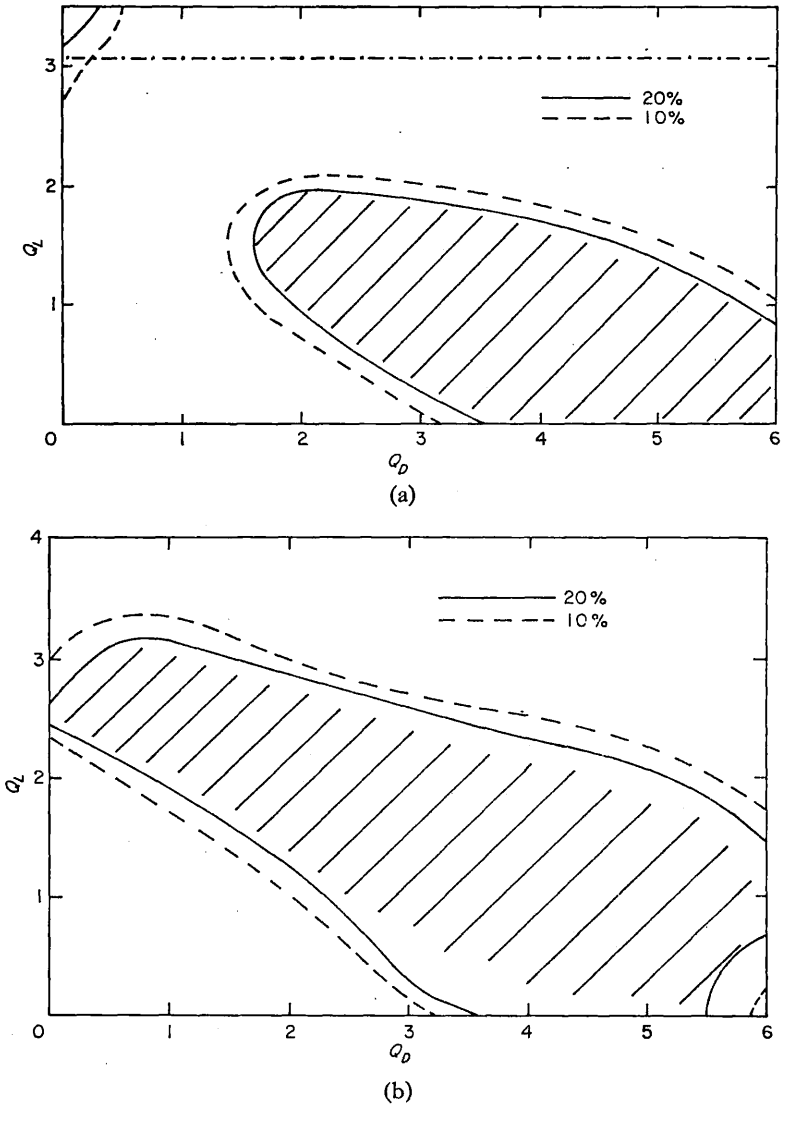

FIG. 10. *Test of combined power-law luminosity and density evolutions,* $Q_L - Q_D$: (a) *Einstein–de Sitter,* (b) *Milne and* (c) *de Sitter models.*

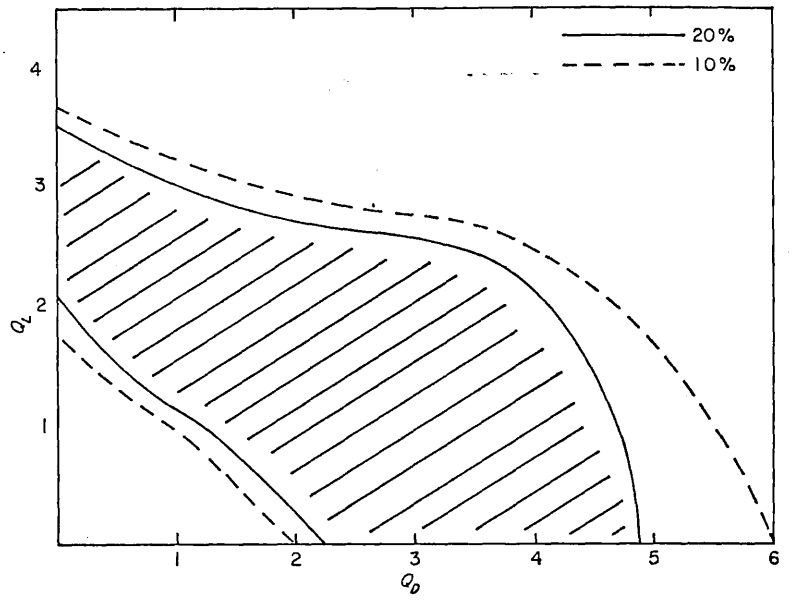

(c)

of the present work are borne in mind. We regard models giving probabilities higher than 20 per cent as acceptable, though many of these will almost certainly be ruled out when more complete data down to a lower flux-level is available. We discuss each of the four evolutionary hypotheses described in Section 6, in turn:

(a) Power-law luminosity evolution, which has been favoured by a number of authors, is the most vulnerable of the four hypotheses to this kind of analysis. There are few models in which this kind of evolution gives consistency with the data. Fig. 7(a) shows that of the models with zero cosmological constant, the only satisfactory models are those with q_0 close to zero. The best values for q_0 are in the range 0·005 to 0·03, corresponding to a smoothed out density at the present epoch of 10^{-31} to 6.10^{-31} g cm^3. The close agreement with values obtained from counting up the actual galaxies observed (**30**) should be regarded as coincidental until there are some strong grounds for believing that evolution of this kind is affecting the distribution of luminosities of quasars.

When a non-zero cosmological constant is included, the most satisfactory models are those with σ_0 close to zero (Figs 4(c), (d); 7(b). Of the completely empty models by far the most satisfactory is the de Sitter model, and those with $q_0 > 1$ are ruled out. Thus exactly those models which might have been expected from consideration of the actual density of material observed to date, and from the problem of the long ages of the oldest stars, are preferred on this evolutionary hypothesis.

(b) Exponential luminosity evolution gives consistency with the data at the 10 per cent level for all the cosmological models tested to date (Fig. 8(a), (b)). In view of the advantage of this form of evolution already discussed, namely that no arbitrary truncation of the distribution is required, this result provides considerable incentive for further investigation of evolutions of this type. At the 20 per cent level models with $\Lambda = 0$, $q_0 > 1$, are ruled out, but all the empty

models are acceptable. For interest we show the 30 per cent contours also in Fig. 8(a), (b): these look very like the 20 per cent contours in Fig. 7(a), (b), suggesting that when more data is available, similar conclusions will be reached as for case (a). The best values for the parameter z_L are in the range 5 to 6: the significance of z_L is that between the epochs corresponding to $z = \infty$ and $z = z_L$ the typical luminosity of quasars has been reduced by a factor $1/e$. At the present epoch the typical luminosity is between 10^{-3} and $10^{-2.5}$ of the value at epoch $t = 0$.

(c) This analysis is extremely insensitive to power-law density evolution, in the sense that for all models quite a wide range of the parameter Q_D is consistent with the data (Fig. 9(a), (b)). Thus the earlier conclusion of the present author (**24**), that density evolution was at least as consistent with the data as luminosity evolution, can now be strengthened to the statement: *density evolution gives much better consistency with the data than luminosity evolution.*

We may note that of the models with zero cosmological constant, the empty models require the least severe evolution: and that of the empty models (including those with non-zero cosmological constant) the de Sitter requires by far the least severe evolution.

(d) Similarly insensitive results are obtained for exponential density evolution, with the best values of z_D being in the range 7–13. Here the significance of the parameter z_D is that between the epochs corresponding to $z = \infty$ and $z = z_D$ the fraction of material in the form of active quasars has decreased by a factor $1/e$. At the present epoch that fraction is only between 10^{-3} and 10^{-5} of the value at $t = 0$. If we consider quasars to be the birth-pangs of galaxies, then we may conclude that most of the galaxies had formed by the epoch corresponding to redshift 10 ± 3.

The comparison of the Milne, de Sitter & Einstein–de Sitter models is very interesting (Fig. 10(a), (b), (c)). Density evolution alone is consistent with the data for all three models, as also are intermediate cases with combined luminosity and density evolution. Luminosity evolution alone is consistent with the de Sitter model for $2 \leqslant Q_L \leqslant 3 \cdot 5$. For the Milne model a rather small range about $Q_L = 2 \cdot 5$ is consistent: with more data a more detailed analysis may enable this possibility to be completely ruled out. For the Einstein–de Sitter model only values of Q_L which give rise to the difficulty discussed in Section 8 are consistent.

11. *Comparison with earlier work.* (i) Longair (**18**) has interpreted the Cambridge radio source-counts in terms of power-law luminosity and density evolutions of the most luminous sources, in the Einstein–de Sitter model. The best parameters he obtained ($Q_L = 3 \cdot 3$, $Q_D = 5 \cdot 7$) agree well with those obtained in this analysis of the available data for quasars, supporting his conjecture that the population causing the steep counts is the quasars. However, as we have remarked in the previous section, luminosity evolution with Q_L of order 3 or more in the Einstein–de Sitter model would require the existence of a large number of sources in 3C to be identified with quasi-stellar objects with redshifts greater than $2 \cdot 2$. This difficulty could only be overcome by supposing that there is a real truncation of the quasars at redshift $2 \cdot 2$: this value is significantly lower than the value required by Longair in his analysis ($z^* = 3$). This difficulty is less severe in the Milne and de Sitter models. Longair argues that the rapid change in slope of the log N–log S curve at low radio flux-levels is evidence of a real truncation at some epoch in the distribution of the sources. However, exponential evolution of the kind we have

TABLE II

$\log_{10} S$ (w m^{-2} Hz^{-1})	−24·0	−24·25	−24·5	−24·75	−25·0	−25·25	−25·5	−25·75	−26·0
$\frac{d(\log N)}{d(\log S)}$	−1·69	−1·76	−1·88	−2·10	−2·49	−2·98	−2·50	−1·08	−0·66

considered in Section 6 may also produce such an effect. Table II shows the number count slope as a function of flux-density for a set of sources uniformly distributed (coordinate number-density independent of epoch) in the Einstein–de Sitter model, when the sources at epoch corresponding to redshift z have luminosity of the form

$$10^{25\cdot5}\left\{\exp 6\left(1-\frac{1}{1+z}\right)\right\},$$

i.e. $z_L = 5$ in our notation of Section 6. Between 3 and 1 flux-units the number-count slope changes rapidly from −2·50 to −0·66. This is even sharper than the observed change of slope, but it is clear that the dispersion in luminosity of the sources would smooth this out to some extent. More detailed analysis of the number-counts to low flux-level will be presented in a subsequent paper.

(ii) Davidson & Davies (**21**) have argued that the hypothesis of galactic collisions can be ruled out (without additional luminosity evolution) on the grounds of the source-counts, for models with $R(t) \propto t^{-n}$. While we do not necessarily wish to advocate this hypothesis, we note that this case, which corresponds to power-law density evolution with $Q_D = 3$, is not ruled out for the quasars in the de Sitter model. Of course the de Sitter model is not of the form considered by Davidson & Davies, but this demonstrates that the the range of models considered by them does not necessarily include the full range of properties shown by the relativistic models.

(iii) Although the density-evolution hypothesis does not allow us to specify the cosmological model, we may compare the results obtained for the luminosity-evolution hypothesis (a) with those obtained using the brightest galaxies in clusters (**29**), (**31**)–(**33**). If the cosmological constant is set equal to zero, and allowance is made for the evolution of the stars in galaxies, both analyses agree in demanding a value for q_0 close to zero. When models with non-zero cosmological constant are considered our analysis gives the de Sitter as the most favourable model. For consistency of this model with the cluster data rather steeper optical luminosity-evolution would be required than has been considered to date (**33**).

12. *Other cosmological models*

(i) *The steady-state model.* Mathematically, the steady-state model is equivalent to the de Sitter model with negative power-law density-evolution, with $Q_D = -3$. The combined optical and radio luminosity-volume tests give a probability of only 0·01 per cent for this model.

(ii) *Brans–Dicke models with $k = 0$.* Brans & Dicke (**47**) have given the solution of the cosmological equations obtained from their scalar–tensor theory of gravitation for the case $k = 0$: the models are given by $R(t) \propto t^{(2+3\omega)/(4+3\omega)}$ where ω is a constant of the theory which can range from zero to infinity. As $\omega \to \infty$ these models tend to the Einstein–de Sitter model. We have tested these models for a range of ω: for $\omega \geqslant 4$ they give results identical to the Einstein–de Sitter model.

The value of ω inferred by Dicke from his interpretation of his measurements of the solar oblateness is about 6 (**48**). Thus there is little prospect of distinguishing between the rival theories of gravitation on the basis of cosmological tests.

13. *Conclusions.* If the redshifts of quasars are cosmological our tentative conclusions are that:

(i) No relativistic model is consistent with the data for quasars without some evolutionary factor that affects both radio and optical distributions.

(ii) The luminosity-evolution hypothesis is far more vulnerable to the luminosity-volume test than density-evolution.

(iii) Luminosity-evolution with a power-law dependence on the scale-factor requires $q_0 < 0{\cdot}035$ if $\Lambda = 0$, with the best value being $0{\cdot}005 \leqslant q_0 \leqslant 0{\cdot}03$, or $10^{-31} \leqslant \rho_0 \leqslant 6{\cdot}10^{-31}$, in very good agreement with Oort's value (**30**) for the average smoothed-out density of matter in galaxies. If models with non-zero cosmological constant are also considered, the best models are those near to the de Sitter model in the σ_0–q_0 plane, which give very long ages to the Universe.

(iv) Luminosity-evolution with an exponential dependence on the scale-factor gives better consistency with the data than power-law evolution, but the best models are the same as those given in (iii).

(v) Density-evolution gives consistency with all models, though the least severe evolution is required in the de Sitter model. With exponential evolution the epoch at which the number-density of quasars is $1/e$ times that at $t = 0$ is given by $z = 10 \pm 3$.

Some of these conclusions may be modified when all quasars in 3C have their redshifts measured, but it seems exceedingly unlikely that (i) and (ii) can be altered. These alone are sufficient to demonstrate the great power of the luminosity-volume test. While some of the features of this test have occurred independently to a number of authors (**14**), (**35**), (**36**), the two factors that enable significant conclusions to be reached are: allowance for selection effects imposed by the limiting flux-levels and the combination of the available information into a single probability.

14. *Future work.* Apart from the obviously urgent programme of the completion of redshift measurements of 3C quasars, important conclusions for cosmology may result from the following work:

(i) The completion of redshift measurements for 3C radio-galaxies, so that the radio luminosity-volume test may be applied. Here we do not have to add the proviso ' if the redshifts are cosmological ', but the results may be less significant since we do not see galaxies out to nearly such large redshifts as quasars. At present the redshifts are 80 per cent complete for radio-galaxies with $m_v \leqslant 15$, but only 20 per cent complete for $15 < m_v < 20$.

(ii) Evolutions with exponential (and other?) dependence on the scale-factor should be investigated for consistency with radio number-counts to low flux-levels and the integrated extragalactic radio background.

(iii) It is a prediction arising from the present work that if the redshifts of quasars are cosmological, and the cosmology relativistic, then optical number-counts of quasars will be significantly steeper than $1{\cdot}5$. The results of optical searches for blue (or infrared (**49**)) quasi-stellar objects are awaited with interest.

(iv) Demonstration that the optical emission from quasars did not arise from a similar mechanism to the radio emission would throw considerable doubt on the luminosity-evolution hypothesis.

(v) Since there are more than ten times as many radio-sources per steradian brighter than the 4C (and Parkes) limiting flux-level than there are in 3C per steradian, it will be some time before the luminosity-volume test may be applied to these sources. Much more powerful conclusions may be expected, since the numbers will be sufficient to investigate the distribution of sources in the luminosity-volume plane in much more detail than our simple division of the observable region into two.

Clearly the observational programmes mentioned above are already being pursued. The present author hopes to present results bearing on (ii) in a subsequent paper: a rough preliminary version of the radio luminosity-volume test for radio-galaxies is also being performed, estimating the unknown redshifts from the optical magnitudes of the galaxies. Although crude, this should indicate whether significant results are to be hoped for, and thus whether the observational programme (i) is of high priority.

Acknowledgments. I would like to thank Mr M. V. Penston, Dr I. Roxburgh, and my supervisor, Professor W. H. McCrea, for stimulating discussions, and for helpful suggestions and criticisms. The computing was performed by the Computing Centre, University of Sussex, to whom thanks are due for much valuable assistance in the writing of the programs. I am indebted to the Science Research Council for a maintenance grant.

I am grateful to a referee for comments that enabled this paper to be improved.

Astronomy Centre,
School of Mathematical and Physical Sciences,
University of Sussex.
1967 *August.*

References

(1) Greenstein, J. L. & Schmidt, M., 1964. *Astrophys. J.*, **140**, 1.
(2) Strittmatter, P., Faulkner, J. & Walmesley, M., 1966. *Nature, Lond.*, **212**, 1441.
(3) Penston, M. V. & Rowan-Robinson, M., 1967. *Nature, Lond.*, **213**, 375.
(4) Burbidge, G. R. & Burbidge, E. M., 1967. *Astrophys. J.*, **148**, 107.
(5) Arp, H., 1966. *Science*, **151**, 1214.
(6) Arp, H., 1967. *Astrophys. J.*, **148**, 321.
(7) Sandage, A. R., 1966. *Astrophys. J.*, **146**, 13.
(8) Terrell, J., 1964. *Science*, **145**, 918.
(9) Hoyle, F. & Burbidge, G. R., 1966. *Astrophys. J.*, **144**, 534.
(10) Faulkner, J., Gunn, J. E. & Peterson, B. A., 1966. *Nature, Lond.*, **211**, 502.
(11) Noedlinger, P. D., Jokipii, J. R. & Woltjer, L., 1966. *Astrophys. J.*, **146**, 523.
(12) Hughes, R. G. & Longair, M. S., 1967. *Mon. Not. R. astr. Soc.*, **135**, 131.
(13) Hoyle, F. & Burbidge, G. R., 1966. *Nature, Lond.*, **210**, 1346.
(14) Kafka, P., 1967. *Nature, Lond.*, **213**, 346.
(15) Ryle, M. & Clarke, R. W., 1961. *Mon. Not. R. astr. Soc.*, **122**, 349.
(16) Davidson, W., 1962. *Mon. Not. R. astr. Soc.*, **123**, 425.
(17) Gower, J. F. R., 1966. *Mon. Not. R. astr. Soc.*, **133**, 151.
(18) Longair, M. S., 1966. *Mon. Not. R. astr. Soc.*, **133**, 421.
(19) Davidson, W., 1962. *Mon. Not. R. astr. Soc.*, **124**, 79.
(20) Davidson, W. & Davies, M., 1964. *Mon. Not. R. astr. Soc.*, **127**, 421.
(21) Davidson, W., & Davies, M., 1966. *Mon. Not. R. astr. Soc.*, **134**, 405.

(22) Longair, M. S., 1966. *Nature, Lond.*, **211**, 949.
(23) Roeder, R. C. & Mitchell, G. F., 1966. *Nature, Lond.*, **212**, 165.
(24) Rowan-Robinson, M., 1966. *Nature, Lond.*, **212**, 1556.
(25) Robertson, H. P., 1933. *Rev. mod. Phys.*, **5**, 62.
(26) McCrea, W. H., 1935. *Z. Astrophys.*, **15**, 69.
(27) McVittie, G. C., 1956. *General Relativity & Cosmology*, Chapman & Hall, London.
(28) Refsdal, S. & Stabell, R., 1966. *Mon. Not. R. astr. Soc.*, **132**, 379.
(29) Solheim, J., 1966. *Mon. Not. R. astr. Soc.*, **133**, 321.
(30) Oort, J. H., 1958. *Solvay Conference on La Structure et l'Evolution de l'Univers*, p. 163.
(31) Humason, M. L., Mayall, N. U. & Sandage, A. R., 1956. *Astr. J.*, **61**, 97.
(32) Baum, W. A., 1962. I.A.U. Symposium No. 15, *Problems of Extragalactic Research*, ed. by G. C. McVittie, p. 390.
(33) Sandage, A. R., 1961. *Astrophys. J.*, **134**, 916.
(34) McCrea, W. H., 1966. *Astrophys. J.*, **144**, 516.
(35) McVittie, G. C. & Stabell, R., 1967. *Nature, Lond.*, **213**, 133.
(36) Rees, M. J. & Sciama, D. W., 1966. *Nature, Lond.*, **211**, 1283.
(37) Edge, D. O. *et al.*, 1959. *Mem. R. astr. Soc.*, **68**, 37.
(38) Bennett, A. S., 1962. *Mem. R. astr. Soc.*, **68**, 163.
(39) Rees, M. J. & Sciama, D. W., 1967. *Nature, Lond.*, **213**, 374.
(40) Petrosian, V., Saltpeter, E. & Szekeres, P., 1967. *Astrophys. J.*, **147**, 1222.
(41) Sandage, A. R., 1965. *Astrophys. J.*, **141**, 1560.
(42) Burbidge, G. R., Burbidge, E. M., Hoyle, F. & Lynds, C. R., 1966. *Nature, Lond.*, **210**, 774.
(43) Lynden-Bell, D., 1967. Herstmonceux Conference on the Helium Problem.
(44) Bahcall, J. N. & Sargent, L. W., 1967. *Astrophys. J.*, **148**, 165.
(45) Wills, D. & Parker, E. A., 1966. *Mon. Not. R. astr. Soc.*, **131**, 503.
(46) Veron, P., 1966. *Ann. Astrophys.*, **29**, 231.
(47) Brans, C. & Dicke, R. H., 1961. *Phys. Rev.*, **124**, 925.
(48) Dicke, R. H., 1967. *Phys. Rev. Lett.*, **18**, 313.
(49) Braccesi, A., 1967, *Nuovo Cim.* (*B*), **49**, 148.
(50) Kellerman, K. I., 1964. *Astrophys. J.*, **140**, 969.
(51) Pauliny-Toth, I. I. K., Wade, C. M. & Heeschen, D. S., 1966. *Astrophys. J., Suppl. Ser.*, **13**, No. 116.
(52) Kafka, P., 1967. Personal communication.

APPENDIX I

Radio and optical K-corrections

We write

$$f_{\text{rad}} = \log_{10} S_{178}$$

where S_{178} is the flux-density at 178 MHz in units of watts $\text{Hz}^{-1}\,\text{m}^{-2}$, taken from the 3C catalogue increased by 8 per cent (**38**), and take the radio K-correction to be

$$-0{\cdot}4\,K = (\alpha - 1)\log_{10}(1+z)$$

where α is the spectral index in the range 178–750 MHz α is taken from Kellerman (**50**) in the case of those sources classified by him as having straight spectra: for the remainder of the sources α is calculated from the relation

$$\alpha = \frac{\log_{10} S_{178} - \log_{10} S_{750}}{\log_{10} 750 - \log_{10} 178}$$

where S_{750} is taken from Pauliny-Toth, Wade & Heeschen (**51**). This procedure is exact for sources having spectra of the form $F(\nu) \propto \nu^{-\alpha}$, and is reasonably accurate even for sources with curved spectra, since the curvatures are not very great.

In order to convert the optical magnitudes to approximately the same absolute scale as the radio flux-densities, we write

$$\mathscr{f}_{\text{opt}} = -22{\cdot}4 - 0{\cdot}4\,V$$

where V is the apparent visual magnitude. We use the optical K-correction calculated by Sandage (52)

APPENDIX II

Calculation of $\mathscr{F}$ and U

By definition

$$U(z) = \int_0^{r_0(z)} \frac{4\pi r^2 dr}{(1+\frac{1}{4}kr^2)^3}$$

and

$$\mathscr{F} - \mathscr{f} + 2{\cdot}5\,K = 2\log_{10}\left\{\frac{r_0 R_0 Z}{1+\frac{1}{4}kr_0{}^2}\right\} \text{ where } Z = 1+z$$

$$= 2\log_{10}(R_0 v Z) \text{ where } v = \frac{r_0}{1+\frac{1}{4}kr_0{}^2}$$

From equations (2), (4) and (5) we find

$$\int_0^{r_0(z)} \frac{dr}{1+\frac{1}{4}kr^2} = \frac{c}{R_0 H_0}\,\chi(z).$$

$k = +1$:

$$R_0 = c/H_0.(3\sigma_0 - 1 - q_0)^{1/2}$$

$$v = \sin\{\chi.(3\sigma_0 - 1 - q_0)^{1/2}\}$$

$$U(z) = 2\pi\{\sin^{-1} v - v(1-v^2)^{1/2}\}.$$

$k = 0$:

$$R_0 = c/H_0$$

$$v = \chi$$

$$U(z) = 4\pi v^3/3.$$

$k = -1$:

$$R_0 = c/H_0(1+q_0-3\sigma_0)^{1/2}$$

$$v = \sinh\{\chi.(1+q_0-3\sigma_0)^{1/2}\}$$

$$U(z) = 2\pi\{v(1+v^2)^{1/2} = \sinh^{-1} v\}.$$

The cases where χ can be evaluated exactly are

$\Lambda = 0$:
$(q_0 \neq 0)$

$$\frac{R_0 H_0 v}{c} = \frac{q_0 z + (q_0 - 1).(\sqrt{1 + 2\,q_0 z} - 1)}{q_0{}^2(1+z)}$$

$\sigma_0 = 0$:
$(q_0 \neq -1)$

$$\frac{R_0 H_0 v}{c} = \frac{\sqrt{(1+q_0)\,Z^2 - q_0} - Z}{q_0}.$$

The three asymptotic models are:

$\sigma_0 = q_0 = 0$ (Milne): $v = (Z^2 - 1)/2Z$;
$\sigma_0 = q_0 = \frac{1}{2}$ (Einstein–de Sitter): $v = 2(1 - Z^{-1/2})$;
$\sigma_0 = 0$, $q_0 = -1$ (de Sitter): $v = z$.

(*Reprinted from Nature, Vol. 216, No. 5122, pp. 1289–1292, December 30, 1967*)

Radio Galaxies as Cosmological Probes

Applying the luminosity-volume test to radio galaxies, it is found that for the data to fit the usual relativistic cosmological models there must be strong evolutionary factors affecting the distribution of the radio galaxies. The steady state model is inconsistent with the present data

by

M. ROWAN-ROBINSON

Department of Mathematics, Queen Mary College, University of London

THIS article reports the results of applying a new cosmological test to the radio galaxies: the distribution of radio galaxies in space is strongly affected by evolutionary factors. In particular, the steady state model, in which evolution is not permitted, does not seem to be consistent with the present data for radio galaxies. This confirms the conclusion of Rees and Sciama[1] based on the data for quasars, although some authors[2–4] continue to cast doubt on the cosmological interpretation of the red-shifts of quasars. The classical cosmological tests, the magnitude-red-shift and the number-count tests, are of value only in situations where the dispersion in luminosity of the sources is small. This condition does not hold for the radio luminosities of radio galaxies, or for either the optical or radio luminosities of quasars (assuming their red-shifts to be cosmological). The additional factor of completeness down to some limiting flux level, however, enables a far more powerful test, the luminosity-volume test, to be applied.

In earlier communications[5,6] I have described the application of this test to the quasars, and the determination of various possible forms of evolution which give consistency with the usual relativistic cosmological models. When the cosmological term is included in Einstein's equations, these models can be characterized by two parameters[7]

$$\sigma_0 = 4\pi G\rho_0/H_0^2 \quad q_0 = -(R\ddot{R}/\dot{R}^2)_0$$

where ρ is the smoothed out cosmological density, $H = \dot{R}/R$, $R(t)$ is the scale factor of the expanding universe and the subscript zero refers to the present epoch. I have examined[6] models with $0 \leq \sigma_0 \leq 3$, $-1 \leq q_0 \leq 3$, and found that for consistency with any of these models some evolutionary factor must be assumed to be affecting the quasars. For example, the fraction of matter in the form of active quasars might have been greater at earlier epochs, or the typical luminosities of quasars at earlier epochs might have been greater.

Luminosity-volume Test

The principle of the luminosity-volume test is that if the distribution of luminosities of a set of sources is independent of epoch, then in any range of luminosity we expect to find equal numbers of sources in equivalent volumes of space. In ref. 5, the radio luminosity-volume diagram was used to demonstrate that for quasars, "density" evolution (the co-ordinate number-density increases with red-shift, but the relative distribution of luminosities is independent of epoch) is at least as consistent with the present observations as "luminosity" evolution (the co-ordinate number-density is independent of epoch, but the typical luminosity increases with red-shift). When proper account is taken of the effects of optical selection, and the optical luminosity-volume diagram is also considered, it is found[6] that only for comparatively empty models ($\sigma_0 \ll 1$) are the quasars consistent with luminosity evolution.

Application to Radio Galaxies

The optical luminosities of radio galaxies show small dispersion[8], so the effect of the limiting visual magnitude of about 20 is simply to confine our identifications to red-shifts smaller than 0·4–0·5. Moreover, we can obtain from the observed visual magnitude of a galaxy a rough estimate of its red-shift in those cases where the red-shift has not yet been determined. At present red-shifts are available in the literature[9–13] for fifty-nine of the one hundred and forty-seven galaxies identified with radio sources in the revised 3*C* catalogue[14], corresponding to 80 per cent of those identified to date with $V \leq 15$ magnitudes, but only 20 per cent of those identified with $15 < V \leq 20$.

Fig. 1 shows the distribution of red-shift of these galaxies against visual magnitude, as estimated by Wyndham[15]: six galaxies with red-shifts less than 0·01 (3*C* 71, 231, 270, 272·1, 274, 386) are omitted. In what follows I shall confine my attention to "strong radio galaxies", that is, those with luminosity greater than 10^{23} W ster^{-1} (c/s)$^{-1}$, so that of these six nearby radio galaxies, only 3*C* 274 will concern us.

Sources of the same luminosity and spectral shape would satisfy a relation of the form

$$V = A + 5 \cdot \log_{10} z + K(z) + 5 \cdot \log_{10}\{D(z)/z\} \ldots \quad (1)$$

where z is the red-shift, $K(z)$ is the K-correction[16] and $D(z)$ is the "luminosity distance"[17].

For small z, equation (1) can be approximated by

$$V = A + 5 \log_{10} z + B z \ldots \quad (2)$$

where A and B are constants[16]. The locus of this form with $A = 20{\cdot}5$, $B = 5$, is shown in Fig. 1; this is the best line of form (2) through the data, from a least squares analysis.

The scatter of the points in Fig. 1 is primarily caused by the approximate nature of the magnitude estimates, which are probably not more accurate than $\pm 1^{m}$. Other factors are the dispersion in intrinsic luminosity of the galaxies, the effect of galactic obscuration and differences in spectral shape for different types of galaxy. Corrections could be applied for the latter two effects, but the approximate nature of the data hardly makes this worthwhile at the present. It will be seen that errors of up to a magnitude do not alter the basic conclusions.

Naturally, I shall not attempt to determine cosmological parameters from equation (2), because there is the possibility of systematic error in the magnitude estimates, quite apart from the random errors already mentioned. In what follows we assume only that equation (2), with $A = 20{\cdot}5$ and $B = 5$, is valid to within a magnitude for the uncorrected visual magnitudes of radio galaxies. For the eighty-eight galaxies identified with $3CR$ radio sources for which no red-shifts are available, we estimate the red-shift from equation (2) with $A = 20{\cdot}5$, $B = 5$. For a total of 142 strong radio galaxies we then investigate the distribution of intrinsic radio luminosity against volume, in various cosmological models: we wish to test whether, in any given range of radio luminosity, equal numbers of sources are found in equivalent volumes of space. The total volume of space in which sources of a given luminosity are visible is limited by (i) the limiting radio flux-level of the $3CR$ catalogue and (ii) for sources of sufficiently high radio luminosity, a more severe limitation arises from the limiting optical magnitude of about 20 magnitudes, which we assume to be equivalent to the restriction $z \leq 0{\cdot}5$. For each range of radio-luminosity considered, the observable volume of space is divided into two. The numbers found are tabulated in Table 1. The columns labelled (a) refer to the nearer half of the observable volume, and (b) the farther.

Because the properties of the relativistic cosmological models do not differ much out to the red-shifts at which these galaxies are found, it is unlikely that the results will

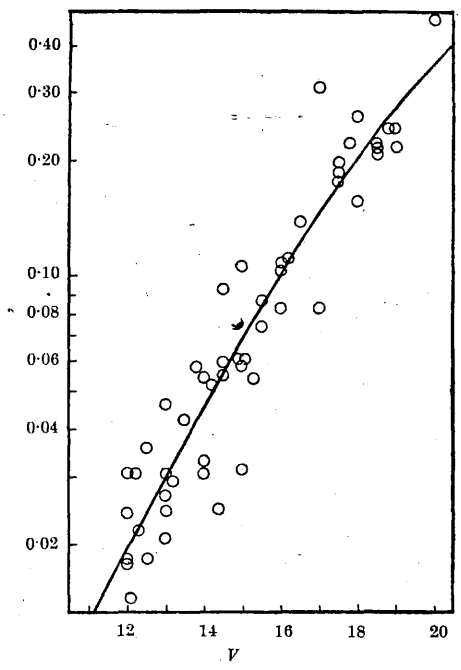

Fig. 1. Red-shift, z, against estimated visual magnitude, V, for fifty-four strong radio galaxies. Solid line: the locus $V = A + 5\log_{10}z + Bz$, with $A = 20{\cdot}5$, $B = 5$. The majority of the points are within one magnitude of this mean locus.

depend very sensitively on the cosmological parameters (the situation is quite different for the quasars, which are visible out to much larger red-shifts). The models we have investigated in detail are the Einstein–de Sitter ($\sigma_0 = q_0 = \frac{1}{2}$), Milne ($\sigma_0 = q_0 = 0$) and de Sitter ($\sigma_0 = 0$, $q_0 = -1$) models. These are the fixed points in the σ–q plane[6], and

Table 1. DISTRIBUTION OF RADIO-LUMINOSITIES OF STRONG RADIO GALAXIES IN TWO EQUIVALENT VOLUMES OF SPACE, FOR FOUR COSMOLOGICAL MODELS; (*a*) NEARER, (*b*) FURTHER, HALF OF THE OBSERVABLE VOLUME

Range of $\log_{10}P$ W (c/s)$^{-1}$ ster^{-1}	Cosmological models: Einstein–de Sitter		Milne		de Sitter		Steady state	
	(*a*)	(*b*)	(*a*)	(*b*)	(*a*)	(*b*)	(*a*)	(*b*)
27·4–27·9	0	0	0	0	0	1	0	1
26·9–27·4	2	1	2	1	3	0	3	0
26·4–26·9	1	0	3	0	4	1	3	1
25·9–26·4	16	19	14	24	14	32	13	34
25·4–25·9	8	33	8	30	6	23	5	24
24·9–25·4	10	15	10	13	11	13	11	13
24·4–24·9	9	7	9	7	8	5	8	5
23·9–24·4	9	5	9	5	10	5	10	5
23·4–23·9	5	2	5	2	4	2	4	2
Totals, $\log_{10}P > 23$	60	82	60	82	60	82	57	85
$\log_{10}P > 24{\cdot}9$	37	68	37	68	38	70	35	73

correspond to asymptotic states of homogeneous, isotropic, pressure-free universes. For comparison, the results obtained for the steady state model are given in column 4. From the last row of Table 1 we see that for all these four models the total number of strong radio galaxies found in the farther region (*b*) is significantly larger than in region (*a*). The distributions do not differ greatly from model to model.

The incompatibility of the steady state model (in which evolutionary effects are not permitted) with the radio galaxy data is perhaps more serious evidence against that model than the distribution of the quasars[1], because doubts have frequently been raised as to the cosmological nature of the large red-shifts of quasars. Conversely, an important impetus to these doubts, the prospect of attributing the steep radio source counts entirely to the quasars[18–20], would be removed if the present results are confirmed by more accurate data.

To test whether the results could be significantly affected by the uncertainties in the estimated magnitudes, the optical magnitudes of the eighty-eight galaxies for which we have estimated the red-shift using equation (2) have been decreased by (i) one magnitude and (ii) two magnitudes (increasing the magnitudes merely reinforces the inequality between the totals for regions (*a*) and (*b*)). The corresponding numbers of sources found in regions (*a*) and (*b*) are shown in Table 2 for all luminosities greater than 10^{23} W (c/s)$^{-1}$ ster^{-1}. Because from Table 1 we see that the inequality between the totals in regions (*a*) and (*b*) is caused primarily by sources with luminosity greater than $10^{24\cdot9}$ W (c/s)$^{-1}$ ster^{-1}, the totals are also shown for this restricted range of luminosity.

The numbers of sources found in regions (*a*) and (*b*) are still significantly different, even if the optical magnitudes of all the galaxies are in error by 2 magnitudes in the same direction, for the higher range of luminosity.

Table 2. MAXIMUM EFFECT OF ERRORS OF ±2 IN ESTIMATED VISUAL MAGNITUDES, AND OF VARYING VARIOUS PARAMETERS, ON THE TOTALS IN TABLE 1

Optical magnitudes all reduced by 1 ($A=20\cdot5$, $B=5$)	Einstein–de Sitter		Milne		de Sitter		Steady state	
	(*a*)	(*b*)	(*a*)	(*b*)	(*a*)	(*b*)	(*a*)	(*b*)
$\text{Log}_{10}P>23$	60	82	60	82	61	81	57	85
$\text{Log}_{10}P>24\cdot9$	35	60	35	61	36	62	31	66
Optical magnitudes all reduced by 2 ($A=20\cdot5$, $B=5$)								
$\text{Log}_{10}P>23$	65	77	65	77	65	77	63	79
$\text{Log}_{10}P>24\cdot9$	36	53	36	53	36	54	35	55

	Milne model, $A=20\cdot5$, $B=4$		Milne model, $A=20\cdot5$, $B=6$		Milne model ($A=20\cdot5$, $B=5$) galaxies with $V\leqslant19$ only	
	(*a*)	(*b*)	(*a*)	(*b*)	(*a*)	(*b*)
$\text{Log}_{10}P>23$	58	84	60	82	50	71
$\text{Log}_{10}P>24\cdot9$	36	71	37	68	27	57

A more likely situation is that errors of up to 1 magnitude exist, but in either direction, so that the totals found in Table 1 are probably not greatly in error. Rows 5 to 6 of Table 2 show the effect of changing the value of B in equation (2), which again does not alter the basic conclusion. Finally, because it may be argued that, in view of the paucity of red-shifts for galaxies with $19 \leq V \leq 20$, it is inadmissible to use an extrapolation of the form (2) in this range, row 6 shows the results obtained when attention is confined to galaxies with $V \leq 19$ ($z \leq 0{\cdot}3$). Incompleteness of the identifications in the fainter ranges of optical magnitude would merely reinforce our conclusions; against this must be offset the greater possibility of incorrect identifications.

These preliminary results provide the strongest impetus for the completion of red-shift measurements of radio galaxies in the 3*CR* catalogue. The evidence seems very strong that, for consistency with the usual cosmological models, some evolutionary factor must affect the distribution of the strong radio galaxies. The effect is clearest for galaxies with radio luminosity greater than $10^{25{\cdot}4}$ W (c/s)$^{-1}$ ster^{-1}, but, because such a small volume of space is visible for the lower ranges of luminosity, no clear effect would be expected for these anyway. Of the models proposed by Longair[19] in his attempt to explain the Cambridge radio source counts, his model (*d*), density evolution of all sources with radio luminosity greater than $10^{26{\cdot}8}$ W (c/s)$^{-1}$ ster^{-1}, is definitely unsuitable. But his model (*b*), luminosity evolution of all sources with luminosity greater than $10^{25{\cdot}4}$ W (c/s)$^{-1}$ ster^{-1}, is entirely in agreement with the present work (though Longair preferred to interpret this evolution as being caused by the quasars only). But it seems unproved that the evolution does not operate down to luminosities a factor of, say, 10 lower than this.

Further evidence of this evolutionary effect is that, if the thirty-four 3*CR* radio galaxies with luminosities less than 10^{25} W (c/s)$^{-1}$ ster^{-1} are excluded, a number-count slope of about $-1{\cdot}9$ is obtained for 3*CR* radio galaxies, as opposed to $-1{\cdot}55$ reported by Veron[20] for all 3*CR* radio galaxies.

Possible Forms of Evolution

To test evolutionary hypotheses, the luminosity-volume test is easily modified; we investigate the distribution of "corrected" luminosity against "weighted" volume[5,6]. The evolutionary hypotheses tested in ref. 6 for the quasars were

luminosity evolution

(i) negative power-law dependence on $R(t)$.

$$\bar{P}(z) \propto (1+z)^{Q_L}$$

(ii) negative exponential dependence on $R(t)$,

$$\bar{P}(z) \propto \exp\left\{(1+z_L)\cdot\left(1-\frac{1}{1+z}\right)\right\}$$

density evolution:

(iii) negative power-law dependence on $R(t)$,

$$\eta(z) \propto (1+z)^{Q_D}$$

(iv) negative exponential dependence on $R(t)$,

$$\eta(z) \propto \exp\left\{(1+z_D)\cdot\left(1-\frac{1}{1+z}\right)\right\}$$

where $\bar{P}(z)$ gives the behaviour with epoch of the luminosity of any particular class of sources, and $\eta(z)$ is the co-ordinate number-density of sources.

The advantage of evolutions of the form (ii) and (iv) is that they do not require arbitrary truncation of the evolving population to obtain a finite contribution to the integrated background radiation.

The values of the parameters Q_L, z_L, Q_D, z_D necessary to give consistency of the radio galaxy data with various cosmological models are given in columns 1 to 4 in Table 3, together with the corresponding values for the quasars, taken from ref. 2. There is remarkably close agreement of the parameters required for the exponential evolutions of both quasars and radio galaxies (columns 2 and 4). In view of the arbitrariness of the particular forms of evolution we have considered, this agreement cannot be taken as evidence of a link between radio galaxies and quasars. But if such a link is accepted (for example, ref. 21), then these forms of evolution seem very promising. Their consistency with radio-source counts to low flux-levels, and with the integrated radio background, will be discussed in subsequent papers.

Although our discussion has been confined to three particular relativistic models, similar results are found for all models in the range

$$0 \leq q_0 \leq 3, \quad -1 \leq q_0 \leq 3$$

It seems that for radio galaxies the evolutionary factor far outweighs any differences between the cosmological models. The explanation of this evolution must await more detailed knowledge of the structure of radio galaxies:

Table 3. EVOLUTIONARY PARAMETERS FOR RADIO GALAXIES (RG) AND QUASARS (Q)

		Luminosity evolution		Density evolution	
		Q_L	z_L	Q_D	z_D
Einstein–de Sitter	RG	4 ± 1	4 ± 1	9 ± 2	9 ± 3
	Q	Not consistent	6 ± 1	6 ± 1	11 ± 3
Milne	RG	4 ± 1	4 ± 1	9 ± 2	10 ± 3
	Q	2·5 ± 0·5	6 ± 1	5 ± 1	11 ± 3
de Sitter	RG	5 ± 1	5 ± 1	9 ± 1	10 ± 1
	Q	3 ± 1	6 ± 2	4 ± 1	11 ± 4

whether, for example, they correspond to early or late stages in the life of a galaxy, and whether interaction with an intergalactic gas or magnetic field is an essential feature of their activity.

I thank Professor W. H. McCrea for advice and encouragement throughout the course of this work, which was performed during the tenure of a Science Research Council studentship at the Astronomy Centre, University of Sussex. Computing was performed by the Computer Centre, University of Sussex. Professor M. Schmidt made helpful criticisms.

Note added in proof. The present results, when combined with those of ref. 6, show that it is not possible to attribute the steep radio source-counts to observational bias, as claimed recently by D. L. Jauncey (*Nature*, **216**, 877; 1967).

Received November 23, 1967.

[1] Rees, M. J., and Sciama, D. W., *Nature*, **213**, 374 (1967).
[2] Burbidge, G. R., and Burbidge, E. M., *Astrophysics J.*, **148**, L107 (1967).
[3] Arp, H., *Astrophys. J.*, **148**, 321 (1967).
[4] Burbidge, G. R., and Hoyle, F., *Nature*, **216**, 351 (1967).
[5] Rowan-Robinson, M., *Nature*, **212**, 1556 (1966).
[6] Rowan-Robinson, M., *Mon. Not. Roy. Astro. Soc.* (in the press).
[7] Refsdal, S., and Stabell, R., *Mon. Not. Roy. Astro. Soc.*, **132**, 379 (1966).
[8] Sandage, A. R., *Astrophys. J.*, **141**, 1560 (1965).
[9] Maltby, P., Matthews, T. A., and Moffet, A. T., *Astrophys. J.*, **137**, 153 (1963).
[10] Matthews, T. A., Morgan, W. W., and Schmidt, M., *Astrophys. J.*, **140**, 35 (1964).
[11] Schmidt, M., *Astrophys. J.*, **141**, 1 (1965).
[12] Sandage, A. R., *Astrophys. J.*, **145**, 1 (1966).
[13] Burbidge, E. M., *Astrophys. J.*, **149**, L51 (1967).
[14] Bennett, A. S., *Mem. Roy. Astro. Soc.*, **68**, 163 (1962).
[15] Wyndham, D. J., *Astrophys. J.*, **144**, 459 (1966).
[16] Humason, M. L., Mayall, N. U., and Sandage, A. R., *Astronom. J.*, **61**, 97 (1956).
[17] McCrea, W. H., *Zeit. Astrophys.*, **15**, 69 (1935).
[18] Sciama, D. W., and Saslaw, W. C., *Nature*, **210**, 348 (1966).
[19] Longair, M. S., *Mon. Not. Roy. Astro. Soc.*, **133**, 421 (1966).
[20] Veron, P., *Ann. d'Astrophys.*, **29**, 231 (1967).
[21] Ryle, M., and Longair, M. S., *Mon. Not. Roy. Astro. Soc.*, **136**, 123 (1967).

Printed in Great Britain by Fisher, Knight & Co., Ltd., St. Albans.

Mon. Not. R. astr. Soc. (1968) **141**, 445–458.

ON COSMOLOGICAL MODELS WITH AN ANTIPOLE

M. Rowan-Robinson

(Received 1968 May 1)

Summary

The properties of Lemaître models are summarized and the luminosity–volume test is used to determine which of these models are consistent with the distributions in space of quasars and radio-galaxies respectively. Ranges of models can be found consistent with either, but not both, of these classes of radio-source, including models which could account for the anomalous absorption redshift of 1·95 in quasars. The integrated extragalactic radio background provides an important additional constraint to the problem. No model is found to agree with the observed radio source-counts, without the introduction of evolutionary effects.

1. *Introduction.* If the redshifts of quasars are cosmological, their distribution in space is inconsistent with a wide range of cosmological models (**1**)–(**3**). The distribution in space of galaxies identified with radio-sources in the 3C catalogue also appears to be inconsistent with relativistic cosmological models having $0 \leqslant \sigma_0 \leqslant 3$, $-1 \leqslant q_0 \leqslant 3$, where $\sigma_0 = 4\pi G\rho_0/H_0^2$, $q_0 = -(R\ddot{R}/\dot{R}^2)_0$, $H = (\dot{R}/R)_0$, $R(t)$ is the scale-factor of the expanding universe and the subscript zero refers to the present epoch (**4**).

Consistency of both quasars and radio-galaxies with such models can be achieved by supposing that the co-moving coordinate number-density of sources, or their luminosity, or both, have a negative exponential dependence on the scale factor, $R(t)$ (**4**).

An alternative approach is to consider the more unusual models associated with the name of Lemaître, in which there is the possibility of an antipole (**5**)–(**9**). In addition to the possibility of accounting for the distribution of quasars and radio-galaxies in space, these models can provide a cosmological explanation of the anomalous absorption redshift reported by Burbidge & Burbidge (**10**). Indeed, Shklovsky (**6**) has suggested that this anomalous absorption redshift is one of the strongest pieces of evidence that the redshifts of quasars are cosmological. Solheim (**9**) has suggested a further possible piece of evidence in favour of models with an antipole, that there exists a positive correlation between radio-sources in the 4C catalogue in opposite directions in the sky.

In this paper the luminosity–volume test (**2**), (**4**) is used to determine which cosmological models are consistent with the distributions in space of the quasars and of the radio-galaxies. Important additional constraints are provided by the radio source-counts to low flux-level and the integrated extra galactic radio background at 178 MHz.

2. *Properties of Lemaître models.* For homogeneous, isotropic, pressure-free cosmological models, Einstein's equations reduce to

$$\Lambda/3 = (\sigma_0 - q_0)H_0^2$$
$$kc^2/R_0^2 = (3\sigma_0 - q_0)H_0^2$$

where, for Lemaître models, $\Lambda > 0$ and $k = +1$. Thus

$$\Lambda = \Lambda_c(1+\epsilon) \qquad \text{where} \qquad \Lambda_c = (c^3/4\pi G\rho_0 R_0^3)^2 \tag{1}$$

and

$$1+\epsilon = \frac{27\sigma_0^2(\sigma_0 - q_0)}{(3\sigma_0 - q_0 - 1)^3}. \tag{2}$$

If $\epsilon = 0$ and $Z = (3\sigma_0 - q_0 - 1)/3\sigma_0 = Z_m$, where $Z = 1 + z = R_0/R$ and z is the redshift, then $\dot{R} = 0$, $\ddot{R} = 0$ and the universe is static with cosmological repulsion just balancing gravity. If $0 < Z_m < 1$, this state is attained as $t \to \infty$, and if $1 < Z_m$, the universe expanded out of this state at $t = -\infty$.

If $\epsilon > 0$, $Z_m > 1$, the scale-factor, $R(t)$, passes through a point of inflection at an epoch given by $Z = Z_m(1+\epsilon)^{1/3}$. If $0 < \epsilon \ll 1$, the universe 'stagnates' near this point of inflection with $Z \simeq Z_m$.

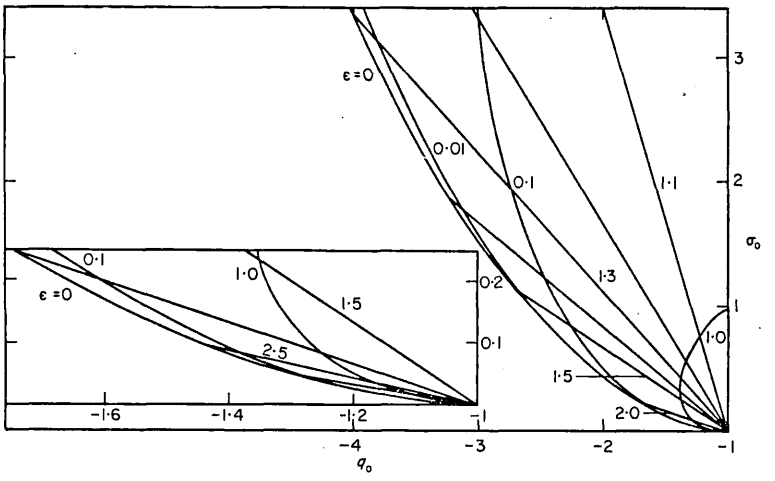

FIG. 1. σ_0–q_0, *the model diagram, showing lines of constant* Z_m *and* ϵ. *The straight lines radiating from* $(\sigma_0, q_0) = (0, -1)$ *are lines of constant* Z_m. *The curved lines are* $\epsilon = 0$, 0·01, 0·1, 1·0. *A portion of the diagram near* $(\sigma_0, q_0) = (0, -1)$ *is shown enlarged (inset).*

Using equations (1) and (2),

$$\sigma_0 = 1/\{Z_m^3(1+\epsilon) + 2 - 3Z_m\} \tag{3}$$

$$q_0 = (1 - Z_m^3(1+\varepsilon))/\{Z_m^3(1+\epsilon) + 2 - 3Z_m\} \tag{4}$$

so

$$1 + q_0 = -3\sigma_0(Z_m - 1).$$

Lines of constant Z_m and ϵ in the $\sigma_0 - q_0$ plane are shown in Fig. 1; the lines of constant Z_m are straight lines radiating from $(0, -1)$. The contribution of observed material in galaxies to ρ_0 is estimated by Oort (**15**) as 7×10^{-31} g cm^{-3}. Thus $\sigma_0 \geqslant 0{\cdot}035$, and from equation (3), $Z_m \leqslant 3{\cdot}3$. We see that $Z_m > 1$ implies $q_0 < -1$, in contradiction to the evidence from the brightest galaxies in clusters (**16**). However, Tinsley (**17**) has recently shown that effects of galactic evolution would be more pronounced in models with $q_0 < -1$, so that they can be reconciled with the observations.

3. *Cosmological explanations of the anomalous absorption redshift at* 1·95

3.1 If $0 < \epsilon \ll 1$, photons from sources with $Z > Z_m$ (> 1) spend a large part of their travel-time traversing material with $Z \simeq Z_m$ (**6**). Using the fact that the anomalous absorption redshifts of quasars satisfy $z = 1{\cdot}95 \pm 0{\cdot}01$ (**10**), Kardashev (**7**) calculates that $\epsilon = 2.10^{-5}$. Actually there is a slight error in this calculation since the optical depth

$$\tau(z) = \bar{n}_0 \bar{\Sigma}_0 \int_1^{1+z} \frac{Z^3 . R dr}{1 + \frac{1}{4}kr^2}$$

where $\bar{n}_0$ is the average particle density, and $\bar{\Sigma}_0$ the average cross-section at the present epoch. Thus

$$\tau(z) = n_0 \bar{\Sigma}_0 R_0 \int_1^{1+z} \frac{Z^2 dZ}{Q}$$

$$Q = \left\{\frac{\sigma_0 - q_0 + (1 + q_0 - 3\sigma_0)Z^2 + 2\sigma_0 Z^3}{3\sigma_0 - q_0 - 1}\right\}^{1/2}$$

$$= \{\tfrac{2}{3}Z^3 Z_m^{-1} + \tfrac{1}{3}Z_m^2(1 + \epsilon) - Z^2\}^{1/2},$$

using equations (3) and (4). Kardashev (**7**) has a factor $(1 + \epsilon)$ multiplying the first term in the bracket (also an incorrect sign for the third term, which is presumably a printing error, since it appears correctly in the Russian version of this letter, in *Astr. Zirk.*, **430** (1967)). His equation (10) should then read

$$\epsilon = 3Q_m^2/(1 + z_m)^2 = 6 \times 10^{-5}.$$

However, since ϵ depends on the square of the dispersion in the absorption redshift and also on the square of the quantity $\bar{n}_0 \bar{\Sigma}_0$, a factor of 3 is not too relevant.

3.2 A further consequence of the stagnation of the universe near $Z = Z_m$ is that the photons from a distant source may have time to make a complete circuit of the closed universe.

The luminosity distance, D, defined by

$$\mathscr{F} = \mathscr{f} + 2 \log_{10} D(z) - 0{\cdot}4K(z) \qquad (6)$$

where $\mathscr{F} = \log_{10} P$; P is the monochromatic luminosity

$\mathscr{f} = \log_{10} S$; S is the monochromatic flux

and $K(z)$ is the K-correction (see, for example, Appendix 1 of Ref. (**2**)), is given by

$$D(z) = R_0 Z \sin \chi(z)$$

where

$$\sin \chi(z) = r/(1 + \tfrac{1}{4}kr^2)$$

and

$$\chi(z) = \int_1^{1+z} \frac{dZ}{Q}.$$

Thus

$$\frac{\partial \chi}{\partial \epsilon} = -\frac{1}{2} \int_1^{1+z} \frac{Z_m^2}{3Q^3} dZ < 0$$

and in fact $\chi(z) \to \infty$ as $\epsilon \to 0$ if $1 + z \geqslant Z_m$. Sources such that $\chi(z)$ is an integral

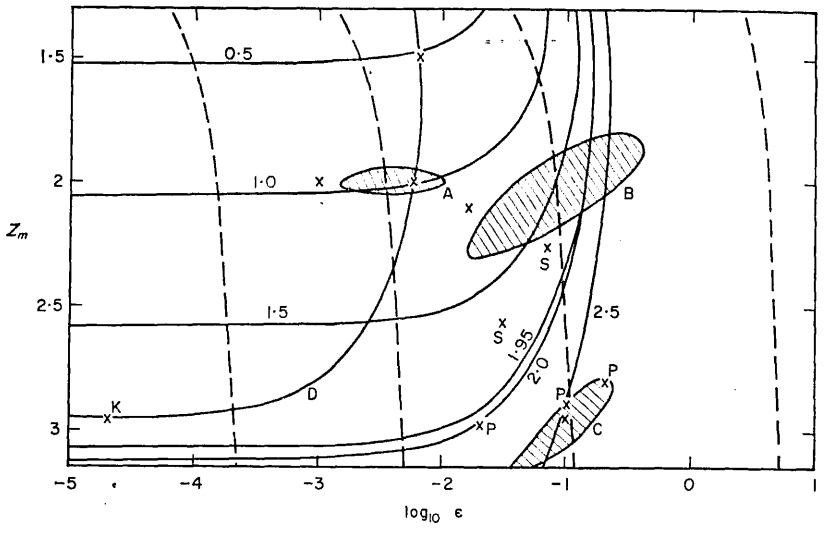

FIG. 2. *Z_m–ϵ. The four broken lines correspond from right to left to $\chi(\infty) = \pi, 2\pi, 3\pi, 4\pi$ respectively. The continuous line labelled D is the locus $\chi(1{\cdot}95) = 2\pi$. The other continuous lines are $\chi(z) = \pi$, where $z = 0{\cdot}5, 1{\cdot}0, 1{\cdot}5, 1{\cdot}95, 2{\cdot}0, 2{\cdot}5$. The shaded areas A,B, C denote models consistent with the distribution in space of the quasars. Crosses denote particular models advocated by various authors (P = Petrosian, Salpeter & Szekeres: S = Solheim: K = Kardashev) and other particular models discussed in this paper.*

multiple of π appear to be infinitely bright. The light from a source at redshift such that $\chi(z) > \pi$ passes through a single point, the antipole. If $\chi(z) > 2\pi$, photons will have passed the observer at an earlier epoch. Thus if sufficiently opaque material is situated at the antipole, or if such material existed in the vicinity of the Earth at an earlier epoch, absorption lines displaced by the corresponding redshifts would be produced.*

The requirement is rather severe,

$$n\Sigma \sim \bar{n}_0\bar{\Sigma}_0 \cdot \frac{20c}{H_0 L}$$

where L is the dimension of the opaque region. Thus for a region of galactic dimensions, $L \sim 10^5$ light years, $n\Sigma \sim 2 \cdot 10^6 \bar{n}_0\bar{\Sigma}_0$.

Fig. 2 shows the loci $\chi(\infty) = \pi, 2\pi, 3\pi, 4\pi$ in the $Z_m - \epsilon$ plane. No antipole occurs in models to the right of the $\chi(z) = \pi$ curve. Also shown are the loci of models such that $\chi(z) = \pi$ for $z = 0{\cdot}5, 1, 1{\cdot}5, 2, 2{\cdot}5$ and such that $\chi(1{\cdot}95) = \pi, 2\pi$. The latter two loci give models that could explain the anomalous absorption redshift of 1·95 by method (b). The line of models $Z_m = 2{\cdot}95$ corresponds to method (a).

4. *Luminosity–volume test.* If the fraction of material in the form of sources in a given range of luminosity is independent of epoch, then the distribution of such sources should be uniform with respect to coordinate volume, $V(z)$, where

$$V(z) = \int_0^z \frac{4\pi r^2 dr}{(1+\frac{1}{4}kr^2)^3}$$

$$= 2\pi(\chi - \sin\chi\cos\chi).$$

* This suggestion was made to me by J. Solheim and M. Rees.

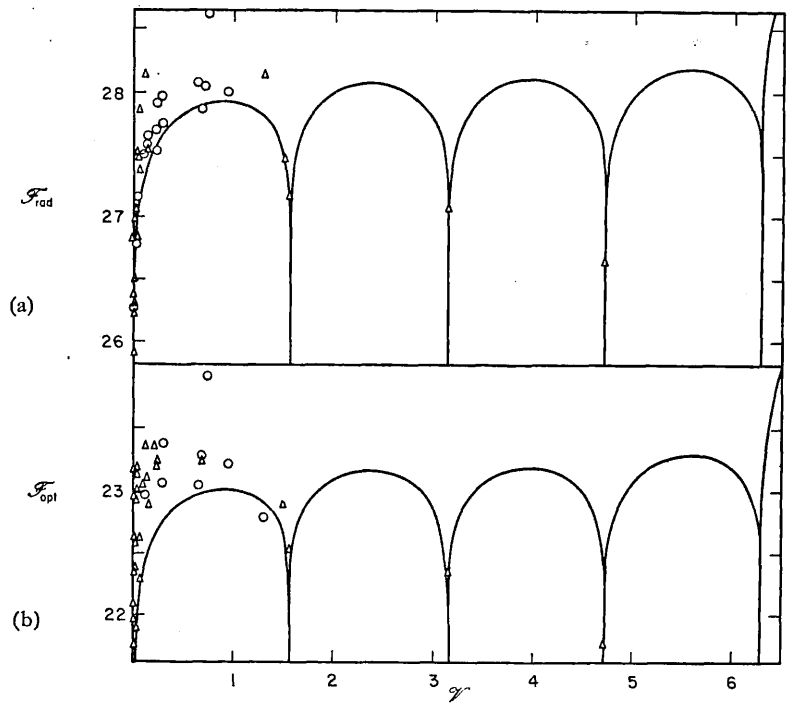

FIG. 3. *The distribution of (a) radio and (b) optical, luminosities of 3C quasars against volume for the model* $Z_m = 2{\cdot}95$, $\epsilon = 0{\cdot}00002$. *In Fig. 3(a), circles denote sources with* $\mathscr{F}_{\text{opt}} \geqslant \mathscr{F}_1 = 23{\cdot}05$; *triangles denote sources with* $\mathscr{F}_{\text{opt}} < \mathscr{F}_1$. *In Fig. 3(b), circles denote sources with* $\mathscr{F}_{\text{rad}} \geqslant \mathscr{F}_2 = 27{\cdot}95$; *triangles denote sources with* $\mathscr{F}_{\text{rad}} < \mathscr{F}_2$. *The units of luminosity are* $w(c/s)^{-1}\ ster^{-1}$ (*and* $\mathscr{F} = \log_{10} P$). *The continuous curves denote the cut-offs imposed by the limiting 3C flux-level of* $9{\cdot}10^{-26}\ w\ m^{-2}(c/s)^{-1}$ *and by the limiting visual magnitude of about 19 for quasars, respectively.*

4.1 *Quasars.* The distributions of radio and optical luminosities of quasars against volume are shown in Fig. 3(a), (b) for the model proposed by Kardashev. The data used is that given in Table I of Ref. (2) and the luminosities are calculated from equation (6) above. The effect of the limiting 3C flux-level of 9.10^{-26} w m^{-2} (c/s)$^{-1}$ is shown by the continuous curve in Fig. 3(a), and the limit $V = 19$ magnitudes in Fig. 3(b). The radio/optical distribution may be corrected for the effect of optical/radio selection by confining attention to sources with higher optical/radio luminosity, i.e. those denoted by a circle. The distributions are strikingly non-uniform.

On the other hand in the model with $Z_m = 2{\cdot}95$, $\epsilon = 0{\cdot}1$, which is close to one of those advocated by Petrosian, Salpeter & Szekeres (5), the distributions are comparatively uniform (Fig. 4(a), (b)). However, since the antipole occurs at redshift (z) 2·58, sources of high flux-density ought to be visible corresponding to this remoter epoch. Some additional hypothesis would be needed to explain the absence of these, for example the gravitational defocusing action of inhomogeneities (5).* Models in the shaded regions B and C of Fig. 2 fall into this category.

* Although the condition for this effect to be significant, that an appreciable fraction of the material in the universe be condensed into galaxies, may not be satisfied at the early epochs corresponding to these large redshifts.

Still more satisfactory are a range of models with $Z_m = 2{\cdot}0$. The radio and optical luminosity-volume diagrams for that with $\epsilon = 0{\cdot}0056$, in which

$$\chi(1{\cdot}95) = 2\pi,$$

are shown in Fig. 5(a), (b). In this model and those which fall in the shaded region A of Fig. 2, the corrected optical and radio distributions are uniform with respect to volume; a natural explanation is provided of the absence of quasars in 3C with redshifts greater than about 2·2.

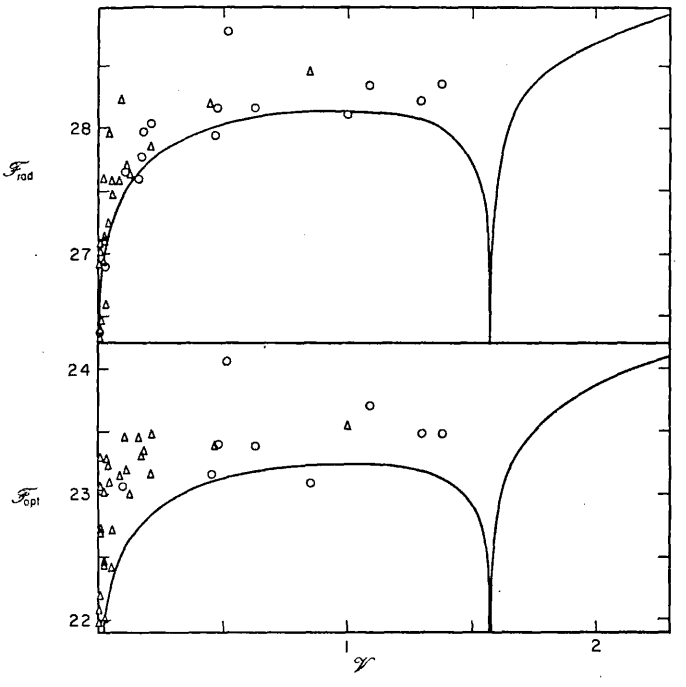

FIG. 4. *As in Fig.* 3, *but with* $\epsilon = 0{\cdot}1, \mathscr{F}_1 = 23{\cdot}15, \mathscr{F}_2 = 28{\cdot}05$.

Models corresponding to values of (Z_m, ϵ) outside the regions A, B, C of Fig. 2 are not consistent with the present data for quasars, unless the coordinate number-density of sources, or their luminosity, varies with epoch. Some examples are shown in Fig. 6: the sources in ranges of luminosity affected by selection effects have been omitted. The situation might change if the identifications of quasars in 3C are very incomplete and unrepresentative. But, for example, if all quasars with visual magnitude fainter than 18 are given a twin, to correct for the selection effect postulated by Penston & Rowan-Robinson (**12**), the regions of the $Z_m - \epsilon$ plane in which consistent models fall do not change significantly.

Thus a rather small range of models is consistent with the present data on the distribution of the quasars in space. Of these, three can also account for the anomalous 1·95 redshift:

$Z_m = 2{\cdot}0, \quad \epsilon = 0{\cdot}0056$ (for which $\chi(1{\cdot}95) = 2\pi$)

$Z_m = 2{\cdot}0, \quad \epsilon = 0{\cdot}14$ (for which $\chi(1{\cdot}95) = \pi$)

and

$Z_m = 2{\cdot}95, \quad \epsilon = 0{\cdot}1.$

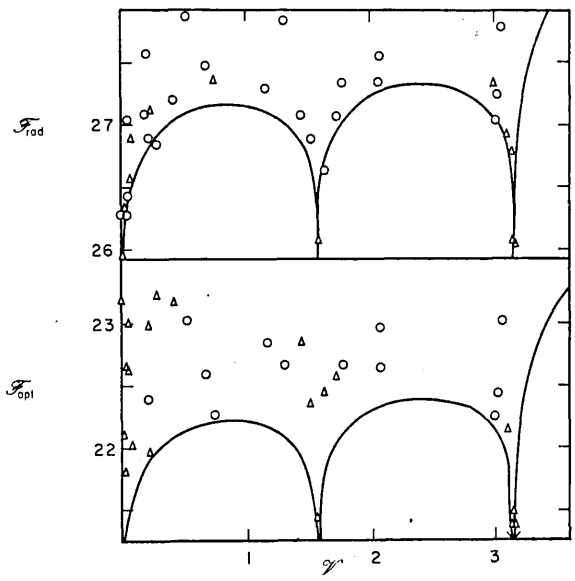

FIG. 5. *As in Fig. 3, but with* $Z_m = 2{\cdot}0$, $\epsilon = 0{\cdot}0056$, $\mathscr{F}_1 = 22{\cdot}35$, $\mathscr{F}_2 = 27{\cdot}25$.

For the latter model, Kardashev's argument would imply an optical depth of only 10^{-2} for objects with $z \simeq Z_m - 1$, so that it is hard to see how absorption lines could be produced.

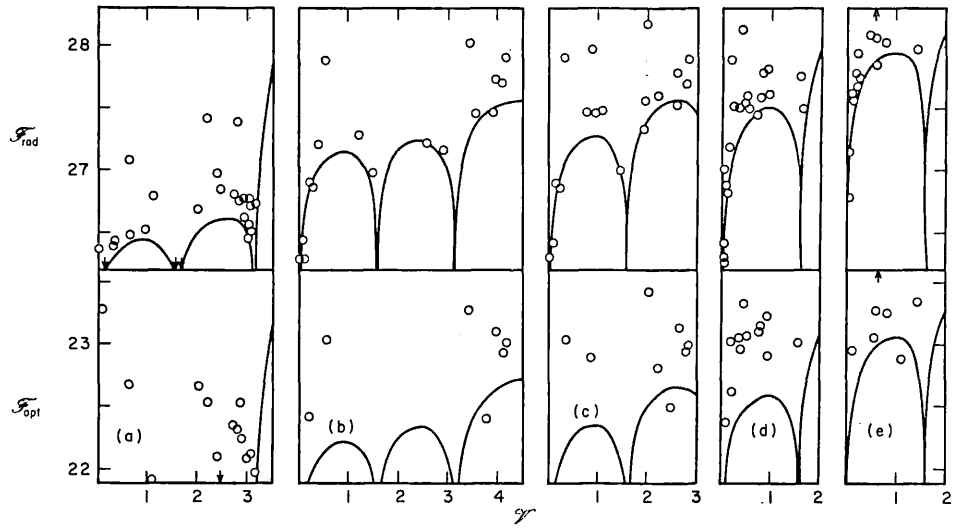

FIG. 6. *Distribution of radio and optical luminosities against volume (corrected for effects of optical and radio selection respectively) for the models:*

(a) $Z_m = 1{\cdot}5$, $\epsilon = 0{\cdot}00626$,
(b) $Z_m = 2{\cdot}0$, $\epsilon = 0{\cdot}001$,
(c) $Z_m = 2{\cdot}1$, $\epsilon = 0{\cdot}016$,
(d) $Z_m = 2{\cdot}262$, $\epsilon = 0{\cdot}068$,
(e) $Z_m = 2{\cdot}98$, $\epsilon = 0{\cdot}02$.

4.2 *Radio-galaxies.* In Ref. (4) the luminosity–volume test was applied to the radio-luminosities of the radio-galaxies in 3C, estimating the redshifts of those galaxies not yet measured from their estimated apparent visual magnitudes. Provided the latter magnitudes are not in error by more than ± 2, the distribution of the radio-galaxies in space is inconsistent with a wide range of cosmological models. The situation is not much altered for most of the cosmological models considered above. In fact, the only models found to be consistent with the present data for the radio-galaxies are those with an antipole at $z < 0{\cdot}45$, which requires $Z_m < 1{\cdot}5$ (from Fig. 2). For example the model with $Z_m = 1{\cdot}4$, $\epsilon = 0{\cdot}006$ is consistent with the distribution of the radio-galaxies and has $\chi(1{\cdot}95) = 2\pi$. However, it is highly inconsistent with the distribution of the quasars and gives an average density of the universe of $3{\cdot}6 \times 10^{-29}$ g cm^{-3}.

Fig. 7 shows the distribution of radio-luminosity against volume for 142 strong ($P \geqslant 10^{23{\cdot}5}$ w ster^{-1} (c/s)$^{-1}$) 3C radio-galaxies for the model $Z_m = 2{\cdot}0$, $\epsilon = 0{\cdot}0056$. Crosses denote galaxies whose redshifts have been measured, circles those whose redshifts have been estimated from

$$V = 20{\cdot}5 + 5 \log_{10} z + 5z \qquad (7)$$

where V is the estimated visual magnitude. Most galaxies whose redshifts are known satisfy this relation to within one magnitude and all to within two magnitudes. The continuous line shows the effect of the limiting 3C flux-level and the limitation $z \lesssim 0{\cdot}4$ imposed by the limiting visual magnitude of 20. The dotted line divides the

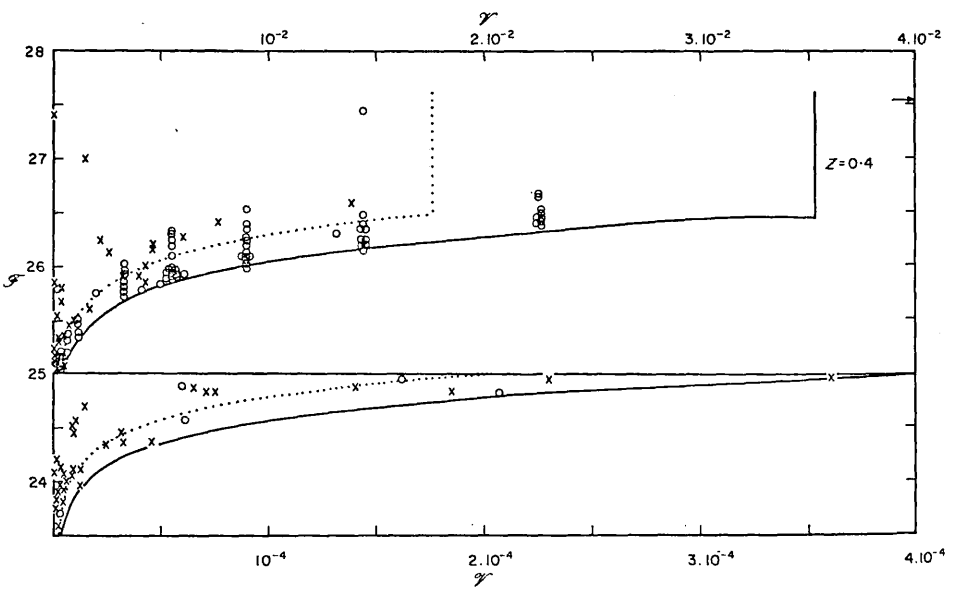

FIG. 7. *Distribution of radio-luminosity of 3C radio-galaxies against volume for the model with $Z_m = 2$, $\epsilon = 0{\cdot}0056$. Crosses denote galaxies whose redshifts are known, circles those whose redshifts have been estimated from equation (7). The upper volume scale refers to luminosities, $\mathscr{F} > 25$: the lower volume scale refers to $\mathscr{F} < 25$. The observable region is limited by the limiting 3C flux-level (continuous curve) and by the limiting optical magnitude of about 20 for galaxies (corresponding to $z \sim 0{\cdot}4$). The dotted curve divides the observable region in half at any given luminosity. The arrow to the right of the diagram denotes 3C 295, which has $V = 0{\cdot}11$ in this model.*

observable region in half at any given luminosity.* The number of radio-galaxies found in the near and further half of space are 61 and 80 respectively, and for sources with $P \geqslant 10^{25}$ w ster^{-1} (c/s)$^{-1}$, 39 and 69 respectively. The latter disposition has a probability of only 0·004 of occurring by chance. If all magnitudes are decreased by 2, these figures change to 65 : 76 and 39 : 54 (probability 0·1): but this is a very large systematic error to postulate.

This conclusion, that unless large errors exist in the present data no Lemaître model is consistent with the distributions in space of both quasars and radio-galaxies, should be contrasted with the result of introducing exponential evolutions into the more familiar models, where very similar rates of evolution were required for consistency with both quasars and radio-galaxies (**2**), (**4**). Of course, if evolutionary effects are now introduced into the Lemaître models, consistent models can be found: this may be necessary if the other evidence in favour of models with an antipole (**6**), (**9**) is confirmed by subsequent observations.

5. *Integrated radio background.* An important additional piece of evidence is the fact that at 178 Mc/s the integrated extragalactic radio background has a brightness temperature $T = 30 \pm 7^\circ$ (**20**). If the coordinate number-density of sources having luminosity between P and $P+dP$ is $\eta(P)dP$, then

$$2KT\nu_0^2/c^2 = \int_0^\infty \eta(P)P\,dP \int_1^{\nu_b/\nu_0} Z^{-\alpha} R \frac{dr}{1+\frac{1}{4}kr^2}$$

where ν_0 is the frequency of observation, K is Boltzmann's constant and

$$P(\nu) \propto \nu^{-\alpha},\ \nu_0 \leqslant \nu \leqslant \nu_b,$$
$$= 0,\ \nu > \nu_b.$$

Thus

$$T = \frac{c^2}{2K\nu_0^2}(c/H_0)\overline{\eta P}.X(\alpha, \sigma_0, q_0) \tag{8}$$

where

$$\overline{\eta P} = \int_0^\infty \eta(P)P\,dP$$

and

$$X(\alpha, \sigma_0, q_0) = \int_1^{\nu_b/\nu_0} Z^{-\alpha} d(H_0 t).$$

X is a weighted age of the universe, where this age is reckoned in units of the Hubble time H_0^{-1}. This is illustrated by Fig. 8, which shows the loci in the $Z_m - \epsilon$ plane of models with equal age and with equal $X(0{\cdot}75, \sigma_0, q_0)$. The ratio of these quantities lies between 1 and 2 for most models considered in this paper.*

If $\alpha \geqslant 0$, $X < H_0 t_0$, which is finite if $\Lambda < \Lambda_c$ (even if $\nu_b \to \infty$). But if $\Lambda = \Lambda_c$ and $\nu_b/\nu_0 > Z_m$, then $Z^{-\alpha} > Z_m^{-\alpha}$ for all t, so that

$$X > \int_1^{Z_m} d(H_0 t),$$

which is divergent. Thus in the Eddington–Lemaître models ($\Lambda = \Lambda_c$), Olber's

* Actually these two loci are dependent on the spectral index of the sources: this has been taken into account in the computations. See, for example, Kafka (**18**).

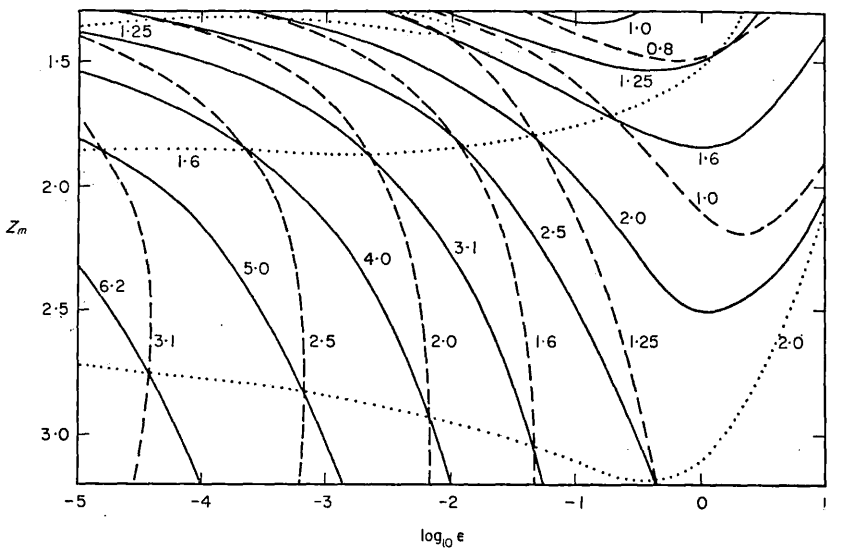

FIG. 8. Z_m–ϵ, *showing lines of constant* H_0t_0 *(continuous curves),* X *(broken curves) and* H_0t_0/X *(dotted curves). The temperature of the integrated extra-galactic radio background is proportional to* X*, which behaves like a weighted age of the universe.*

paradox is unresolved even though the universe is expanding (but is resolved by assuming sources radiated only for a finite time in the past).

If a dispersion in spectral indices is assumed, and the fraction of sources having spectral index between α and $\alpha+d\alpha$ is $\phi(\alpha)d\alpha$ (assumed independent of P and t), then

$$T = \frac{c^2}{2K\nu_0^2}\,(c/H_0)\overline{\eta P}.\bar{X}(\alpha_0, q_0) \tag{9}$$

where

$$\bar{X}(\alpha_0, q_0) = \int_{-\infty}^{\infty} X(\alpha, \sigma_0, q_0)\phi(\alpha)\,d\alpha$$

$$= \int_1^{\nu_b/\nu_0} d(H_0t) \int_{-\infty}^{\infty} Z^{-\alpha}\phi(\alpha)\,d\alpha.$$

The observed distribution (13) can be reasonably well represented by a Gaussian distribution, that is

$$\phi(\alpha) = (1/s\sqrt{2\pi}).\exp\{-(\alpha-\bar{\alpha})^2/2s^2\}$$

with $\bar{\alpha} = 0{\cdot}75$, $s = 0{\cdot}2$. Thus

$$\int_{-\infty}^{\infty} Z^{-\alpha}\phi(\alpha)\,d\alpha = Z^{-\bar{\alpha}+1/2s^2\log_e Z}$$

and

$$\bar{X}(\alpha_0, q_0) = \int_1^{\nu_b/\nu_0} Z^{-\bar{\alpha}+1/2s^2\log_e Z}\,d(H_0t).$$

The requirement that ν_b/ν_0 be finite is now essential to the resolution of Olber's paradox.

* Felten's calculation (22) of the energy density of starlight, in which he took $X \sim 1$, would have to be modified for the cosmological models considered here. The same applies to Veron's calculation (23) of the integrated extragalactic radio background.

In the de Sitter, Milne and Einstein–de Sitter models, $\bar{\chi}$ may be evaluated as a series of incomplete gamma-functions. For example, in the de Sitter model

$$\bar{X}(0, -1) = \int_1^{\nu_b/\nu_0} Z^{-\bar{\alpha}+1/2s^2 \log_e Z} dZ/Z$$

$$= \frac{1}{\bar{\alpha}} \int_0^x \exp(-y + \tfrac{1}{2}s^2y^2/2\bar{\alpha}^2) dy \qquad (10)$$

where $y = \bar{\alpha} \log_e Z$, $x = \bar{\alpha} \log_e \nu_b/\nu_0$

$$= \frac{1}{\bar{\alpha}} \int_0^x e^{-y} \left\{ \sum_{n=0}^{\infty} \frac{1}{n!} (s^2y^2/2\bar{\alpha}^2)^n \right\} dy$$

$$= \frac{1}{\bar{\alpha}} \sum_{n=0}^{\infty} \frac{1}{n!} (s^2/2\bar{\alpha}^2)^n \gamma(2n+1, x) \qquad (11)$$

where the incomplete Γ-function,

$$\gamma(a, x) = \int_0^x e^{-y} y^{a-1} dy.$$

So if $\bar{\alpha} = 0{\cdot}75$, $s = 0{\cdot}2$ and $\nu_b = 2 \times 10^5$ MHz, the first few terms give (23)

$$\bar{X}(0, -1) \simeq 1{\cdot}333\{0{\cdot}996 + 1{\cdot}60(s^2/2\bar{\alpha}^2) + 5{\cdot}64(s^2/2\bar{\alpha}^2)^2\}$$

$$= 1{\cdot}413.$$

whereas

$$X(\bar{\alpha}, 0, -1) = \frac{0{\cdot}996}{0{\cdot}75} = 1{\cdot}328.$$

Thus the error in assuming all sources to have the mean spectral index is considerably less than the uncertainties in $\overline{\eta P}$ and T. The situation is very similar for the Milne and Einstein–de Sitter models, except that $\bar{\alpha}$ should be replaced in equations (10) and (11) by $\bar{\alpha}+1$ and $\bar{\alpha}+3/2$, respectively. In the remainder of this paper we shall neglect the effect of the dispersion in spectral indices.

The application of the luminosity–volume test described in Section 4.2 above showed that for the radio-galaxies $\eta(P)$ was not independent of redshift for models with $Z_m \geqslant 1{\cdot}5$. Nevertheless the mean value of $\eta(P)$ over the observable volume of space can be estimated in each model and the corresponding integrated background predicted. For 'weak' radio-galaxies, i.e. those with luminosities less than $10^{23{\cdot}5}$ w ster^{-1} (c/s)$^{-1}$ at 178 MHz, the luminosity function of Caswell & Wills (14) can be used, since $\eta(P)$ is practically independent of cosmological model for such sources.

The quantity $(c/H_0)\overline{\eta P}$, which is independent of H_0, depends only slightly on cosmological model. It is practically independent of ϵ, is a slowly decreasing function of Z_m and is of the order of

$$13 . 10^{-23} \text{ w m}^{-2} \quad \text{for} \quad 1{\cdot}4 \leqslant Z_m \leqslant 3{\cdot}0, \; 10^{-5} \leqslant \epsilon \leqslant 1.$$

Slightly over half this figure is contributed by weak radio-galaxies: the contribution of the quasars is negligible, about $0{\cdot}5 \times 10^{-23}$ w m^{-2}. Radio-wise, it is reasonable to regard the quasars as a subclass of the radio-galaxies, visible at large redshift by virtue of exceptionally large optical emission. From this point of view it is not necessary to include their contribution to $\eta(P)$.

Now $c^2/2K\nu_0^2 = 10^{23{\cdot}01}$ deg m^2 w^{-1} so $T \sim 13\bar{X}°$. The dependence of T on model is shown more precisely in Fig. 9. The models in the regions B and C (see

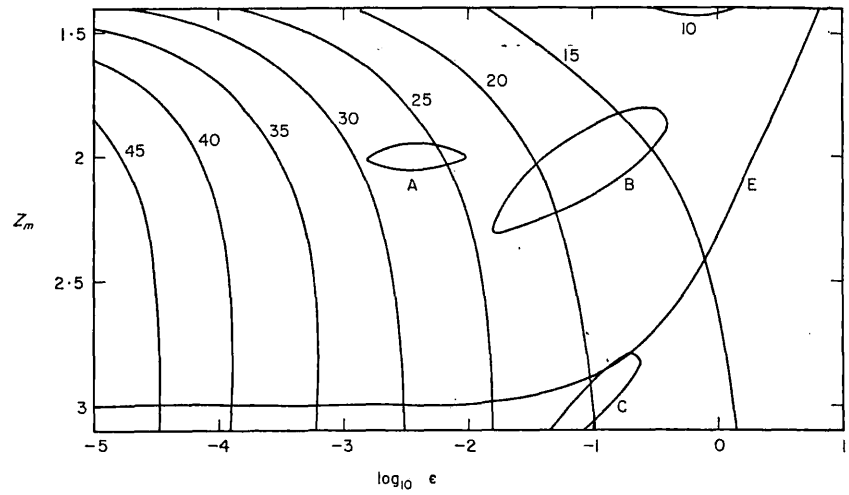

FIG. 9. *Z_m–ϵ, showing lines of constant integrated extra-galactic background temperature at 178 MHz. Models in the region A fall in the observed range $30\pm7°$. The curve labelled E corresponds to $\sigma_0 = 0{\cdot}05$, or $\rho_0 = 10^{-30}$ g cm^{-3}.*

Section 4.1) give rather low background temperatures, in the range 15–20°. The models in the region A fall within the strip corresponding to the observed values $30\pm7°$ (**20**). Comparing this strip with Fig. 8, the corresponding ages of the universe are in the range 2–$4(H_0^{-1})$. The model proposed by Kardashev gives a background temperature at 178 MHz of 46°, in the absence of evolutionary effects.

The strip of models consistent with the observed integrated background could change very drastically if evolutionary effects are introduced. For consistency of the Kardashev model with the distributions in space of radio-galaxies and quasars, the number-density or luminosity of sources should increase with redshift in the range $0<z<0{\cdot}5$, and decrease in the range $1<z<2$.

6. *Number-counts to low flux-level.* In calculating the theoretical number-count relationship for models with antipoles, both Kardashev (**7**) and McVittie & Stabell (**8**) have neglected the contribution of sources in the vicinity of epochs such that $\chi(z) = \pi, 2\pi, 3\pi$ etc. This, however, is incorrect. Suppose $\chi(z_n) = n\pi$, $n = 1, \ldots, N$, and that the values of z for which sources of luminosity P and spectral index are observed to have flux-level S are given by $z = z_n \pm \beta_n$, $n = 1 \ldots N$ and $z = \beta_0$.

Let the corresponding values of χ be $n\pi \pm \delta_n$, and δ_0. Then if

$$\delta_n \ll 1,\ D(z_n \pm \beta_n) \simeq R_0 Z_n \delta_n,$$

so

$$S = P/R_0^2 Z_n^{1+\alpha} \delta_n^2.$$

Also

$$v(z_n \pm \beta_n) \simeq \tfrac{1}{2} n\pi \pm \delta_n^3/3.$$

The number of sources brighter than S is proportional to

$$\begin{aligned} R_0^3\{v(\beta_0) + \sum_{n=1}^{N} [v(z_n+\beta_n) - v(z_n-\beta_n)]\} &= 1/3\left(\delta_0^3 + 2\sum_1^N \delta_n^3\right) R_0^3 \\ &= 1/3(P/S)^{1\cdot5}\left\{1 + 2\sum_1^N Z_n^{-3(1+\alpha)/2}\right\} \\ &= 1/3(P/S)^{1\cdot5}\xi \text{ say.} \end{aligned}$$

Kardashev and McVittie & Stabell, assumed that $\xi \simeq 1$, but in fact, for the Kardashev model, $Z_1 = 2{\cdot}84117$, $Z_2 = 2{\cdot}94829$, $Z_3 = 3{\cdot}02076$, $Z_4 = 4{\cdot}92604$ (Kardashev has different values for Z_3 and Z_4 as a consequence of his incorrect expression for Q: see Section 3.1 above), and so $\xi = 1{\cdot}355$. Moreover, as $\epsilon \to 0$ the number of solutions of $\chi(z) = n\pi$ with $1+z \simeq Z_m$ tends to infinity, so $\xi \to \infty$.

Fig. 10 shows the exact log N–log S relation for sources of luminosity 10^{25} w ster^{-1} (c/s)$^{-1}$, for three models with antipoles and also the relations obtained when the observed dispersion in luminosity is taken into account. These theoretical log N–log S curves are very much less steep than that observed at 178 MHz. This failure to account for the radio source-counts to low flux-level applies to all models within the range considered in this paper: $1{\cdot}4 \leqslant Z_m \leqslant 3{\cdot}0$; $10^{-5} \leqslant \epsilon \leqslant 1$.

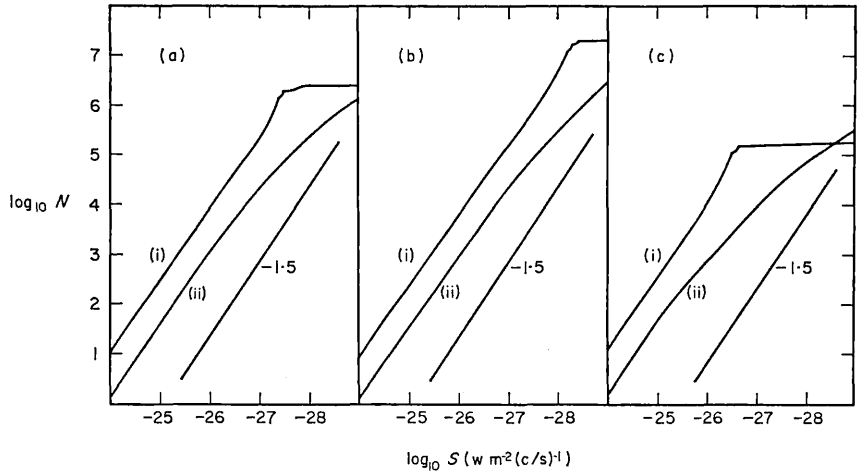

FIG. 10. log N–log S *curves at* 178 *MHz* (*i*) *for sources with luminosity* 10^{25} *w ster*$^{-1}$ (*c*/*s*)$^{-1}$ *and coordinate number density* 10^6 $(c/H_0)^{-3}$, (*ii*) *for the observed distribution of luminosities, for three models. Lines of slope* $-1{\cdot}5$ *are shown in each case.*

(*a*) $Z_m = 2{\cdot}0$, $\epsilon = 0{\cdot}0056$
(*b*) $Z_m = 2{\cdot}95$, $\epsilon = 0{\cdot}00002$
(*c*) $Z_m = 1{\cdot}4$, $\epsilon = 0{\cdot}006$.

Conclusions

(i) A small range of models is consistent with the distribution in space of 3C quasars, including three models that might also explain the anomalous absorption redshift of 1·95: $(Z_m, \epsilon) = (2{\cdot}0, 0{\cdot}0056)$, $(2{\cdot}0, 0{\cdot}14)$ and $(2{\cdot}95, 0{\cdot}1)$.

The first of these gives an integrated background temperature at 178 MHz for extragalactic sources of 26°, in agreement with the observed value of $30 \pm 7°$ and provides a natural explanation of the absence of 3C quasars with redshift greater than 2·2. The average density of the universe in this model is about $5 . 10^{-30}$ g cm^{-3}, requiring the existence of an appreciable quantity of intergalactic or intercluster material.

(ii) For consistency with the distribution in space of 3C radio-galaxies, it is necessary that an antipole occur at $z \leqslant 0{\cdot}45$. It would then be the most remarkable coincidence that the galaxy identified with 3C295, with $z = 0{\cdot}46$, satisfies the Hubble relation (**21**). Very large systematic errors must be present in the data for

models with $Z_m \geqslant 1{\cdot}5$ to be consistent with the distribution of 3C radio-galaxies, without the introduction of evolutionary effects.

(iii) None of the models considered in this paper predict source-count curves as steep as that observed. Evolutionary effects have to be introduced and there seems no reason for preferring models with an antipole to the more familiar models with $\Lambda = 0$, unless further evidence (confirmation of the anomalous absorption redshift, or of the correlation of radio-sources in opposite directions in the sky) points towards them. The interpretation of the radio source-counts to low flux-level in terms of exponential evolutionary effects will be discussed in a subsequent paper.

Acknowledgments. The computing was performed by the Computer Centre Staff, Queen Mary College, to whom thanks are due for helpful assistance. I am grateful to a referee, and to Dr R. Stabell, for comments that enabled this paper to be improved.

Queen Mary College,
Mile End Road,
London E.1.
1968 *May.*

References

(1) Rees, M. J. & Sciama, D. W., 1967. *Nature, Lond.*, **213**, 374.
(2) Rowan-Robinson, M., 1968. *Mon. Not. R. astr. Soc.*, **138**, 445.
(3) Schmidt, M., 1968. *Astrophys. J.*, **151**, 393.
(4) Rowan-Robinson, M., 1967. *Nature, Lond.*, **216**, 1289.
(5) Petrosian, V., Salpeter, E. & Szekeres, P., 1967. *Astrophys. J.*, **147**, 1222.
(6) Shklovsky, I., 1967. *Astrophys. J.*, **150**, L1.
(7) Kardashev, N., 1967. *Astrophys. J.*, **150**, L135.
(8) McVittie, G. C. & Stabell, R., 1967. *Astrophys. J.*, **150**, L141.
(9) Solheim, J. E., 1968. *Nature, Lond.*, **217**, 41.
(10) Burbidge, G. R. & Burbidge, E. M., 1967. *Astrophys. J.*, **148**, 107.
(11) Wagoner, R. V., 1967. *Astrophys. J.*, **149**, 465.
(12) Penston, M. V. & Rowan-Robinson, M., 1967. *Nature, Lond.*, **213**, 375.
(13) Long, R. J., Smith, M. A., Stewart, P. & Williams, P. J. S., 1966. *Mon. Not. R. astr. Soc.* **134**, 371.
(14) Caswell, J. L. & Wills, D., 1967. *Mon. Not. R. astr. Soc.*, **135**, 231.
(15) Oort, J. H., 1958. Solvay Conference on *La Structure et l'Evolution de l'Univers*, p. 163.
(16) Humason, M. L., Mayall, N. U. & Sandage, A. R., 1956. *Astr., J.*, **61**, 97.
(17) Tinsley, B. M., 1967. Ph.D. Thesis, University of Texas.
(18) Kafka, P., 1967. Max-Planck Institute für Physik und Astrophysik, München, preprint.
(19) Veron, P., 1967. *Ann. d'Astrophys.*, **30**, 719.
(20) Bridle, A. H., 1967. *Mon. Not. R. astr. Soc.*, **136**, 219.
(21) Sandage, A. R., 1965. *Astrophys. J.*, **141**, 1560.
(22) Felten, J. E., 1966. *Astrophys. J.*, **144**, 241.
(23) Pearson, K., 1922. *Tables of the Incomplete Gamma-Function*, London.